http://researchcommons.waikato.ac.nz/

Research Commons at the University of Waikato

Copyright Statement:

The digital copy of this thesis is protected by the Copyright Act 1994 (New Zealand).

The thesis may be consulted by you, provided you comply with the provisions of the Act and the following conditions of use:

- Any use you make of these documents or images must be for research or private study purposes only, and you may not make them available to any other person.
- Authors control the copyright of their thesis. You will recognise the author's right to be identified as the author of the thesis, and due acknowledgement will be made to the author where appropriate.
- You will obtain the author's permission before publishing any material from the thesis.

The Role of the Deposit Feeding Bivalve *Macomona liliana* in a Simple Biophysical Model for Predicting Estuarine Ecosystem Tipping Points

A thesis

submitted in partial fulfilment

of the requirements for the degree

of

Master of Science (Research) In Environmental Sciences

at

The University of Waikato

by

Taylor Scott Thomson

THE UNIVERSITY OF
WAIKATO
Te Whare Wānanga o Waikato

2022

Abstract

Estuaries are highly productive, coastal marine environments that provide vital ecosystem functions supporting human health. Throughout history, many major settlements have been established adjacent to estuaries, so to take advantage of the resources they provide. After centuries of exploitation and heavy pollution, the health of estuaries have experienced a notable decline. The need for effective management strategies has arisen, but their efficacy continues to be questioned due to the dynamic and unpredictable nature of these environments. Non-linear processes, such as regime shifts, make long-term predictions of ecosystem health a point of concern. To combat this issue in New Zealand, ecosystem interaction networks (EINs) have been used to predict the future health of estuaries using long-term statistical modelling. Unfortunately, these models fail to capture the coupling interactions between biotic and abiotic variables that occur in such a volatile environment. Therefore, we have created a simple model design that replicates the dynamic ecosystem interactions found within the benthic environments of New Zealand estuaries, with a specific focus on the behaviour of the keystone bivalve species *Macomona liliana*. A multitude of biophysical dynamical models currently exist in this field (e.g. Delft3D and DELWAQ); however none with the ability to replicate the exchange of nutrients between the sediment and benthic layer caused by *M. liliana* pumping behaviour. Consequently, this makes our model the first of its kind. Our model design simulates the variation of three dynamic variables (biomass, nutrients, detritus) corresponding to the interactions of *M. liliana* and microphytobenthos (MPB) at a representative site of New Zealand sandy bottom estuaries (Tuapiro Point, Tauranga Harbour). Extensive testing was conducted to ensure that, at the baseline level, the model's output was consistent with field sampling data seen within the literature. Once completed, the model was tested against external forcing factors that are likely to occur within New Zealand estuaries – turbidity, sedimentation, and external nutrient loading. We found that our system is light limited, with *M. liliana* and MPB biomasses both declining with increasing turbidity. MPB populations fluctuate significantly following a sediment mud content increase, which we believe demonstrates a reaction to an ecological tipping point being surpassed. Furthermore, we found that a significant influx of external nutrient loading is required to initiate a MPB bloom, which the system cannot maintain despite nutrient levels remaining high. Our model's results are in agreement with estuarine responses seen in the past, with our design exceeding the guidelines surrounding the efficacy

in predicting ecosystem tipping points. Therefore, due to its unique ability to demonstrate the interactions within coupled systems and its broad applicability globally, we believe our model can become a central component of future estuarine management strategies. Recommendations are made for future improvements to the model design, increasing both its range of simulated ecological processes and the validity of its predictions.

Acknowledgements

I would like to express my sincere gratitude to the Sustainable Seas National Science Challenge for their funding throughout my project. You gave me the key to my next journey in science and for that I am forever grateful.

I am deeply grateful to my supervisor Karin Bryan for her assistance throughout the length of this project. Despite some setbacks, your ongoing support and enthusiasm kept me pushing through the hard yards to the end. Your knowledge and guidance have been truly inspiring, and it has been an honour to work alongside you.

I would like to offer special thanks to Conrad Pilditch, Simon Thrush, and Dong Sheng Jeng for their insightful comments and suggestions. The privilege of gaining feedback from such reputable authors in this field has not gone unnoticed, and increased the quality of my work exponentially, so for that, thank you.

Many thanks to the School of Science for their continued support throughout my research. Your flexibility and willingness to lend a hand helped to shape my project into what it is today.

Finally, I would like to thank those in my life, both past and present, who have supported me along the way. To my parents, thank you for encouraging my love of the water and providing endless opportunities to explore. To all my friends, thank you for keeping me sane and involved in life outside of research. To my dog Zeke, thank you for making me want to be a better person.

Table of Contents

Abstract ii

Acknowledgements iv

Table of Contents v

List of Figures ix

List of Tables xix

List of Equations xxi

Chapter 1 22

1.1 Background and Motivation of the Study 22

1.2 Research Aims and Objectives 24

1.3 Thesis Outline 25

Chapter 2 26

2.1 Estuaries 26

2.2 M. liliana 28

2.3 Microphytobenthos (MPB) 30

2.4 Benthic Layer 31

2.5 Interactions Within the Benthic Layer 37

2.6 Regime Shifts 37

2.7 Alternate stable states 39

2.8 Tipping points 42

Chapter 3 46

3.1 Model Design 46

3.2 Model Domain Characteristics 48

3.3 Biomass dynamics 49

3.4 Light Intensity 52

3.5 *M. liliana* Growth Dynamics 54

3.6 MPB growth dynamics 60
3.7 Detrital pool dynamics 61
3.8 Nutrient pool dynamics 62
3.9 Initial boundary conditions 67
3.10 Flushing Coefficient 68
3.11 Summary 74
Chapter 4 75
4.1 Model Testing Structure 75
4.2 *M. liliana* and MPB Mortality Values 76
4.3 Observations Trials one to ten 80
4.3.1 Biomass 80
4.3.2 Nutrients 83
4.3.3 Detritus 84
4.3.4 Key Findings 86
4.4 Observations Trials ten to 15 86
4.4.1 Biomass 86
4.4.2 Nutrients 89
4.4.3 Detritus 91
4.4.4 Key Findings 92
4.5 Observations Trials 18 to 27 93
4.5.1 Biomass 93
4.5.2 Nutrients 96
4.5.3 Detritus 98
4.5.4 Key Findings 102
4.6 Observations Following the Addition of *DR* – Trials 28 to 31 103
4.6.1 Biomass 103
4.6.2 Nutrients 109

4.6.3 Detritus 111
4.6.4 Key Findings 115
4.7 Observations Following the Addition of *DR* – Trials 32 to 46 115
4.7.1 Biomass 115
4.7.2 Nutrients 118
4.7.3 Detritus 120
4.7.4 Key findings 122
4.8 Preliminary Results of the Model 123
4.9 The Model's Reaction to Changing Turbidity 123
4.9.1 Biomass 123
4.9.2 Nutrients 124
4.9.3 Detritus 125
4.9.4 Key Findings 126
4.10 The Model's Reaction to Increasing Sediment Mud Content 127
4.10.1 Biomass 127
4.10.2 Nutrients 128
4.10.3 Detritus 129
4.10.4 Key Findings 130
4.11 The Model's Reaction to a Single External Nutrient Loading Event 131
4.11.1 Biomass 131
4.11.2 Nutrients 132
4.11.3 Detritus 133
4.11.4 Key Findings 134
Chapter 5 135
5.1 Successful Modelling of Interactions Between Three Dynamic Variables 135
5.1.1 Relationships Observed During Model Testing 135
5.1.2 Possible Tipping Point Events 137

5.2 Preliminary Results of External Forcing Tests 138
5.2.1 Turbidity 138
5.2.2 Sediment Mud Content 140
5.2.3 External Nutrient Loading Event 142
5.3 Increasing the Model's Efficacy in Predicting Estuarine Tipping Points 144
5.3.1 Adding Wind, Tidal, and Wave Effects 144
5.3.2 External Nutrient Loading 146
5.3.3 Turbidity 147
5.3.4 Sediment Mud Content 147
Chapter 6 149
6.1 Conclusions 149
6.2 Recommendations for Future Research 150
References 152

List of Figures

Figure 2.1. Weighted importance across all taxa (overall importance) of natural environmental variables and stressors from land in predicting benthic macroinvertebrate compositional turnover in New Zealand estuaries. R^2 evaluated by boot-strapped gradient forest models. The average contribution by each predictor across 100 bootstraps is demonstrated by the grey bars, with error bars denoting the standard deviation (Clark et al., 2021). 28

Figure 2.2. Illustration of a New Zealand estuarine benthic interaction web (Thrush et al., 2014). 29

Figure 2.3. EIN situated within a (A) clear (>420 $\mu mol \cdot L^{-1} \cdot m^{-2} \cdot s^{-1}$ PAR) and (B) turbid (<350 $\mu mol \cdot L^{-1} \cdot m^{-2} \cdot s^{-1}$ PAR) sites. Pink boxes refer to the abundance of shellfish >20mm shell length; NH_4^+ flux between the sediment-water layer and denitrification (N_2) are indicated by the yellow boxes; benthic oxygen consumption outline within the blue box; purple boxes indicate mud, mud in the sediment, and the standing stock of microphytobenthos (Chl a); and teal boxes identify the experimental manipulation of nutrient addition and turbidity's effect on available photosynthetically active radiation (average daily max PAR). Arrow thickness demonstrates the relationship strength, with black arrows identifying negative relationships and red positive (Thrush et al., 2021). 33

Figure 2.4. Denitrification enzyme activity in low mud (a) and high mud (b) sediments, shown by structural equations modelling ecosystem interactions. Path thickness is determined by the path coefficient (significant at p), with r^2 variables displayed for each response variable. Black paths identify negative relationships, with red positive (Douglas et al., 2019). 34

Figure 2.5. Box plots depicting the ecosystem constituents (a) mud content, (b) organic content, (c) Chl a, (d) total taxa, (e) abundance of macrofauna, and (f) large bivalves present in the sandy (10% mud) dataset (n=57). 25th and 75th percentiles and shown, 10th10th and 90th percentiles identified by whiskers, and black dots showing the 5th and 95th percentiles. The mean is shown by a dashed line, with the solid line indicating the median (Douglas et al., 2019). 36

Figure 2.6. Alternative forms of regime shifts, ranging from smooth/linear responses to discontinuous change (Selkoe et al., 2015). 38

Figure 2.7. Illustration depicting ecosystem response over five distinct ecosystems. The grey components represent the external forcing needed for the five ecosystems to switch ecological state. The centre component represents an ecosystem with a strong positive feedback, while the components at either end depict ecosystems residing deep within their ecological state. Unstable ecosystems are depicted with smaller hills, having little resilience and need only small/moderate perturbations to shift state, while stable ecosystems have large valleys and require larger perturbations to undergo a regime shift. The yellow segment beneath illustrates an equilibrium curve, depicting a regime shift. The grey components can be matched to their respective positions along the curve, demonstrating where they sit regarding changing ecological state. F1 and F2 identify where on the curve an ecosystem will change state (Scheffer et al., 2001). 39

Figure 2.8. Ecosystem responses to external forcing. (a) Represents external forces changing with time. (b) Depicts an ecosystem undergoing gradual change in response to external forcing and has no positive feedback system present. (c) Demonstrates a rapid response to external forcing, occurring when there is a weak positive feedback system present. (d) Portrays an ecosystem with a strong positive feedback system. System (d) resists change until a tipping point is reached, causing an abrupt change from one state to another once surpassed. Such response is classified as hysteresis, which requires external conditions to decrease to a point that is smaller than where the shift occurred. (b-d) therefore demonstrate that the response of an ecosystem to external forcing is dependent on the strength of the positive feedback system between biotic and abiotic factors (Kéfi et al., 2016). 41

Figure 2.9. Monitoring design recommendations for detecting marine system tipping points. Fewer years and data points are needed to detect change when rapid change in the response variables correspond with rapid change in a driver (Hewitt & Thrush, 2019). 43

Figure 2.10. Monitoring design recommendations for detecting early warning signals in marine systems (Hewitt & Thrush, 2019). 44

Figure 3.1. Monthly growth rates of *M. liliana* across eight sites within a transplant experiment. Mean growth rate is denoted by the grey bars, with standard error bars in black shown (Auckland Regional Council, 2008) 56

Figure 3.2. Scatter plot demonstrating the relationship between *M. liliana* biomass and ammonia concentrations within sediment. The y-axis represents the number of *M. liliana* present, while the x-axis represents the NH_4^+ concentration (µmol L) 5-7cm below the sediment surface. Dots are indicative of measurements taken at individual sampling sites within Thrush et al. (2021). An exponential curve is fitted to the graph as a solid line, with the dotted line representing the upper 99% prediction bound. 59

Figure 3.3. Recurrent pressurisation of porewater affiliated with deposit-feeding by *M. liliana* (4.9cm shell length) in sediment with a permeability of 4.3×10^{-12} m^2 (Volkenborn et al., 2012). 71

Figure 3.4. Porewater pressure dynamics corresponding to the hydraulic activity of *M. liliana* (5.0cm shell length) in sediment with a permeability of 4.3×10^{-12} m^2. The spikes represent burrowing episodes, with the recurrent pressurisation and positive and negative hydraulic pulses affiliated with siphon movements, and pseudofeces and feces expulsions. Box A demonstrates the entire 22-hour sequence, while box B and C are enlargements of the data outlined by the dashed boxes in A (Volkenborne et al., 2012). 72

Figure 4.1. Timeseries plot of biomass values (g C m^{-2}) per time step for trials one to ten for *M. liliana* (a) and MPB (b). Trials are plotted along a colour scale progressing from blue to magenta (MATLAB's 'cool colormap'). Trial ten was run to on an unrestricted timeframe, to identify if an increased t_{max} would significantly alter results. 82

Figure 4.2. Scatter graphs demonstrating the biomass of *M. liliana* and MPB. The graph includes values from all results across trials one to ten. The vertical red line illustrates an average MPB biomass (1.056 g C m^{-2}) within the Tauranga Harbour ((Flowers et al., in review) and the horizontal blue line illustrates an average *M. liliana* biomass (41.768 g C m^{-2}) found within Tauranga Harbour (Thrush et al., 2021). The colour scale in (a) denotes the different *M. liliana* mortality rate (per time step) log formed in each trial; the colour scale in (b) denotes the different MPB mortality rates (per time step) log formed in each trial; the colour scale in (c) corresponds to the 'variant' number for MPB mortality across trials (see Table 4.1); and the colour scale in (d) refers to the 'trial' number for *M. liliana* mortality rate across trials (see Table 4.1). 83

Figure 4.3. Timeseries plot of nutrient values (mmol N m^{-2}) per time step for trials one to ten for *M. liliana* (a) and MPB (b). Trials are plotted along a colour scale progressing from blue to magenta (MATLAB's 'cool colormap').....84

Figure 4.4. Timeseries plot of detrital values (g C m^{-2}) per time step for trials one to ten for *M. liliana* (a) and MPB (b). Trials are plotted along a colour scale progressing from blue to magenta (MATLAB's 'cool colormap').....85

Figure 4.5. Timeseries plot of biomass values (g C m^{-2}) per time step for trials 11 to 15 for *M. liliana* (a) and MPB (b). Trials are plotted along a colour scale progressing from red to yellow (MATLAB's 'autumn colormap').....88

Figure 4.6. Timeseries plot for biomass values (g C m^{-2}) per time step for trials one to 15 for *M. liliana* (a) and MPB (b). Trials are plotted along a colour scale, with colours for trials one to ten progressing from blue to magenta (MATLAB's 'cool colormap'), and colours for trials 11 to 15 progressing from red to yellow (MATLAB's 'autumn colormap').....88

Figure 4.7. Scatter graphs demonstrating the biomass of *M. liliana* and MPB at the conclusion of all results from trial one to 15. The vertical red line illustrates an average MPB biomass (1.056 g C m^{-2}) within Tauranga Harbour (Flowers et al., in review) and the horizontal blue line illustrates an average *M. liliana* biomass (41.768 g C m^{-2}) found within Tauranga Harbour (Thrush et al., 2021). The colour scale in (a) denotes the different *M. liliana* mortality rate (per time step) log formed in each trial; the colour scale in (b) denotes the different MPB mortality rates (per time step) log formed in each trial; the colour scale in (c) corresponds to the 'variant' number for MPB mortality across trials (see Table 4.1 & 4.2); and the colour scale in (d) refers to the 'trial' number for *M. liliana* mortality rate across trials (see Table 4.1 & 4.2).....89

Figure 4.8. Timeseries plot of nutrient values (mmol N m^{-2}) per time step for trials 11 to 15 for *M. liliana* (a) and MPB (b). Trials are plotted along a colour scale progressing from red to yellow (MATLAB's 'autumn colormap').....90

Figure 4.9. Timeseries plot of nutrient values (mmol N m^{-2}) per time step for trials one to 15 for *M. liliana* (a) and MPB (b). Trials are plotted along a colour scale, with colours for trials one to ten progressing from blue to magenta (MATLAB's 'cool colormap'), and colours for trials 11 to 15 progressing from red to yellow (MATLAB's 'autumn colormap').....90

Figure 4.10. Timeseries plot of detrital values (g C m^{-2}) per time step for trials 11 to 15 for *M. liliana* (a) and MPB (b). Trials are plotted along a colour scale progressing from red to yellow (MATLAB's 'autumn colormap'). 91

Figure 4.11. Timeseries plot of detrital values (g C m^{-2}) per time step for trials one to 15 for *M. liliana* (a) and MPB (b). Trials are plotted along a colour scale, with colours for trials one to ten progressing from blue to magenta (MATLAB's 'cool colormap'), and colours for trials 11 to 15 progressing from red to yellow (MATLAB's 'autumn colormap').....92

Figure 4.12. Timeseries plot of biomass values (g C m^{-2}) per time step for trials 18 to 27 for *M. liliana* (a) and MPB (b). Trials are plotted along a colour scale progressing from dark green to lime (MATLAB's 'summer colormap'). 94

Figure 4.13. Timeseries plot for biomass values (g C m^{-2}) per time step for *M. liliana* (a) and MPB (b). Data was used from trials one through to 27, excluding trials 16 & 17 due to errors. Trials are plotted along several colour scales; trials one to ten are plotted in colours progressing from blue to magenta (MATLAB's 'cool colormap'), 11 to 15 are plotted in colours progressing from red to yellow (MATLAB's 'autumn colormap'), and 18 to 27 are plotted in colours progressing from dark green to lime (MATLAB's 'summer colormap'),..95

Figure 4.14. Scatter graphs demonstrating the biomass of *M. liliana* and MPB at the conclusion of each trial (excluding trial 16-17) from trials one to 27. The vertical red line illustrates an average MPB biomass (1.056 g C m^{-2}) within Tauranga Harbour (Flowers et al., in review) and the horizontal blue line illustrates an average *M. liliana* biomass (41.768 g C m^{-2}) found within Tauranga Harbour (Thrush et al., 2021). The colour scale in (a) denotes the different *M. liliana* mortality rate (per time step) log formed in each trial; the colour scale in (b) denotes the different MPB mortality rates (per time step) log formed in each trial; the colour scale in (c) corresponds to the 'variant' number for MPB mortality across trials (see Table 4.1, 4.2, & 4.3); and the colour scale in (d) refers to the 'trial' number for *M. liliana* mortality rate across trials (see Table 4.1, 4.2, & 4.3).....96

Figure 4.15. Timeseries plot of nutrient values (mmol N m^{-2}) per time step for trials 18 to 27 for *M. liliana* (a) and MPB (b). Trials are plotted along a colour scale progressing from dark green to lime (MATLAB's 'summer colormap'). 97

Figure 4.16. Timeseries plot of nutrient levels (mmol N m^{-2}) per time step for *M. liliana* (a) and MPB (b). Data was used from trials one to 27 excluding trials 16 & 17 due to errors.

Trials are plotted along several colour scales; trials one to ten are plotted in colours progressing from blue to magenta (MATLAB's 'cool colormap'), 11 to 15 are plotted in colours progressing from red to yellow (MATLAB's 'autumn colormap'), and 18 to 26 are plotted in colours progressing from dark green to lime (MATLAB's 'summer colormap')...98

Figure 4.17. Timeseries plot of detrital values (g C m^{-2}) per time step for trials 18 to 27 for *M. liliana* (a) and MPB (b). Trials are plotted along a colour scale progressing from dark green to lime (MATLAB's 'summer colormap'). 99

Figure 4.18. Timeseries plot of detrital values (g C m^{-2}) per time step for *M. liliana* (a) and MPB (b). Data was used from trials one to 27, excluding trials 16 & 17 due to errors. Trials are plotted along several colour scales; trials one to ten are plotted in colours progressing from blue to magenta (MATLAB's 'cool colormap'), 11 to 15 are plotted in colours progressing from red to yellow (MATLAB's 'autumn colormap'), and 18 to 27 are plotted in colours progressing from dark green to lime (MATLAB's 'summer colormap'). 100

Figure 4.19. Timeseries plot of MPB biomass values (g C m^{-2}) per time step (a) and MPB detrital values (g C m^{-2}) (b). Data was used from trials one to 27, excluding trials 16 & 17 due to errors. Trials are plotted along several colour scales; trials one to ten are plotted in colours progressing from blue to magenta (MATLAB's 'cool colormap'), 11 to 15 are plotted in colours progressing from red to yellow (MATLAB's 'autumn colormap'), and 18 to 27 are plotted in colours progressing from dark green to lime (MATLAB's 'summer colormap'). 101

Figure 4.20. Timeseries plot of biomass and detrital values (g C m^{-2}) per time step for *M. liliana* (a) and MPB (b). Data was used from trials one to 27, excluding trials 16 & 17 due to errors. Red lines correspond to biomass values, while blue lines identify detrital values.....102

Figure 4.21. Timeseries plot of biomass values (g C m^{-2}) per time step for trials 28 to 31 for *M. liliana* (a) and MPB (b). Trials are plotted along a colour scale progressing from black to copper (MATLAB's 'copper colormap').....104

Figure 4.22. Timeseries plot of biomass values (g C m^{-2}) per time step for *M. liliana* (a) and MPB (b). Data was used from trials one to 31, excluding trials 16 & 17 due to errors. Trials are plotted along several colour scales; trials one to ten are plotted in colours progressing from blue to magenta (MATLAB's 'cool colormap'), 11 to 15 are plotted in colours progressing from red to yellow (MATLAB's 'autumn colormap'), 18 to 27 are plotted in

colours progressing from dark green to lime (MATLAB's 'summer colormap'), and 28 to 31 are plotted in colours progressing from black to copper (MATLAB's 'copper colormap')..105

Figure 4.23. Scatter graphs demonstrating the biomass of *M. liliana* and MPB at the conclusion of each trial (excluding trial 16 & 17) from trials one to 31. The vertical red line illustrates an average MPB biomass (1.056 g C m^{-2}) within Tauranga Harbour (Flowers et al., in review) the horizontal blue line illustrates an average *M. liliana* biomass (41.768 g C m^{-2}) found within Tauranga Harbour (Thrush et al., 2021). The colour scale in (a) denotes the different *M. liliana* mortality rate (per time step) log formed in each trial; the colour scale in (b) denotes the different MPB mortality rates (per time step) log formed in each trial; the colour scale in (c) corresponds to the 'variant' number for MPB mortality across trials (see Table 4.1, 4.2, 4.3, 4.4, & 4.5); and the colour scale in (d) refers to the 'trial' number for *M. liliana* mortality rate across trials (see Table 4.1, 4.2, 4.3, 4.4, & 4.5). 106

Figure 4.24. Timeseries plot of nutrient values (mmol N m^{-2}) per time step for trials 28 to 31 for *M. liliana* (a) and MPB (b). Trials are plotted along a colour scale progressing from black to copper (MATLAB's 'copper colormap'). 110

Figure 4.25. Timeseries plot of nutrient values (mmol N m^{-2}) per time step for trials one to 31 for *M. liliana* (a) and MPB (b). Data was used from trials one to 31, excluding trials 16 & 17 due to errors. Trials are plotted along several colour scales; trials one to ten are plotted in colours progressing from blue to magenta (MATLAB's 'cool colormap'), 11 to15 are plotted in colours progressing from red to yellow (MATLAB's 'autumn colormap'), 18 to 26 are plotted in colours progressing from dark green to lime (MATLAB's 'summer colormap'), and 27 to 31 are plotted in colours progressing from black to copper (MATLAB's 'copper colormap').....111

Figure 4.26. Timeseries plot of detrital values (g C m^{-2}) per time step for trials 28 to 31 for *M. liliana* (a) and MPB (b). Trials are plotted along a colour scale progressing from black to copper (MATLAB's 'copper colormap').....112

Figure 4.27. Timeseries plot of detrital values (g C m^{-2}) per time step for *M. liliana* (a) and MPB (b). Data was used from trials one to 31, excluding trials 16 & 17 due to errors. Trials are plotted along several colour scales; trials one to ten are plotted in colours progressing from blue to magenta (MATLAB's 'cool colormap'), 11 to 15 are plotted in colours progressing from red to yellow (MATLAB's 'autumn colormap'), 18 to 26 are plotted in

colours progressing from dark green to lime (MATLAB's 'summer colormap'), and 27 to 31 are plotted in colours progressing from black to copper (MATLAB's 'copper colormap')..113

Figure 4.28. Timeseries plot of biomass values (g C m^{-2}) per time step for trials 32 to 46 for *M. liliana* (a) and MPB (b). Trials are plotted along a colour scale progressing from dark blue to green (MATLAB's 'winter colormap'). 116

Figure 4.29. Timeseries plot of biomass values (g C m^{-2}) per time step for *M. liliana* (a) and MPB (b). Data was used from trials one to 46, excluding trials 16 & 17 due to errors. Trials are plotted along several colour scales; trials one to ten are plotted in colours progressing from blue to magenta (MATLAB's 'cool colormap'), 11 to 15 are plotted in colours progressing from red to yellow (MATLAB's 'autumn colormap'), 18 to 27 are plotted in colours progressing from dark green to lime (MATLAB's 'summer colormap'), 28 to 31 are plotted in colours progressing from black to copper (MATLAB's 'copper colormap'), and 32 to 46 are plotted in colours progressing from dark blue to green (MATLAB's 'winter colormap').....117

Figure 4.30. Scatter graphs demonstrating the biomass of *M. liliana* and MPB at the conclusion of each trial (excluding trial 16 & 17) from trials one to 46. The vertical red line illustrates an average MPB biomass (1.056 g C m^{-2}) within Tauranga Harbour (Flowers et al., in review) and the horizontal blue line illustrates an average *M. liliana* biomass (41.768 g C m^{-2}) found within Tauranga Harbour (Thrush et al., 2021). The colour scale in (a) denotes the different *M. liliana* mortality rate (per time step) log formed in each trial; the colour scale in (b) denotes the different MPB mortality rates (per time step) log formed in each trial; the colour scale in (c) corresponds to the 'variant' number for MPB mortality across trials (see Table 4.1, 4.2, 4.3, 4.4, 4.5, & 4.6); and the colour scale in (d) refers to the 'trial' number for *M. liliana* mortality rate across trials (see Table 4.1, 4.2, 4.3, 4.4, 4.5, & 4.6). 118

Figure 4.31. Timeseries plot of nutrient values (mmol N m^{-2}) per time step for trials 32 to 46 for *M. liliana* (a) and MPB (b). Trials are plotted along a colour scale progressing from dark blue to green (MATLAB's 'winter colormap'). 119

Figure 4.32. Timeseries plot of nutrient values (mmol N m^{-2}) per time step for trials one to 46 for *M. liliana* (a) and MPB (b). Data was used from trials one to 31, excluding trials 16 & 17 due to errors. Trials are plotted along several colour scales; trials one to ten are plotted in colours progressing from blue to magenta (MATLAB's 'cool colormap'), 11 to15 are plotted

in colours progressing from red to yellow (MATLAB's 'autumn colormap'), 18 to 27 are plotted in colours progressing from dark green to lime (MATLAB's 'summer colormap'), 28 to 31 are plotted in colours progressing from black to copper (MATLAB's 'copper colormap'), and 32 to 46 are plotted in colours progressing from dark blue to green (MATLAB's 'winter colormap'). 120

Figure 4.33. Timeseries plot of detrital values (g C m^{-2}) per time step for trials 32 to 46 for *M. liliana* (a) and MPB (b). Trials are plotted along a colour scale progressing from dark blue to green (MATLAB's 'winter colormap'). 121

Figure 4.34. Timeseries plot of detrital values (g C m^{-2}) per time step for *M. liliana* (a) and MPB (b). Data was used from trials one to 46, excluding trials 16 & 17 due to errors. Trials are plotted along several colour scales; trials one to ten are plotted in colours progressing from blue to magenta (MATLAB's 'cool colormap'), 11 to 15 are plotted in colours progressing from red to yellow (MATLAB's 'autumn colormap'), 18 to 27 are plotted in colours progressing from dark green to lime (MATLAB's 'summer colormap'), 28 to 31 are plotted in colours progressing from black to copper (MATLAB's 'copper colormap'), and 32 to 46 are plotted in colours progressing from dark blue to green (MATLAB's 'winter colormap'). 122

Figure 4.35. Timeseries plots of light variation trials one to 19 (excluding trials one, three, five, and seven due to errors). Biomass values (g C m^{-2}) per time step are plotted for *M. liliana* (a) and MPB (b). Results are plotted along a colour scale progressing from blue to magenta (MATLAB's 'cool colormap'). 124

Figure 4.36. Timeseries plot of light variation trials one to 19 (excluding trials one, three, five, and seven due to errors). Nutrient values (mmol N m^{-2}) per time step are plotted for *M. liliana* (a) and MPB (b). Results are plotted along a colour scale progressing from blue to magenta (MATLAB's 'cool colormap'). 125

Figure 4.37. Timeseries plots of light variation trials one to 19 (excluding trials one, three, five, and seven due to errors). Detrital values (g C m^{-2}) per time step are plotted for *M. liliana* (a) and MPB (b). Results are plotted along a colour scale progressing from blue to magenta (MATLAB's 'cool colormap'). 126

Figure 4.38. Timeseries plots of sediment mud content trials one to ten. Biomass values (g C m^{-2}) per time step are plotted for *M. liliana* (a) and MPB (b). Results are plotted along a colour scale progressing from blue to magenta (MATLAB's 'cool colormap'). 128

Figure 4.39. Timeseries plots of sediment mud content trials one to ten. Nutrient values (mmol N m^{-2}) per time step are plotted for *M. liliana* (a) and MPB (b). Results are plotted along a colour scale progressing from blue to magenta (MATLAB's 'cool colormap').....129

Figure 4.40. Timeseries plots of sediment mud content trials one to ten. Detrital values (g C m^{-2}) per time step are plotted for *M. liliana* (a) and MPB (b). Results are plotted along a colour scale progressing from blue to magenta (MATLAB's 'cool colormap'). 130

Figure 4.41. Timeseries plots of external nutrient loading trials one to six. Biomass values (g C m^{-2}) per time step are plotted for M. liliana (a) and MPB (b). Results are plotted along a colour scale progressing from blue to magenta (MATLAB's 'cool colormap'). 132

Figure 4.42. Log transformed timeseries plots of external nutrient loading trials one to six. Nutrient values (mmol N m^{-2}) per timestep are plotted for *M. liliana* (a) and MPB (b). Results are plotted along a colour scale progressing from blue to magenta (MATLAB's 'cool colormap').....133

Figure 4.43. Timeseries plots of external nutrient loading trials one to six. Detrital values (g C m^{-2}) per time step are plotted for *M. liliana* (a) and MPB (b). Results are plotted along a colour scale progressing from blue to magenta (MATLAB's 'cool colormap'). 134

List of Tables

Table 3.1. Model Parameters 47

Table 4.1. *M. liliana* (mac) and MPB mortality rates and their corresponding trial and variant number, for trials one to ten. Note that every combination of row (trial) and column (variant) was run. 76

Table 4.2. *M. liliana* (mac) and MPB mortality rates and their corresponding trial and variant number, for trials 11 to 15. Note that every combination of row (trial) and column (variant) was run. 76

Table 4.3. *M. liliana* (mac) and MPB mortality rates and their corresponding trial and variant number, for trials 18 to 26. Trials 16 and 17 were excluded from analyses (and this table) due to errors. Note that every combination of row (trial) and column (variant) was run. 76

Table 4.4. *M. liliana* (mac) and MPB mortality rates and their corresponding trial and variant number for trial 27. Note that every combination of row (trial) and column (variant) was run. 77

Table 4.5. *M. liliana* and MPB mortality rates and their corresponding trial and variant number, for trials 28 to 31. Note that every combination of row (trial) and column (variant) was run. 77

Table 4.6. *M. liliana* and MPB mortality rates and their corresponding trial and variant number, for trials 32 to 46. Note that every combination of row (trial) and column (variant) was run. 78

Table 4.7. Light availability test trial numbers and their corresponding light attenuation (k_d) depth (m). Trials one, three, five, and seven are excluded due to errors. 79

Table 4.8. Mud content test trial numbers and their corresponding sediment mud content (M_c) (%).....79

Table 4.9. External nutrient test trial numbers and their corresponding external nutrient (IN) value (mmol N m^{-2}).....79

Table 4.10. Rapid biomass jumps for trials 28 to 31. Size of the jump and time taken to occur are evaluated and ranked from largest to smallest. 107

Table 4.11. Double biomass jumps within trial 28. Size of the jump and time taken to occur are evaluated and ranked from largest to smallest. 108

Table 4.12. Rapid detritus jumps for trials 28 to 31. Size of the jump and time taken to occur are evaluated and ranked from largest to smallest. 114

Table 4.13. Comparison between rapid jumps in MPB biomass and detrital values (g C m^{-2}). The difference in time between the biomass and detritus jumps and their difference in size is examined. Values are positive or negative to indicate the direction of time difference. 114

List of Equations

MPB Biomass Dynamics (1) ……49
MPB Growth (2) ...……...50
Light Limitation (3) ……....50
Nutrient Limitation Water Column (4) ……50
Nutrient Limitation Sediment Layer (5) ……...50
Light Attenuation (6) ……...52
M. liliana Biomass Dynamics (7) ..……..54
M. liliana Growth (8) ……...54
M. liliana Maximum Growth Rate (9) ……..55
M. liliana Carrying Capacity (10) ……57
M. liliana Nutrient Poisoning (11) ……...58
MPB Detrital Dynamics (12) ……...62
M. liliana Detrital Dynamics (13) ……62
Nutrient Concentration Gradient (14) ……..62
MPB Nutrient Dynamics (15) ……..62
M. liliana Nutrient Dynamics (16) ……...63
Total Nutrients (17) ……..63
Nutrient Conversion from Grams to Millimoles (18) ……..66
Areal Coverage of *M. liliana* (19) ……68
Formulation of a Porous Seabed with Varying Permeabilities (20) ……69
Flux of Fluid Through a Porous Medium (21) ……..69
Pressurisation at Sediment Surface During *M. liliana* Feeding (22) ……72
Constant Pressurisation at the Sediment Surface by *M. liliana* (23) ……73
Flushing of Nutrients from Sediment (24) ……73
Mixing Coefficient (25) ……...73

Chapter 1

General Introduction

1.1 Background and Motivation of the Study

Anthropogenic influences are putting pressure on estuarine ecosystems along New Zealand's coastlines. Land derived stressors from human occupation and resource exploitation within estuaries are causing a decline in ecological health (Wells et al., 2019; Clark et al., 2021). Over time, estuaries undergo natural shifts in biotic and abiotic factors, having a gradual impact on an estuary's physical condition. Urbanisation has created a non-linear response within estuaries to anthropogenic pressures (Green, 2013), reducing ecosystem resilience. In ecological terms, resilience is an ecosystem's ability to respond to disturbance and retain the same function (Walker et al., 2004). An ecosystem's state will decline more quickly if it has low resilience (Scheffer et al., 2001), making it more susceptible to biodiversity loss and a change in ecosystem state.

Benthic macrofauna, such as the bivalve *Macomona liliana*, are imperative for nutrient cycling within coastal marine ecosystems (Douglas et al., 2017). *M. liliana* is a filter feeding shellfish species that regulates the exchange of nutrients between the water column and seabed sediment. They dwell 10-15cm beneath the marine sediment surface, excreting waste from material on the seabed by pumping water into the sediments. Their pumping behaviour pressurises sediments, generating a net upward flow of nutrient rich water, feeding algae dwelling at the sediment-water interface. This action is responsible for enhancing primary production and ecosystem function (Volkenborn et al., 2012; Woodin et al., 2012; Huettel et al., 2014; Kristensen et al., 2014). Anthropogenic influences are negatively impacting the bivalves' ability to perform their key functional roles, such as decreasing their growth rate (Wells et al., 2019), contributing to a decreasing resilience in estuaries.

Microphytobenthos (MPB) are also important to the health of New Zealand estuaries. Critical roles they serve within estuaries include primary production, carbon fixation, nutrient cycling, and sediment stabilisation (Borum & Sand-Jensen, 1996; Sundbäck et al., 2006; Jones et al., 2016; Joensuu et al., 2017; Hope et al., 2019). Crucially, they are the food source of *M. liliana,* which eat MPB using an inhalant siphon they protrude through the sediment surface. MPB live atop sediments, in what is known as the benthic layer. This region begins

at the shoreline and is considered to be an ecological hotspot within estuaries, responsible for preventing excess nutrient enrichment. Anthropogenic activity is causing an increase in fine sediment within benthic areas, reducing their resilience and the health of the organisms that dwell within it (Thrush, 2004; Douglas et al., 2018; Clark et al., 2021). Consequently, nutrient processing and removal is being dampened by such activity (Mermillod-Blondin & Rosenberg, 2006; Huettel et al., 2014).

New Zealand's estuaries are particularly prone to the addition of fine sediments and nutrients entering through river run-off. The array of negative effects that ensues increases the biotic and abiotic shifts in condition an estuary already experiences. Slowly shifting physical conditions are manageable by an estuarine system, but anthropogenic activity is generally accompanied by an increase in the rate of physical change (Scheffer et al., 2001). Estuaries can function with multiple stable states operating within them (Wang & Temmerman, 2013), but should anthropogenic activity reduce an estuary's health past its tipping point, a regime shift may occur – a change in species and chemical composition within an estuary due to the conversion from one stable ecological state to another (Walker & Meyers, 2004). Despite the recent expansion in research surrounding tipping points, they are not a new phenomenon. Many ecosystem tipping points have been documented in the past, the crash of the horse mackerel (*Trachurus trachurus*) population in the North Sea in the 1980s being a famous example. Tipping points are hard to predict, with regime shifts often being sudden and occurring after non-linear changes in estuarine conditions. Therefore, it is difficult to implement management practices surrounding these incidents, making it harder for governing bodies to restrict anthropogenic activity that negatively impacts estuaries.

New Zealand's coastal zones underpin many facets of its economy. Within its Exclusive Economic Zone (EEZ), which is the fourth largest in the world and 20 times larger than its land mass (New Zealand Ministry for Culture and Heritage Te Manatu Taonga, 2006), New Zealand waters house industry in renewable energy, tourism, minerals, oil and gas, aquaculture, and fisheries. To ensure that the multitude of practices do not interfere with each other or harm the environment, a holistic management approach is needed. This MSc research is sponsored by National Science Challenge: Sustainable Seas; a New Zealand wide endeavour to generate foundational research for the creation of a coastal Ecosystem Based Management (EBM) system. The National Science Challenge combines scientific research and Mātauranga Māori to produce adaptable resources for ecosystem management, while providing for Treaty of Waitangi partnerships. This project will contribute to determining the

factors causing estuarine ecosystem 'tipping points'. Specifically, it focuses on the role *M. liliana* have in regulating the exchange of nutrients between seabed sediment and the water column within estuarine environments.

1.2 Research Aims and Objectives

The aim of this research was to determine the factors which cause estuarine ecosystem tipping points, using a simple ecosystem model. Specifically, we have created an ecosystem interaction model (EIN), built upon a prototype developed by Dr Karin Bryan and Dr Giovanni Coco. Our version models biotic and abiotic interactions within an estuary to identify the impact sediment and nutrient loading has on the estuary's functionality. This data can be used to determine the health of the estuary and the organisms within it. Similar EINs have been created for New Zealand estuaries previously (Thrush et al., 2014, 2021); however, using different methodologies and creating statistical models, rather than dynamic. EINs allow researchers to model the flow of energy within a system, and identify how an ecosystem may react to change, in a relatively short amount of time and without having to conduct field experiments. In our case, our research focussed on the adjustments in *M. liliana* behaviour, and the changes that might occur as water column nutrients and suspended sediments vary, reflecting real world circumstances at Tuapiro Point (Tauranga Harbour, New Zealand). The goal was to be able to predict an estuarine tipping point. The creation of our model is important, as New Zealand estuaries are under immense stress from fine sediments and nutrients. Identifying tipping points before they occur within the Tauranga Harbour is crucial, as a regime shift within this ecosystem would cause widespread loss of biodiversity, function, and recreational potential.

Our model incorporates a positive feedback system, imitating the relationship between three components within New Zealand estuaries. These are 1) the changing biomass of MPB and *M. liliana*; 2) MPB and *M. liliana* detritus; and 3) nutrients within the top layer of benthic sediment and within the water column. *M. liliana* live within the top layer of benthic sediment, pumping nutrients to the sediment surface where they are consumed by MPB. These creatures live and die, contributing to their biomass and detrital 'pools' respectively. Sources and sinks generated in the exchange processes between these pools change their mass with time, which are coded within the model to create an interpretable output.

Key questions that were addressed, to determine estuarine 'tipping points' include: (i) How did changing nutrient and sediment loading in the model, change the balance between *M. liliana* and MPB biomass? (ii) Under what conditions did the (simplified) benthic food web access nutrients from the water column verses surviving only on regenerated (sediment sourced) nutrients? (iii) How does light availability (turbidity) effect the relationship between *M. liliana* and MPB, and their biomasses.

Three objectives were identified for this research:

Objective one: Create a dynamic model that can accurately synthesise basic ecological relationships in benthic communities within New Zealand estuaries.

Objective two: Subject the model to external forcing patterns that occur within New Zealand estuaries and evaluate the model's response.

Objective three: Identify issues within the model and outline resolutions.

1.3 Thesis Outline

This thesis is divided into chapters based upon the construction and evaluation of the model and its outputs.

Chapter 2: Literature Review

Chapter two consists of a literature review, encompassing biotic and abiotic relationships within estuarine benthic communities, and estuarine ecosystem tipping points.

Chapter 3: Methodology

Chapter three consists of the methodology used in the construction of the model. The chapter explains the choice of parameters and gives background on their sources. It also describes the equations used within the model and their interactions.

Chapter 4: Results

Chapter four evaluates the functionality and output of the model, based upon the key questions aforementioned (*see Section 1.2*).

Chapter 5: Discussion

Chapter five explores the relevance of the model's output to the literature. Recommendations are made regarding the model's efficacy in estuarine management.

Chapter 6: Conclusions and Recommendations

Chapter six is a summary of the key results and findings within our research. Opportunities for future research are identified.

Chapter 2

Literature Review

2.1 Estuaries

Estuaries are partially enclosed, coastal bodies of water subject to waves, tides, and the influx of saline and riverine inputs – more simply, they are where rivers meet the ocean (Pritchard, 1967). They constitute a small portion of the marine environment, being only 11% of the ocean and 4% of land (Barbier, 2017). Estuaries are one of the most productive biological regions globally, with a vast variety of fish species using these areas for spawning and development (McDowall, 1976). However, estuaries are distinguished by little permanent ecological structure (such as kelp or coral) and high degree of organism mobility, due to their harsh and altering abiotic conditions (Costanza et al., 1995). Their productivity is abused by humans, as 50% of the international fishing harvest takes place within nearshore oceanic areas and estuaries (Kennish, 2019). With over 2.4 billion people living within 100 km of the coast, estuaries are under immense pressure from decades of use as repositories for anthropogenic waste (SEDAC, 2011).

Contaminants enter estuaries through several key pathways; runoff from land, dumping and discharges from ships, atmospheric deposition, riverine input, and direct pipeline discharges from settlements (Bourdeau & Barth, 1986). Most of the pollution is derived from land-based sources (>40%) and atmospheric deposition (30%) (GESAMP, 1990). Pollutants harm estuaries long past their visual signature, accumulating in sediments where ongoing legacy effects cause detrimental consequences to life in the years following (Attrill & Thomes, 1995; Birch, 2000; Hewitt et al., 2009). Legacy effects can manifest as an increase in organic carbons, pathogens, or nutrient enrichment (Kennish, 2002). These disturbances interrupt key ecological functions, many of which are imperative for human health. An ecosystem function is an action that alters the movement of organic matter, nutrients, or energy through an environment, such as photosynthesis (Cardinale et al., 2012). Storm protection, nutrient regeneration, and food provisioning are amongst the most important services estuaries provide to humans (Waikato Regional Council, n.d.). Ecosystem services – ecological functions, processes, and characteristics that sustain human wellbeing (Costanza, 2020) – have been valued at more than US$33 Trillion per year (Costanza et al.,

1997). After accounting for inflation since the publishing of this figure, ecosystem services' value has risen to over US$52 Trillion annually. Estuarine ecosystem services are expected to decay as anthropogenic discharge of pollutants into these environments continues to rise (Kennish, 2002). An estuary's type can determine its predisposition to anthropogenic stressors such as sedimentation, with New Zealand alone having eight different classes of estuaries (NIWA, 2014). For example, large shallow drowned valley estuaries encourage a diverse benthic community, as their size permits greater wind fetch (Clark et al., 2021). The resulting wind-generated mixing and circulation improves recruitment (Commito et al., 1995), increases the food supply (Fréchette & Bourget 1985), and strengthens the estuary's resilience to storm events (Thrush et al., 2003). Other estuary types are not as fortunate, and their benthic environments are more vulnerable to anthropogenic stress.

Nutrient and sediment inputs are often associated with a gradual change in estuarine health; however, in general, current rates exceed an estuary's ability to offset negative change. In the USA, nutrient enrichment impacts between 30-60% of estuaries (Bricker et al., 2008), while sedimentation rates have increased by as much as 100-fold in some parts of the world (Thrush et al., 2004). Sediment and nutrients enter estuaries naturally, but are exacerbated by ongoing land use changes. Switching from native forest to agricultural land, or creating urbanised settlements near the sea, creates non-permeable surfaces for sediments to shift across without being trapped, all of which accumulate within estuaries (Vitousek, 1994; Matthaei et al., 2006; Green, 2013). As climate change threatens more storm events, sedimentation within estuaries will increase (Williams, 2012; Herring et al., 2015). Sedimentation is frequently coupled with greater nutrient availability, creates muddier substrate that buries organisms, alters community composition, and reduces ecosystem function (Lovelock et al., 2007; Pratt et al., 2013). On the local scale, environmental elements such as grain size and salinity are crucial in determining community structure, while temperature is also important across expansive geographic scales (Denis-Roy et al., 2020). In a model created by Clark et al (2021), community composition frequently altered above 20°C sea surface temperature (SST), suggesting that as species' temperature tolerances and distributional boundaries change with climate change, we may see a notable restructuring of communities (Johnson et al., 2011). It was further found that in New Zealand these natural environmental variables, plus wind-wave exposure, are more significant in predicting shifts in community composition than land-derived stressors (Clark et al., 2021). However, there is

uncertainty surrounding this claim in regions of excessive land-derived stress, as New Zealand estuaries are typically low in mud and nutrient content.

Figure 2.1. Weighted importance across all taxa (overall importance) of natural environmental variables and stressors from land in predicting benthic macroinvertebrate compositional turnover in New Zealand estuaries. R^2 evaluated by bootstrapped gradient forest models. The average contribution by each predictor across 100 bootstraps is demonstrated by the grey bars, with error bars denoting the standard deviation (Clark et al., 2021).

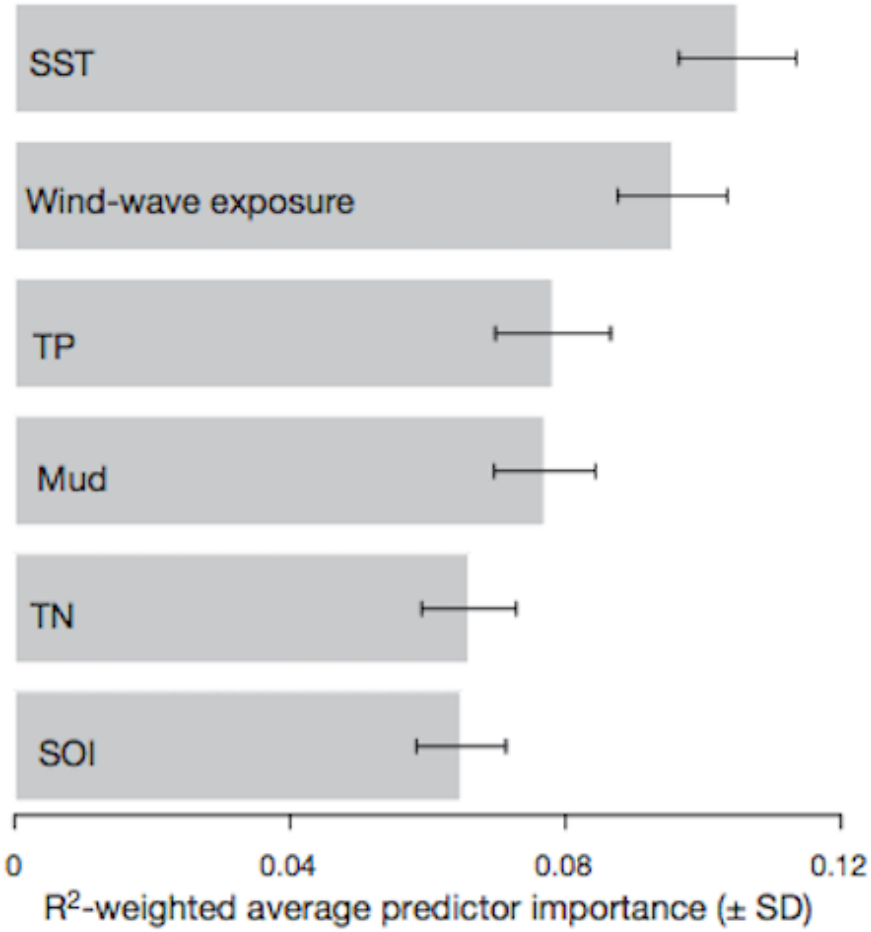

The model designed in this project will focus on an estuarine system's response to nutrients and sediments. Its output will help in the understanding of patterns and relationships within New Zealand estuaries, and further progress toward creating a tool useful for predicting estuarine ecosystem tipping points.

2.2 M. liliana

M. liliana is a keystone species within New Zealand estuarine ecosystems (Pratt et al., 2013). It is a tellinid bivalve that dwells within the top 10cm of sandy sediment, deposit feeding on microphytobenthos (MPB) at the sediment surface through an inhalant siphon (Pridmore et al., 1990). It is part of a wider benthic macrofauna community that are critical

for preserving the health of estuaries and have long been observed conducting key functions within intertidal sandflats (Pratt et al., 2013). Bivalves carry out imperative functions within coastal environments, such as providing a source of food (Thrush et al., 1994), nutrient cycling (Henriksen et al., 1983; Magni et al., 2000; Woodin et al., 2016), increasing primary production (Marinelli & Williams, 2003; Lohrer et al., 2004; Volkenborn et al., 2012; Huettel et al., 2014; Kristensen et al., 2014), regulating phytoplankton biomass (Cloern, 1982; Newell, 2004), and the oxygenation and flux of nutrients out of subsurface sediment (Woodin et al., 2016).

M. liliana are ecosystem engineers, as they regularly hydraulically alter the sediment boundary layer in benthic systems (Woodin et al., 2016). During feeding bouts, waste and water is excreted from the organism. This generates pore-water pressure gradients that flush nutrient rich pore-water through the sediment surface, oxygenating subsurface sediment and accelerating MPB production (Woodin et al., 2010; Woodin et al., 2012; Volkenborn et al., 2012). The process changes the structure of the benthic boundary layer, increasing ecosystem functioning (Lohrer et al., 2004). Therefore, *M. liliana* serve a pivotal role in the functioning of estuarine environments, a role demonstrated by the benthic interaction model produced by Thrush et al. (2014).

Figure 2.2. Illustration of a New Zealand estuarine benthic interaction web (Thrush et al., 2014). Reproduced by permission of John Wiley & Sons.

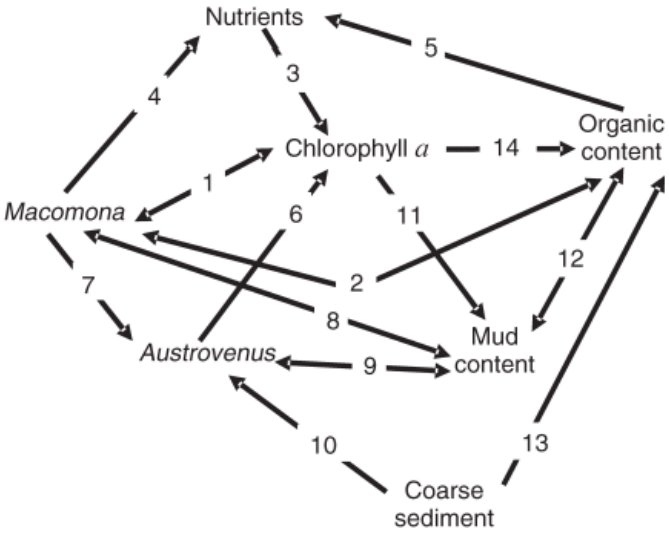

Species within benthic macroinvertebrate communities, such as *M. liliana*, are regularly used to evaluate anthropogenic impacts on estuaries. These species can demonstrate

the consequence of numerous stressors over time, display distinct stress-tolerances, and they are included in multiple trophic levels (Dauer 1993; Borja et al. 2000). In a study completed by Hope et al. (2020), lipid reserves in *M. liliana* tissue were reduced by a maximum of six orders of magnitude, following medium and high nitrogen addition to sample plots. Despite an increase in food availability following nutrient enrichment, *M. liliana* nutritional quality to higher trophic levels decreased, shown by the lower ratio of essential fatty acids in their tissue. Therefore, nutrient enrichment from anthropogenic activities can reduce carbon flow and ecosystem productivity. Alongside the reduced intake of food, there may be several factors for this phenomenon. The bivalve's lower nutritional quality may be explained by chemical stress from the accumulation of ammonium in sediment (Camargo & Alonso, 2006; Simpson et al., 2013) or lipid peroxidation and oxidative stress – as seen in other bivalve species (Coutteau et al., 1996; Alves de Almeida et al., 2007). Bivalves often increase their metabolic activity as a stress response to prolonged exposure to pollutants (Smolders et al., 2004; Alves de Almeida et al., 2007; Patil, 2011), meaning that their fatty acid and lipid reserves, and their biomass, would further decrease.

This project will model the interactions of *M. liliana* with the external forces most likely to be encountered in New Zealand estuaries, to investigate how the behaviour and density of this species affect the stability of the system. With this, we hope to prove that *M. liliana* are biotic stabilisers of estuarine ecosystems that maintain the health and functionality of New Zealand's coastal waters.

2.3 Microphytobenthos (MPB)

MPB, a descriptive term for microscopic autotrophs affiliated with benthic sediments, perform a variety of functions that are imperative for the health of estuarine ecosystems. Within New Zealand estuaries, MPB perform a larger role in the food web than pelagic phytoplankton and are the most significant primary producer when accounting for their productivity and biomass (Jones et al., 2016). As a result, MPB account for a large portion of total marine carbon fixation (Borum & Sand-Jensen, 1996). Alongside their role in climate control, MPB contribute to nutrient recycling, sediment stabilisation, and the improvement of water quality (Sundbäck et al., 2006; Joensuu et al., 2017; Hope et al., 2019). They are the only source of omega-3 and omega-6 essential fatty acids to higher trophic organisms; a pathway highly influenced by nutrient and light conditions (Hill et al., 2011). For many bivalve species, the consumption of Omega-3 fatty acids contained in MPB is essential for their reproductive success (Fearman et al., 2009). MPB also facilitate denitrification, by

supplying nitrogen cycling bacteria with a labile carbon source through their oxygenation of the sediment surface (Tobias et al., 2003; Cnudde et al., 2015)

Increasing nutrient concentrations may elevate the biomass and productivity of primary producers, which can cause an overflow of effects throughout the estuarine food web (Human et al., 2018). MPB are no exception, and a population explosion (bloom) of these organisms create eutrophic waters, often associated with fish kills, the modification of community composition, and the loss of submerged macrophytes (Human et al., 2016). The ensuing death of MPB creates further toxic water conditions, as dissolved oxygen concentrations plummet due to their decomposition (Nixon, 1995; Anderson et al., 2008).

Despite fine sediments stimulating MPB by increasing nutrient availability (Drylie et al., 2018), the concurrent light limitation decreases their photosynthetic potential (Kromkamp et al., 1995; Cahoon & Safi, 2002; Du et al., 2017). MPB have been known to adapt to light limitation physiologically and behaviourally (Cartaxana et al., 2016), through migration and photo acclimation (Consalvey et al., 2004; Migné et al., 2007; Jesus et al., 2009; Serôdio et al., 2012). Through this process, MPB quality, biosynthesis, and the ability to transfer essential fatty acids, may decrease. In lakes, nutrient availability and light intensity are crucial in governing algae quantity and quality (Sterner et al., 1997), something seldom considered within estuaries (Hope et al., 2020).

MPB are included in this model as their populations alone can induce mass change to an ecosystem's health, reducing its resilience and increasing the chance of a regime shift. Exploring the governing effects nutrient and light have on MPB is crucial for gaining an understanding of the importance of their ecosystem functions and their role as prey. The model simulates MPBs reaction to increasing external forcing variables. MPB's interaction with these parameters can be interpreted to identify the effect of nutrient loading and sedimentation on the stability of estuarine health.

2.4 Benthic Layer

The benthic layer is the area at the lowest depth of the water column. It is an ecological region including the bottom layer of water, the sediment surface, and the topmost layer of sediment effected by the water. The benthic region begins at the shoreline and progresses to the depths of the ocean. Estuarine benthic zones are highly influenced by the surrounding catchment and continental region bordering their entrance to the ocean. A large proportion of marine denitrification from land sourced nitrogen occurs within coastal

sediments (Galloway et al., 2008). This removal of bioavailable nitrogen is imperative in preventing excess nutrient enrichment and is considered a vital function of soft sediment habitats in coastal environments (Thrush et al., 2021). Intertidal sandflats within estuaries sustain productive ecosystems that are crucial for nutrient cycling and primary production (Volkenborn et al., 2012; Huettel et al., 2014; Kristensen et al., 2014). Biota such as MPB and *M. liliana* facilitate community growth within benthic environments. MPB are primary producers, while bioturbation from *M. liliana* in the benthic layer dissolves silicate rich pore waters and inorganic carbon, displaces ammonium, and oxygenates subsurface sediments (Woodin et al., 2016). The process of exchanging nutrients from sediments to the water column creates a positive feedback loop between biotic and abiotic factors within the ecosystem (Kéfi et al., 2016). Fine sediment from land run-off and riverine input clog pore spaces, creating muddy substrate unsuitable for inhabitancy by marine macrofauna (Pratt et al., 2013). In the Tauranga Harbour, intertidal sediment transport is largely shaped by wind waves, while tidal currents and swell waves govern transport at the harbour entrance (Davies-Colley & Healy, 1978). Here, tidal currents have altered the textural qualities of sediment, which mostly originates from marine sand on the Bay of Plenty continental shelf (Davies-Colley & Healy, 1978). However, compared to other estuaries along New Zealand's east coast, sedimentation rates within Tauranga harbour are low (Hancock et al., 2009). A shift from rural to urban environments is substantially reducing sediment inputs; however, urbanisation is creating a new issue. Concrete substrates provide an impermeable surface for sediment transport, creating a non-linear response to sedimentation (Green, 2013). This means that while less fine sediment is running off farmland, heavy rainfall events cause large quantities of sediment from the city to be deposited into the harbour. As climate change increases the risk of heavy storm events (Herring et al., 2015), sedimentation is likely to increase (Williams, 2012).

Sedimentation can reduce the functionality of the benthic layer significantly. The process is known to reduce the maximum density of *M. liliana*, the ammonium efflux from the sea floor to the water column from bioturbation activity, and the maximum rates of sediment oxygen consumption (Pratt et al., 2013). Therefore, a negative relationship exists between *M. liliana* and sediment silt content (thereafter, mud). As mud content increases, nutrient processing may be restricted, facilitating more eutrophic conditions (Douglas et al., 2018) and reducing benthic community composition. Turbidity levels increase also, which can reduce light penetration to the sea floor. High turbidity negatively influences

phytoplankton growth, reducing the available energy in an estuarine system (Thrush et al., 2004).

During the creation of an ecosystem interaction network (EIN), Thrush et al. (2021) discovered that during periods of elevated turbidity, sediments had a reduced ability to process nutrient additions. Therefore, the adverse impacts of nutrient additions to estuarine ecosystems may be intensified by the sediment's diminished denitrification capacity.

Figure 2.3. EIN situated within a (A) clear (>420 μmol·L^{-1}·m^{-2}·s^{-1} PAR) and (B) turbid (<350 μmol·L^{-1}·m^{-2}·s^{-1} PAR) sites. Pink boxes refer to the abundance of shellfish >20mm shell length; NH_4^+ flux between the sediment-water layer and denitrification (N_2) are indicated by the yellow boxes; benthic oxygen consumption outline within the blue box; purple boxes indicate mud, mud in the sediment, and the standing stock of microphytobenthos (Chl a); and teal boxes identify the experimental manipulation of nutrient addition and turbidity's effect on available photosynthetically active radiation (average daily max PAR). Arrow thickness demonstrates the relationship strength, with black arrows identifying negative relationships and red positive (Thrush et al., 2021).

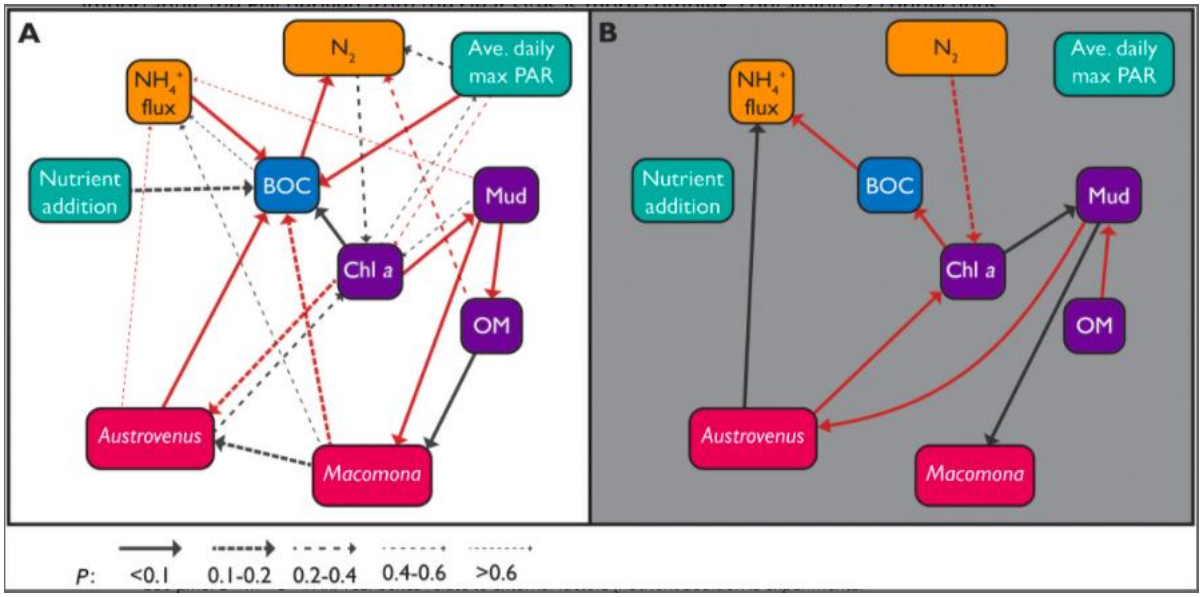

In turbid sites, benthic oxygen consumption was disconnected from the role of nutrient addition and light, demonstrating a reduced ability within the ecosystem to manage a nutrient increase. Within these sites, only MPB influenced oxygen consumption, as opposed to MPB and both *M. liliana* and *A. stutchburyi* directly impacting benthic oxygen consumption in clear sites (Thrush et al., 2021).

Figure 2.4. Denitrification enzyme activity in low mud (a) and high mud (b) sediments, shown by structural equations modelling ecosystem interactions. Path thickness is determined by the path coefficient (significant at p), with r^2 variables displayed for each response variable. Black paths identify negative relationships, with red positive (Douglas et al., 2019).

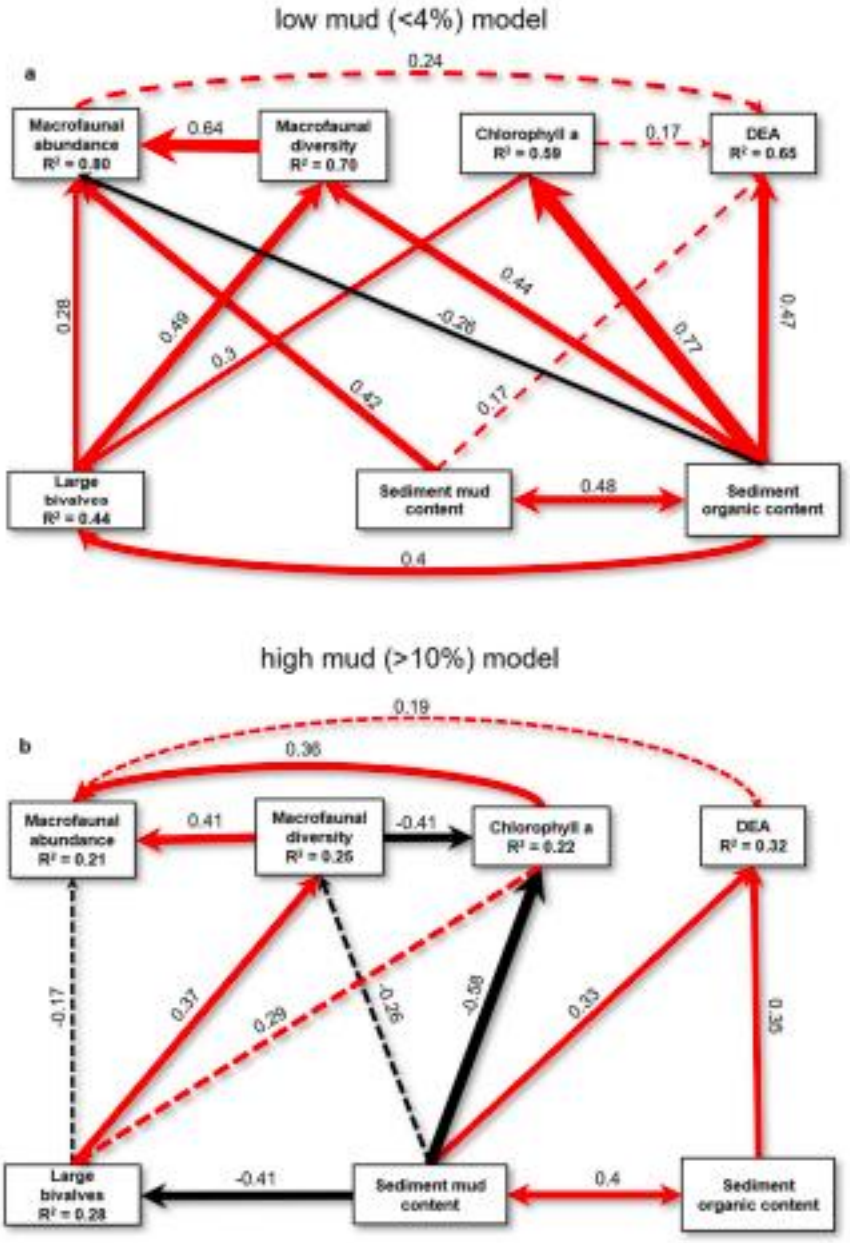

Research completed by Douglas et al. (2019) demonstrated how structural equation models (SEMS) can be used to assess changes in ecosystem dynamics within muddy and sandy environments. They found that the interaction networks within the sandy system are meaningfully different to those within the muddy model. Significant negative network interactions increase three-fold within the muddy system, and significant positive network interactions decrease in number. These changes indicate a breakdown in the functioning of an

ecosystem, and therefore a reduction of its resilience, following the transition from sandy sediments to muddy.

Nitrogen transformation rates, processed by microbial nitrogen cycling, are slower in muddier sediments compared to sandy (Huettel et al., 2014). Despite organic content generally being higher in muddier sediments, slower pore water advection limits the movement of solutes (Mermillod-Blondin & Rosenberg, 2006). This slow movement, paired alongside a decrease in macrofaunal trait-based indices (such as nutrient cycling) when mud content surpasses 10% (Rodil et al., 2013), creates a combination of factors ideal for generating hypoxic conditions. Once nutrient levels reach 1200mg kg^{-1}, community composition within New Zealand estuaries has regularly been found to change (Clark et al., 2021). Additionally, compositional shifts in community structure were found to be better explained by a sediment total nitrogen (TN) gradient, over mud content or total phosphorous (TP) (Clark et al., 2021). This may be the case as nitrogen is frequently the limiting nutrient within coastal ecosystems (Howarth & Marino, 2006). These results are consistent with eight Californian estuaries, with a TN threshold of 1000 mg kg^{-1}, that experienced a shallowing of apparent redox potential discontinuity (aRPD) to almost zero (Sutula et al., 2014). Unsurprisingly, the shrinking of the aRPD depth is regularly connected to hypoxic events (Clark et al., 2021). Therefore, functional traits within the ecosystem that increase sediment mixing within muddy sediments, such as bioturbation from macrofauna, may be crucial in facilitating the bioadvection of solutes and increasing denitrification enzyme activity (DEA) (Douglas et al., 2019). Model outputs within Douglas et al. (2019) indicate that increasing sediment mud content decreases the relationship strength between DEA and several ecosystem components that are important for the removal of nutrients from sediments: MPB biomass, macrofauna diversity, and macrofauna abundance. Many of New Zealand's estuaries are experiencing increases in mud content linked to anthropogenic activity on land (Swales et al., 2015; Urlich & Handley, 2020), which has further been recognised as an indicator of stress within estuarine ecosystems (Thrush et al., 2003, 2005; Ellis et al., 2017, Douglas et al., 2019). Even at compositions as low as 10% mud content within sediments, a reduction in sensitive taxa populations and functional redundancy can be seen within the ecosystem (Figure 2.5) (Thrush et al., 2003; Anderson, 2008; Robertson et al., 2015; Ellis et al., 2017). Specifically, mud accumulation has shown to cause a swift decrease in the abundance of *M. liliana* (Clark et al., 2021).

Figure 2.5. Box plots depicting the ecosystem constituents (a) mud content, (b) organic content, (c) Chl a, (d) total taxa, (e) abundance of macrofauna, and (f) large bivalves present in the sandy (10% mud) dataset (n=57). 25th and 75th percentiles and shown, 10th10th and 90th percentiles identified by whiskers, and black dots showing the 5th and 95th percentiles. The mean is shown by a dashed line, with the solid line indicating the median (Douglas et al., 2019).

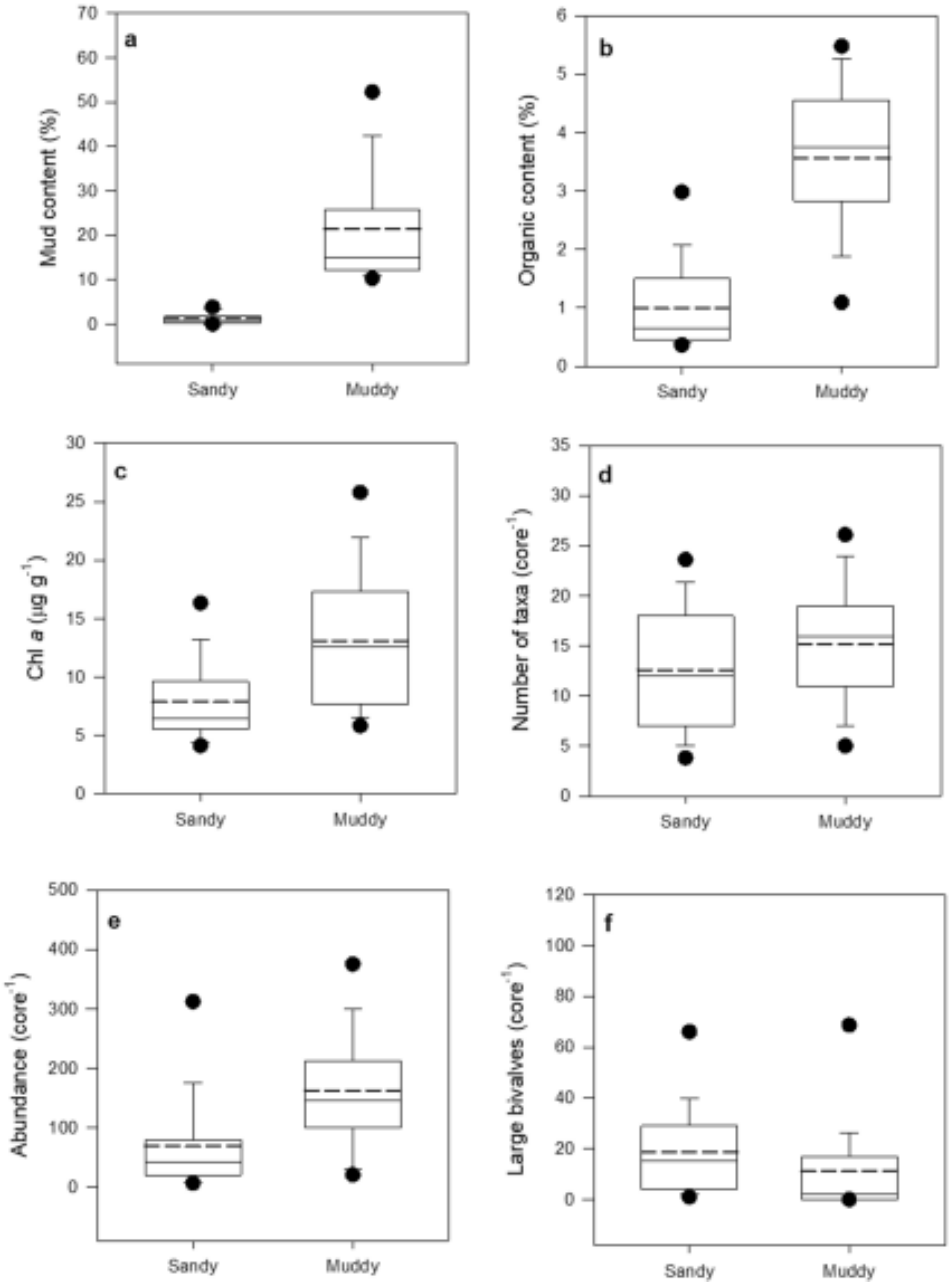

Our model will simulate the effect of sedimentation (increasing mud content) on the behaviour and density of *M. liliana*. The consequent effects on MPB biomass, estuarine nutrient content, and *M. liliana* and MPB detrital values will also be demonstrated. This data can be interpreted to identify the effect of sedimentation on the benthic community and the estuary's health.

2.5 Interactions Within the Benthic Layer

The key focus of this project is to model the interaction of *M. liliana* and MPB with components of the benthic layer when stressed by external forcing. To do this, we must first understand the interaction network itself, so that responses of the two species and the feedbacks they produce can be modelled accurately.

Extrapolating upon Figure 2.2, the interaction network of benthic ecosystems in New Zealand estuaries can be better understood. (1) *M. liliana* consume MPB (represented as chlorophyll *a* in Figure 2.2), decreasing their biomass (Lelieveld et al., 2004). A positive relationship between *M. liliana* and MPB biomasses exist, as the nutrients pumped from sediments during feeding bouts increases MPB populations more than *M. liliana* grazing decreases them (Thrush et al., 2006). Therefore, a decline in *M. liliana* ecosystem functions would decrease MPB production, further altering food web dynamics and existing functional roles within the benthic food web (Mangan et al., 2020). (2) Skilleter and Peterson (1994) confirm, in a study of the functionally similar species *Macoma balthica*, that the presence of organic content within sediment increased food resources available to bivalves. (3) Pore-water nutrient concentrations are increased indirectly by *M. liliana* feeding activity (pathways 2 and 5) and directly through pathways 4, maintaining a highly productive MPB biomass (Cahoon et al., 1999). (8) Bioturbation from *M. liliana* in high densities separates fine sediment, enhancing erosion and reducing mud content (Thrush et al., 1997). (11) The binding of fine sediment by a coagulant released by MPB is moderated by predation by *M. liliana*, reducing sediment mud content (Lelieveld et al., 2003). (14) *M. liliana* recycle detritus deposited into sediment from dead MPB, which returns to the water column's nutrient pool (Ehrenhauss et al., 2004; Volkenborn et al., 2012; Woodin et al., 2012).

2.6 Regime Shifts

With time, estuarine environments naturally experience compositional shifts in chemicals, biotic factors, and sediment composition, as well as changes in climate conditions. An estuary may undergo a 'regime shift' once the threshold of a governing variable, or the 'tipping point', is exceeded. Walker & Meyers (2004) define a regime shift as the conversion from one stable ecological state to another, altering both the chemical and species composition. Tipping points are explained in more detail in Section 2.8. Regime shifts occur in response to stressors and are generally large and sudden (Selkoe et al., 2015). While a slow shift in physical conditions is manageable, anthropogenic activity is exacerbating negative

impacts in coastal regions (Scheffer et al., 2001). Even so, gradual changes to external forcing factors can reduce an ecosystem's resilience to change, meaning only a small perturbation is required to surpass its tipping point (Kéfi et al., 2016). External forces are considered any factor outside the production of an ecosystem that alters its functionality, such as heavy metal pollutants. To put this into context, an estuary's resilience to change will gradually decrease with consistent pollution input from an external factor such as road run off.

Figure 2.6. Alternative forms of regime shifts, ranging from smooth/linear responses to discontinuous change (Selkoe et al., 2015).

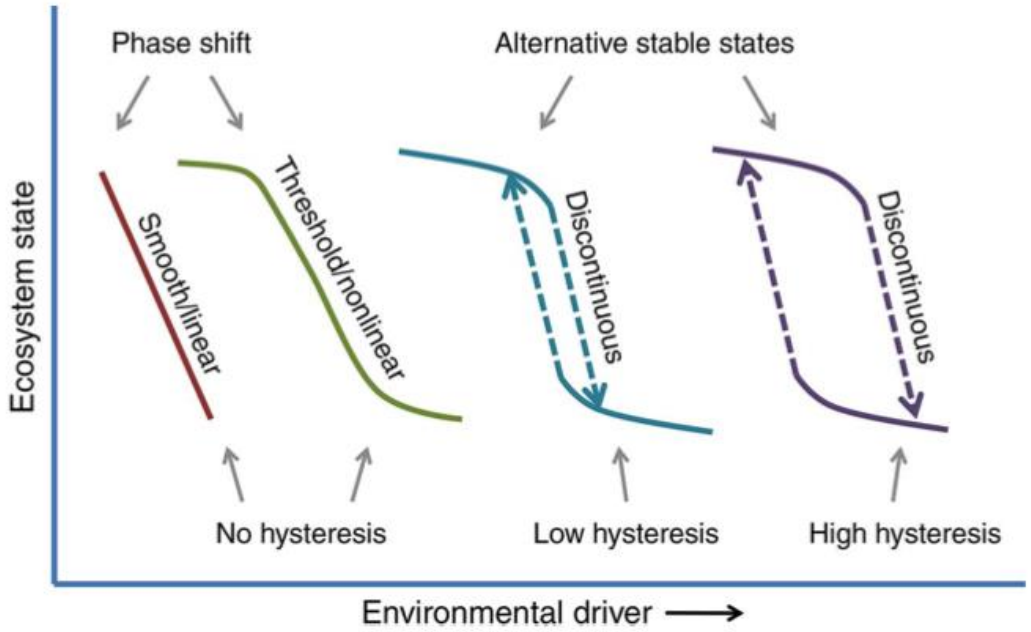

Regime shifts can follow a linear progression, where a gradual and predictable change in conditions is followed; however, this is often not the case. Such instances of non-linear change can be seen throughout nature, examples being the Allee effect or dose-response curves in physiology (Selkoe et al., 2015). These examples both demonstrate a sudden change of condition in response to external stressors, suggesting that natural systems may operate in a stable state until a threshold is surpassed. Estuaries are no exception; a common, and likely familiar, occurrence of marine tipping points being exceeded is the abrupt blooming of algae. The nonlinearity of an estuary's response to stressors may be increased by its connection with the ocean (Selkoe et al., 2015). As such, this connection can allow for the restoration of an estuary's ecosystem or the spread of its regime shift (Olds et al., 2012).

2.7 Alternate stable states

An estuary may function in one of two alternate stable states, in which the chemical and biotic composition of one is completely different from the other. Restoration of ecosystems that function in this manor is difficult and costly, as its pathway of recovery is different to its deterioration (Suding & Hobbs, 2009). It is common for the restoration of these systems to be plagued with time lags following the reduction, or eradication, of stressors (Montefalcone et al., 2011). Random events coinciding with restoration in estuaries, such as the establishment of new industry, can determine the ensuing restoration pathway – a sequence known as hysteresis (Selkoe et al., 2015).

Figure 2.7. Illustration depicting ecosystem response over five distinct ecosystems. The grey components represent the external forcing needed for the five ecosystems to switch ecological state. The centre component represents an ecosystem with a strong positive feedback, while the components at either end depict ecosystems residing deep within their ecological state. Unstable ecosystems are depicted with smaller hills, having little resilience and need only small/moderate perturbations to shift state, while stable ecosystems have large valleys and require larger perturbations to undergo a regime shift. The yellow segment beneath illustrates an equilibrium curve, depicting a regime shift. The grey components can be matched to their respective positions along the curve, demonstrating where they sit regarding changing ecological state. F1 and F2 identify where on the curve an ecosystem will change state (Scheffer et al., 2001). Reproduced with permission of Springer Nature.

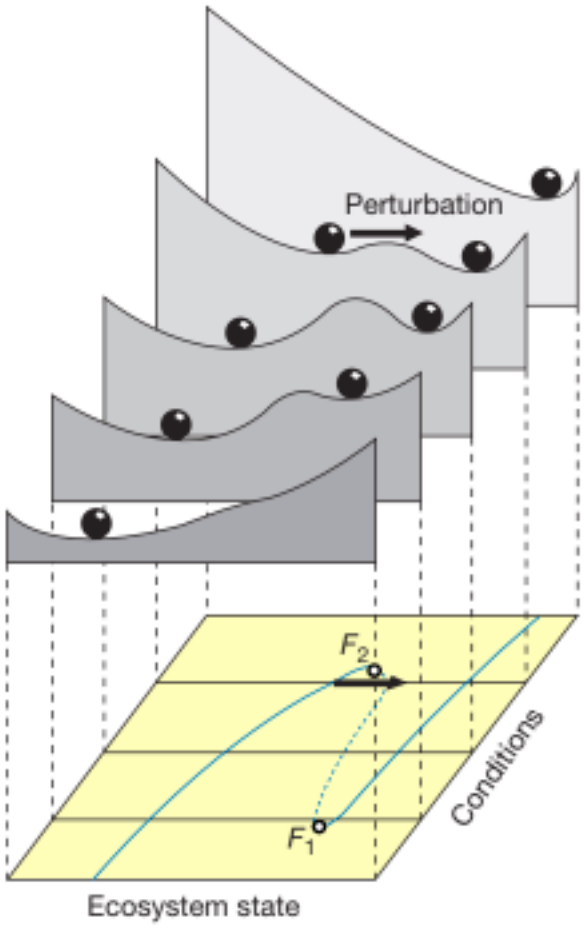

An ecosystem that can alternate between stable states often contains a positive feedback system within it (May, 1977). These positive feedback systems include interspecific links between abiotic conditions and species within a community. Positive interactions occur when the biotic or abiotic environment is enriched for one species by another (Kéfi et al., 2016). The positive feedback is created when interactions benefit the same species, or a group of species, involved in the interaction (Wilson & Agnew, 1992). Interactions can be indirect or direct, with examples for *M. liliana* being the facilitation of phytoplankton biomass (Cloern, 1982; Newell, 2004) and the modification of sediment composition (Woodin et al., 2016). Research shows that ecosystem states may be stabilised by biotic interactions, suggesting that the sensitivity of keystone species to environmental change is critical in maintaining community composition (Hall et al., 1992; Hare & Mantua, 2000; Marani et al., 2010). Therefore, positive interactions between *M. liliana* and its community act as biotic stabilisers, preventing the occurrence of regime shifts induced by external forces (Hare & Mantua, 2000; Fleeger et al., 2003).

Benthic environments experience cyclic patterns, normally in the realm of five to seven years, which may be effected by oceanographic rhythms (Gray & Christie, 1983). These ecosystems may respond to internal interactions and external forcing in different ways (Kéfi et al., 2016). Responses may be progressive (Figure 2.8 (a) & (b)), or sudden following the exceedance of a limit during a static period (Figure 2.8 (c)). Regime shifts occur in rare circumstances when an ecosystem has multiple stable states it can function within (Figure 2.8 (d))

Figure 2.8. Ecosystem responses to external forcing. (a) Represents external forces changing with time. (b) Depicts an ecosystem undergoing gradual change in response to external forcing and has no positive feedback system present. (c) Demonstrates a rapid response to external forcing, occurring when there is a weak positive feedback system present. (d) Portrays an ecosystem with a strong positive feedback system. System (d) resists change until a tipping point is reached, causing an abrupt change from one state to another once surpassed. Such response is classified as hysteresis, which requires external conditions to decrease to a point that is smaller than where the shift occurred. (b-d) therefore demonstrate that the response of an ecosystem to external forcing is dependent on the strength of the positive feedback system between biotic and abiotic factors (Kéfi et al., 2016).

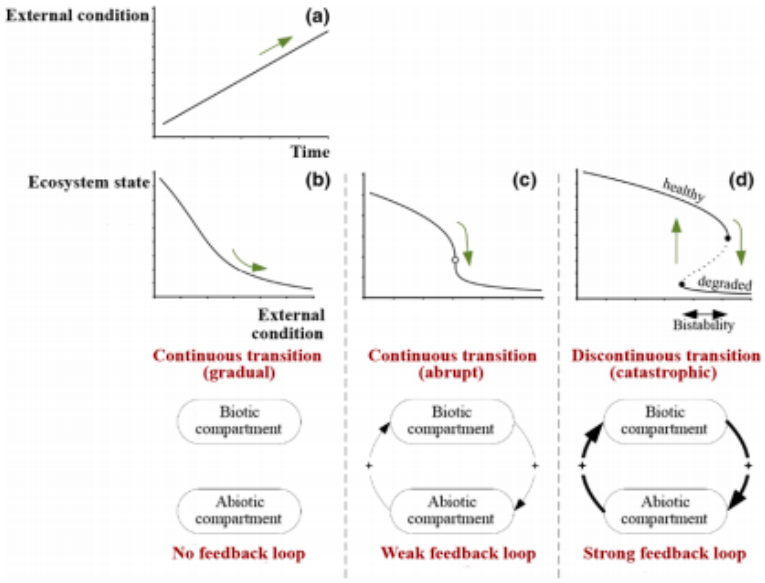

Alternative stable states within estuarine environments are regularly controlled by two factors: sediments and nutrients. Estuaries often have multiple stable states functioning within them: lowly-elevated intertidal sandflats and highly elevated vegetated marshes (Wang & Temmerman, 2013). Sedimentation increases the elevation of the intertidal zone, increasing the growth of mangroves and ultimately causing a regime shift from sandflat to mudflat (Li et al., 2017; Suyadi et al., 2019). Nutrient loading can shift an estuary from a healthy state filled with macrophytes, to a eutrophic state overrun with macroalgae and phytoplankton (Dahlgren & Kautsky, 2004; Lemley et al., 2019; Adams et al., 2020). In this thesis, the process of regime shifts, and biotic stabilisations will be modelled, with a focus on the reaction of *M. liliana* and MPB to nutrient and sediment loading. The literature demonstrates that a density decrease in *M. liliana* leads to a change in sediment composition and an increase in phytoplankton density. By coding this interaction, the model will be able to identify when a regime shift is likely to occur following increasing nutrient and sediment levels.

2.8 Tipping points

Tipping points are a focal point in modern ecological study. They are hard to predict, and just as difficult to manage. Confidence in their predictions can be increased through multivariate analyses of data taken over 10-32 years, and the use of supporting information (Peters, 1991; Anderson & Thompson, 2004; van Nes et al., 2007; Warwick et al., 2002; Weijerman et al., 2005). While stressors and disturbances are often viewed in a negative light, some may be of benefit to benthic marine habitats. Unlike anthropogenic disturbance, small scale natural disturbances create heterogeneity, which is imperative for the functioning of these ecosystems (Thrush & Dayton, 2002). Until a tipping point is reached, few impacts may be noticed; however, once surpassed, the consequences are widespread (Selkoe et al., 2015).

There are many examples of tipping points being exceeded within marine environments, notably in the North Sea. To name several, the devastation of the horse mackerel population in the 1980s, paired alongside gradual physicochemical changes in oxygen and nutrient concentrations and SST rise, led to a distinct change in the benthic community (Montefalcone et al., 2011). The once dominant Brittle star's (*Amphiura filifomis)* population was reduced to <10% of its original size, becoming replaced by the burrowing mud-shrimp *Callianassa subterranea*. In a local example, macroalgae populations replaced seagrass meadows following a shift in estuarine ecological state. Seagrass is invaluable within coastal areas, as it is a primary producer, nursery, sediment trap, and wave energy attenuator (Nordlund et al., 2017). By 2010, up to 20% of seagrass meadows had been lost from coastal areas (Boudouresque et al., 2009). Within the Tauranga harbour, this number is closer to 50% (Ha et al., 2021). In Tunisia, waterfowl have been displaced by the replacement of seagrass by *Ruppia sp.*, and in the French Atlantic coast seagrass has been superseded by the brown alga *Sargassum muticum* (Boudouresque at al., 2009; Montefalcone et al., 2011). Physiochemical changes within intertidal zones, such as pollution and climate, may also lead to the eradication of seagrass, being replaced only with mud (Li et al., 2017; Suyadi et al., 2019). Finally, overfishing within the Caribbean enabled the spiny sea urchin population to flourish as the lack of herbivory fish saw a bloom in algal growth and spread of disease within the coral. A once resilient coral ecosystem became algal dominated, changing the interactions and feedbacks between species (Selkoe et al., 2015).

In a New Zealand study conducted by Thrush et al. (2017) it was found that the regions within an estuarine sandflat did not functionally respond the same to increased

nutrient loading, as the sandflat was not uniform. Therefore, threshold responses across expanses of a sandflat may be surpassed following separate levels of environmental stress. This creates a problem for generating detection thresholds and predicting tipping points within an estuarine ecosystem, as the process of mapping ecosystem function across entire sandflats is a time consuming and expensive process. It may result in information not representative of the ecosystem being used for prediction and management strategies, which can lead to unsuccessful outcomes

Figure 2.9. Monitoring design recommendations for detecting marine system tipping points. Fewer years and data points are needed to detect change when rapid change in the response variables correspond with rapid change in a driver (Hewitt & Thrush, 2019). Reproduced with permission of Elsevier.

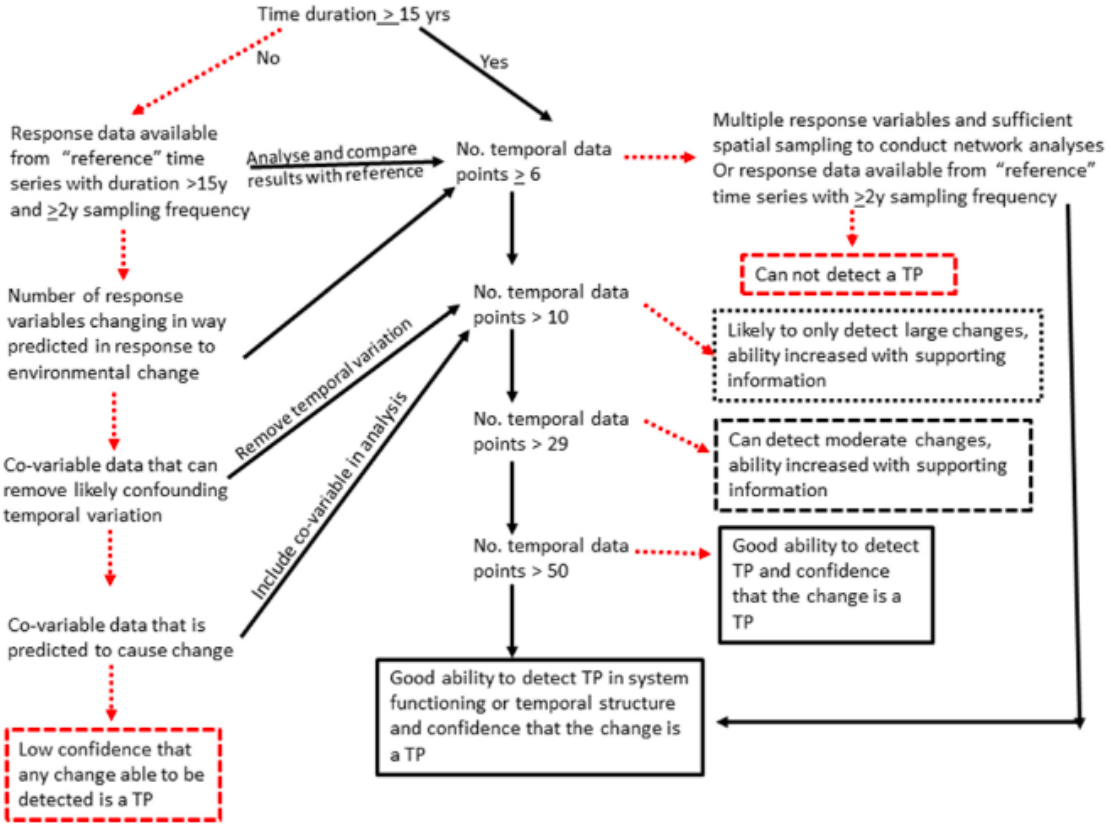

Figure 2.10. Monitoring design recommendations for detecting early warning signals in marine systems (Hewitt & Thrush, 2019). Reproduced with permission of Elsevier.

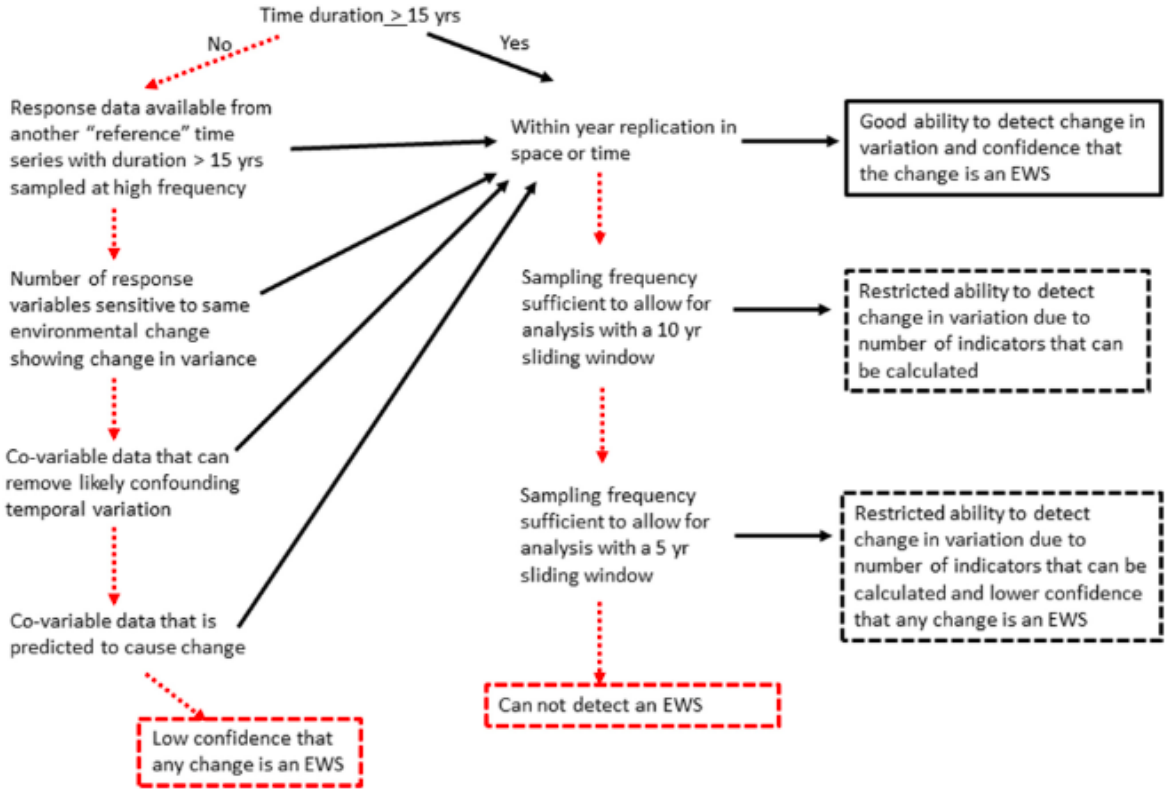

In an investigation of the literature, Hewitt & Thrush (2019) discovered several key components that are needed to create successful marine monitoring programmes for tipping points in New Zealand. Most importantly, an understanding of what is 'usual' within an ecosystem is necessary. Data becomes more reliable when supporting information is used, analysis is flexible, monitoring is consistent and conducted over a long-term period, and within-year sampling is included in the programme. This last factor is particularly important if the programme intends to identify early warning signals for tipping points, rather than simply detect that they have occurred. Furthermore, they identified that many New Zealand monitoring programmes would be unable to detect tipping points (Figure 2.9 & 2.10), due to their limited sampling frequency and duration. Finally, if New Zealand's monitoring programmes improve, there may still be insufficient time to carry out management actions. As early warning signals often present once a tipping point has begun, this leaves very little time for management strategies to be implemented (Perretti & Munch, 2012; Spanbauer et al., 2014).

To preserve our coastal marine ecosystems, it is not enough to protect species on their own, but to maintain the interactions and functions within them (Bradbury & Seymour, 2009). This can only be achieved if early warning indicators of tipping points can be identified and managed. Large collections of spatial data, identifying relationships between ecosystem and anthropogenic stressors can also be useful for determining indicators (Selkoe et al., 2015). This thesis combines both approaches; large amounts of spatial data were used to model the effect of anthropogenic stressors on an estuarine environment. Ultimately, we are testing the resilience of estuaries to anthropogenic stress. Our approach should enable the identification of early warning indicators of a tipping point within the time series data. As parameters within the model are interchangeable, it could be used globally, allowing for regionally specific indicators to be identified.

Chapter 3

Methods

3.1 Model Design

This study was designed to emulate conditions in typical *M. liliana* dominated sandy estuaries in New Zealand. Specifically, Tuapiro Point in Tauranga Harbour was chosen as a representative site, as many modelling studies have been completed here over the last 40 years. A particular focus has been taken on creating water quality, sediment, and hydrodynamic models to manage flooding and sediment within the harbour (Bryan et al., 2022). Therefore, Tauranga Harbour studies and values were used where available. When not available, parameters were sourced from relevant studies completed across an international scale.

Our work models a positive feedback system, largely focusing on the relationship between three distinct facets of an estuarine environment: the biomass of *M. liliana* and MPB; *M. liliana* and MPB detritus; and nutrients within the top layer and on the surface of the sediments. The MPB access the nutrients at the surface of sediments, and *M. liliana* live in the top layer. Their existence effects top layer nutrients through their influence on pore-water advection currents. The temporal change in mass in each of these 'pools' is modelled by tracking the sources and sinks caused by exchange processes between pools. The governing equations and representation of exchange processes is detailed in this chapter, along with justification for formulae and constants used within them.

Table 3.1. Model Parameters

Abbreviation	Denotes	Units
Model parameters		
Mac	*Macomona liliana*	Unitless
MPB	Microphytobenthos	Unitless
B	Biomass	g C m^{-2}
N	Nutrients, meant to represent total dissolved inorganic nitrogen in mmol	mmol ml m^{-2}
D	Detritus	g C m^{-2}
t	Time	Time steps♣
d_w	Depth of the water	m
d	Dwelling depth of species	m
G	Growth	g C m^{-2} day^{-1}
M	Mortality rate	Proportion day^{-1}
I	Light intensity at sea bed	µE m^{-2} s^{-1}
GR	Growth rate	Proportion day^{-1}
Ki	Light uptake rate	µE m^{-2} s^{-1}
N_W	Nutrients in the water column	mmol N m^{-2}
K_N	Nutrient uptake rate	mmol N m^{-2}
$G_{macgraz}$	Grazing rate of MPB by *M. liliana*	Proportion day^{-1}
I_0	Sea surface light intensity	µE m^{-2} s^{-1}
K_d	Light attenuation	m
K	Carrying capacity	g C m^{-2}
L	M. liliana growth rate	mm day^{-1}
WW	The conversion of *M. liliana* from their wet weight to their ash-free dry weight†	g C
C_2	Volume of two macrofaunal cores*	m^2
M_c	Mud content within sediment	%
T_{feed}	Feeding rate of *M. liliana*	s^{-1}
C	Biomass decay rate	g C m^{-2} day^{-1}
Kz	Mixing coefficient	m^{-2} s^{-1}
C2N	The weight of nitrogen produced per gram of carbon during breakdown in the detrital pool (g N m2) - the Redfield ratio - multiplied by N_{conv}	mmol N m^{-2} / g N m^{-2}
DR	Denitrification rate	N_2 m^{-2} day^{-1}
A	Areal coverage of a species	% m^2

L_{mac}	Length of an individual *M. liliana*	m
K_x, K_y, *and* K_z	Sediment permeability in the x-, y-. and z-direction	Unitless
P	Wave induced pore pressure	Pa
Yw	Unit weight of pore-water	N m^3
n'	Soil porosity	Unitless
β	Compressibility of pore fluid	Unitless
ε	Volume strain	m^3
q	Flux of fluid through porous medium	m s^{-1}
CF	Coefficient of mixing between the surface and top layer due to flushing	m^2 s^{-1}
K_H	Hydraulic conductivity	m s^{-1}
P_W	Wave pressure at the seabed	Pa
N_{conv}	Conversion of g N to mmol of N	mmol N / g N
IN	External nutrients	mmol N m^{-2}
P_{mac}	Pumping and porewater rate	m^3 s^{-1}

♣ One time step is equivalent to one day.

† WW is needed to convert numbers of individuals to g C

*C_2 is needed because literature values are often reported as the number of individuals counted in two cores.

3.2 Model Domain Characteristics

The model domain consists of one spatial dimension (vertical) and a time dimension, measured in metres and days respectively. The vertical dimension is divided into the water and sediment layers, where the water layer has one grid cell and the sediment has two grid cells (the surface layer where the MPB live and the top layer where the *M. liliana* live). The water layer is d_w and is variable; however *M. liliana* are continually submerged underwater. In our model, *dw* operates under a long period variation, which could represent seasonal or interannual changes, the tide, or even sea level rise. We have allowed for changing conditions associated with a predicted rise in sea level of 1.4 m by 2100 (Turner et al., 2009). Future versions could easily incorporate periods of exposure.

The d_{mac} parameter defines the depth beneath the sediment surface that the bivalves dwell. d_{mac} is used in multiple calculations: *M. liliana* carrying capacity, the vertical pressure gradient caused by *M. liliana* feeding behaviour, and the amount of nutrients produced from the *M. liliana* detrital pool. The flux between the detrital and the nutrient pool requires a

conversion from concentration (the nutrient units) to total mass in the upper layer where the *M. liliana* live (the carbon units). The d_{mac} parameter is derived from Thrush et al. (2021). In their study, increasing sediment nitrogen concentrations were applied to multiple *M. liliana* populations at various life stages. A census was conducted across the experimental plots to identify the relationship between sediment ammonia levels and *M. liliana* carrying capacity. Based on their observations, a population of adult *M. liliana* dwelling 5–7 cm beneath the sediment surface was chosen for our model. An average depth of 6 cm was chosen for *M. liliana*'s dwelling depth.

The d_{MPB} parameter defines the dwelling depth of *MPB* within the benthic sediment layer. The benthic layer is assumed to be a well-mixed, very thin layer found between the pelagic habitat and the sediment surface (Jäger & Diehl, 2014). d_{MPB} is used for calculating the addition of nutrients into the MPB nutrient pool. It also acts as a depth measurement when calculating the movement of water through sediments, due to wave pumping or bed pressurisation from *M. liliana* feeding. The d_{MPB} was derived from Sinha (2017). Their study designed a numerical model to examine the reaction of benthic and pelagic primary producers within the water column of a riverine ecosystem to changes in the flow and nutrient levels. The dwelling depth of MPB was measured as 0.01m beneath the sediment surface, which we have incorporated in our model.

3.3 Biomass dynamics

The change in MPB biomass (B_{MPB}) can be calculated using the balance between sources (growth) and sinks (mortality and grazing):

Growth *Mortality* *Grazing*

$$\frac{\partial B_{MPB}}{\partial t} = G_{MPB}B_{MPB}\left(1-\frac{B_{MPB}}{K_{MPB}}\right) - M_{MPB}\left(B_{MPB}-B_{MPB}^{min}\right) - G_{mac}B_{mac}\left(1-\frac{B_{mac}}{K_{mac}}\right), \quad (1)$$

where G_{MPB} is growth rate, M_{MPB} is mortality (set as a portion lost per day); the grazing term depends on the feeding activity of *M. liliana* and is defined below. B_{MPB}^{min} is a minimum value of biomass, which is presented in more detail later. This term could represent biomass advected into the region from the surrounding estuary. The growth rate depends on light limitation I_{lim}, nutrient limitation N_{lim}, and the maximum possible growth rate GR_{MPB}. The growth rate equation is:

$$G_{MPB} = GR_{MPB} I_{lim} N_{lim}, \quad (2)$$

Where:

$$I_{lim} = 1 - e^{I(d_w)/K_i}, \quad (3)$$

K_i is the light uptake rate, and I is the light intensity at the seabed (at depth d_w). The degree to which growth is limited by nutrients depends on the nutrient availability in the MPB layer N_{MPB}. We assume that since the MPB are in contact with pore water and the water column they can use either source, and are therefore limited only by the source with the highest concentration. Therefore, if the nutrient concentration in the surface layer of sediments is lower than that of the water column N_w, then the limitation is modelled as:

$$N_{lim} = \frac{N_w}{K_N + N_w}, \quad (4)$$

and if $N_{MPB} > N_w$ then:

$$N_{lim} = \frac{N_{MPB}}{K_N + N_{MPB}}, \quad (5)$$

where K_N is the nutrient uptake rate. This functionality allows the MPB to switch between their dependence from benthic to pelagic supply under high nutrient loading scenarios. The light availability at the seabed is calculated using the Beer-Lambert law (presented in a section below).

GR_{MPB} defines the maximum growth rate of MPB. GR_{MPB} is coded as the maximum amount the standing biomass of MPB can change at the current time step. The term was derived from Naithani et al. (2016), who developed an ecosystem model for the Scheldt estuary and tidal river network (in the Netherlands) to simulate seasonal and longitudinal variations in plankton. The growth rate within Naithani et al. (2016) is a maximum growth rate constant at 0°C for marine chlorophytes - 0.3 day^{-1}. Temperature, nutrients, and the availability of light govern growth in their model, with all biological rates doubling as temperature increases by 10°C (Eppley, 1972; Kremer & Nixon, 1978).

Summer water temperatures in the Tauranga harbour vary substantially, shifting by as much as 4°C with changing wind and river flood conditions (Tay et al., 2013). During calm weather, water temperatures are usually >22°C, but can drop to as low as 18°C, following heavy rain and wind. Therefore, we increased the growth rate used in the Naithani model to reflect our higher temperature setting, and the growth rate of MPB was set to 0.9 day^{-1}. This

is broadly consistent with the maximum growth rate for phytoplankton in 20°C of between 0.5–5 day^{-1} reported in Parsons et al. (1984). Further validation comes from Mariotti & Fagherazzi's (2012) benthic biofilm model, which coded a maximum growth rate ranging between 0.0078–1.11 day^{-1}.

M_{MPB} defines the mortality rate of *MPB*. M_{MPB} is coded as the mortality of *MPB* as a proportion of standing biomass per timestep. The M_{MPB} parameter was obtained through extensive model testing following the completion of our parameter list. Arbitrary values for M_{MPB} were set in a series of model test runs. These tests were run in parallel with the M_{mac} parameter tests, to identify whether a change in MPB biomass (*M. liliana's* food source), resulting from a change in their mortality rate, would impact the biomass of *M. liliana*. The M_{MPB} value was chosen based on which combination of M_{MPB} and M_{mac} values produced B_{MPB} values closest to field observations. As no data on the mortality rate of *MPB* could be found in the literature, this process ensures that the value set is as representative as possible to what is seen in an average estuary in New Zealand. M_{MPB} is set to 0.009.

B_{MPB}^{min} defines the minimum possible biomass of MPB in grams of carbon per m^2. Like the B_{mac}^{min} value, discussed in Section 3.5, B_{MPB}^{min} accounts for recruitment of individuals should the existing standing stock be entirely consumed or buried by sediment. Findings to support this parameter come from Larson & Sundbäck (2012), who conducted an experiment in which MPB biomass dropped to 25% of that found in controls following seven days of induced deposition events (1.5mm fine grained sediment daily, 10.5mm total). MPB populations began to increase linearly in a trend that would cause the biomass recover after 50 days. The initial increase was likely due to the upward migration of diatoms through sediment. The parameter B_{MPB}^{min} has been set at 0.001 g C m^{-2}.

$G_{macgraz}$ is coded as a percentage decrease of MPB biomass consumed by *M. liliana* per time step. This parameter allows the biomass of *M. liliana* to increase, due to a transfer of carbon from the MPB population. The grazing rate was derived from Pratt et al. (2015), whose study used feeding traces as a proxy of recent *M. liliana* deposit feeding activity to determine the relationship between MPB concentration in sediment and *M. liliana* density. During deposit feeding, *M. liliana* destabilise sediments at the surface using their inhalant siphon, consuming MPB and leaving behind diverging, radial traces (Lelieveld et al., 2004). Since traces are washed away with the changing ebb and flood tides, they can be used as indicators for recent feeding activity over a tidal cycle (Pratt et al., 2015). In Pratt et al. (2015) feeding traces were measured in 55 35 × 35 cm gridded quadrat plots within the

Manukau Harbour, New Zealand. *M. liliana* feeding trace area (FTa) averaged 12.5% of each plot, with a range of 1.58 – 28.5%. MPB concentrations (chl-a, μg cm^{-2}) were calculated using sixteen 1cm deep subsamples extracted using syringes. The depth was chosen, because in sandy sediments the most active MPB resides in the top centimetre (Mitbavkar & Anil, 2004; Du et al., 2010). Subsample cores from plots where sediments had not recently been grazed were compared to plots where feeding traces were present, to identify a change in MPB biomass. When FTa increased from 2 to 28%, MPB biomass declined by 28%, demonstrating a significant relationship between FTa and MPB (std. coefficient = -0.24, p = 0.01). For our model, we assume that MPB cover 100% of sandy sediments (there is no patchiness), and that deposit feeding is 100% effective, meaning 1% FTa = 1% MPB consumed. The grazing parameter was set to the mean FTa coverage from Pratt et al., (2015) – 0.125 proportion of MPB biomass day^{-1}. In our model area unit of 1m by 1m, the maximum that the *M. liliana* could consume would be 12.5% of the biomass in one day, and this is modified downward by the biomass availability and the carrying capacity of *M. liliana.* The carrying capacity (discussed later) simulates the competition for resources that occurs at higher densities, which ultimately limits growth.

3.4 Light Intensity

Beer's law describes the attenuation of light through the material in which it is traveling through (Berberan-Santos, 1990). Shortwave radiation from the sun is attenuated by water, exponentially decreasing the light's intensity with depth. The irradiance attenuation coefficient, K_d, describes the attenuation of light with depth (Kirk, 1977; Lee & Rast, 1997). Particles in the water column reflect and absorb light, so as the light encounters more suspended matter light intensity decreases. Beer's Law is written as $A = \varepsilon L c$, where A is absorbance, ε is the molar absorptivity constant ($Lmol^{-1}cm^{-1}$), L is the length of the sample (cm), and c is the solution concentration (mol L^{-1}). Light moving through transparent matter is attenuated as:

$$I = I_0 \, e^{-\mu x} \tag{6}$$

where I is the intensity of light at the seafloor, I_0 is the surface light intensity, x is the distance in km, and μ is the attenuation coefficient in km^{-1}.

K_d defines the attenuation of light within the Tauranga Harbour. It was derived from field measurements conducted by Cussioli et al. (2019). Discrete measurements (coloured dissolved organic matter (CDOM), chlorophyll-*a*, suspended particulate matter, and irradiance profiles) were measured within the Tauranga Harbour to identify the constituents controlling the penetration of light through the water column. Relationships between K_d and the drivers listed above were identified, allowing for the prediction of K_d within a system using turbidity measurements. Measured K_d ranged from $0.16 m^{-1}$ to $0.98 m^{-1}$, with an average $0.40 m^{-1}$. The average value was chosen for our model.

I is defined as the intensity of light available at MPB dwelling depth. In context, *I* determines the availability of food for MPB, and thus is a component of their growth rate calculations. Light limitation *I* is modelled using Equation 3, where d_w defines the changing water depth with time. Therefore, *I* varies as the model progresses with time. K_i defines the light saturation half constant of MPB in $\mu E\ m^{-2}\ s^{-1}$. K_i is coded as the light intensity at which the photosynthetic rate occurs at half the maximum possible photosynthetic rate (Pmax).

K_i was derived from Flowers et al. (in review), who in January 2020 used field observations in a unvegetated site at Tuapiro Point, Tauranga Harbour to determine the light uptake rate. Flowers et al. (in review) conducted experiments involving benthic incubation chambers to calculate relative photosynthetic-irradiance (PI) curves for eight separate light availability treatments (8%, 15%, 31%, 45%, 60%, 85%) and the 0% light. Benthic incubation chambers are sealed compartments that sit on the sea floor, allowing for in-situ measurement of dissolved substances exchanged between the floor and water column. Productivity within the chambers was measured using ten-minute averaged dissolved oxygen measurements, taken at the start and the end of a four-hour incubation period. Gross primary production (GPP) by fauna was calculated from net primary production (NPP) flux values, by measuring respiration in dark. The value of K_i calculated by Flowers et al. (in review) used in this model is 541 $\mu E\ m^{-2}\ s^{-1}$.

Daily averaged light intensity at the surface of the water, I_0 *(6)*, measured as photosynthetically-active radiation (PAR), defines the spectral range of light used for photosynthesis by photosynthetic organisms. PAR wavelengths range between 400–700 nanometres, which is approximately the range of visible light by humans. In this model, I_0 defines the photosynthetic irradiance of light at the surface at Tuapiro Point, Tauranga Harbour. I_0 changes regularly due to cloud cover and shading from land, and with latitudinal and seasonal variations also. This parameter was derived from Manghan (2020). An

experiment was conducted at 22 intertidal sites in 14 estuaries throughout New Zealand between March and November 2017, in which PAR was measured every ten minutes for a total of 201 to 260 days (depending on site). Measurements were taken using Odyssey PAR loggers deployed 10cm above the sediment surface. Immersed and emerged periods, determined by the time of high or low tide ± 2 h, are presented in the data to demonstrate a separation of tidal state and a four-hour period where the sensor was either completely emerged or completely covered by water. Measurements taken at night were excluded by removing PAR measurements of 0 µmol m^{-2} s^{-1}. Light intensity at Tuapiro Point, Tauranga, averaged 503 µmol m^{-2} s^{-1} over the sample period.

3.5 *M. liliana* Growth Dynamics

The change in *M. liliana* biomass is calculated by balancing the sources (growth due to grazing on MPB) and sinks (mortality):

$$B_{mac} = B_{mac} + \partial t * (\underbrace{G_{mac}}_{Growth} - \underbrace{M_{mac} * B_{mac}}_{Mortality}), \quad (7)$$

M. liliana grow by consuming MPB, before reaching a maximum sustainable biomass (carrying capacity) within the sediment:

$$G_{mac} = G_{mac}^{max}\left(B_{MPB} * G_{macgraz}\right)\left(1 - \frac{B_{Mac}}{K_{mac}}\right), \quad (8)$$

where G_{mac}^{max} is the maximum growth an individual *M. liliana* can achieve in a day, B_{MPB} is the MPB biomass available to consume, and K_{mac} is the species' carrying capacity. Biomass growth is dependent on the available MPB biomass and limited by the maximum individuals a habitat can sustain. The carrying capacity considers other factors that limit population abundance which are not explicitly in the model, such as competition between individuals.

G_{mac}^{max} defines the maximum growth rate of *M. liliana* in grams of carbon per m^{-2} per time-step. G_{mac}^{max} is a constant multiplied by a variable exponent. This term increases exponentially with the shell length of *M. liliana*. G_{mac}^{max} was derived from Pratt et al. (2015), which measured the spatial distributions of MPB against *M. liliana* grazing activity. The experiment's aim was to identify if a scale-dependent relationship exists across a sedimentary

gradient. During their study, Pratt et al. (2015) examined *M. liliana* biomass' effect on their grazing activity, as energy requirements and metabolic activity of invertebrates are partly in consequence of body size (Banse, 1982). From their research, the authors could estimate the biomass of *M. liliana* within experimental plots based upon the shell length and ash-free dry weight of individuals.

G_{mac}^{max} is calculated using the equation:

$$G_{mac}^{max} = 0.0023e^{0.164L}, \quad (9)$$

where L is the *M. liliana* growth rate – 0.00167 mm day^{-1}.

L is defined as the growth rate of *M. liliana* shell length in mm per day. In this model, the *M. liliana* population is measured in grams of carbon per m^{-2}. L is a component of the maximum growth rate calculation of *M. liliana*, which is converted from growth in mm to the growth in ash-free dry weight (carbon) in grams. L was derived from an Auckland Regional Council (2008) report. The Auckland Regional Council conducted a field transplant experiment, where juvenile *M. liliana* were transferred from one site within the Whitford embayment (Auckland, New Zealand) to nine others. These sites were predicted to experience contrasting suspended sediment concentrations, meaning their calculated growth rate is averaged across the varying conditions seen within estuaries. Ten *M. liliana* were transplanted to each site in a cage measuring 30 × 30 × 10 deep (cm). All sites were exposed to air for 1.5 hours before the mean low tide, with the length measurements of individuals being recorded monthly over a three-month period. *M. liliana* growth rate decreased with increasing median suspended sediment concentrations and increased with increasing settling flux. This shows that *M. liliana* biomass would increase at a lower rate as mud content increases, which is represented within the model as a decrease in carrying capacity.

Figure 3.1. Monthly growth rates of *M. liliana* across eight sites within a transplant experiment. Mean growth rate is denoted by the grey bars, with standard error bars in black shown (Auckland Regional Council, 2008)

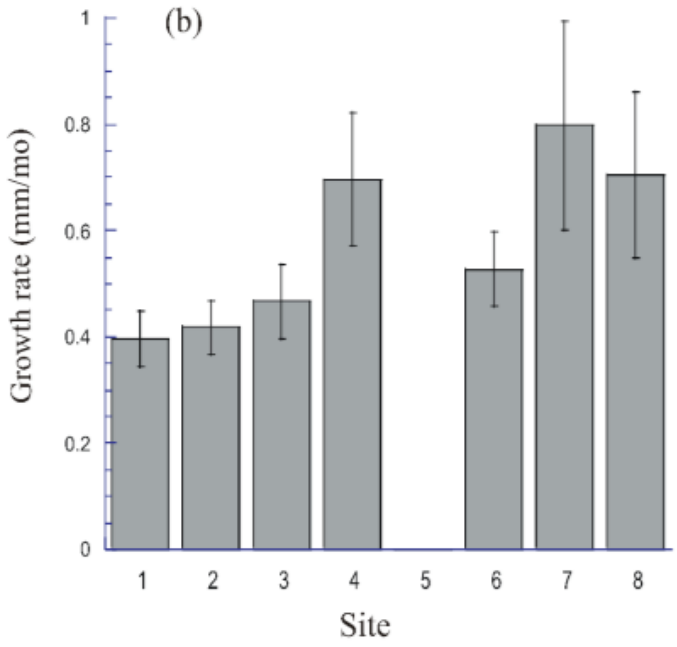

The daily growth of *M. liliana* in the model has been taken as the average growth of transplanted individuals across all sites. It should be noted that measurements were taken from individuals smaller than the size class used throughout the rest of the model. Growth measurements from a similar bivalve species, *M. balthica*, have been found to decrease with the age and size of individuals at a rate of $-0.46x + 3.14$, where x is the age in years (McGreer, 1983). Therefore, *L* may not be representative of our *M. liliana* size class.

WW defines the conversion from individual *M. liliana* at their wet weight to their dry weight in ash-free carbon. *WW* converts the weight of *M. liliana* from grams to grams of carbon, to keep calculations and outputs consistent. Using this parameter allows the model to calculate the change in *M. liliana* biomass in units g C m^{-2} day^{-1}. *WW* was calculated from Thrush et al. (2021) who provided data from an experiment conducted on *M. liliana* within the Tauranga Harbour. The data outlines the condition of *M. liliana* across multiple sites within the summer and winter seasons. We averaged the ash-free dry weight (AFDW) of individuals across the three sites within the summer months. These individuals ranged in length from 6.88mm to 50.48mm, with an average length of 26.27mm. The conversion equation from wet-weight to AFDW was obtained from Riccardi & Bourget (1998), who found that the AFDW of bivalves is 5.5% that of their wet weight. This was discovered by

incinerating freshly harvested bivalves in a muffle furnace at 450 - 500°C, converting them to particulate matter which is then weighed. *WW* is equivalent to 0.22 g C per individual.

K_{mac} defines the carrying capacity of *M. liliana* in grams of carbon per m^{-2}. K_{mac} is modelled as the maximum number of individual *M. liliana*, as a function of average sediment mud content. K_{mac} is reached when the biomass of *M. liliana* can no longer increase, or when the average sediment grain size becomes too small for suitable inhabitation by macrofauna. For K_{mac} to be coded in units g C m^{-2}, the value must be divided by the volume of the macrofaunal cores (C_2), multiplied by the *M. liliana* detrital pool (D_{mac}) and *WW*. K_{mac} can be estimated using published relationships between biomass and limitations using a regression model:

$$K_{mac} = \frac{21.6+0.146*(M_C*100)-0.005*\left((M_C*100)^2\right)}{\left(\frac{C_2}{2}\right)*D_{mac}*WW} \quad (10)$$

The equation demonstrates a second-order polynomial relationship, where the maximum density of *M. liliana* the sediment can support is a function of sediment mud content. In this study, the biomass is estimated by counting the number of individuals in two standard benthic cores (13cm diameter, 15cm height). To convert between individuals and g C m^{-2}, a constant conversion rate of 0.22 g C m^{-2} per individual is applied (represented as *WW* in Table 3.1)

K_{mac} was derived from Thrush et al. (2003). The study monitored the effects of terrestrial sediment deposits on benthic communities across six intertidal sandflats within the Whitianga Harbour, New Zealand, for 212 days. The authors found a negative relationship between the recovery of macrobenthos biomass, and the size of disturbance caused by terrestrial sediment deposition. The size and dwelling depth of macrobenthos also influenced recovery rate, with deeper dwelling adult *M. liliana* and larger biota recovering more slowly than smaller macrofauna or inhabitants of the sediment surface layer (0-2cm). This result coincides with other literature, where decreasing sediment particle size can alter the diversity of deposit feeders and coupled biogeochemical fluxes (Woodin et al., 1998; Boudreau & Jørgensen, 2001; Thrush, 2014). When mud content is set at the base rate of 0.1, K_{mac} is 129.174 g C m^{-2}; however, once M_c exceeds 0.8, K_{mac} is arbitrarily set to 1 g C m^{-2}, in response to the unfavourable sediment and nutrient conditions when M_c is this large.

K_{mac} can also reduce due to the species' sensitivity to high levels of ammonia, which can accumulate within the seabed sediments if porewaters are inadequately flushed. The

relationship between nutrient enrichment and K_{mac} (explained in more detail below) produces a coefficient that can be implemented into the reduction equation:

$$K_{mac_{new}} = K_{mac} * \exp\left(-1.045e^{-4} * 1000 * N_{old_{mac}}\right). \quad (11)$$

where the degree to which the carrying capacity is reduced depends on the concentration of nutrients within the *M. liliana* sediment layer ($N_{old_{mac}}$) at the previous time step.

$K_{mac_{new}}$ is the nutrient poisoning term, demonstrating *M. liliana* mortality that occurs due to excessive nutrient enrichment within sediments. $K_{mac_{new}}$ simulates the reduction of K_{mac} as nutrients increases at the dwelling depth of the bivalve (d_{mac}). Nutrients increase within sediments as *M. liliana* die and add carbon to the detrital pool (biomass decay explained in Section 3.7). Therefore, as more individuals die and the nutrient levels within the detrital pool increase, K_{mac} decreases due to nutrient poisoning.

$K_{mac_{new}}$ was derived from Thrush et al. (2021). The study manipulated sediment nitrogen concentrations to increase incident light at the seafloor within 24 sites, in 15 estuaries throughout New Zealand. Slow-release fertiliser was injected at 15cm beneath the sediment surface, elevating pore water nitrogen concentrations over a prolonged period. Adult *M. liliana* populations were measured using two macrofaunal cores (13cm diameter, 15cm deep) at each plot, alongside pore water NH_4^+ concentrations by using benthic flux chambers. Data from this study was extrapolated to examine the relationship between nutrient enrichment and *M. liliana* carrying capacity, producing the coefficient $-1.045e^{-4}$ at the upper 99th percentile.

Figure 3.2. Scatter plot demonstrating the relationship between *M. liliana* biomass and ammonia concentrations within sediment. The y-axis represents the number of *M. liliana* present, while the x-axis represents the NH_4^+ concentration (µmol L) 5-7cm below the sediment surface. Dots are indicative of measurements taken at individual sampling sites within Thrush et al. (2021). An exponential curve is fitted to the graph as a solid line, with the dotted line representing the upper 99% prediction bound.

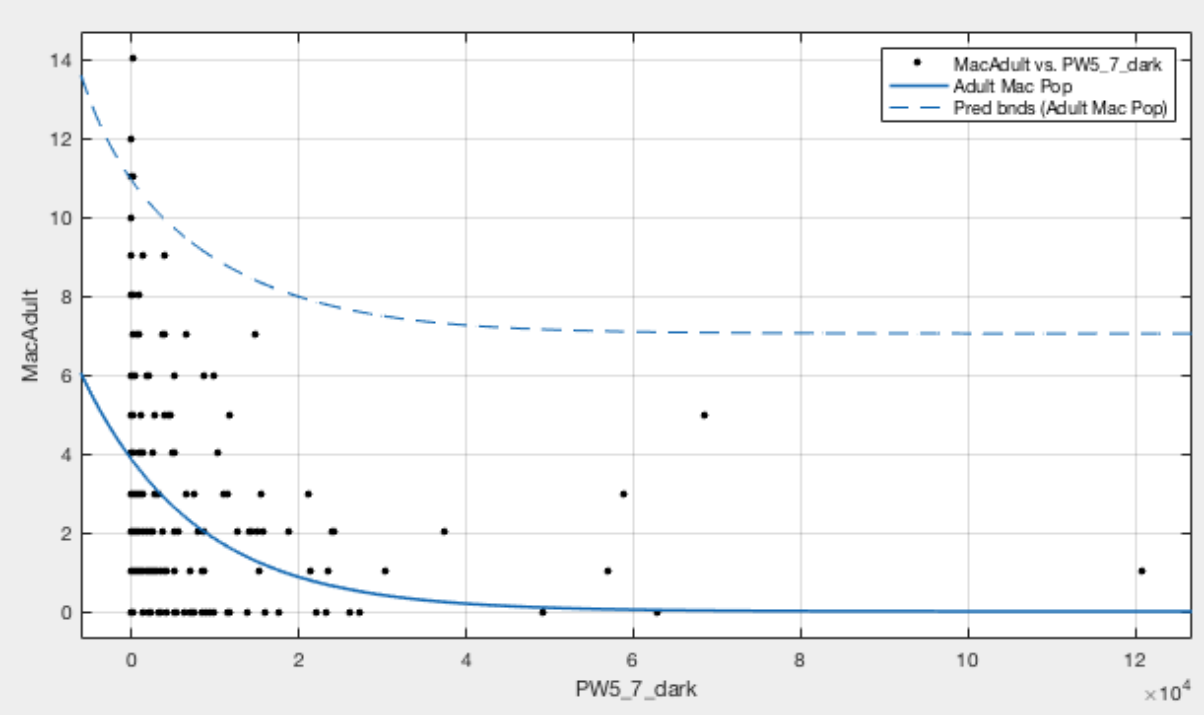

M_{mac} is coded as a proportional loss to B_{mac} per time step. We obtained M_{mac} through extensive model testing following the completion of our parameter list. Arbitrary values for M_{mac} were set in a series of model test runs, with our chosen M_{mac} value producing a B_{mac} value closest to field observations. As no data on the mortality rate of *M. liliana* could be found in the literature, this process ensures that the value set is as representative as possible to what is seen in an average estuary in New Zealand. The M_{mac} is set as a proportional loss of 0.000004 for B_{mac} per day.

T_{feed} defines the feeding cycle period of *M. liliana* on MPB in seconds. T_{feed} is coded as the length of time *M. liliana* feed upon MPB. This parameter is used within a flushing coefficient equation (Equation 22), allowing the model to simulate intermittent *M. liliana* feeding bouts. This is crucial, as the pressurisation of sediment by *M. liliana* occurs as the organism excretes water inhaled during their time feeding. T_{feed} was derived from Volkenborn et al. (2012), who modelled the oxygen dynamics and bioirrigation of *M. liliana* following an experiment on three tellinid bivalves in New Zealand. In their work, *M. liliana* were collected from Tuapiro Point (Tauranga Harbour) and placed within individual laboratory containers to monitor their hydraulic activities. Porewater pressure waveforms were identified using time-

lapse photography and porewater pressure sensors. What was found is that larger individuals (4.1-5cm) were hydraulically active 94% of the time, with 88% of time spent deposit feeding. During deposit feeding, porewater was pressurised for 8.3 minutes (± 2.5), followed by 10 minutes (± 1.8) of rest; this is considered one feeding bout. On average, there were 3.3 feeding bouts within an hour, with sediment being pressurised for 45% of the feeding time.

A period of nine minutes per feeding bout was chosen to simplify the mechanics within the model. It should be noted that sediment type had no effect on the hydraulic activity, meaning that as sedimentation increases within the model, this parameter will not be adjusted.

B_{mac}^{min} defines the minimum possible biomass of *M. liliana* in grams of carbon per m^{-2}. B_{mac}^{min} has an arbitrary value set above zero, to allow the model to restart if B_{mac} reaches zero. Setting at this value simulates immigration of *M. liliana* should B_{mac} becomes zero, and is the only time *M. liliana* transport is considered. Juveniles can travel as far as 3.3km during a tidal cycle, which allows for disturbed habitats to repopulate (Petuha et al., 2006). A barren area can further repopulate with the reintroduction of adult *M.* liliana, as they can increase the number of juveniles through recruitment (Roper et al., 1992). B_{mac}^{min} is equivalent to 0.001 g C m^{-2}.

3.6 MPB growth dynamics

K_{MPB} defines the carrying capacity of MPB in g C m^{-2}. K_{MPB} is coded as the maximum volume of MPB that can inhabit one metre squared of surface sediments. K_{MPB} was derived from Sinha's (2017) numerical model, which was designed to measure the effect of nutrient and flow on benthic and pelagic primary producers within the Bode River riverine ecosystem, Germany. The model coded K_{MPB} in mgCh-a/m^{-2} and has been converted to g C m^{-2} within our model to maintain consistency. The term was originally sourced from Flynn et al. (2013), a study that modelled the lateral variation of attached algae in rivers. K_{MPB} is an approximation coinciding with the photosynthetic rate (following light and nutrient limitation) needed to sustain diurnal river dissolved oxygen measurements and the maximum unlimited growth rate of MPB (disregarding nutrient or light effects at 20°C). Further validation of this value comes from a similar estimate in Turner et al. (2009), who modelled dissolved oxygen and pH changes in the South Umpqua River, Oregon, to predict nutrient enrichment patterns. Marine estimates of K_{MPB} are placed closer to 2.4 ± 0.35 g C m^{-2} (Morris, 2005), between 0.2-0.025 g per gram of sediment (Orvain et al., 2003), or as small

as 0.012 g C m^{-2} for a photosynthetically active MPB biomass (Méléder et al., 2005). As estimates between freshwater studies are more consistent than marine, freshwater values have been chosen for this model. K_{MPB} is valued at 1.2 gCh-a/m^{-2}.

K_N defines MPB's daily uptake of nutrients from the water column in mmol N m^{-2}. K_N allows B_{MPB} within the model to grow when nutrients are unavailable within the sediment. Typically, MPB source nutrients from sediment, but as nutrient requirements increase with available light MPB must also consume nutrients from the water column. K_N was derived from Sundbäck & Granéli (1988), who studied the relationship between inorganic nutrients in bottom water and MPB by experimentally exposing sediment to varying light quantities. Sediment was sourced 15m beneath the water's surface from Laholm Bay, Sweden. As sampling was carried out in October, a time where algae are not abundant at 15m, surficial sediment from Salviken Bay, Sweden, taken from 0.5m depth was mixed with sediment from Laholm Bay to increase algae biomass. Microflora species were not found to be essentially different between the two locations. The experiment was run for 81 days, with a 16/8 h light and dark cycle. Samples were exposed to two of four different light regimes (0, 5, 10, and 30 µE m^{-2} s^{-1}) within independent aquaria; a range alike the light exposure at 15m depth at the sediment's source. 36 days into the experiment, light treatments were inverted to measure the reaction speed to an altered light condition and to determine if differences between samples were due to separate light regimes (5 µE to 10µE and vice versa; 0µE to 30µE and vice versa). NH_4^+ concentrations in the water were initially low in each aquarium. NH_4^+ concentrations within aquaria kept in the dark increased by 0.6 to 0.7 mmol m^{-2} day^{-1}. Once light conditions were inverted to 30 µE, NH_4^+ concentrations promptly decreased at a mean rate of 1.5 mmol m^{-2} day^{-1}, demonstrating the nutrient uptake rate of MPB. Therefore, this model defines K_N as 1.5 mmol m^{-2} day^{-1}.

3.7 Detrital pool dynamics

The MPB detrital pool (D_{MPB}) increases through the addition of deceased individuals that have been removed from the biomass pool by mortality. The change in D_{MPB} can be calculated as the removal of nutrients that decay from deceased individuals:

$$\underset{Mortality}{} \quad \underset{Decay}{}$$

$$\frac{\partial D_{MPB}}{\partial t} = M_{MPB} B_{MPB} - C_{MPB} D_{MPB}, \tag{12}$$

where M_{MPB} is mortality (set as a portion lost per day), and C_{MPB} is the biomass decay rate (g C m^{-2} day^{-1}) from the detrital pool.

The *M. liliana* detrital pool also increases through the addition of deceased individuals. The change in the *M. liliana* detrital pool can be calculated as the removal of nutrients that decay from deceased individuals:

$$\underset{Mortality}{} \quad \underset{Decay}{}$$

$$\frac{\partial D_{mac}}{\partial t} = M_{mac} B_{mac} - C_{mac} D_{mac}, \tag{13}$$

where M_{mac} is mortality (set as a portion lost per day), and C_{MPB} is the biomass decay rate (g C m^{-2} day^{-1}) from the detrital pool.

3.8 Nutrient pool dynamics

A nutrient concentration gradient between the MPB (surface) and *M. liliana* layer must be calculated to determine the effect of mixing across the gradient. This can be done by:

$$\partial N / \partial z = \frac{N_{MPB} - N_{mac}}{d_{mac}}, \tag{14}$$

where the addition of nutrients to the MPB nutrient pool can be calculated by looking at the balance of sources (decay and addition) and sinks (growth):

$$\underset{Decay}{} \quad \underset{Growth}{} \quad \underset{Addition}{}$$

$$\frac{\partial N_{MPB}}{\partial t} = \frac{d_{MPB}}{C2N} \left(C_{MPB} D_{MPB} - G_{MPB} B_{old} \left(1 - \frac{B_{MPB}}{K_{MPB}}\right)\right) * \ Kz \ \partial N \partial z, \tag{15}$$

where C_{MPB} is the biomass decay rate (g C m^{-2} day^{-1}), G_{MPB} is growth (g C m^{-2} day^{-1}) from the consumption of nutrients produced by the decay of carbon in the detrital pool (g N m^{-2}

day^{-1}). *M. liliana* add nutrients from depth through their pumping behaviour (which is explained in more depth later).

Nutrients accessible by *M. liliana* at depth within sediment can be calculated by looking at the balance between sources (decay) and sinks (pumping behaviour). This can be done by:

$$\partial N_{mac} = \underbrace{\frac{d_{mac}}{C2N}\, C_{mac}\, D_{mac}}_{Decay} - \underbrace{Kz * \partial N \partial z}_{Removal}, \quad (16)$$

where the decay of dead *M. liliana* (C_{mac}) at depth in g C m^{-2} day^{-1} is converted to nitrogen (g N m^{-2} day^{-1}) and added to the nutrient pool. *M. liliana* pumping behaviour causes a net flux of nutrients from depth upwards to the MPB layer. Therefore, the collective sum of nutrients within the seabed can be calculated as the addition of nutrients within the MPB and *M. liliana* layers. This can be done by:

$$N = N_{MPB} + N_{mac}, \quad (17)$$

C_{mac} and C_{MPB} define the proportion of standing stock (biomass) that is transferred to the detrital pool in g C m^{-2} day^{-1}. C_{mac} and C_{MPB} are coded to allow the addition of carbon to the detrital pools from the decay of MPB and *M. liliana* biomass. Within the benthic ecosystem, nutrients circulate through the present organic biomass, detrital pool, and inorganic nutrients. Detritus is a broad term that encompasses any non-living organic matter (Moore et al., 2004). Nutrients are added to the detrital pool through faeces and dead organic matter, while the inorganic nutrient pool increases in size with the remineralisation of detritus. The microbial food web rapidly remineralise small quantities of organic nutrients into inorganic nutrients, as a function of temperature. Their biological rate doubles following a 10°C increase in water temperature (Eppley, 1972; Kremer & Nixon, 1978), providing more readily accessible nutrients for organisms within the ecosystem's organic biomass.

C_{mac} and C_{MPB} were derived from van Oevelen et al. (2006), who quantified the carbon flow through a benthic food web in the Molenplaat intertidal flat within the Scheldt estuary (The Netherlands). Data were collected through a mixture of literature review, and extensive site sampling between 1996 and 1999. A range of data were used to compile the

results, such as tracer data on fixed carbon by MPB, isotope signatures, carbon production and processing, and the biomass of benthos. What resulted was a minimum and maximum measurement of g C m^{-2} day^{-1} between all components of the food web. We took the median flow of carbon from MPB standing stock to detritus to use as our benthic detrital parameter for MPB. The value was converted to a proportion of MPB standing stock, by dividing the weight of carbon added to the detrital pool by the weight of MPB standing stock:

$$\frac{26(mgCm^{-2}day^{-1})}{2090(mgCm^{-2}day^{-1})} = 0.0124$$

As these data were collected from water averaging 13.6°C in temperature (Maes et al., 2005), the biological breakdown rate must be increased to reflect the average temperature of the Tauranga Harbour in summer (22°C). An 8.4°C increase would constitute an 84% increase in the breakdown rate, meaning the proportion of MPB standing stock that transfers to the detrital pool is:

$$0.0124 * 1.84 = 0.0228.$$

van Oevelen et al. (2006) also measured the flow of carbon from the macrobenthos population to the detrital pool. This was broken down into subcategories of suspension feeders, deposit feeders, and surface deposit feeders. The median value of carbon transfer from deposit feeders to detritus was used in our model. Deposit feeders constituted 51.5% of the macrobenthos population (12,172 mg C $m^{-2}day^{-1}$), which equates to 6270 mg C m^{-2} day^{-1}. We assumed that deposit feeders contributed to 51.5% of the flow of carbon from macrobenthos to detritus. Therefore, the proportion of deposit feeder standing stock that transitioned to the detrital pool was calculated by dividing their flow of carbon to detritus by their standing stock:

$$\frac{88.84(mgCm^{-2}day^{-1})}{6270(mgCm^{-2}day^{-1})} = 0.0142$$

When adjusting for the temperature discrepancy, the proportion of deposit feeder standing stock that transfers to the detrital pool is:

$$0.0142 * 1.84 = 0.0261$$

It should be noted that detritus constitutes more than dead individuals, including both animal tissue and faeces, to which MPB will contribute both. It should also be noted that these values have been updated from an original, constant coefficient for benthic detritus. The original value was 0.00064 g C m^{-2} day^{-1} and was sourced from Naithani et al. (2016). Naithani et al. (2016) created an ecological model, also for the Scheldt estuary and tidal rivers ecosystem. The value from this study is considerably smaller than the values obtained from van Oevelen et al. (2006); however, values from van Oevelen et al. (2006) were chosen as it provides data specific to fauna, rather than a constant value for all remineralisation within the benthic environment. Something to be considered is the effect of sediment type on remineralisation rates. Remineralisation rates can increase tenfold in muddy sediments, compared to sandy tidal flats (Nowicki & Nixon, 1985). The Scheldt estuary is known for high sedimentation rates and sand extraction (Gils et al., 1993), which may have influenced the outputs from the above studies. The values used in the model for C_{mac} and C_{MPB} are 0.0261 g C m^{-2} day^{-1} and 0.0228 g C m^{-2} day^{-1} respectively.

C2N defines the weight of nitrogen produced per gram of carbon, during the breakdown of carbon in the detrital pool. *C2N* calculates the amount of available nitrogen (*N*) in the water column that can be re-assimilated by MPB (see K_N). Therefore, *C2N* allows MPB growth to be modelled following nutrient enrichment sourced from the detrital pool (Fransz & Verhagen, 1985). *C2N* was derived from Naithani et al. (2016), who based this value on several similar studies (Lingeman-Kosmerchock, 1978; Los, 1982; Fransz & Verhagen, 1985). These studies examine and model the production of phytoplankton in relation to nutrient loading within the water column. Naithani et al. (2016) chose a conversion value that fell within the scope of the other studies' findings. The resulting *N* output in g N m^{-2} is then converted to mmol *N* using the equation:

$$N_{mmol} = \frac{1}{(14.0067)} * 1000, \quad (18)$$

where 14.0067 is the molar mass of *N* in g mol. Therefore, *C2N* is valued at 5.88 g N m^{-2}.

DR defines the denitrification rate of nutrients within the modelled estuarine system in mmol N m^{-2} day^{-1}. *DR* was derived from O'Meara et al. (2020) who examined and compared denitrification rates across four sites within the Mahurangi Harbour (New Zealand). The sites were chosen based on their proximity to the Mahurangi River in the upper reaches of the estuary, with site one located in the upper harbour, and the remaining sites distributed towards the outer harbour. The site selection allowed the examination of denitrification rates across a natural declining gradient of sediment organic matter and nitrogen loading. Denitrification was evaluated relative to macrofaunal communities, nutrient and dissolved gas fluxes, and decreasing sediment grain size. The denitrification rate from site one (22.35 ± 13.34 μmol N_2 m^{-2} $h^{-}1$) has been chosen for our model, as compared to the other sample sites it is situated the closest to intertidal flats. The calculations to convert the denitrification to units consistent within our model are as follows: The units μmol were converted to mmol:

$$\frac{22.35 \pm 13.34}{1000} = 0.02235 \pm 0.01334$$

With the result being multiplied by 24 to convert from an hourly to a daily rate:

$$(0.02235 \pm 0.01334) * 24 = 0.5364 \pm 0.32016$$

And finally, a lower and upper limit of the denitrification rate was identified by adding or subtracting one standard deviation from the median rate:

$$0.5364 - 0.32016 = 0.21624$$
$$0.5364 + 0.32016 = 0.85656$$

Therefore, the resulting lower, median, and upper limits of denitrification within our model are 0.216, 0.536, and 0.857 mmol N m^{-2} day^{-1} respectively.

3.9 Initial boundary conditions

Initial boundary conditions for the three dynamic variables in the model were updated following the completion of mortality trail testing. Trial 46 variant two (*see Section 4.7*) produced biomass values that reflected field sample observations for both species. We assumed that detrital and nutrient values would also be reflective of natural levels. Therefore, the initial boundary conditions for our three dynamic variables within the model are equal to their equivalent final value from trial 46 variant two. These are:

$B_{mac}(1)$ = 31.918 g C m^{-2}

$B_{MPB}(1)$ = 1.133 g C m^{-2}

$N(1)$ = 0.0043 mmol N m^{-2}

$N_{mac}(1)$ & $N_{MPB}(1)$ = 0.0022 mmol N m^{-2}

$D_{mac}(1)$ = 0.11 g C m^{-2}

$D_{MPB}(1)$ = 0.409 g C m^{-2}

Before mortality testing could be conducted, initial biomass values were obtained from the literature, with nutrient and detrital values being arbitrarily set.

$B_{mac}(1)$ defines the starting biomass of *M. liliana* within the model in g C m^{-2}. Initially, $B_{mac}(1)$ was derived from Thrush et al. (2021). An average of 6.3 *M. liliana* were found within two sediment cores (13cm diameter x 15cm height) per sample. This number has been multiplied by *C2N*, to give the total weight of the individuals in grams of carbon. This value is then divided by C_2 and multiplied by d_{mac}. What is produced is the biomass of *M. liliana* in g C m^{-2} from Tuapiro Point at the time of sampling. This value is assumed to be an average, baseline value of *M. liliana* present at this location, or an indication of an expected biomass. $B_{mac}(1)$ is 71.82 g C m^{-2}.

$B_{MPB}(1)$ defines the starting biomass of MPB within the model in g C m^{-2}. Initially, $B_{MPB}(1)$ was also derived from Thrush et al. (2021). An average of 8.11 µg of MPB were found per gram of sediment. This was multiplied by the sediment density and sediment porosity to give the weight of MPB in kg m^3. This was further converted to the weight of MPB in g C m^{-2}, by multiplying the value by d_{MPB}. What was produced is assumed to be an average, baseline biomass of MPB present at this location. $B_{MPB}(1)$ is 0.159 g C m^{-2}.

3.10 Flushing Coefficient

The flushing parameter (*CF*) is dependent on two factors; the movement of water through a porous sediment of finite thickness due to wave pumping ($flush_{wave}$), and the pressurisation of sediment caused by *M. liliana* (Equation 22 & 23). Therefore, $flush_{wave}$ and $flush_{mac}$ have been assigned to each of these factors respectively, to model wave interactions and pressurisation of the seabed by *M. liliana*. Firstly, we must calculate the areal coverage of *M. liliana* to identify the areal size of pressurised seabed. The degree of pressurisation caused by *M. liliana* are for each individual, and so need to be converted to our unit of 1 m^2. We assume that if the areal coverage of *M. liliana* is >1 m^2, then 100% of the area is pressurised. The areal coverage of *M. liliana* is calculated first by converting from biomass to individuals, and then by approximating the area of an individual by the area of a circle with diameter equal to the length of the shell:

$$A_{mac} = \left(\frac{B_{mac_{old}}}{WW}\right)\pi * \left(\pi * \frac{L_{mac}}{2}\right)^2, \quad (19)$$

where the dry weight of *M. liliana* is multiplied by the circumference of *M. liliana*, to produce a percentage coverage of *M. liliana* within a m^2 area.

To determine the pressure variations caused by waves within the seabed sediments, first the pressure at the seabed surface is needed (which can be calculated from linear wave theory), then that pressure needs to be attenuated within the sediments. Attenuation can be calculated using Biot's equation, assuming the following:

1) Pore pressure within sediment is a consequence of elastic interactions between water and sediment within a porous sandy bed (dilation effects are neglected).
2) Darcy's law governs flow within the porous bed.
3) Unimpeded, reversible, and linear mechanical properties are assumed for the sediment matrix predominantly obeying Hooke's law, regardless of a pore pressure phase lag in fine sediment.
4) A uniformly compressible pore fluid and sediment matrix exist.
5) A horizontal, porous seabed exists that is of finite thickness, hydraulically anisotropic (with the same properties in all dimensions), and homogeneously unsaturated.

The functions to calculate attenuation of waves in seabed sediments were provided by Hsu & Jeng (1994), which were provided in Matlab form by Dong Sheng Jeng (pers. comm.). Following the assumptions above, a porous seabed with varying permeabilities in the x-, y-, and z-directions can be formulated as:

$$\frac{K_x}{K_z}\frac{\partial^2 P}{\partial x^2} + \frac{K_y}{K_z}\frac{\partial^2 P}{\partial x^2} + \frac{\partial^2 P}{\partial z^2} - \frac{\gamma_w n' \beta}{K_z}\frac{\partial P}{\partial t} = \frac{\gamma_w}{K_z}\frac{\partial \varepsilon}{\partial t}, \quad (20)$$

where K_x, K_y, and K_z define sediment permeability in the *x*-, *y*-, and *z*-directions. The wave-induced pore pressure above that of the hydrostatic condition is denoted by *P*, the unit weight of pore-water is γ_w, soil porosity is *n'*, the compressibility of the pore fluid is β, volume strain is ε, and time is *t*. This formula produces the pressure field, from which Darcy's law can be used to formulate a flow speed/discharge that is the basis for flushing parameter/pore-water velocity:

$$q = -\frac{k}{\mu L}\Delta, \quad (21)$$

where the flux of fluid through a porous medium, q (m s^{-1}), is equal to the permeability of the medium (k), the fluid viscosity of the fluid (μ), and the drop in pressure (Δp) over a specified distance (L).

CF was obtained in part from Hsu & Jeng (1994) and Volkenborn et al., (2012). It combines the work of multiple studies, to define the benthic flushing rate. *CF* depends on the movement of water through sediments due to wave pumping, sourced in part from the second stage in a study series by Hsu & Jeng (1994), and the pressurisation caused by *M. liliana* (Equation 22 & 23), sourced in part from Volkenborn et al. (2012).

In the first of their study series, Hsu & Jeng (1993) provide an analytical solution for the wave-induced soil response in a three-dimensional wave domain for soil of infinite thickness. As field measurements and laboratory experiments on this subject were often conducted in porous soil of finite thickness, Hsu & Jeng set out to develop a solution to this question. Existing literature surrounding the subject, such as equations developed by Yamamoto (1977) and Mei & Foda (1981), could not produce conclusive closed form solutions within the two-dimensional and three-dimensional wave domain. By expanding upon their earlier work, Verruijt's (1969) storage equation, and Biot's (1941) three-

dimensional consolidation theory, Hsu & Jeng (1994) create an equation suited to soil of finite thickness within short-crested wave systems. The equation models the attenuation of pressure with depth, the displacement of sediment, the upward pressure within the sediment (not normalised by the surface pressure), and the downward flow (calculated by Darcy's law) in m s^{-1}. Variables within this equation have been altered to suit the needs of our model, formulating $flush_{wave}$. The velocity of the pressure response (initially non-dimensional) was changed to a dimensional force by multiplying it with the pressure at the surface. Hydraulic conductivity (as a function of soil grain size), sourced from Oh et al. (2013), was also added to the equation. These alterations were made so the speed in which waves permeate through sediment could be calculated.

Volkenborn et al. (2012) modelled the intermittent bioirrigation and oxygen dynamics of three tellinid bivalves in permeable sediments. *M. liliana* were collected from the northern entrance of Tauranga Harbour and Tuapiro Point (a well-known dwelling spot for *M. liliana* in Tauranga Harbour). Porewater pressure measurements were collected from individuals placed in circular containers submerged in running artificial seawater. Large individuals (4.1-5.0cm) were placed in either muddy or sandy sediment, while small individuals (2.3-2.4cm) were placed only in muddy sediment. Porewater pressure dynamics were identified from time-lapse photography (every 15s) and pressure sensors within the sediment. Results showed that *M. liliana* pressurise 4cm of water for 30-60 minutes at a time. Larger individuals were found to be hydraulically active 94% of the time, with 88% of time spent deposit feeding. Deposit feeding is characterised by approximately nine minutes of pressurisation, followed by roughly nine minutes of rest. On average, there were 3.3 feeding bouts within an hour, with sediment being pressurised for 45% of the feeding time.

Figure 3.3. Recurrent pressurisation of porewater affiliated with deposit-feeding by *M. liliana* (4.9cm shell length) in sediment with a permeability of 4.3 x 10^{-12} m^2 (Volkenborn et al., 2012). Reproduced with permission of author.

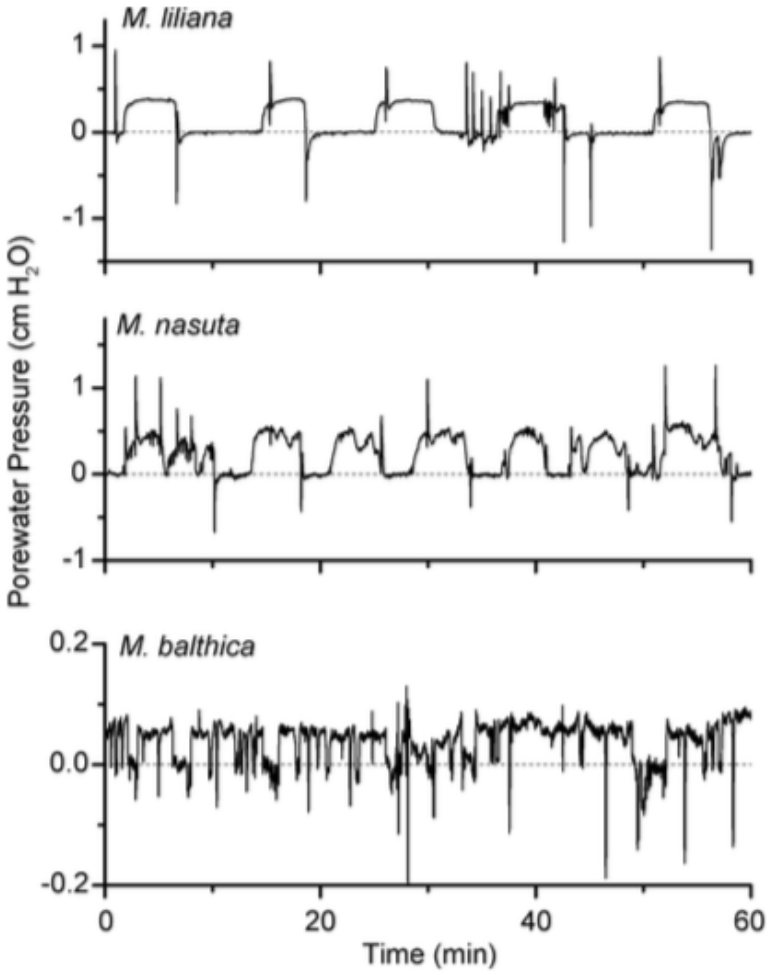

Figure 3.4. Porewater pressure dynamics corresponding to the hydraulic activity of *M. liliana* (5.0cm shell length) in sediment with a permeability of 4.3 x 10^{-12} m^2. The spikes represent burrowing episodes, with the recurrent pressurisation and positive and negative hydraulic pulses affiliated with siphon movements, and pseudofeces and faeces expulsions. Box A demonstrates the entire 22-hour sequence, while box B and C are enlargements of the data outlined by the dashed boxes in A (Volkenborne et al., 2012). Reproduced with permission of author.

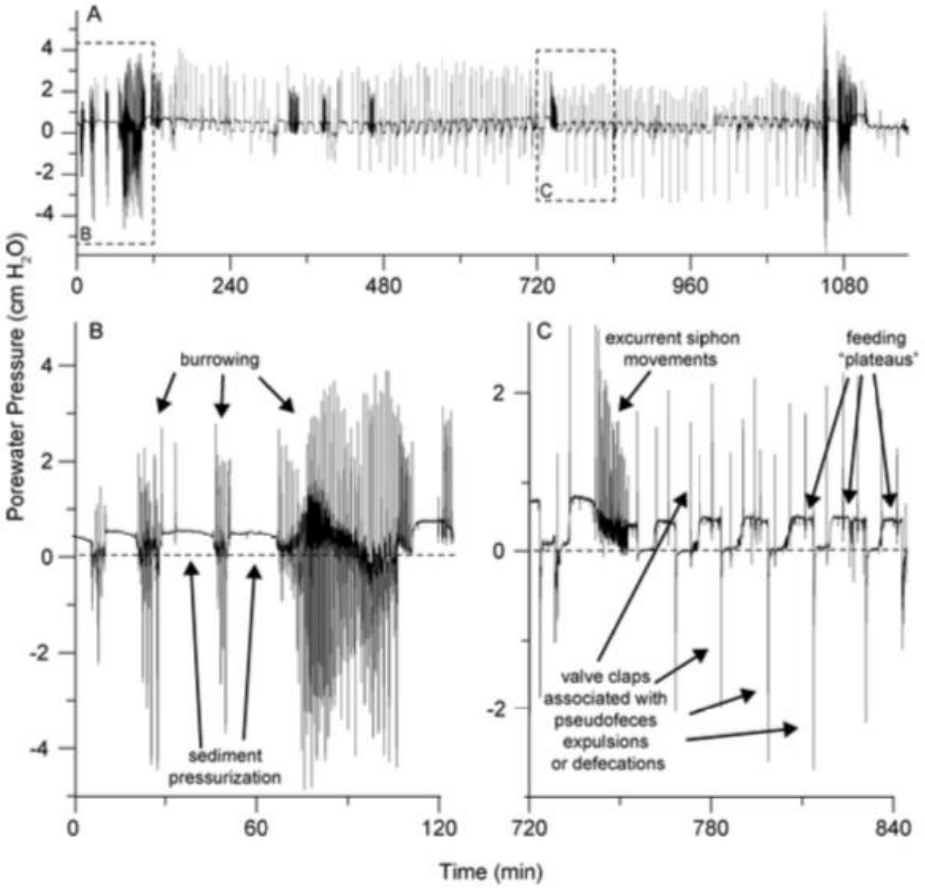

As the pressurisation of benthic sediments by *M. liliana* is not constant, the behaviour must be modelled to reflect active and inactive periods of pressurisation by the present B_{mac}. Our model has been coded so that cyclic flushing by *M. liliana* can be turned on or off – on meaning that flushing occurs during feeding bouts (Equation 22), and off meaning flushing is continuous (Equation 23). *M. liliana* pressurise the bed to 0.5cm H_2O. This was converted to pascals, and defines the vertical conductivity, or the pressurisation caused at the sediment surface, by *M. liliana*:

$$flush_{mac} = -\left(\frac{K_H}{\rho * g} * \frac{\left(0.008 * round\left(0.5 * \left(1 + \cos\left(2 * pi * \frac{time}{T_{feed}}\right)\right)\right) * \rho * g\right) - P_W}{d_{mac}}\right) * A_{mac} \quad (22)$$

when cyclic flushing is on, $flush_{mac}$ is the output of the pressurisation at the sediment surface from *M. liliana* (rounded to the nearest decimal), multiplied by the density of water, the acceleration of gravity, and feeding bouts of *M. liliana* (oscillating between nine minutes of feeding and nine minutes of rest), minus the pressurisation of sediment at the depth of *M. liliana* dwelling, and multiplied by the areal coverage of *M. liliana* as a percentage:

$$flush_{mac} = -\left(\frac{K_H}{\rho * g} * \frac{(0.008 * \rho * g) - P_W}{d_{mac}}\right) * A_{mac} \quad (23)$$

when cyclic flushing is off, $flush_{mac}$ is the output of the pressurisation at the sediment surface from *M. liliana*, multiplied by the density of water, the acceleration of gravity, minus the pressurisation of sediment at the dwelling depth of *M. liliana*, and multiplied by the areal coverage of *M. liliana* as a percentage.

Therefore, the flushing of nutrients from sediment by *M. liliana* is calculated as:

$$CF = flush_{wave} + flush_{mac} \quad (24)$$

The flushing coefficient is the sum of $flush_{wave}$ and Equation 22 or 23, the latter of which being dependent on whether cyclic flushing is turned on or off. Finally, continuity of mass means that if there is a flow upward through the sediments, it would be matched by a flow downward, so that the effect of flushing is the same as mixing across a concentration gradient. This can be simulated by using the flushing to define a mixing coefficient (*Kz*) that measures the diffusion of nutrients in $m^2\ s^{-1}$ (this is the way horizontal salinity gradients are diffused by the effect of tidal currents in estuaries). The mixing coefficient can be approximated by the velocity scale multiplied by a length scale (the depth of the *M. liliana* layer):

$$Kz = |CF| * \frac{d_{mac}}{2}, \quad (25)$$

An absolute value must be used so that the mixing always reduces the concentration gradient to equalise concentration between the surface and the depth where *M. liliana* live.

3.11 Summary

We developed a model grid with three layers of operation. Three dynamic variables (biomass, nutrients, and detritus) for both benthic dwelling species *M. liliana* and MPB are connected in the model and parameterised by distinct source and sink relationships. The system shifts carbon by *M. liliana* living within estuarine benthic sediment feeding upon MPB at the sediment surface. Detritus, and corresponding nutrients released by detrital breakdown, from *M. liliana* is transferred to the sediment surface through the species' pumping behaviour. These nutrients are consumed by MPB populations, fuelling their growth. Sediment porosity (mud content) and external nutrient loading influence the efficiency of functioning within each model layer and in the transfer of matter between layers.

Chapter 4

Results

4.1 Model Testing Structure

The first task was to manipulate the only parameters in the model which could not be found in the literature, the mortality rates (*M*), so that the biomass (*B*) in the *M. liliana* (B_{mac}) and MPB (B_{MPB}) pools reflected real world values. The biomass of both species interacted non-linearly, and so varying one caused the other to vary as well. The mortality rate was deemed appropriate if B_{mac} and B_{MPB} values were close or equivalent to their biomasses found within field studies. Observed natural values were used from studies completed in Tauranga Harbour. These values were 41.768 g C m^{-2} for *M. liliana* (Thrush et al., 2021; *see Section 3.5 for explanation on study*) and 1.056 g C m^{-2} for MPB (Flowers et al., in review; *see Section 3.4 for explanation on study*). All parameters within the model remained at control values, except for *M. liliana* and MPB mortality (M_{mac} and M_{MPB}), and the maximum length of the simulation (t_{max}).

The results were stored in Matlab structure files (with name mortB(x)results(y), where 'x' is replaced by an index number for the M_{mac} rate used, and 'y' refers to an index for M_{MPB} (see Table 4.1 to 4.6 for the values assigned to each index). For example, mortB3results11 corresponds to a *M. liliana* mortality rate of 0.001 and a MPB mortality rate of 0.1 (Table 4.1). A 'structure' file is a master variable which allows a number of different variables to be stored with a common name. In this case, the structure file contained a complete timeseries of all of the dynamical variables. As testing was conducted, mortality rates were refined to decrease the difference between our observed species' biomass and values seen in nature. Time (t_{max}) was increased from trial eleven to allow the simulation to stabilise further. This file naming system was chosen so that the results of each variation could be automatically identified when plotted against each other. Henceforth, 'trial' will be used to refer to M_{mac} values, and 'variant' refers to M_{MPB} values. However, the testing structure changed following trial 31, with M_{mac} altering with the variant number, rather than M_{MPB} (Table 4.6). Despite this change, language when referring to the trial and variant number remains the same.

Please note, symbol definitions can be found in Table 3.1. The Pearson Correlation Coefficient was used to identify the relationships found in this section, with the *p-value*

calculated at the 95% confidence interval. Values from specific trial and variant numbers were chosen as representative values from trial sets (Tables 4.1 to 4.6 each represent a trial set) during relationship analysis. Specific trials and variants were chosen when their biomass values were closest to values seen in nature.

4.2 *M. liliana* and MPB Mortality Values

Table 4.1. *M. liliana* (mac) and MPB mortality rates and their corresponding trial and variant number, for trials one to ten. Note that every combination of row (trial) and column (variant) was run.

Mac \ MPB	1E-11	1E-10	1E-09	0.00000001	0.0000001	0.000001	0.00001	0.0001	0.001	0.01	0.1	tmax
0.1	1.1	1.2	1.3	1.4	1.5	1.6	1.7	1.8	1.9	1.10	1.11	150000000
0.01	2.1	2.2	2.3	2.4	2.5	2.6	2.7	2.8	2.9	2.10	2.11	150000000
0.001	3.1	3.2	3.3	3.4	3.5	3.6	3.7	3.8	3.9	3.10	3.11	150000000
0.0001	4.1	4.2	4.3	4.4	4.5	4.6	4.7	4.8	4.9	4.10	4.11	150000000
0.00001	5.1	5.2	5.3	5.4	5.5	5.6	5.7	5.8	5.9	5.10	5.11	150000000
0.000001	6.1	6.2	6.3	6.4	6.5	6.6	6.7	6.8	6.9	6.10	6.11	150000000
0.0000001	7.1	7.2	7.3	7.4	7.5	7.6	7.7	7.8	7.9	7.10	7.11	150000000
0.00000001	8.1	8.2	8.3	8.4	8.5	8.6	8.7	8.8	8.9	8.10	8.11	150000000
0.000000001	9.1	9.2	9.3	9.4	9.5	9.6	9.7	9.8	9.9	9.10	9.11	150000000
1E-10	10.1	10.2	10.3	10.4	10.5	10.6	10.7	10.8	10.9	10.10	10.11	150000000

Table 4.2. *M. liliana* (mac) and MPB mortality rates and their corresponding trial and variant number, for trials 11 to 15. Note that every combination of row (trial) and column (variant) was run.

Mac \ MPB	0.00001	0.0001	0.001	0.01	0.1	tmax
1E-11	11.1	11.2	11.3	11.4	11.5	20000000
1E-12	12.1	12.2	12.3	12.4	12.5	20000000
1E-13	13.1	13.2	13.3	13.4	13.5	20000000
1E-14	14.1	14.2	14.3	14.4	14.5	20000000
1E-15	15.1	15.2	15.3	15.4	15.5	20000000

Table 4.3. *M. liliana* (mac) and MPB mortality rates and their corresponding trial and variant number, for trials 18 to 26. Trials 16 and 17 were excluded from analyses (and this table) due to errors. Note that every combination of row (trial) and column (variant) was run.

Mac \ MPB	0.03	0.05	0.07	0.09	tmax
0.000001	18.1	18.2	18.3	18.4	20000000
0.000002	19.1	19.2	19.3	19.4	20000000
0.000003	20.1	20.2	20.3	20.4	20000000
0.000004	21.1	21.2	21.3	21.4	20000000
0.000005	22.1	22.2	22.3	22.4	20000000
0.000006	23.1	23.2	23.3	23.4	20000000
0.000007	24.1	24.2	24.3	24.4	20000000
0.000008	25.1	25.2	25.3	25.4	20000000
0.000009	26.1	26.2	26.3	26.4	20000000

Table 4.4. *M. liliana* (mac) and MPB mortality rates and their corresponding trial and variant number for trial 27. Note that every combination of row (trial) and column (variant) was run.

Mac \ MPB	0.07	tmax
7E-10	27.1	20000000
0. 000000007	27.2	20000000
0. 00000007	27.3	20000000
0. 0000007	27.4	20000000
0. 000007	27.5	20000000

Table 4.5. *M. liliana* and MPB mortality rates and their corresponding trial and variant number, for trials 28 to 31. Note that every combination of row (trial) and column (variant) was run.

Trial	*M. liliana* mortality rate	Variant	MPB mortality rate	tmax
28	0.000001	1	0.1	20000000
28	0.00001	2	0.1	20000000
28	0.0001	3	0.1	20000000
28	0.001	4	0.1	20000000
28	0.01	5	0.1	20000000
28	0.1	6	0.1	20000000
29	0.000001	1	0.01	20000000
29	0.00001	2	0.01	20000000
29	0.0001	3	0.01	20000000
29	0.001	4	0.01	20000000
29	0.01	5	0.01	20000000
29	0.1	6	0.01	20000000
30	0.000001	1	0.001	20000000
30	0.00001	2	0.001	20000000
30	0.0001	3	0.001	20000000
30	0.001	4	0.001	20000000
30	0.01	5	0.001	20000000
30	0.1	6	0.001	20000000
31	0.000001	1	0.0001	20000000
31	0.00001	2	0.0001	20000000
31	0.0001	3	0.0001	20000000
31	0.001	4	0.0001	20000000
31	0.01	5	0.0001	20000000
31	0.1	6	0.0001	20000000

Table 4.6. *M. liliana* and MPB mortality rates and their corresponding trial and variant number, for trials 32 to 46. Note that every combination of row (trial) and column (variant) was run.

Trial	*M. liliana* mortality rate	Variant	MPB mortality rate	tmax
32	0.000002	1	0.00001	20000000
32	0.000004	2	0.00001	20000000
32	0.000006	3	0.00001	20000000
32	0.000008	4	0.00001	20000000
33	0.000002	1	0.00003	20000000
33	0.000004	2	0.00003	20000000
33	0.000006	3	0.00003	20000000
33	0.000008	4	0.00003	20000000
34	0.000002	1	0.00005	20000000
34	0.000004	2	0.00005	20000000
34	0.000006	3	0.00005	20000000
34	0.000008	4	0.00005	20000000
35	0.000002	1	0.00007	20000000
35	0.000004	2	0.00007	20000000
35	0.000006	3	0.00007	20000000
35	0.000008	4	0.00007	20000000
36	0.000002	1	0.00009	20000000
36	0.000004	2	0.00009	20000000
36	0.000006	3	0.00009	20000000
36	0.000008	4	0.00009	20000000
37	0.000002	1	0.0001	20000000
37	0.000004	2	0.0001	20000000
37	0.000006	3	0.0001	20000000
37	0.000008	4	0.0001	20000000
38	0.000002	1	0.0003	20000000
38	0.000004	2	0.0003	20000000
38	0.000006	3	0.0003	20000000
38	0.000008	4	0.0003	20000000
39	0.000002	1	0.0005	20000000
39	0.000004	2	0.0005	20000000
39	0.000006	3	0.0005	20000000
39	0.000008	4	0.0005	20000000
40	0.000002	1	0.0007	20000000
40	0.000004	2	0.0007	20000000
40	0.000006	3	0.0007	20000000
40	0.000008	4	0.0007	20000000
41	0.000002	1	0.0009	20000000
41	0.000004	2	0.0009	20000000
41	0.000006	3	0.0009	20000000
41	0.000008	4	0.0009	20000000
42	0.000002	1	0.001	20000000
42	0.000004	2	0.001	20000000
42	0.000006	3	0.001	20000000
42	0.000008	4	0.001	20000000
43	0.000002	1	0.003	20000000
43	0.000004	2	0.003	20000000
43	0.000006	3	0.003	20000000
43	0.000008	4	0.003	20000000
44	0.000002	1	0.005	20000000
44	0.000004	2	0.005	20000000
44	0.000006	3	0.005	20000000
44	0.000008	4	0.005	20000000
45	0.000002	1	0.007	20000000
45	0.000004	2	0.007	20000000
45	0.000006	3	0.007	20000000
45	0.000008	4	0.007	20000000
46	0.000002	1	0.009	20000000
46	0.000004	2	0.009	20000000
46	0.000006	3	0.009	20000000
46	0.000008	4	0.009	20000000

Table 4.7. Light availability test trial numbers and their corresponding light attenuation (k_d) depth (m). Trials one, three, five, and seven are excluded due to errors.

Trial	k_d
2	0.2
4	0.4
6	0.6
8	0.8
9	1.0
10	1.2
11	1.4
12	1.6
13	1.8
14	2.0
15	2.2
16	2.4
17	2.6
18	2.8
19	3.0

Table 4.8. Mud content test trial numbers and their corresponding sediment mud content (M_c) (%).

Trial	M_C
1	0.1
2	0.2
3	0.3
4	0.4
5	0.5
6	0.6
7	0.7
8	0.8
9	0.9
10	1

Table 4.9. External nutrient test trial numbers and their corresponding external nutrient (IN) value (mmol N m^{-2}).

Trial	*IN*
1	1
2	10
3	100
4	1000
5	10000
6	100000

4.3 Observations Trials one to ten

Trial 6 variant 10 (Table 4.1) was used as a base case when analysing relationships between variables in trials one to ten. B_{MPB} values across trials and variants were consistently different from what is seen in nature (except for several outliers), meaning more weight was given to the matching of B_{mac} values when selecting results for relationship analysis.

4.3.1 Biomass

Figure 4.1 (a) demonstrates a large disparity in biomass across various M_{mac} values. B_{mac} values increase on a positive trend until trial five variant nine, where values begin to drop below that of previous variants. This pattern is followed throughout the rest of the trials, where once M_{MPB} reaches 0.001 (g C m^{-2}) (see Table 4.1) M_{mac} begins to decrease. From this, we assumed that a smaller M_{mac} will result in a larger B_{mac} and that M_{MPB} influences M_{mac}. While our assumptions partially were correct, as a very strong negative relationship exists between B_{mac} and M_{MPB} (r = -.979, p = <.00001), no significant relationship exists between B_{mac} and M_{mac} (r = -.423, p = .178). B_{mac} has a range of over 70 g C m^{-2}, with the majority of trials appearing to have not reached a stable biomass by t_{max}. A stable biomass, as seen in Figure 4.1 (b), will oscillate around the organism's carrying capacity (K_{MPB}), as the biomass rises and falls around this value. In Figure 4.1 (a), we see a continuation of the growth or reduction of B_{mac} at t_{max}. In some instances, B_{mac} dropped to near zero g C m^{-2} and remained consistently low for long periods of time. B_{mac} is much larger than this in nature (Figure 4.2), meaning these results are unfavourable.

B_{MPB} values in Figure 4.1 (b) behave much differently to those in Figure 4.1 (a). Irrespective of the trial number, B_{MPB} approaches carrying capacity (K_{MPB}) within 300 days. The oscillation of B_{MPB}, shown by the magenta line between 0.7-1 g C m^{-2}, demonstrates the MPB population fluctuating above and below K_{MPB}. While K_{MPB} within the model is set to 1.2 g C m^{-2}, it is not unexpected to see results below this threshold, as different variations of the model across trials may reduce K_{MPB} naturally. This is due to a larger B_{mac} being present (from their mortality rate being reduced), which allows for more predation of MPB to occur. A reduction in K_{MPB} can also occur with an increasing M_{MPB}, further explaining the varying K_{MPB} values observed. A very strong negative relationship exists between B_{MPB} and M_{MPB} (r = -1, p = <.00001), while there is no significant relationship between B_{MPB} and M_{mac} (r = -.493, p = .147).

B_{mac} at Tuapiro Point is 41.768 g C m^{-2}, while an expected B_{MPB} is 1.056 g C m^{-2}. Figure 4.2 demonstrates that only one result from trials one to ten produced a B_{mac} value close to that seen in nature (Trial six, variant ten – 41.51 g C m^{-2}). There is a fairly even spread of B_{mac} values above and below natural levels. No trials produced a B_{MPB} value close to natural levels, with nearly all values being too large. Figure 4.2 (c) shows that there is little variation in B_{MPB} (shown by the large overlap in results), despite a change in M_{MPB}. B_{MPB} sits above 1.195 g C m^{-2} throughout all variants of all trials, until variants ten and 11. Here, we see a significant drop in biomass at the 95% confidence interval (t = -3.312, p = .0091, df = 1). This further highlights the negative relationship between B_{MPB} and M_{MPB}. We have also identified our threshold in which B_{MPB} can be sustained, before dropping below K_{MPB} by a significant value. We assumed that a secondary variable, the consumption of MPB by *M. liliana* ($G_{macgraz}$), may also be important for controlling B_{MPB}. This theory was considered in later testing. Figure 4.2 was used alongside Figure 4.1 to progress our trial runs, with the objective of producing results that fit the centre of the red and blue lines. t_{max} was increased from $1.5e^{-6}$ to $2e^{-6}$ time steps, as no significant change in results were identified in trial ten (where t_{max} was considerably extended). Time restraints on the project did not permit such large t_{max} values (taking several days of processing time to complete). Following our interpretations from trials one through ten, we continued with the assumption that a smaller M_{mac} would lead to a larger B_{mac}, and tested this theory in more depth by extending the length of the trial from $1.5e^{6}$ to $2.0e^{6}$ time steps.

Figure 4.1. Timeseries plot of biomass values (g C m^{-2}) per time step for trials one to ten for *M. liliana* (a) and MPB (b). Trials are plotted along a colour scale progressing from blue to magenta (MATLAB's 'cool colormap'). Trial ten was run to on an unrestricted timeframe, to identify if an increased t_{max} would significantly alter results.

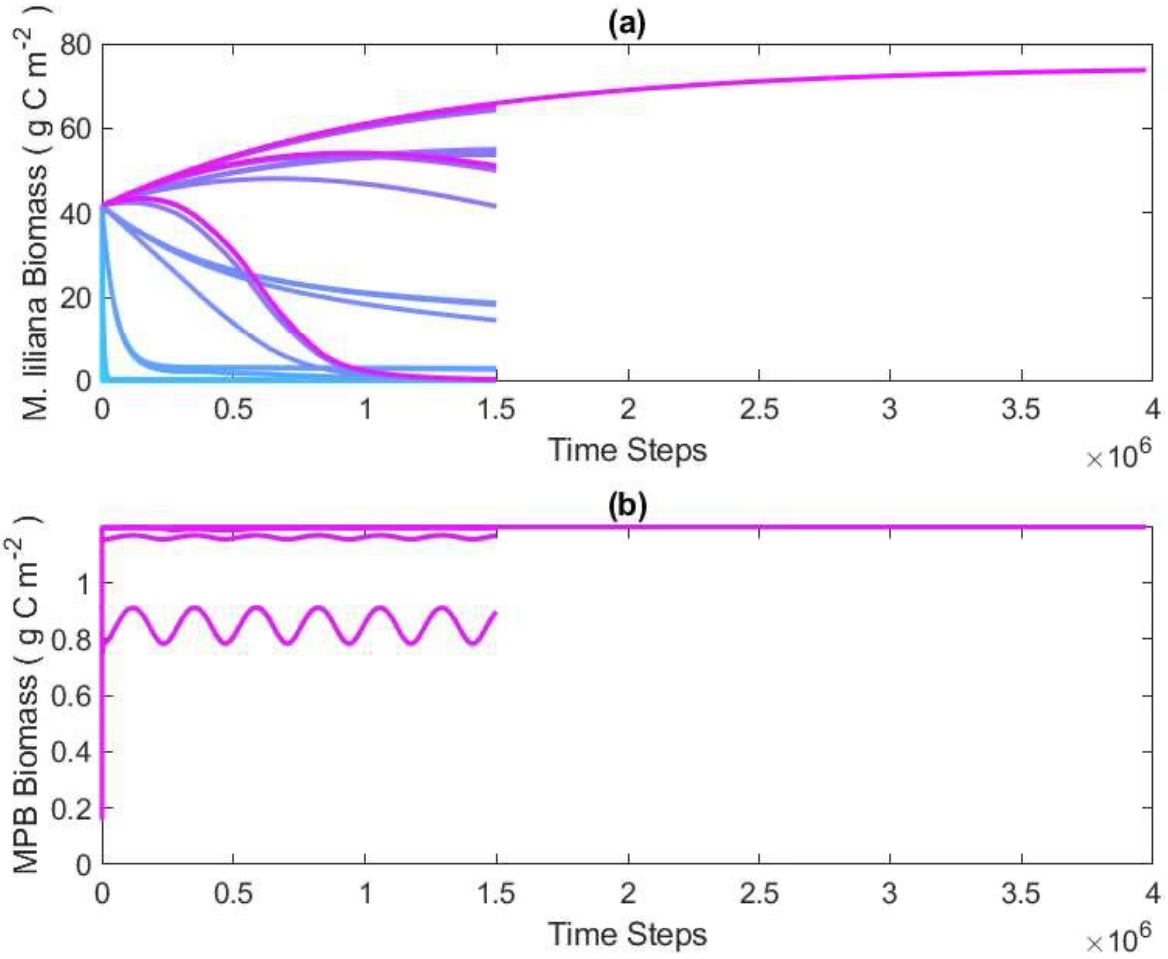

Figure 4.2. Scatter graphs demonstrating the biomass of *M. liliana* and MPB. The graph includes values from all results across trials one to ten. The vertical red line illustrates an average MPB biomass (1.056 g C m^{-2}) within the Tauranga Harbour ((Flowers et al., in review) and the horizontal blue line illustrates an average *M. liliana* biomass (41.768 g C m^{-2}) found within Tauranga Harbour (Thrush et al., 2021). The colour scale in (a) denotes the different *M. liliana* mortality rate (per time step) log formed in each trial; the colour scale in (b) denotes the different MPB mortality rates (per time step) log formed in each trial; the colour scale in (c) corresponds to the 'variant' number for MPB mortality across trials (see Table 4.1); and the colour scale in (d) refers to the 'trial' number for *M. liliana* mortality rate across trials (see Table 4.1).

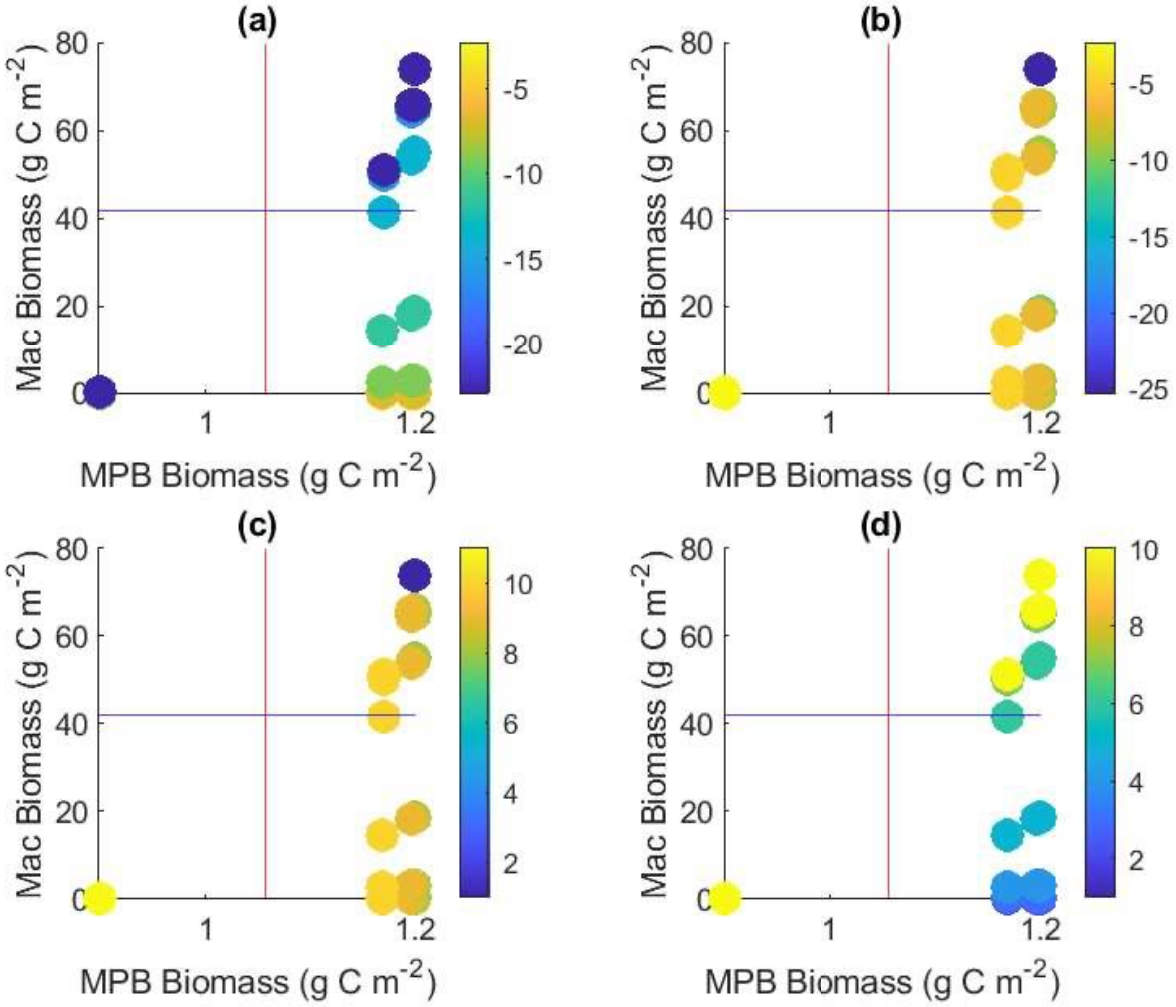

4.3.2 ***Nutrients***

Nutrients in the system increase throughout the duration of trials one through ten (Figure 4.3). This is to be expected, as nutrients from within the sediment are added to the system by *M. liliana* pumping behaviour. Both (a) and (b) in Figure 4.3 have a range of 0 to 60,000 mmol N m^{-2}, showing that the model is mixing nutrient pools until equilibrium is reached. There is no significant relationship between M_{mac} and N_{mac} or N_{MPB} (r = .460, p = .181). However, a very strong positive relationship exists between the M_{MPB} and both nutrient pools (r = 1, p = <.00001). When comparing Figure 4.1 (b) and Figure 4.3 (b), we see that increasing nutrients does not fuel an MPB bloom. A couple of assumptions were

made following this finding; 1) MPB have reached K_{MPB}, meaning additional nutrients cannot increase their biomass further, or 2) MPB are not nutrient limited, but light limited, so additional nutrients cannot increase their biomass further. Figure 4.3 (b) also highlights the need for a toxicity parameter within the water column, as nutrients are allowed to increase past the rate of consumption with no impact on MPB's carrying capacity (Figure 4.1 (b).

Figure 4.3. Timeseries plot of nutrient values (mmol N m^{-2}) per time step for trials one to ten for *M. liliana* (a) and MPB (b). Trials are plotted along a colour scale progressing from blue to magenta (MATLAB's 'cool colormap').

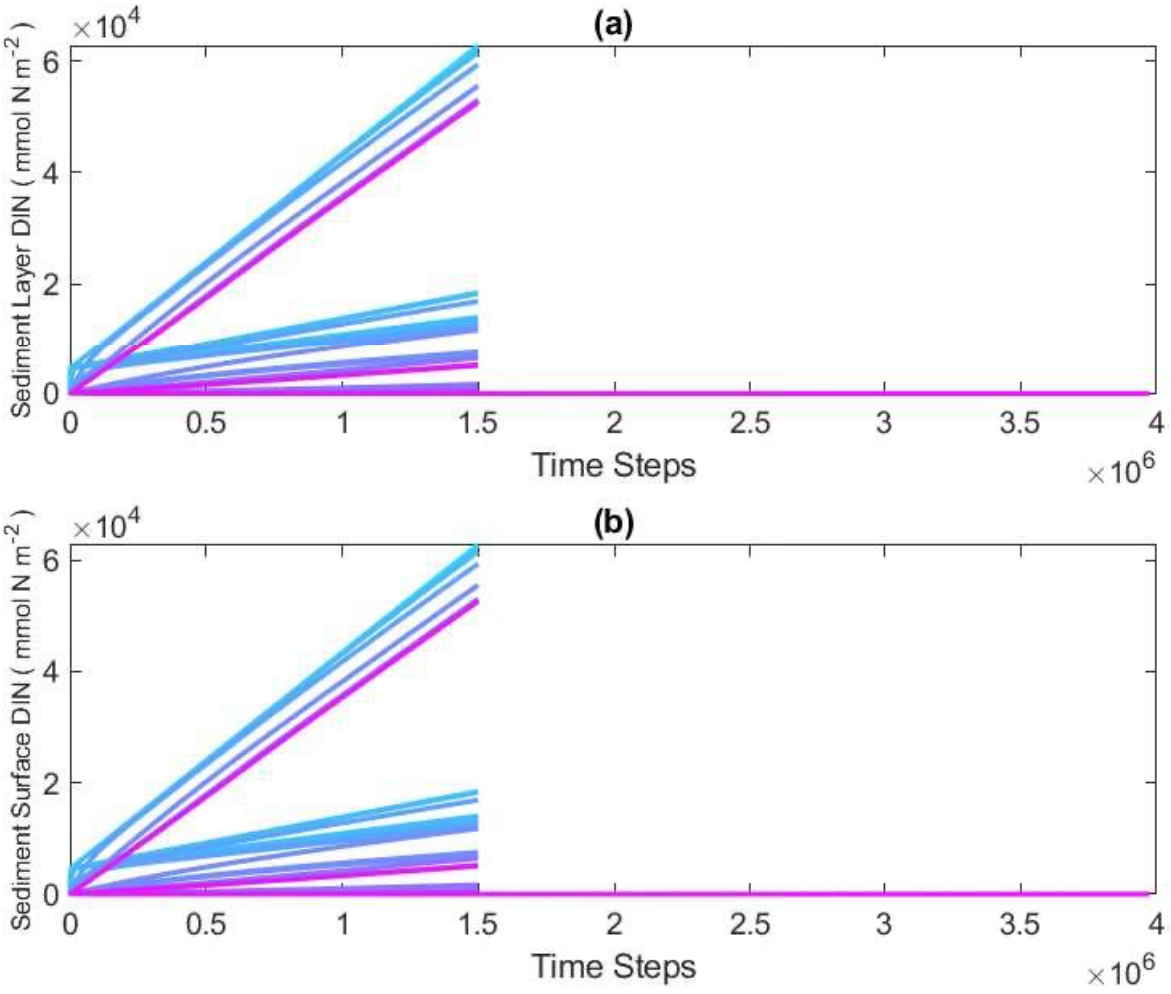

4.3.3 ***Detritus***

D_{mac} levels in trials one to ten rapidly drop from their initial boundary conditions to <0.21 g C m^{-2} within 20,000 time steps, and stay below this level for the remainder of the trial (Figure 4.4 (a)). D_{mac} values have a range from 0.0243 2.201e^{-9} g C m^{-2}, showing no significant relationship with M_{mac} (r = .484, p = .155). However, a very strong negative

relationship exists between D_{mac} *and* M_{MPB} (r = -.989, p = <.00001). Our results demonstrate that detritus is rapidly transitioning back into nitrogen and entering the sediment layer (Figure 4.3). This is likely due to a combination of the carbon breakdown parameter (*C2N*) and *M. liliana* pumping behaviour (P_{mac}) working to remove detritus from the sediment layer, and the biomass decay rate (C_{mac}) being too small (see *section 3.8 & 3.10*).

D_{MPB} values in trials one to ten range from 3.60 to 4.81e^{-5} g C m^{-2} (Figure 4.4 (b)), considerably larger than that of B_{MPB}. Only variant 11 has results that sit above 1 g C m^{-2}, demonstrating that the M_{MPB} is the controlling factor for D_{MPB} A very strong positive relationship exists between the D_{MPB} and M_{MPB} (r = .999, p = <.00001), while no significant relationship exists with M_{mac} (r = -.479, p = .161). As there is no set carrying capacity for D_{MPB}, D_{MPB} is able to be maintained in considerably larger quantities than B_{MPB}. D_{MPB} values are also considerably larger than D_{mac}; the largest D_{MPB} value is 300% larger than K_{MPB}, compared to *M. liliana's* being <0.02% of the K_{mac}.

Figure 4.4. Timeseries plot of detrital values (g C m^{-2}) per time step for trials one to ten for *M. liliana* (a) and MPB (b). Trials are plotted along a colour scale progressing from blue to magenta (MATLAB's 'cool colormap').

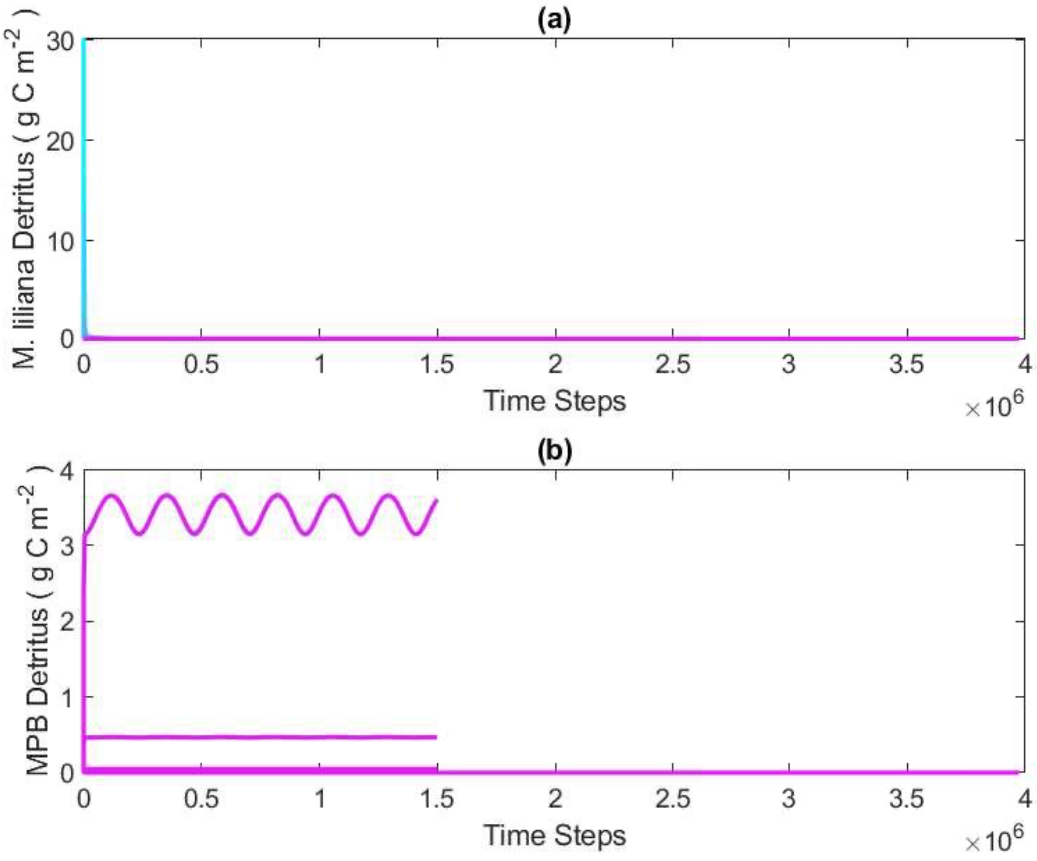

4.3.4 *Key Findings*

- Very strong relationships exist between M_{MPB} and the biomass, nutrient, and detrital values for both species.
- No significant relationships exist between M_{mac} and biomass, nutrients, or detritus.
- B_{mac} does not stabilise across all trials and variants, but B_{MPB} does.
- Trial ten variant six closest B_{mac} values to what is seen in nature.
- Nutrients increasing within the system do not fuel an MPB bloom.
- D_{mac} is rapidly converted into nitrogen and removed from sediments.
- Detrital values are considerably higher (MPB) or lower (*M. liliana*) than the corresponding species' biomass values.

4.4 Observations Trials ten to 15

Results from trial 11 variant four were used in the analysis of relationships within trials 11-15. Due to limited colormaps available in Matlab, results can be hard to interpret. Trials 11 to 15 were chosen for Matlab's 'autumn colormap' due to their low variance and high overlap, meaning few intricacies between trials need to be interpreted.

4.4.1 *Biomass*

Trials 11-15 are difficult to distinguish. Despite the colormap in Figure 4.5 ranging from red to yellow, only yellow is seen as biomass values from later trials overlap values from earlier ones. The range of biomass values is similar to that of trials one to ten, >70 g C m^{-2}. Finding similar results for B_{mac} was unsurprising, given that our assumption of a negative relationship existing between M_{mac} and B_{mac} was proven to not be significant in previous trials. We continued trial a reducing M_{mac}, as we suspected this may change. In trials 11 to 15, no relationship exists between M_{mac} and B_{mac}; however, a very strong negative relationship exists between B_{mac} and M_{MPB} (r = -.966, p = .00749). B_{mac} continues to not stabilise, despite the increase in t_{max}. From this we assumed two things; 1) B_{mac} will continue to decline, possibly due to a lack of food or toxicity levels becoming too large to sustain the population, or 2) B_{mac} is beginning to oscillate around the carrying capacity (like B_{MPB} in Figure 4.1 (b)), but oscillates over a much longer period than MPB. Option two is plausible, as despite K_{mac} being set at 74.8 g C m^{-2}, this value will decrease as nutrients levels in the sediment increase.

Following an increase in nutrients, the sediment begins to become toxic and can no longer support the existing biomass (leading to a reduction in K_{mac}) (*see Section 3.5*). Regardless of the plausibility of this assumption, time limitations meant we could not extend t_{max} to test the theory. Additionally, we believed B_{mac} would stabilise once M_{mac} was set to an appropriate value.

Figure 4.5 (b) demonstrates a refinement in M_{MPB}, as only the largest five mortality values from trials one to ten (0.0001 to 0.1, increasing by one order of magnitude in each trial) were used in trials 11 to 15 (Table 4.2). Unfortunately, these changes did little to alter B_{MPB} results, when compared to trials one to ten (Figure 4.1 (b)). This is further highlighted in Figure 4.6 (b), where B_{MPB} results from trials 11 to 15 can be seen to overlap with results from trials one to ten. We found no relationship between B_{MPB} and the M_{mac}, but a very strong negative relationship between B_{MPB} and M_{MPB} continues to exist (r = -1, p = <.00001).

Figure 4.7 demonstrates that, despite the refining of the M_{mac} and M_{MPB} in trials 11-15, still no trials produce results that are the same as values in nature. While more results now sit closer to B_{mac} values in nature, B_{MPB} values from all trials are either too high or too low. The spread of B_{MPB} values for trials 11 to 15 are near identical to that from trials one to ten, meaning that continuing to reduce M_{mac} to achieve the desired result was not working. However, what has become more apparent in Figure 4.7 is the relationship between B_{mac} and M_{MPB}. This is shown prominently in Figure 4.7 (d), where B_{mac} values in variations of trial 15 range from 69.09 g C m^{-2} to 0.05 g C m^{-2} (shown by the yellow dots).

Figure 4.5. Timeseries plot of biomass values (g C m^{-2}) per time step for trials 11 to 15 for *M. liliana* (a) and MPB (b). Trials are plotted along a colour scale progressing from red to yellow (MATLAB's 'autumn colormap').

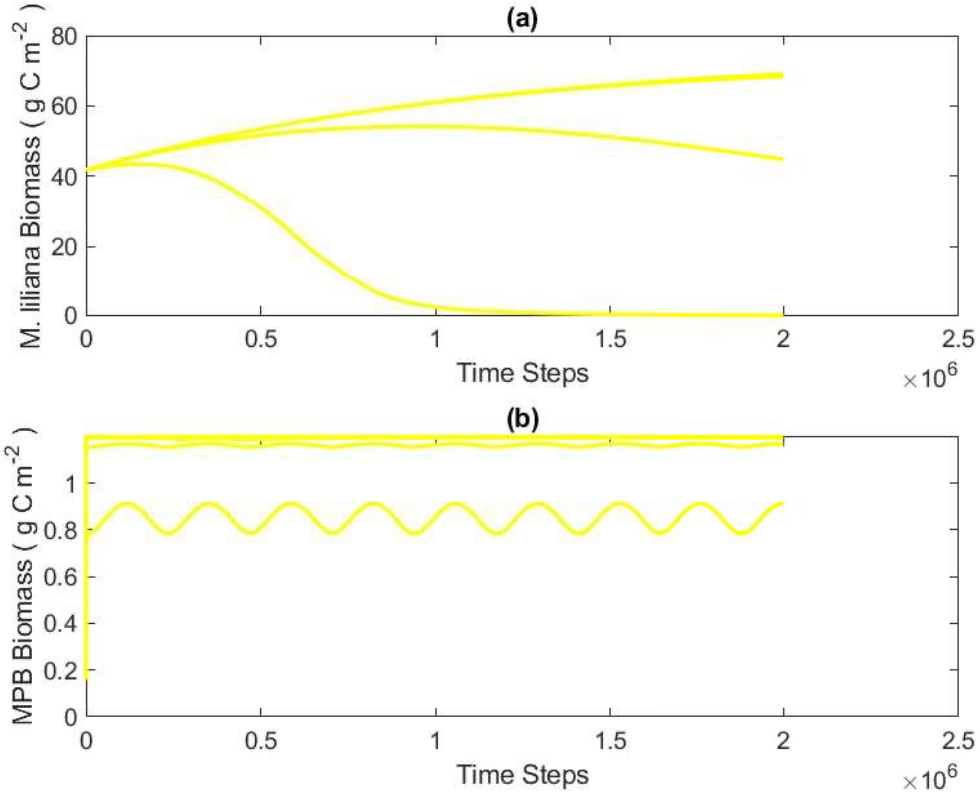

Figure 4.6. Timeseries plot for biomass values (g C m^{-2}) per time step for trials one to 15 for *M. liliana* (a) and MPB (b). Trials are plotted along a colour scale, with colours for trials one to ten progressing from blue to magenta (MATLAB's 'cool colormap'), and colours for trials 11 to 15 progressing from red to yellow (MATLAB's 'autumn colormap').

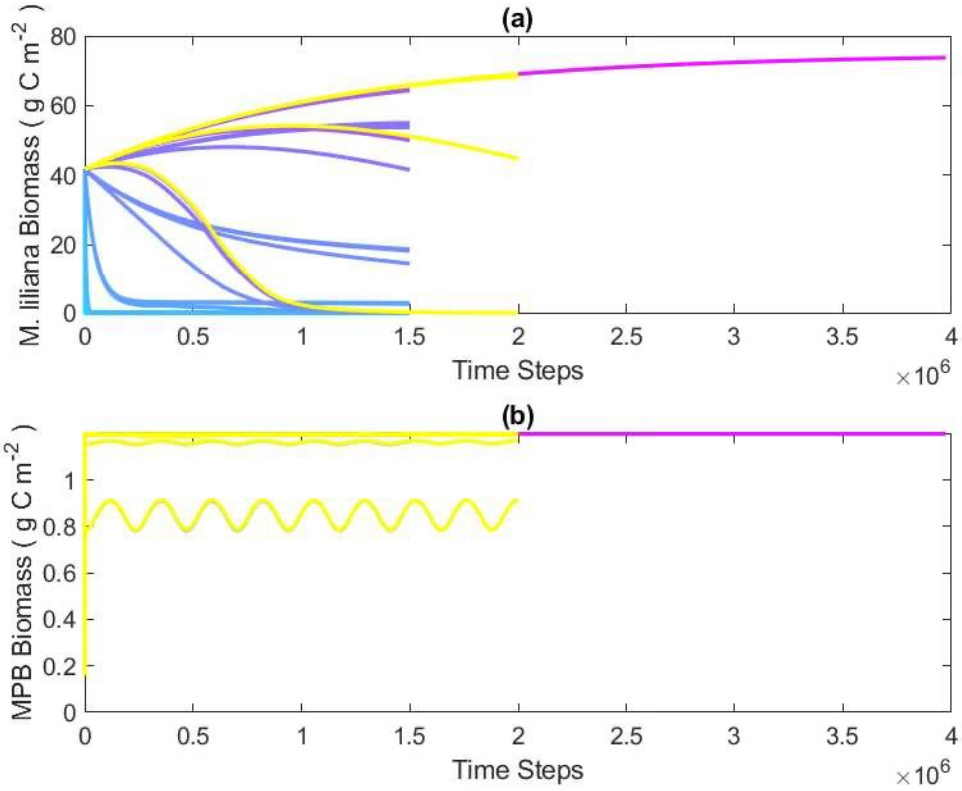

Figure 4.7. Scatter graphs demonstrating the biomass of *M. liliana* and MPB at the conclusion of all results from trial one to 15. The vertical red line illustrates an average MPB biomass (1.056 g C m^{-2}) within Tauranga Harbour (Flowers et al., in review) and the horizontal blue line illustrates an average *M. liliana* biomass (41.768 g C m^{-2}) found within Tauranga Harbour (Thrush et al., 2021). The colour scale in (a) denotes the different *M. liliana* mortality rate (per time step) log formed in each trial; the colour scale in (b) denotes the different MPB mortality rates (per time step) log formed in each trial; the colour scale in (c) corresponds to the 'variant' number for MPB mortality across trials (see Table 4.1 & 4.2); and the colour scale in (d) refers to the 'trial' number for *M. liliana* mortality rate across trials (see Table 4.1 & 4.2).

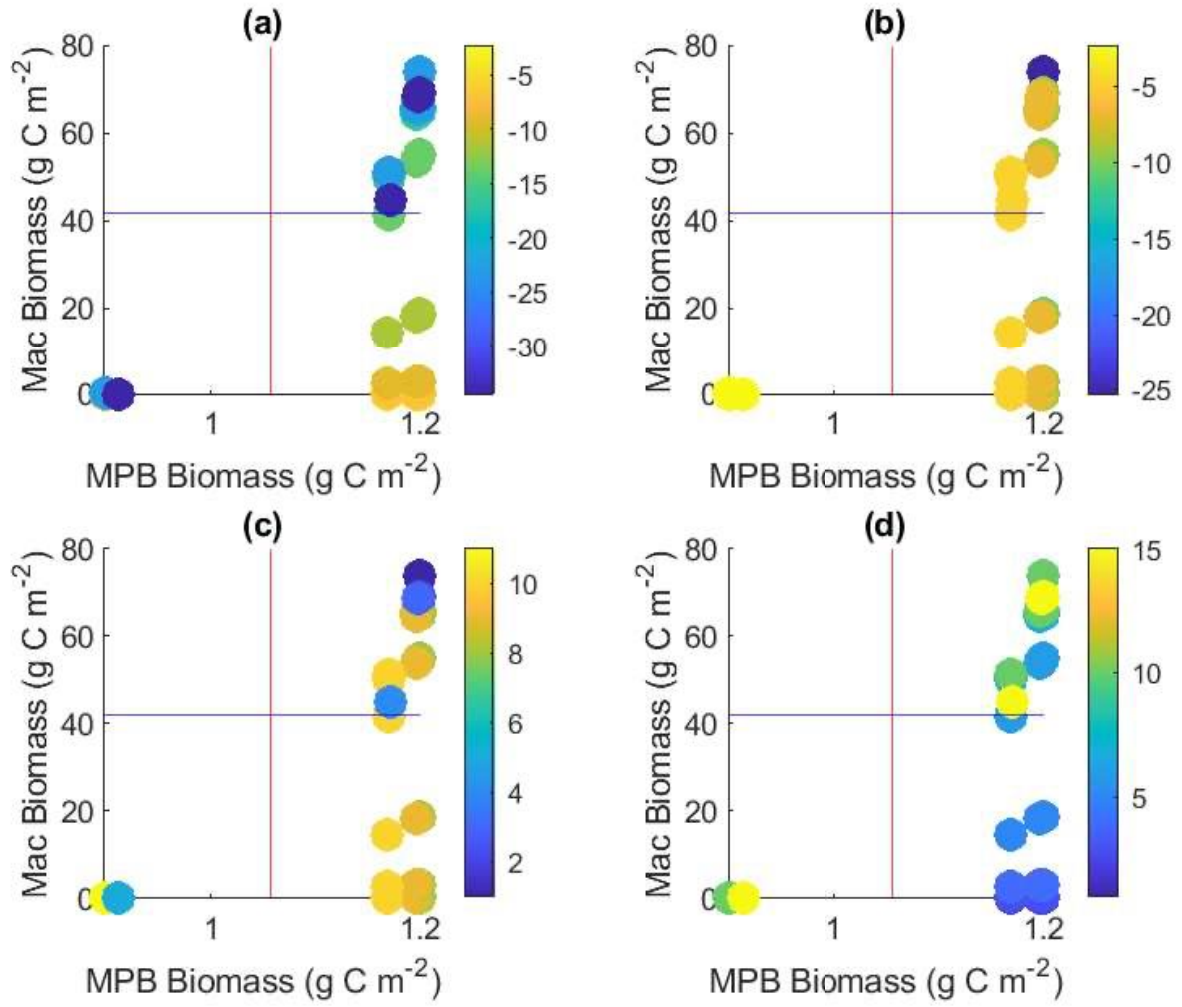

4.4.2 Nutrients

N_{mac} and N_{MPB} values continue to increase with time, and mix until equilibrium. Nutrients in trials 11 to 15 have a larger range than previous trials, ranging from 69,942 to 0.133 mmol N m^{-2} (Figure 4.8). N_{mac} and N_{MPB} values do no change with M_{mac}, with analysis showing no relationship between the two variables. However, there continues to be a very strong positive relationship between M_{MPB} and nutrients (Trials 11 to 15, $r = 1$, $p = <.00001$).

Figure 4.8. Timeseries plot of nutrient values (mmol N m^{-2}) per time step for trials 11 to 15 for *M. liliana* (a) and MPB (b). Trials are plotted along a colour scale progressing from red to yellow (MATLAB's 'autumn colormap').

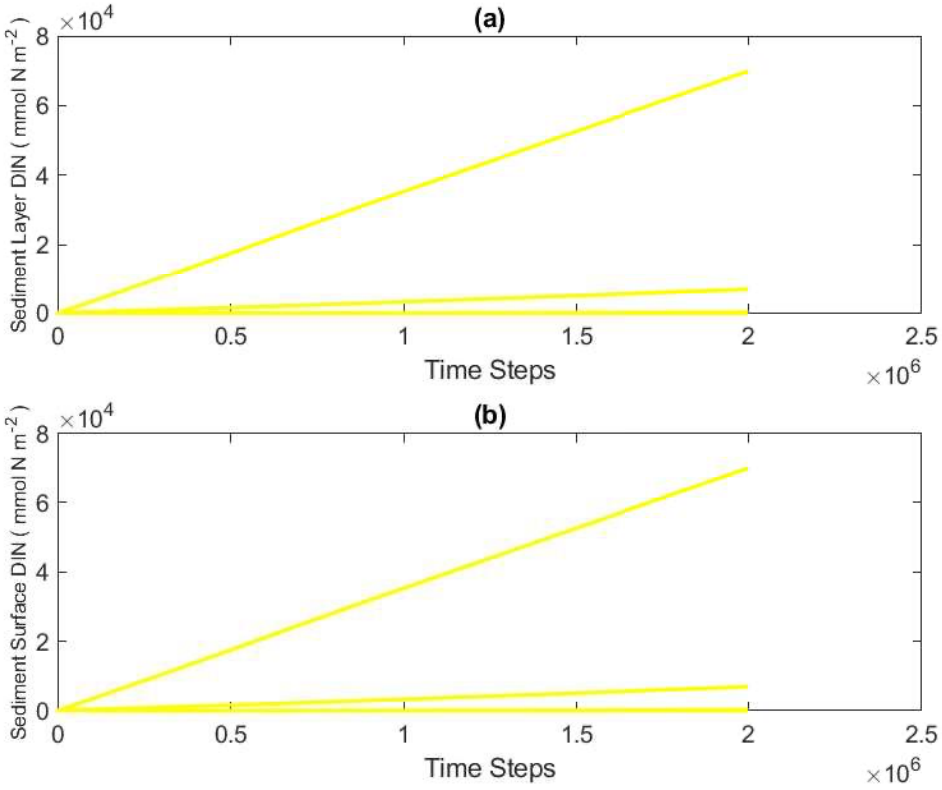

Figure 4.9. Timeseries plot of nutrient values (mmol N m^{-2}) per time step for trials one to 15 for *M. liliana* (a) and MPB (b). Trials are plotted along a colour scale, with colours for trials one to ten progressing from blue to magenta (MATLAB's 'cool colormap'), and colours for trials 11 to 15 progressing from red to yellow (MATLAB's 'autumn colormap').

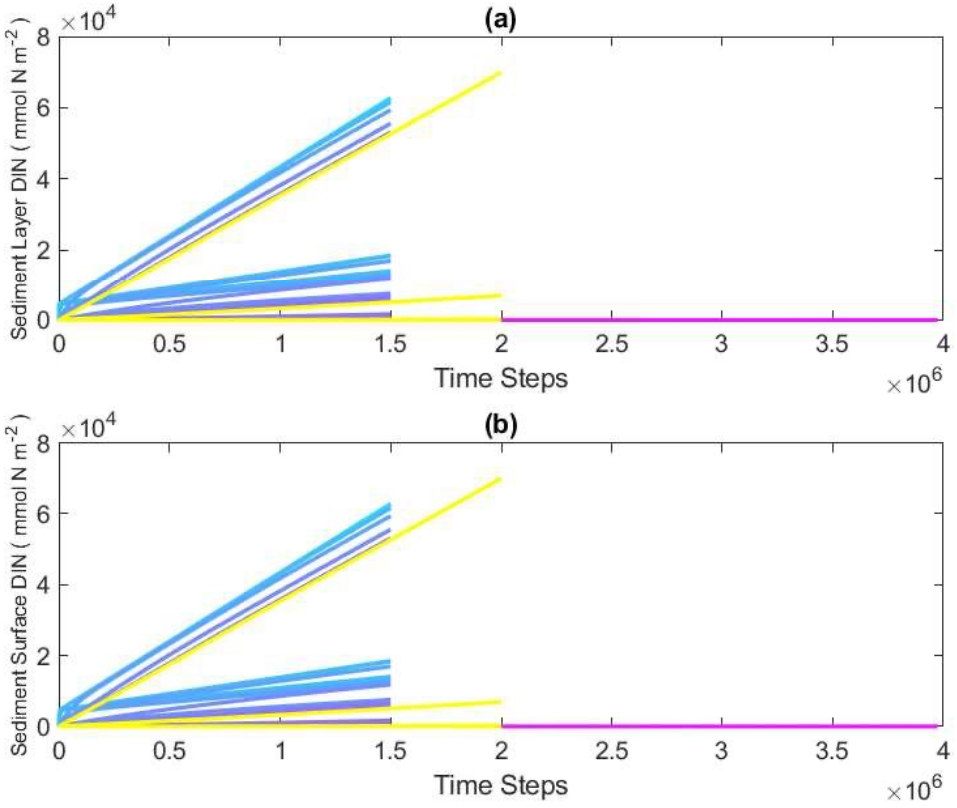

4.4.3 ***Detritus***

D_{mac} values in trials 11 to 15 (Figure 4.10 (a)) range from $3.534e^{-10}$ to $4.865e^{-8}$ g C m^{-2}, and continue on the same trend as previous trials (*see 4.3.3*). However, unlike trials one to ten, D_{mac} values in trials 11 to 15 have a very strong positive relationship with M_{mac} (r = 1, p = <.00001), with D_{mac} and M_{mac} values decreasing by one order of magnitude with each trial. A very strong negative relationship exists between D_{mac} and M_{MPB} (r = -.966, p = .0085) also. D_{mac} values continue to remain at levels considerably lower than corresponding B_{mac} values.

D_{MPB} values in trials 11 to 15 (Figure 4.10 (b)) range from 3.662 to $4.82e^{-4}$ g C m^{-2}, nearly identical to previous trials (*see 4.3.3*) and still considerably larger than B_{MPB}. No relationship exists between D_{MPB} and M_{mac}. Therefore, the factor influencing D_{MPB} must be the M_{MPB}, to which a very strong positive relationship exists (r = .999, p = .000038).

Figure 4.10. Timeseries plot of detrital values (g C m^{-2}) per time step for trials 11 to 15 for *M. liliana* (a) and MPB (b). Trials are plotted along a colour scale progressing from red to yellow (MATLAB's 'autumn colormap').

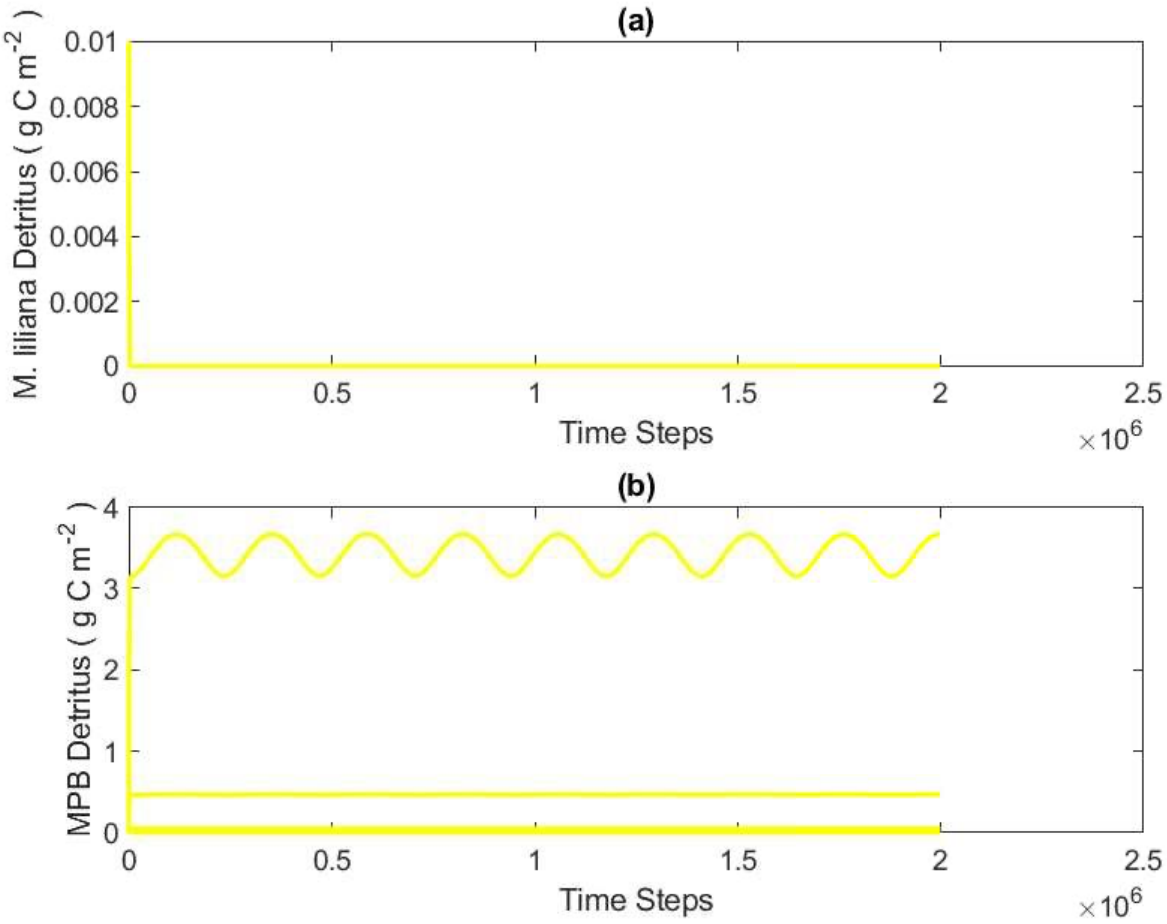

Figure 4.11. Timeseries plot of detrital values (g C m^{-2}) per time step for trials one to 15 for *M. liliana* (a) and MPB (b). Trials are plotted along a colour scale, with colours for trials one to ten progressing from blue to magenta (MATLAB's 'cool colormap'), and colours for trials 11 to 15 progressing from red to yellow (MATLAB's 'autumn colormap').

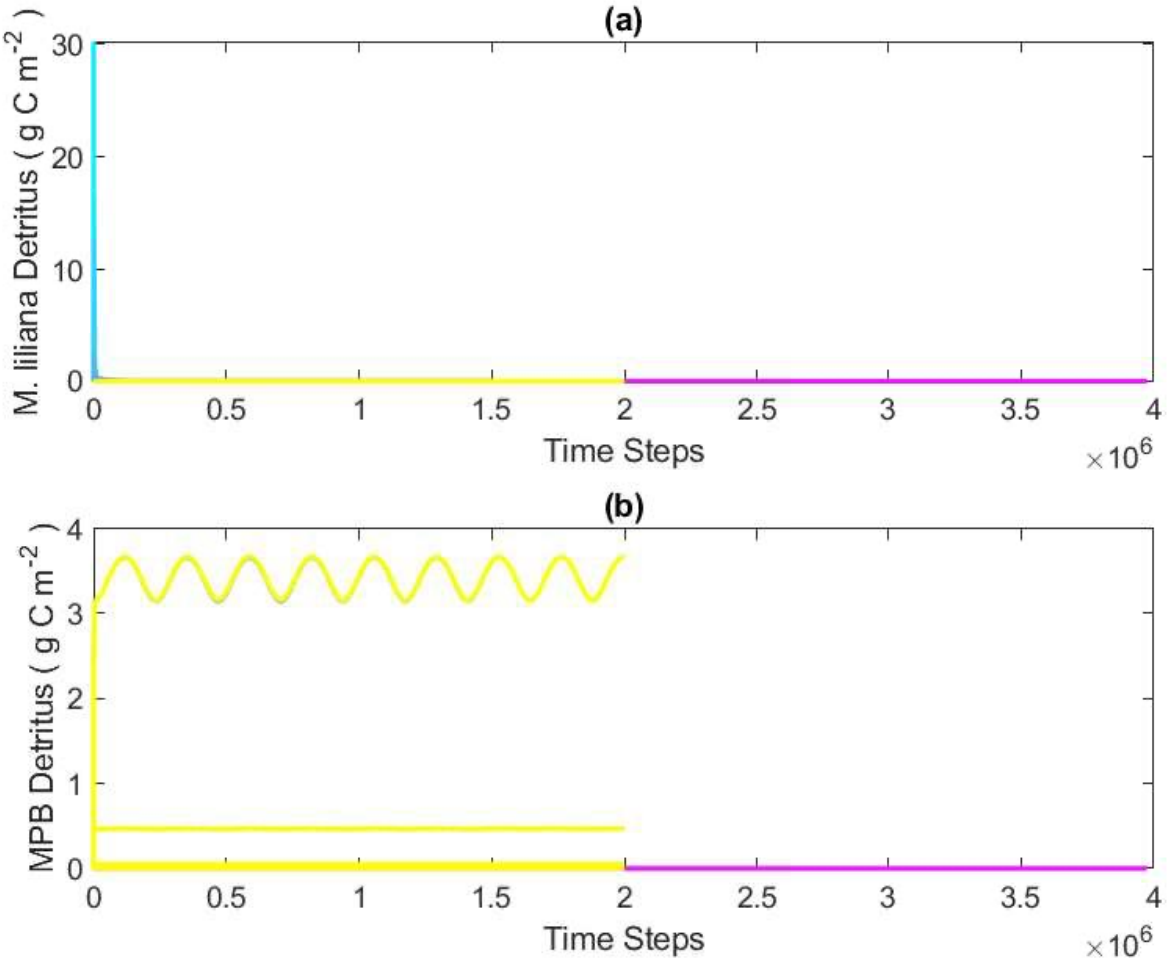

4.4.4 *Key Findings*

- M_{mac} only shares a relationship with D_{mac}.
- Very strong relationships exist between M_{MPB} and the biomass, nutrient, and detrital values for both species.
- Biomass results for both species are further from their natural values across all trials, when compared to trials one to ten.

4.5 Observations Trials 18 to 27

For trials 18 to 26, we no longer continued on the trend of reducing M_{mac} by one order of magnitude (see Table 4.3), but instead chose to set M_{mac} values between that seen in trials six and seven – trial six produced a B_{mac} most similar to that seen in nature (Figure 4.2 and 4.7). A similar change was made with M_{MPB} values (Table 4.3). As no variant had produced B_{MPB} values close to what is seen in nature, M_{MPB} was also refined based upon trial six, using variant ten. M_{mac} in trial 27 was structured differently to trials 18 to 26 (Table 4.4), with M_{MPB} staying within a similar range. We chose to group trial 27 with trials 18 to 26 as they showed similar results. Results from variant two across trials 18 to 27 (Table 4.3 & 4.4) were used when analysing relationships between variables. Due to the structure of testing in trials 18 to 27 (Table 4.3 & 4.4), insufficient data was available to test for relationships with M_{MPB}. Trials 16 and 17 were excluded from analyses due to errors.

4.5.1 Biomass

Variants amongst trials 18 to 27 in Figure 4.12 (a) produce results that follow a similar trend to one another; B_{mac} gradually reduces from boundary conditions to low levels. This trend is different to results we have seen from the first 15 trials thus far, as earlier trials have often produced results that overlap or show very little variation. A very strong negative relationship exists between B_{mac} and M_{mac} (r = -.966, p = .000023).

Figure 4.12 (b) does not confirm our assumption that $G_{macgraz}$ was a variable controlling B_{MPB}. Figure 4.12 (b) demonstrates a distinct overlap in B_{MPB} values across all four M_{MPB} variants, indicating that a change in M_{MPB} is responsible for the variations in B_{MPB}. If B_{mac} was controlling B_{MPB} through consumption (which increases in rate with increasing B_{mac}), we would likely see nine identifiable B_{MPB} values that align with the nine variants of M_{mac}. Instead, B_{MPB} increases alongside B_{mac}, which may infer that the nutrient cycling occurring through $G_{macgraz}$ is more beneficial for B_{MPB} than detrimental (*see sections 3.4, 3.6, and 3.10*. Unfortunately, the sample size for trials 18 to 27 is too small to confidently identify a relationship between B_{MPB} and M_{MPB}; however, in earlier trials we identified a strong negative relationship (Trial 15, r = -.999, p =.000038) that appears to continue on in later trials. Therefore, we continue to assume that M_{MPB} is the primary influence of B_{MPB}.

Figure 4.12. Timeseries plot of biomass values (g C m^{-2}) per time step for trials 18 to 27 for *M. liliana* (a) and MPB (b). Trials are plotted along a colour scale progressing from dark green to lime (MATLAB's 'summer colormap').

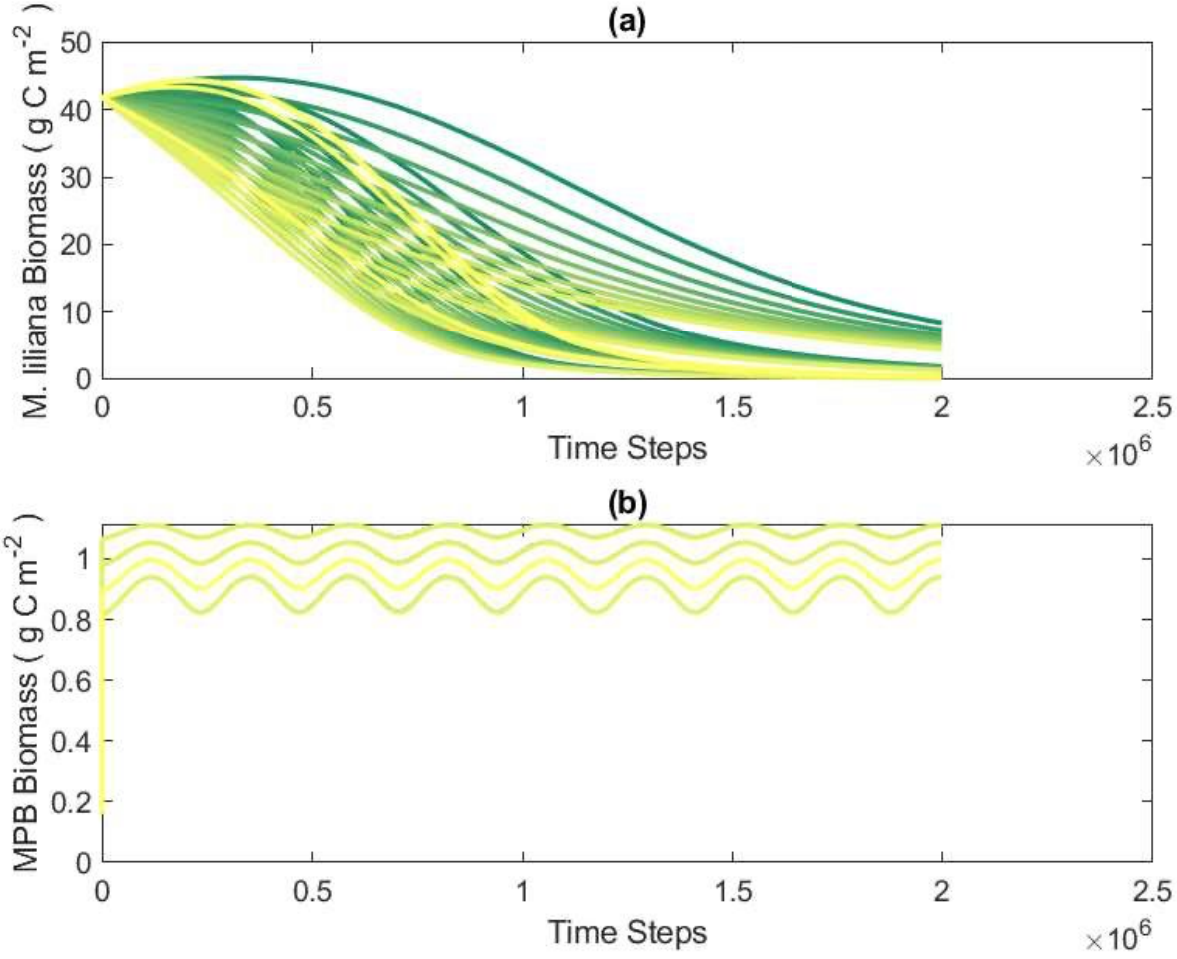

Figure 4.13. Timeseries plot for biomass values (g C m^{-2}) per time step for *M. liliana* (a) and MPB (b). Data was used from trials one through to 27, excluding trials 16 & 17 due to errors. Trials are plotted along several colour scales; trials one to ten are plotted in colours progressing from blue to magenta (MATLAB's 'cool colormap'), 11 to 15 are plotted in colours progressing from red to yellow (MATLAB's 'autumn colormap'), and 18 to 27 are plotted in colours progressing from dark green to lime (MATLAB's 'summer colormap'),

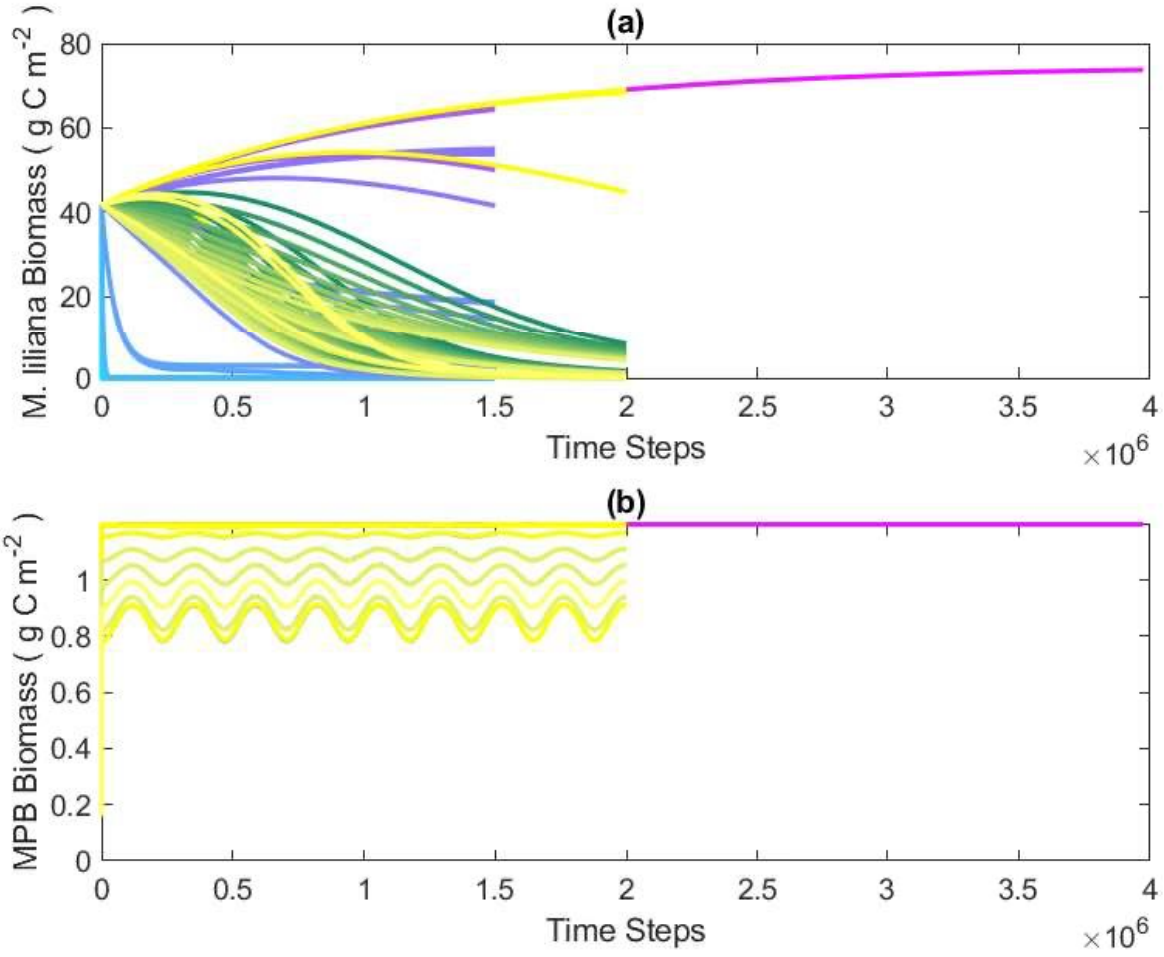

Figure 4.14. Scatter graphs demonstrating the biomass of *M. liliana* and MPB at the conclusion of each trial (excluding trial 16-17) from trials one to 27. The vertical red line illustrates an average MPB biomass (1.056 g C m^{-2}) within Tauranga Harbour (Flowers et al., in review) and the horizontal blue line illustrates an average *M. liliana* biomass (41.768 g C m^{-2}) found within Tauranga Harbour (Thrush et al., 2021). The colour scale in (a) denotes the different *M. liliana* mortality rate (per time step) log formed in each trial; the colour scale in (b) denotes the different MPB mortality rates (per time step) log formed in each trial; the colour scale in (c) corresponds to the 'variant' number for MPB mortality across trials (see Table 4.1, 4.2, & 4.3); and the colour scale in (d) refers to the 'trial' number for *M. liliana* mortality rate across trials (see Table 4.1, 4.2, & 4.3).

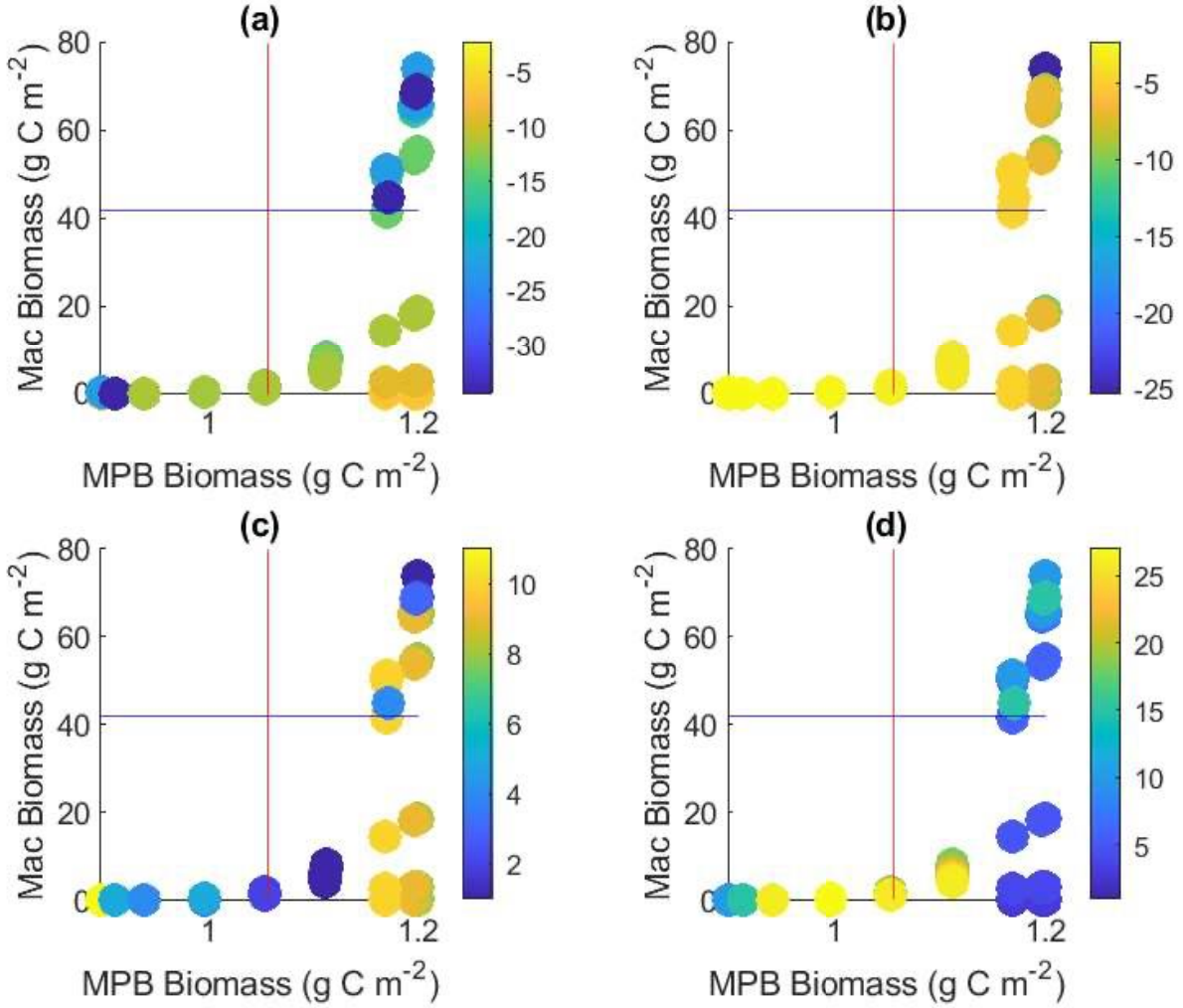

4.5.2 ***Nutrients***

N_{mac} and N_{MPB} in trials 18 to 27 follow a similar trend to previous trials (Figure 4.16). Despite trial 27 having five variants, its results still fit within four distinct groups – trials 18 to 26 having four variants (*see Section 4.5 for explanation on grouping trial 27*). Nutrient values increase with time across trials, with nutrient values increasing with the variants within trials also. This is shown by the progression of dark green to lime colouring in Figure 4.15. This pattern is broken by trial 27, where there is the distinct lime, dark green, lime sequence in one of the groupings. In trials 18 to 27 a very strong positive relationship exists

between the M_{mac} and nutrients (r .991, p = <.00001). In previous trials, this relationship has been moderately positive (*see Section 4.3.*2) and undetectable (*see Section 4.4.*2).

Figure 4.14 shows that refining mortality values has not produced biomass values similar to that seen in nature for both species simultaneously. Therefore, a new question was raised. Was N_{mac} becoming too large, creating a toxic environment and causing K_{mac} to reduce too far? Highlighting trial 20, which we knew to have B_{mac} values reducing well below the levels found in nature, we found that N_{mac} increased from 10 mmol N m^{-2} at the beginning of the trial to 64,313 mmol N m^{-2} at the end (Figure 4.15 (a)). These values are well above nutrient levels that *M. liliana* naturally dwell in, as shown in Figure 3.2 (*see Section 3.5*). Therefore, total nutrient levels were reaching up to 128,630 mmol N m^{-2}. To test this nutrient overload theory, a new denitrification parameter was created (see *DR* in Chapter 3) and used within the model following trial 27.

Figure 4.15. Timeseries plot of nutrient values (mmol N m^{-2}) per time step for trials 18 to 27 for *M. liliana* (a) and MPB (b). Trials are plotted along a colour scale progressing from dark green to lime (MATLAB's 'summer colormap').

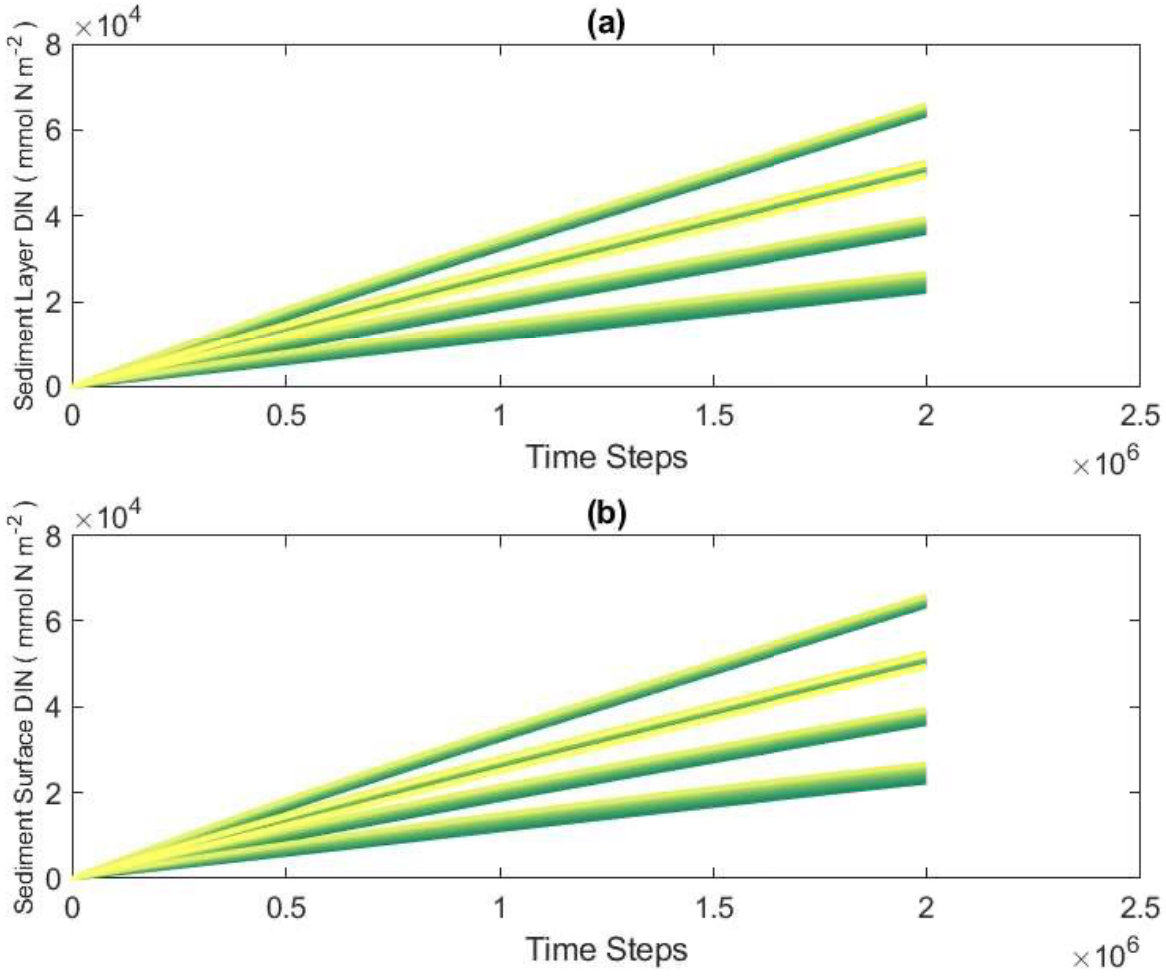

Figure 4.16. Timeseries plot of nutrient levels (mmol N m^{-2}) per time step for *M. liliana* (a) and MPB (b). Data was used from trials one to 27 excluding trials 16 & 17 due to errors. Trials are plotted along several colour scales; trials one to ten are plotted in colours progressing from blue to magenta (MATLAB's 'cool colormap'), 11 to 15 are plotted in colours progressing from red to yellow (MATLAB's 'autumn colormap'), and 18 to 26 are plotted in colours progressing from dark green to lime (MATLAB's 'summer colormap').

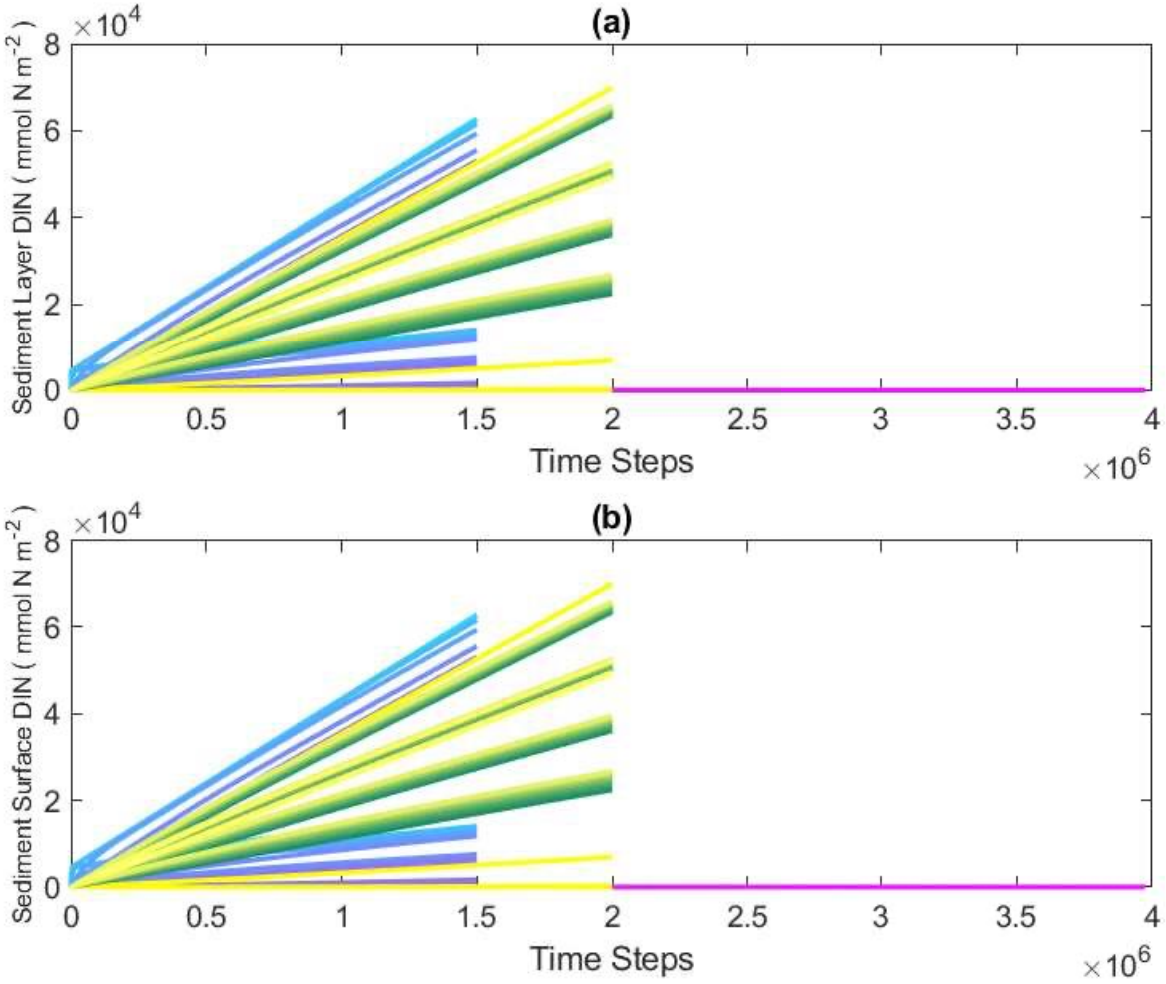

4.5.3 ***Detritus***

D_{mac} values in trials 18 to 27 range from 2.203e^{-8} to 0.00279 g C m^{-2} (Figure 4.17 (a)). A very strong positive relationship continues to exist between D_{mac} and M_{mac} in trials 18 to 27 (r = .966, p = <.00001).

D_{MPB} in trials 18 to 27 range from 3.396 to 1.339 g C m^{-2} (Figure 4.17 (b)), meaning all values sit above K_{MPB}. A moderate negative relationship exists between D_{MPB} and M_{mac} rates in trials 18 to 27 (r = -.725, p = .0271). This is the first instance across trials that a significant relationship exists between these variables. When looking at Figure 4.17 (b) we can see that as D_{MPB} values increase, their oscillating pattern become larger in value also. Previously, we thought that this was due to D_{MPB}'s relationship with had with M_{MPB};

however, as a relationship with M_{mac} is now evident (and we cannot test the relationship with the M_{MPB}) we cannot be sure which variable is causing this pattern.

When comparing B_{MPB} to D_{MPB} values across trials one to 27 (Figure 4.19 & 4.20), the amount of carbon in each pool can be seen to oscillate in near unison, demonstrating the appropriate transfer of carbon within the model.

Figure 4.17. Timeseries plot of detrital values (g C m^{-2}) per time step for trials 18 to 27 for *M. liliana* (a) and MPB (b). Trials are plotted along a colour scale progressing from dark green to lime (MATLAB's 'summer colormap').

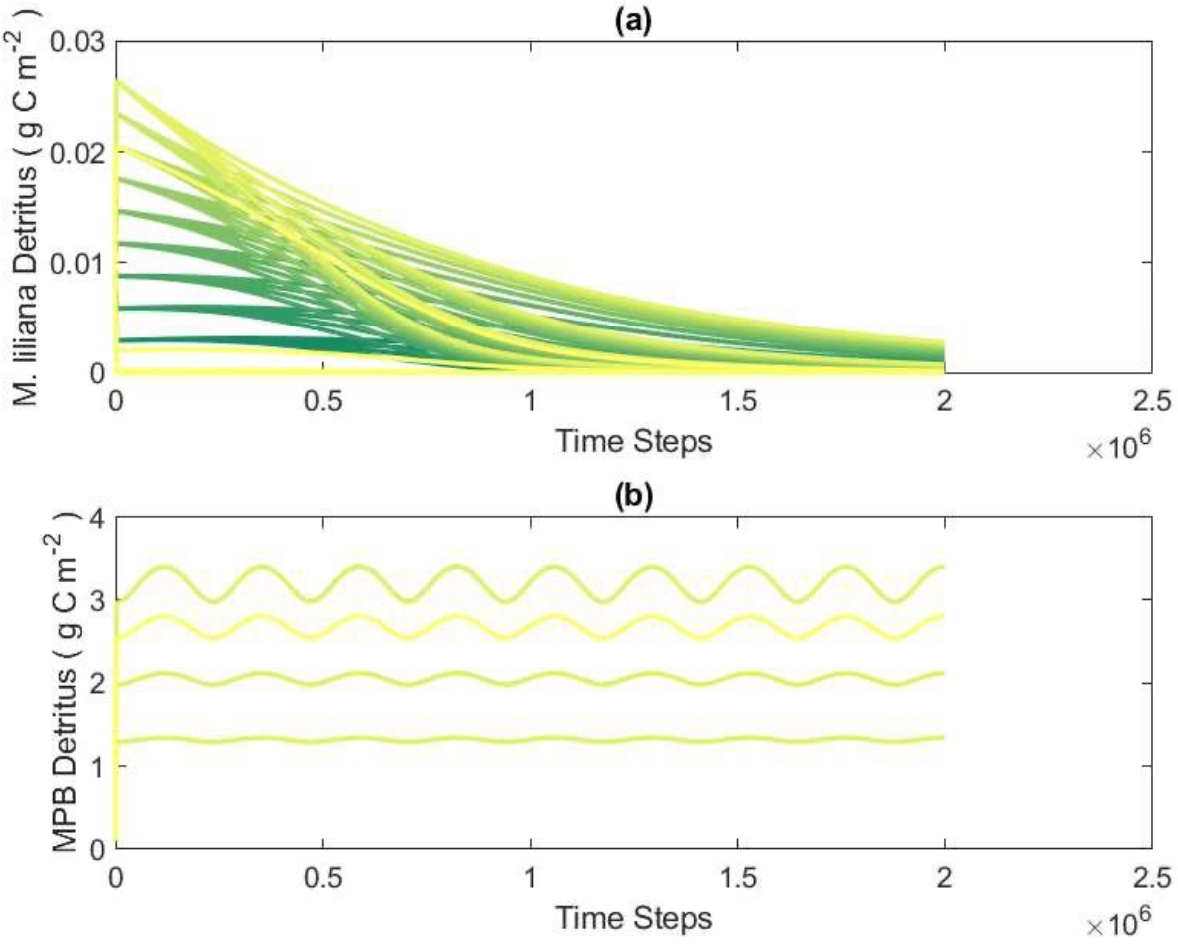

Figure 4.18. Timeseries plot of detrital values (g C m^{-2}) per time step for *M. liliana* (a) and MPB (b). Data was used from trials one to 27, excluding trials 16 & 17 due to errors. Trials are plotted along several colour scales; trials one to ten are plotted in colours progressing from blue to magenta (MATLAB's 'cool colormap'), 11 to 15 are plotted in colours progressing from red to yellow (MATLAB's 'autumn colormap'), and 18 to 27 are plotted in colours progressing from dark green to lime (MATLAB's 'summer colormap').

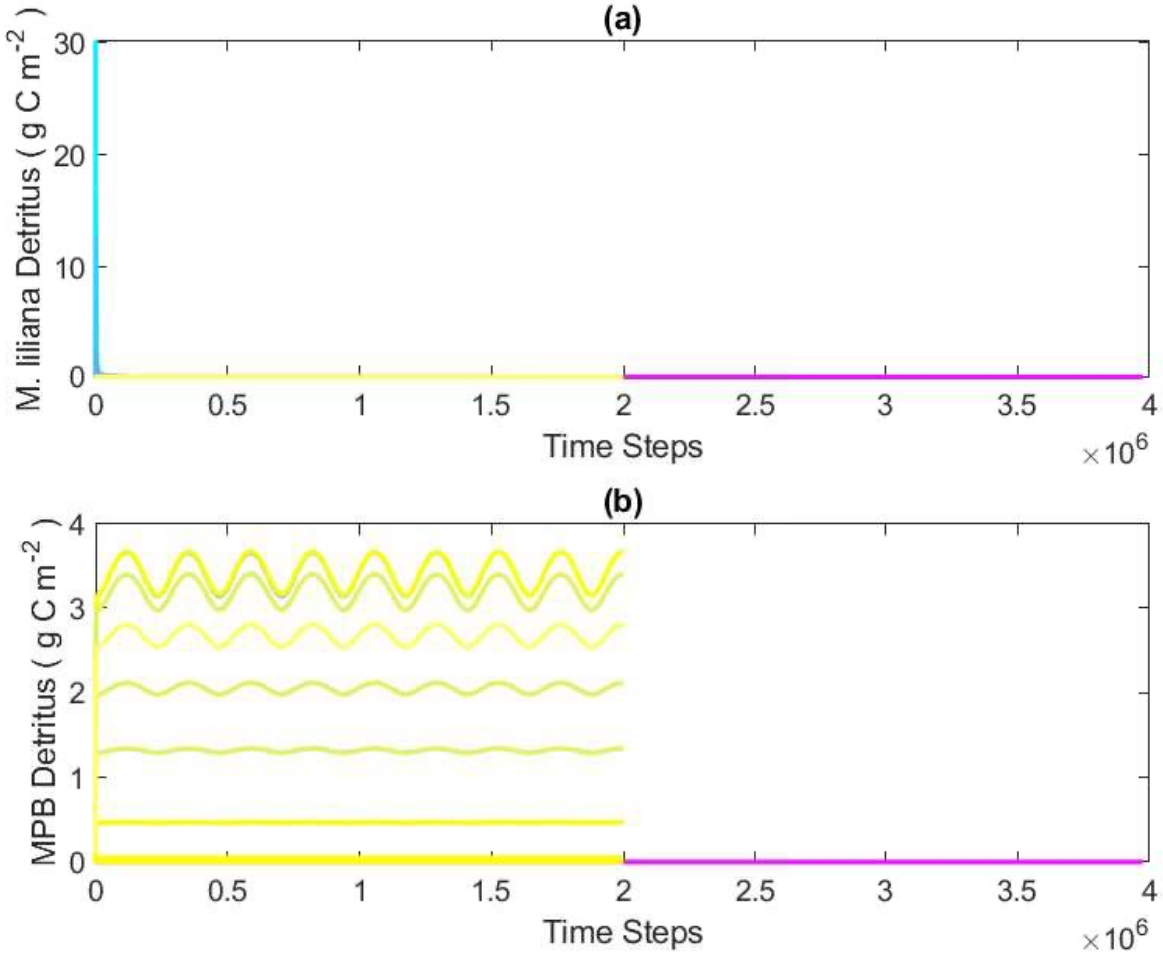

Figure 4.19. Timeseries plot of MPB biomass values (g C m^{-2}) per time step (a) and MPB detrital values (g C m^{-2}) (b). Data was used from trials one to 27, excluding trials 16 & 17 due to errors. Trials are plotted along several colour scales; trials one to ten are plotted in colours progressing from blue to magenta (MATLAB's 'cool colormap'), 11 to 15 are plotted in colours progressing from red to yellow (MATLAB's 'autumn colormap'), and 18 to 27 are plotted in colours progressing from dark green to lime (MATLAB's 'summer colormap').

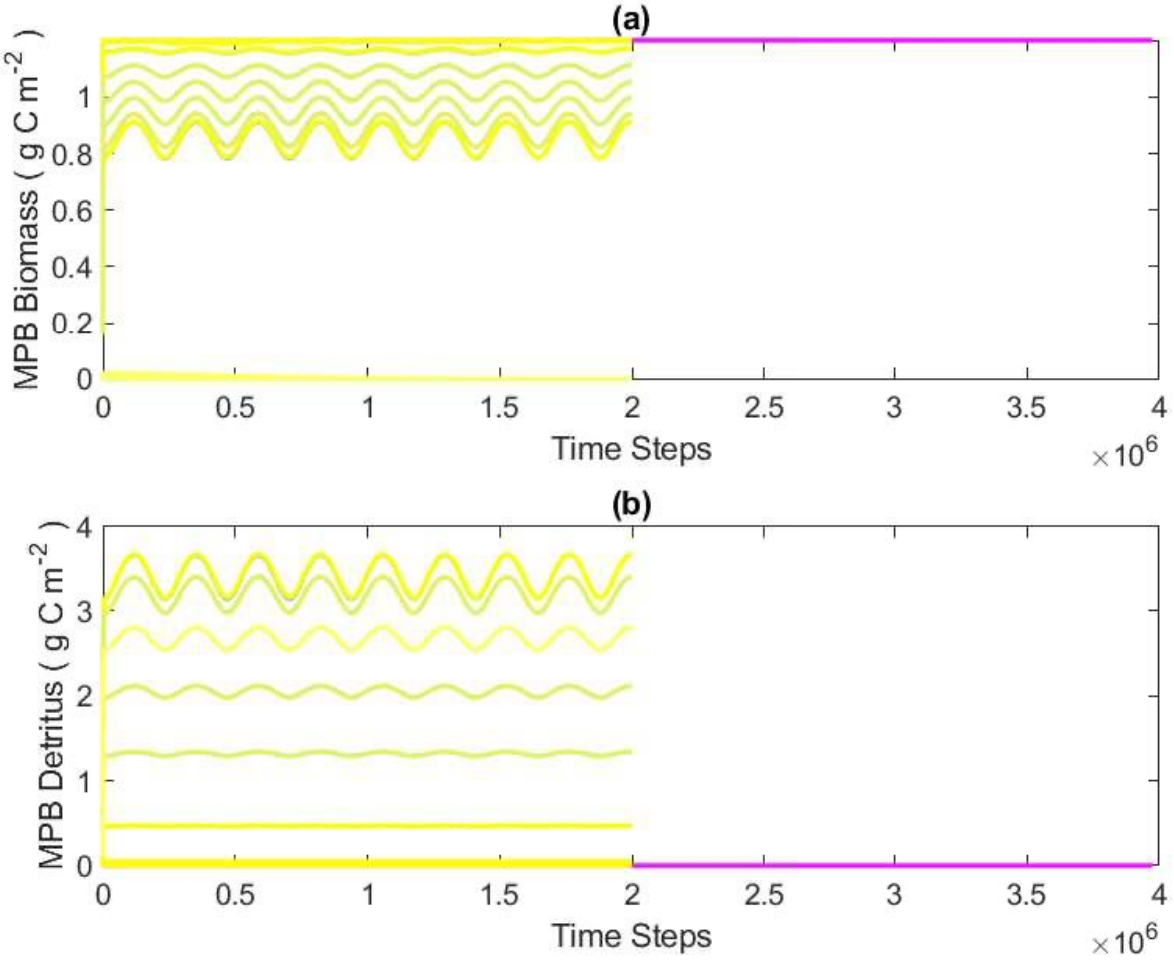

Figure 4.20. Timeseries plot of biomass and detrital values (g C m^{-2}) per time step for *M. liliana* (a) and MPB (b). Data was used from trials one to 27, excluding trials 16 & 17 due to errors. Red lines correspond to biomass values, while blue lines identify detrital values.

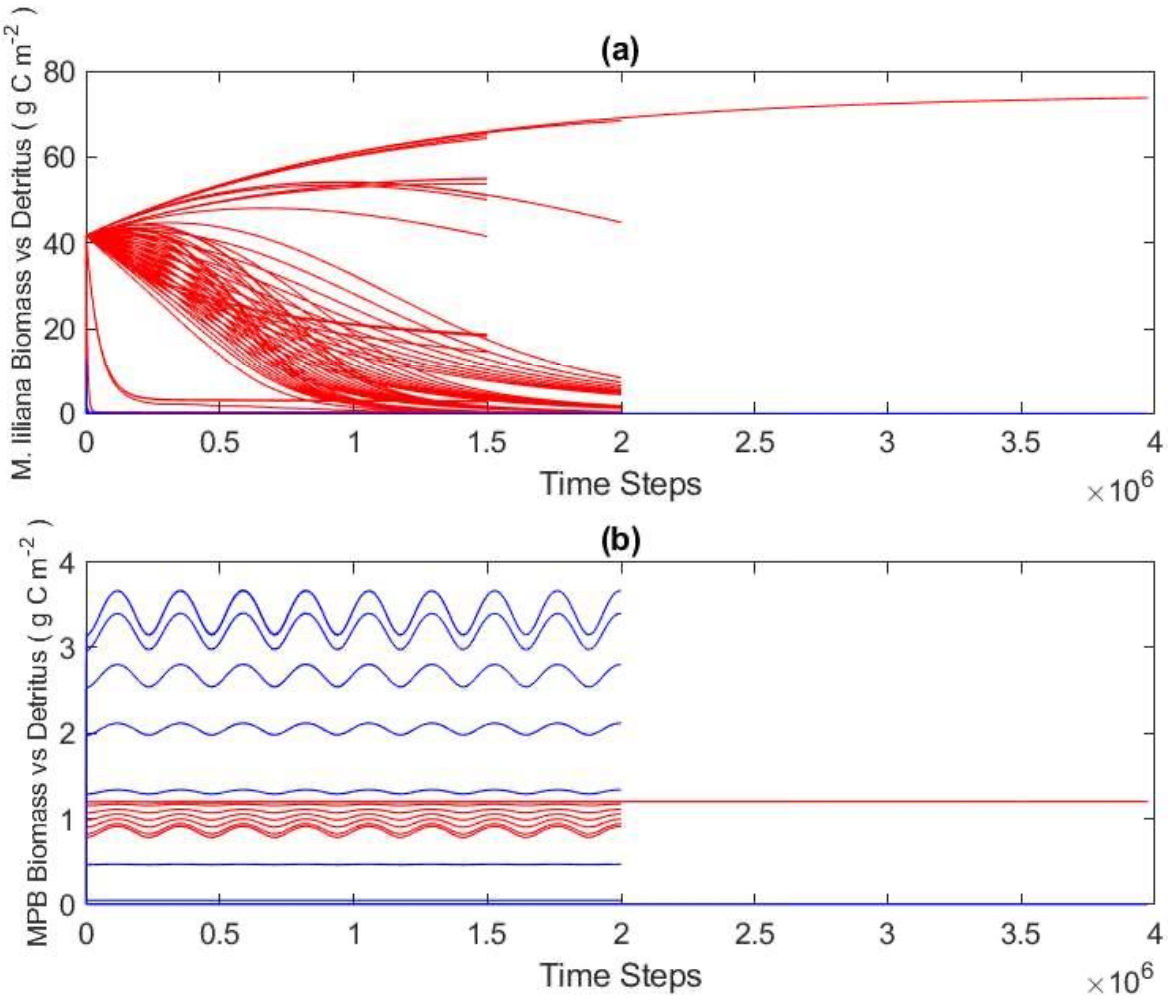

4.5.4 Key Findings

- Stronger relationships have occurred between M_{mac} and the model's three dynamic variables, demonstrating that we are closer to finding an appropriate mortality rate.
- Continual rise of nutrients creating concentrations well above natural levels, which are likely poisoning *M. liliana.*
- B_{MPB} and D_{MPB} values oscillate in near unison with time across trials.

4.6 Observations Following the Addition of *DR* – Trials 28 to 31

Trial 29 was selected to represent the relationships seen in trials 28-31. Due to the structure of testing in trials 28 to 31 (Table 4.5), relationships with M_{MPB} could not be analysed.

4.6.1 Biomass

Following the addition of the *DR* parameter, the model produced much more stable B_{mac} results compared to earlier trials (Figure 4.22 (a)). These results are highlighted in Figure 4.21 (a), which demonstrates B_{mac} results that plateau considerably faster than previous trials. B_{mac} results in trials 28 to 31 have range from 59.15 to 0.023 g C m^{-2}. Surprisingly, no significant relationship between B_{mac} and M_{mac} exists (r = -.333, p = .519), which goes against all our current findings. More trials are producing results where B_{mac} is similar to that seen in nature (Figure 4.23); however, still none are simultaneously accurate for *M. liliana* and MPB. B_{mac} values stabilising supports our assumption that B_{mac} was decreasing below levels seen in nature due to the growth of N_{mac}, as nutrients no longer remain at high volumes.

B_{MPB} results in trials 28 to 31 show a similar trend to previous trials (Figure 4.22 (b)); however, there is a much larger range than previously seen. B_{MPB} values range from 1.97 to 0.54 g C m^{-2}. Results from trials that have a lower B_{MPB} oscillate in larger fluctuations around their carrying capacity, than those with a larger B_{MPB}. The results with the smaller B_{MPB} values have a lower carrying capacity than is set in the model, due to the interactions between species following the alteration of their mortality rates. An anomaly arose when testing B_{MPB}'s relationship with M_{mac}; no significant relationship between these variables exist in trials 29 to 31, but a very strong positive relationship exists in trial 28 (r = 0.995, p .000037). Figure 4.21 (b) highlights a variance in results not seen until the addition of the *DR* value; B_{MPB} values shift almost instantaneously to oscillate below a new K_{MPB} value. Variant three and four of trial 28 saw the largest shifts in B_{MPB} over short periods of time (Table 4.10 & 4.11), with these variants also experiencing a double shift; B_{MPB} quickly reduces and then increases again within a short period of time (Table 4.11). Rapid shifts in B_{MPB} decrease in size as the trial and variant number increase (Table 4.10), likely caused by the relationship between B_{MPB} and M_{MPB}. As M_{MPB} decreases through trials, B_{MPB} and K_{MPB} values increase, demonstrating that M_{MPB} has less control over these variables than previously. These rapid changes in value may be the system responding to a regime shift.

Trials 28 to 31 have produced more results that are close to B_{MPB} values measured in natural settings; however, none are accurate (Figure 4.23). Notably, trials and variants that experienced larger rapid shifts in B_{MPB} than others (Table 4.10) produced values that sit below those seen in nature.

Figure 4.21. Timeseries plot of biomass values (g C m^{-2}) per time step for trials 28 to 31 for *M. liliana* (a) and MPB (b). Trials are plotted along a colour scale progressing from black to copper (MATLAB's 'copper colormap').

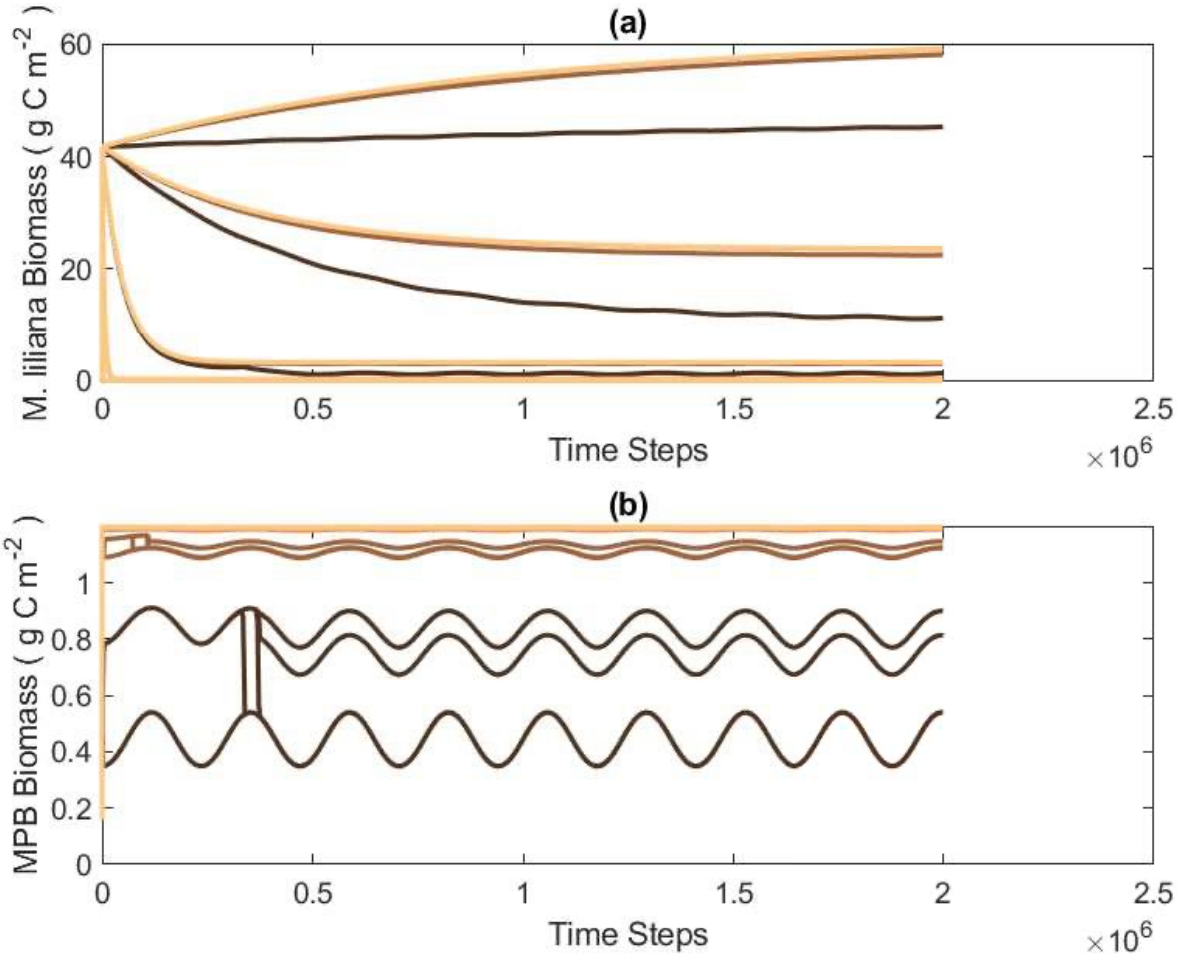

Figure 4.22. Timeseries plot of biomass values (g C m^{-2}) per time step for *M. liliana* (a) and MPB (b). Data was used from trials one to 31, excluding trials 16 & 17 due to errors. Trials are plotted along several colour scales; trials one to ten are plotted in colours progressing from blue to magenta (MATLAB's 'cool colormap'), 11 to 15 are plotted in colours progressing from red to yellow (MATLAB's 'autumn colormap'), 18 to 27 are plotted in colours progressing from dark green to lime (MATLAB's 'summer colormap'), and 28 to 31 are plotted in colours progressing from black to copper (MATLAB's 'copper colormap').

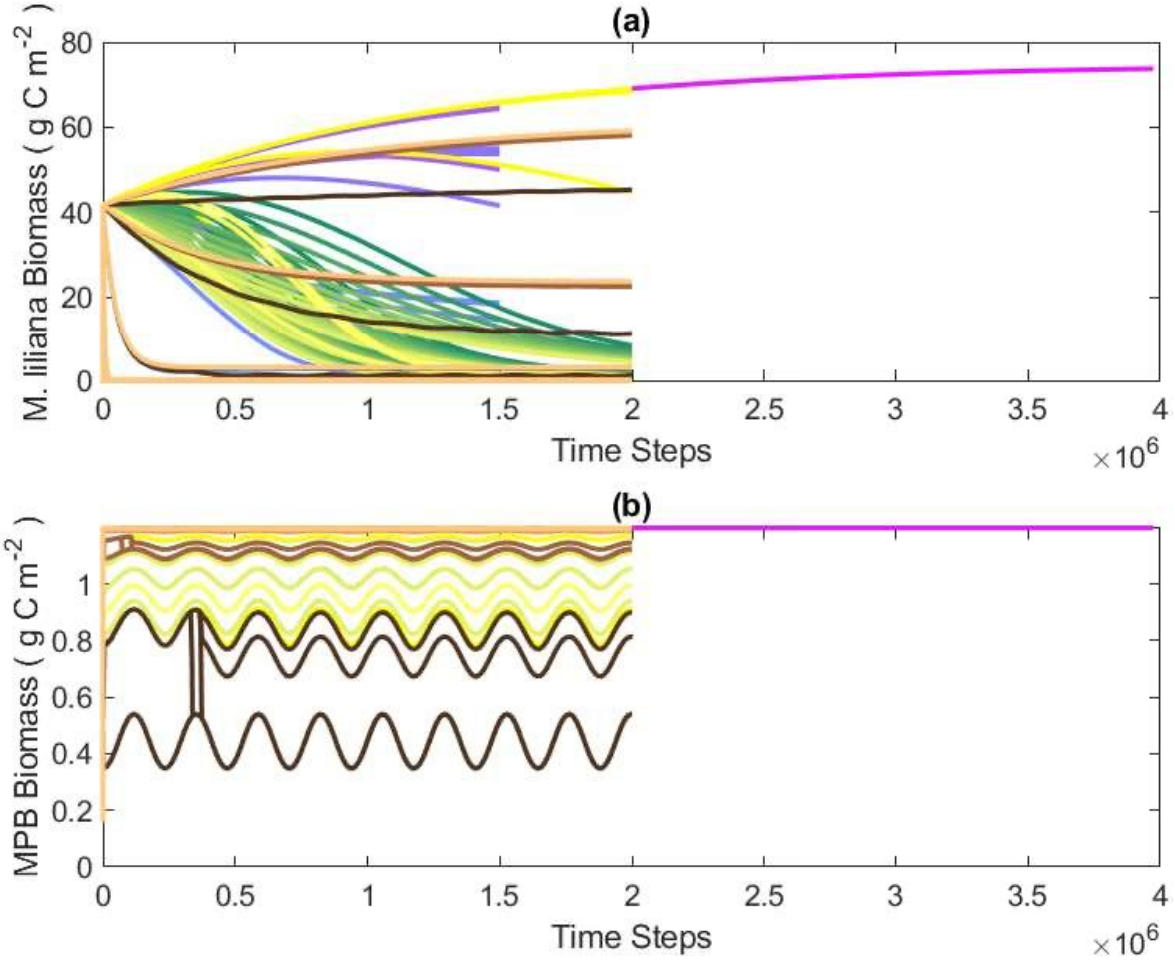

Figure 4.23. Scatter graphs demonstrating the biomass of *M. liliana* and MPB at the conclusion of each trial (excluding trial 16 & 17) from trials one to 31. The vertical red line illustrates an average MPB biomass (1.056 g C m^{-2}) within Tauranga Harbour (Flowers et al., in review) the horizontal blue line illustrates an average *M. liliana* biomass (41.768 g C m^{-2}) found within Tauranga Harbour (Thrush et al., 2021). The colour scale in (a) denotes the different *M. liliana* mortality rate (per time step) log formed in each trial; the colour scale in (b) denotes the different MPB mortality rates (per time step) log formed in each trial; the colour scale in (c) corresponds to the 'variant' number for MPB mortality across trials (see Table 4.1, 4.2, 4.3, 4.4, & 4.5); and the colour scale in (d) refers to the 'trial' number for *M. liliana* mortality rate across trials (see Table 4.1, 4.2, 4.3, 4.4, & 4.5).

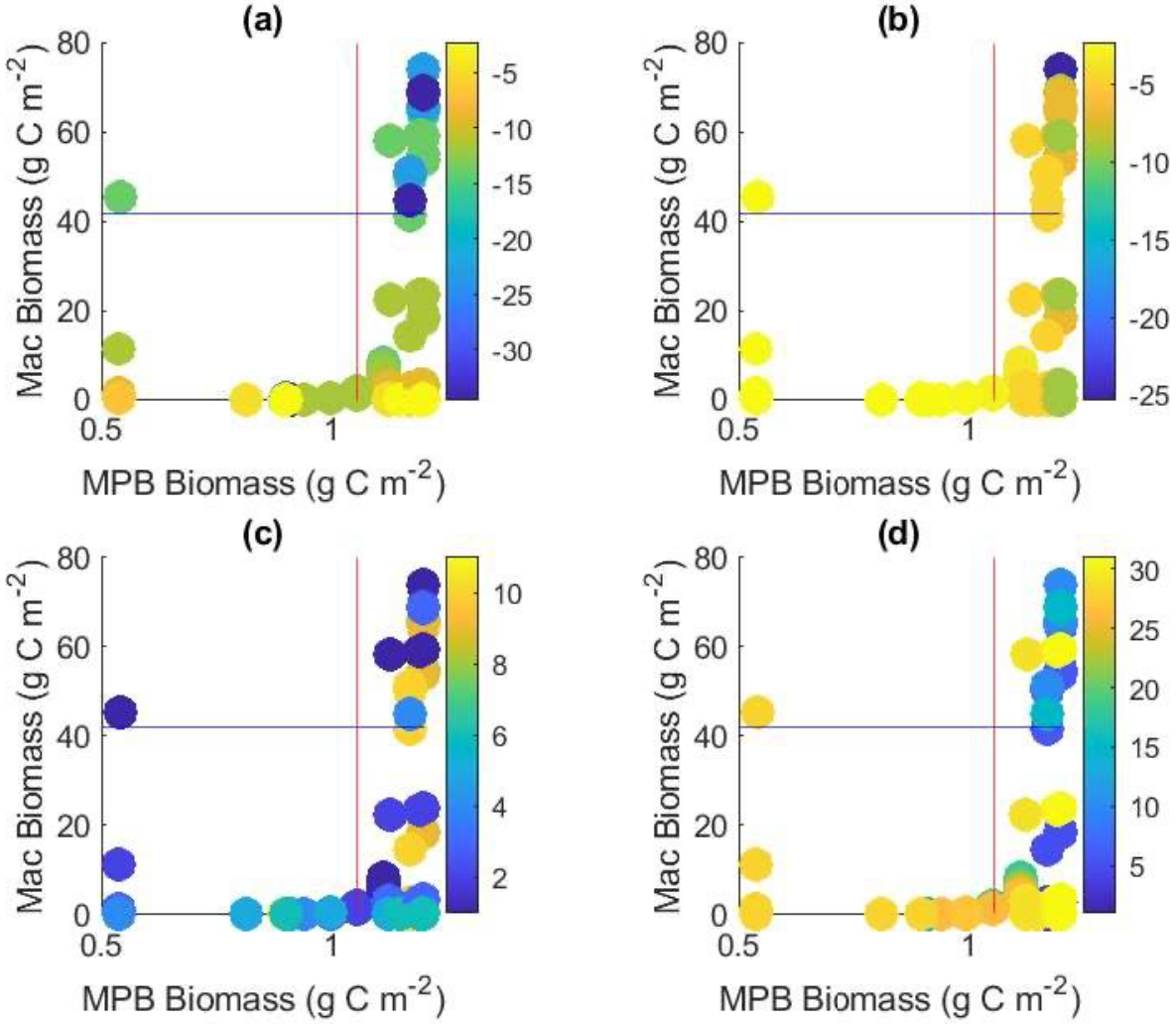

Table 4.10. Rapid biomass jumps for trials 28 to 31. Size of the jump and time taken to occur are evaluated and ranked from largest to smallest.

Trial	Variant	Value 1 (g C m^{-2})	Time Step 1 (*t*)	Value 2 (g C m^{-2})	Time Step 2 (*t*)	Difference (g C m^{-2})	Percentage Change	Difference (*t*)	Rank (difference percentage)	Rank (difference time step)
28	2	0.741	170	0.349	1951	-0.392	-0.529	1781	1	5
	3	0.886	334168	0.533	338707	-0.353	-0.398	4539	3	2
	4	0.888	367649	0.527	372267	-0.361	-0.407	4618	2	1
	5	0.892	370615	0.805	374152	-0.087	-0.098	3537	4	3
	6	0.898	370741	0.894	372051	-0.004	-0.004	1310	13	7
29	3	1.147	469	1.091	858	-0.056	-0.049	389	6	15
	3	1.091	3634	1.148	4777	0.057	0.052	1143	5	10
	3	1.163	72523	1.115	73630	-0.048	-0.041	1107	7	11
	4	1.166	107776	1.124	108271	-0.042	-0.036	495	8	14
	5	1.166	108986	1.124	109537	-0.042	-0.036	551	8	13
	6	1.168	108942	1.148	112320	-0.02	-0.017	3378	10	4
30	3	1.194	637	1.189	1005	-0.005	-0.004	368	13	16
	3	1.187	3996	1.194	5222	0.007	0.006	1226	11	8
	3	1.194	63802	1.189	64061	-0.005	-0.004	259	13	17
	4	1.195	100922	1.19	101125	-0.005	-0.004	203	13	20
	4	1.195	102146	1.19	102330	-0.005	-0.004	184	13	23
	5	1.195	102153	1.19	102333	-0.005	-0.004	180	13	24
	6	1.196	102107	1.19	103287	-0.006	-0.005	1180	12	9
31	2	1.199	584	1.197	769	-0.002	-0.002	185	18	22
	3	1.199	656	1.197	886	-0.002	-0.002	230	18	18
	3	1.197	3989	1.199	4705	0.002	0.002	716	18	12
	3	1.198	62917	1.197	63133	-0.001	-0.001	216	22	19
	4	1.198	100275	1.197	100462	-0.001	-0.001	187	22	21
	5	1.198	101557	1.197	101649	-0.001	-0.001	92	22	25
	6	1.199	101068	1.197	102543	-0.002	-0.002	1475	18	6

Table 4.11. Double biomass jumps within trial 28. Size of the jump and time taken to occur are evaluated and ranked from largest to smallest.

Trial	Variant	Value 1 (g C m^{-2})	Time Step 1 (*t*)	Value 2 (g C m^{-2})	Time Step 2 (*t*)	Difference (g C m^{-2})	Percentage Change	Difference (*t*)	Value 3 (g C m^{-2})	Time Step 3 (*t*)	Difference (g C m^{-2})	Percentage Change	Difference (t)
28	3	0.741	163	0.508	543	-0.233	-0.314	380	0.764	3391	0.256	0.50393701	2848
	4	0.745	163	0.508	544	-0.237	-0.318	381	0.78	1470	0.272	0.53543307	926

4.6.2 ***Nutrients***

Following the addition of the *DR* value, Figure 4.24 (a) and (b) show that the system is losing nutrients, rather than continuing to increase with time, like previous trials. Nutrient conditions are nearly identical within N_{mac} and N_{MPB}, further demonstrating the effectiveness of mixing in the model. Trials 29 to 31 show considerable overlap in results, with nutrients being removed from N_{mac} entirely (Figure 4.24 (a)) or N_{MPB} dropping to low levels (Figure 4.24 (b)) faster across each trial. Trial 28 variant five produced the largest N_{mac} value (4,260 mmol N m^{-2}) that also remain in the system the longest (373,431 timesteps), before reducing to zero. A very strong positive relationship exists between M_{mac} and N_{mac} ($r = 1$, $p = <.00001$).

Trial 28 variant six has the largest N_{MPB} value (4,293 mmol N m^2) (Figure 4.24 (b)). N_{MPB} remain above zero throughout all trials and variants; however, trial 28 variant six has N_{MPB} levels that remain at the highest levels (>40 mmol N m^{-2}). As M_{MPB} decreases, we see nutrient levels reduce faster, but there is insufficient data to identify a relationship at the 95% confidence interval. However, we have identified a very strong positive relationship between M_{mac} and N_{MPB} ($r = 1$, $p = <.00001$). Six of the largest rapid shifts in B_{MPB} (Table 4.10 & 4.11), in respect to a percentage increase or decrease in g C m^{-2}, all occur in variations of trial 28, where nutrients remain in the system for the longest period of time.

Figure 4.24. Timeseries plot of nutrient values (mmol N m^{-2}) per time step for trials 28 to 31 for *M. liliana* (a) and MPB (b). Trials are plotted along a colour scale progressing from black to copper (MATLAB's 'copper colormap').

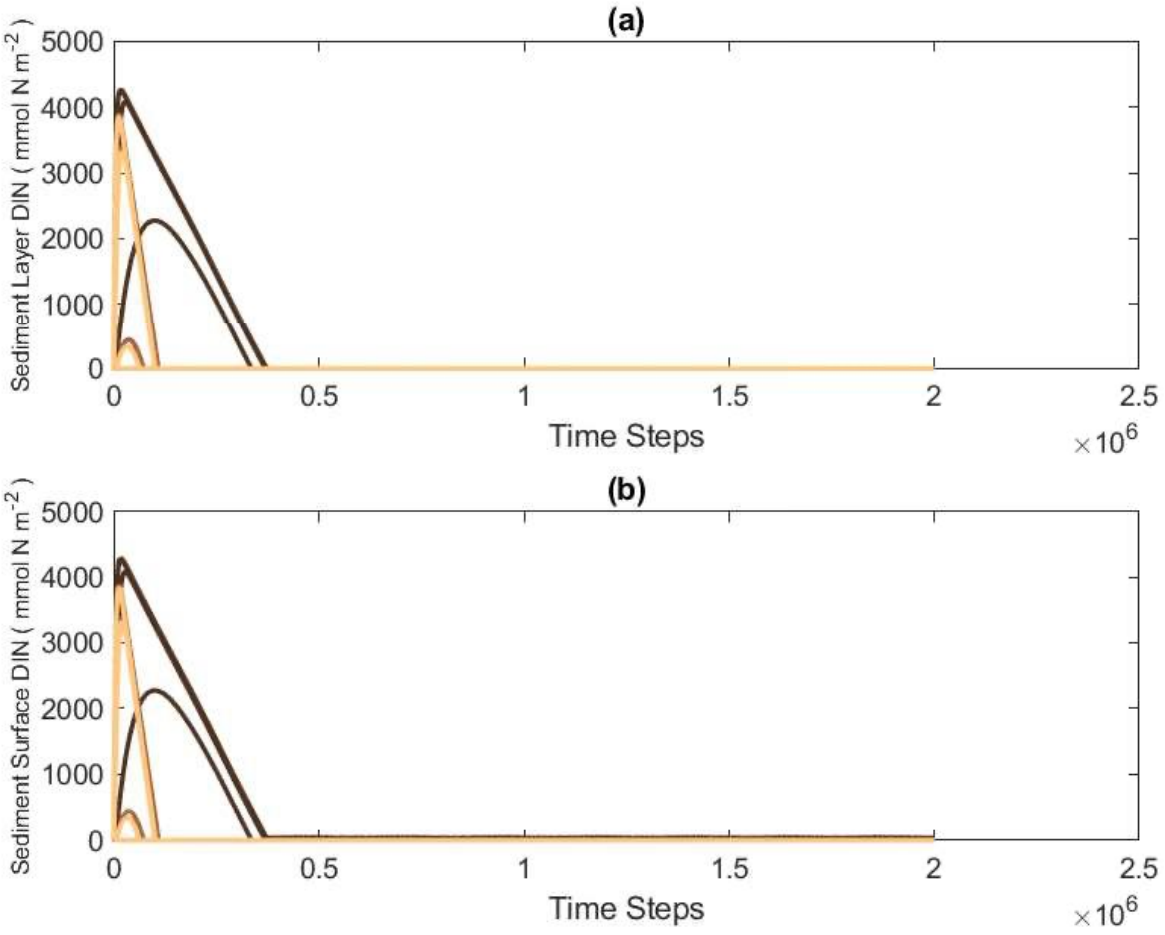

Figure 4.25. Timeseries plot of nutrient values (mmol N m^{-2}) per time step for trials one to 31 for *M. liliana* (a) and MPB (b). Data was used from trials one to 31, excluding trials 16 & 17 due to errors. Trials are plotted along several colour scales; trials one to ten are plotted in colours progressing from blue to magenta (MATLAB's 'cool colormap'), 11 to15 are plotted in colours progressing from red to yellow (MATLAB's 'autumn colormap'), 18 to 26 are plotted in colours progressing from dark green to lime (MATLAB's 'summer colormap'), and 27 to 31 are plotted in colours progressing from black to copper (MATLAB's 'copper colormap').

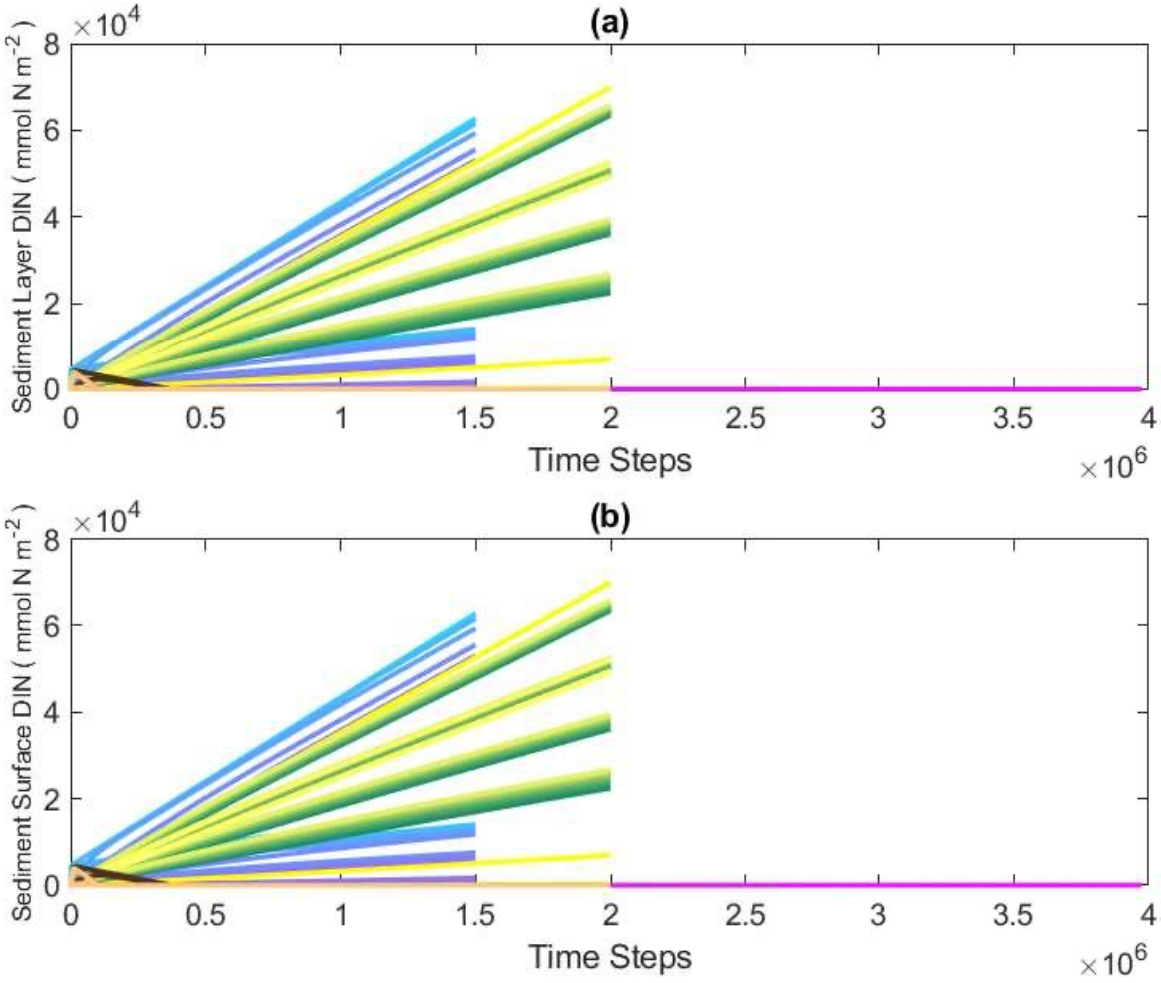

4.6.3 ***Detritus***

Following the addition of the *DR* parameter, D_{MPB} show a slight variation from that seen in previous trials (Figure 4.26 (a)). D_{mac} values range from 0.243 to 0.0319 g C m^{-2}, and remain larger for a longer period of time. Values plateau as late as 176,329 timesteps, as opposed to 25,168 timesteps in earlier trials. Results overlap between trials, indicating no relationship between D_{mac} and the duration nutrients remain in the system. No significant relationship exists between M_{mac} and D_{mac} (r = .356, p = .489). D_{mac} continues to transition into nitrogen at a rapid rate, keeping D_{mac} values low throughout the majority of each trial.

D_{MPB} from trials 28 to 31 range from 3.61 to 0.00481 g C m^{-2} (Figure 4.26 (b)) and show a similar trend to previous trials (Figure 4.27 (b)). A very strong relationship exists

between M_{mac} and the D_{MPB} (r = .989, p = 0.000181). Rapid shifts in D_{MPB}, alike that seen with B_{MPB} (Figure 4.21 (b)), have occurred. Once again, the largest jumps in values occur in variations of trial 28, with rapid shifts in B_{MPB} and D_{MPB} values occurring almost simultaneously throughout trials (Table 4.12). From this, we can be sure that the model is appropriately transferring carbon between these two pools.

Figure 4.26. Timeseries plot of detrital values (g C m^{-2}) per time step for trials 28 to 31 for *M. liliana* (a) and MPB (b). Trials are plotted along a colour scale progressing from black to copper (MATLAB's 'copper colormap').

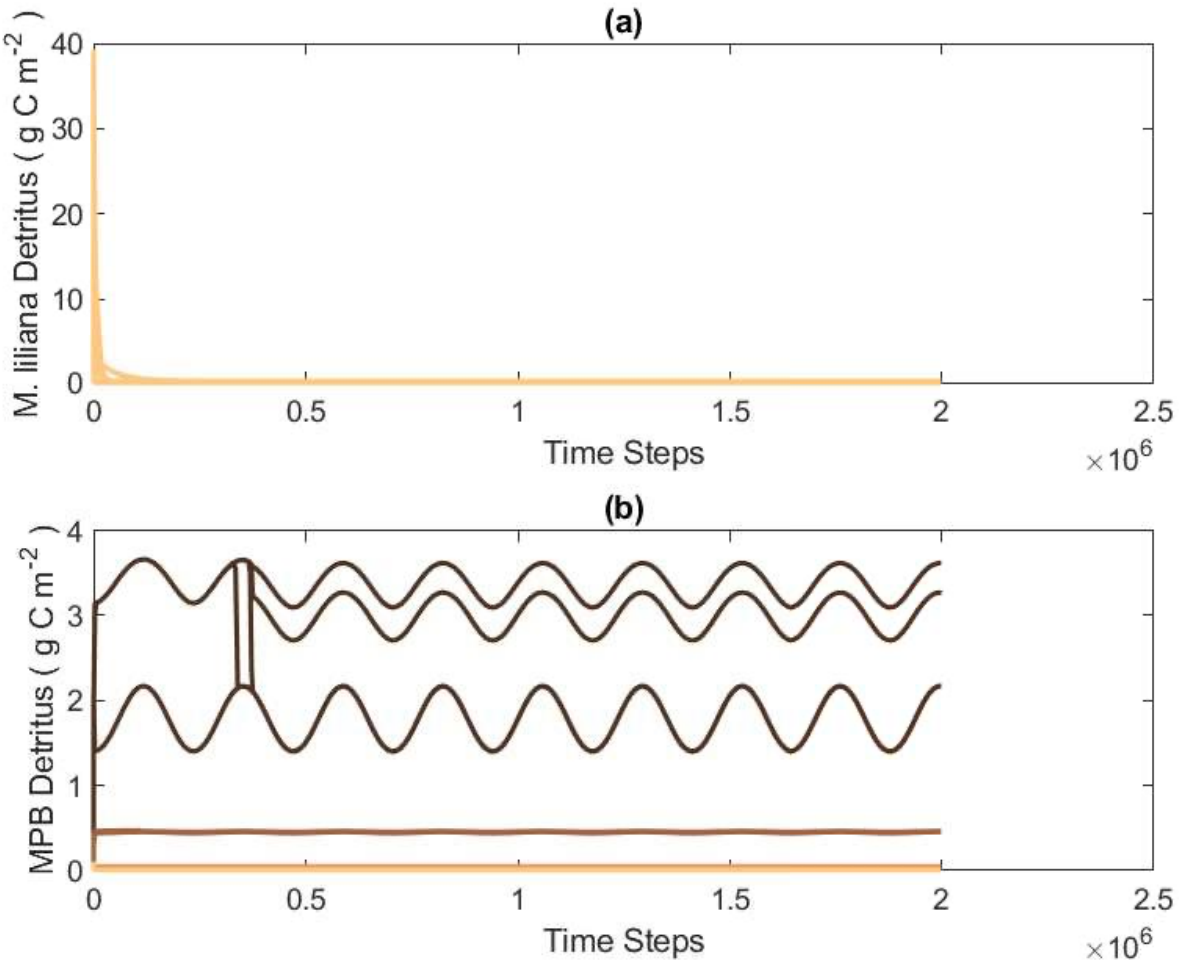

Figure 4.27. Timeseries plot of detrital values (g C m^{-2}) per time step for *M. liliana* (a) and MPB (b). Data was used from trials one to 31, excluding trials 16 & 17 due to errors. Trials are plotted along several colour scales; trials one to ten are plotted in colours progressing from blue to magenta (MATLAB's 'cool colormap'), 11 to 15 are plotted in colours progressing from red to yellow (MATLAB's 'autumn colormap'), 18 to 26 are plotted in colours progressing from dark green to lime (MATLAB's 'summer colormap'), and 27 to 31 are plotted in colours progressing from black to copper (MATLAB's 'copper colormap').

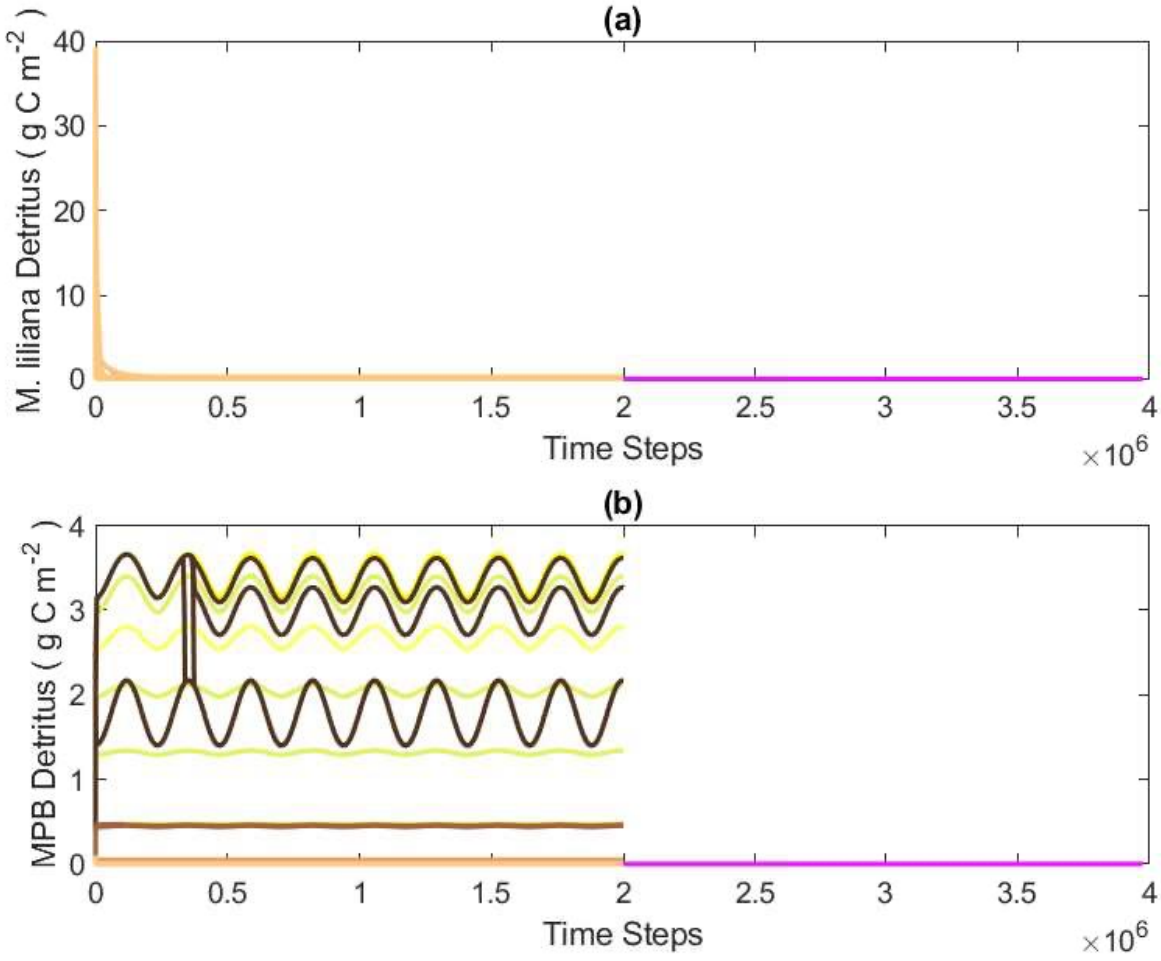

Table 4.12. Rapid detritus jumps for trials 28 to 31. Size of the jump and time taken to occur are evaluated and ranked from largest to smallest.

Trial	Variant	Value 1 (g C m^{-2})	Time Step 1 (*t*)	Value 2 (g C m^{-2})	Time Step 2 (*t*)	Difference (g C m^{-2})	Percentage Change	Difference (*t*)	Rank (difference percentage)	Rank (difference time step)
28	1	2.081	363	1.408	1934	-0.673	-0.3234022	1571	4	15
	2	2.084	365	1.404	2475	-0.68	-0.3262956	2110	3	8
	3	3.587	332843	2.141	339443	-1.446	-0.4031224	6600	2	1
	4	3.579	367509	2.111	373030	-1.468	-0.4101704	5521	1	2
	5	3.586	370642	3.231	374730	-0.355	-0.0989961	4088	5	3
	6	3.605	370795	3.589	372377	-0.016	-0.0044383	1582	12	13
29	3	0.438	3594	0.463	6241	0.025	0.05707763	2647	6	6
	3	0.467	72440	0.448	74142	-0.019	-0.0406852	1702	7	11
	4	0.469	107510	0.451	109002	-0.018	-0.0383795	1492	8	16
	5	0.469	108684	0.451	110735	-0.018	-0.0383795	2051	8	9
	6	0.469	108761	0.461	112151	-0.008	-0.0170576	3390	10	4
30	3	0.0477	3350	0.048	6223	0.0003	0.00628931	2873	11	5
	3	0.048	63108	0.0478	64832	-0.0002	-0.0041667	1724	13	10
	4	0.048	100558	0.0478	102131	-0.0002	-0.0041667	1573	13	14
	5	0.048	102032	0.0478	102873	-0.0002	-0.0041667	841	13	17
	6	0.048	102052	0.0478	104386	-0.0002	-0.0041667	2334	13	7
31	1	0.0048	4049	0.00481	5633	1E-05	0.00208333	1584	17	12
	1	0.00481	62962	0.0048	63592	-1E-05	-0.002079	630	18	18

Table 4.13. Comparison between rapid jumps in MPB biomass and detrital values (g C m^{-2}). The difference in time between the biomass and detritus jumps and their difference in size is examined. Values are positive or negative to indicate the direction of time difference.

Trial	Variant	Difference at First Time Step (t)	Difference at Second Time Step (t)	Difference (%)
28	2	195	524	0.20271926
	3	-1325	736	-0.0047025
	4	-140	763	-0.0036389
	5	27	578	-0.0014625
	6	54	326	1.6063E-05
29	3	-40	1464	0.00483198
	3	-83	512	0.00058735
	4	-266	731	-0.0023589
	5	-302	1198	-0.0023589
	6	-181	-169	6.5718E-05
30	3	-646	1001	0.00039209
	3	-694	771	2.0938E-05
	4	-364	1006	1.7434E-05
	5	-121	540	1.7434E-05
	6	-55	1099	0.00085006

4.6.4 *Key Findings*

- Following the addition of *DR*, biomass values across both species become closer to those measured in nature.
- No significant relationship existed between M_{mac} and B_{mac}, B_{MPB} *(trials 29-31), or* $D_{mac.}$
- Very strong positive relationship existed between M_{mac} and B_{MPB} in trial 28.
- Rapid shifts occur in B_{MPB} and D_{MPB} values with time, decreasing in size as trial number increases. **Possible detection of regime shift.**
- Nutrients are removed from the system more quickly as M_{MPB} increases.
- The size of the rapid shifts in B_{MPB} and D_{MPB} decrease when nutrients are removed from system more quickly (through *DR*).
- Jumps in B_{MPB} and D_{MPB} occur in near unison across trials.

4.7 Observations Following the Addition of *DR* – Trials 32 to 46

Variant two was selected to represent the relationships seen in trials 32 to 46. Unfortunately, due to the structure of testing, sample sizes were too small to test (at the 95% confidence level) M_{mac}'s relationship between the biomass, nutrient, and detrital values.

4.7.1 *Biomass*

B_{mac} values across trials 32 to 46 range from 51.360 to 26.327 g C m^{-2} (Figure 4.28 (a)), the smallest range across trials so far. Trials 32 to 46 have produced much more uniform results when compared to previous trials (Figure 4.29 (a) & 4.30). B_{mac} values across trials and variants congregate based upon M_{mac} values. Variant two across trials produced results closest to a B_{mac} seen in nature, ranging from 40.163 to 38.918 g C m^{-2} (Figure 4.30). B_{mac} continues to have a very strong negative relationship with M_{MPB} (r = -1, p = <.00001), demonstrated by the progression from dark blue to green as biomass values decrease in Figure 4.28 (a).

B_{MPB} values range from 1.199 to 1.132 g C m^{-2} for trials 32 to 46 (Figure 4.28 (b)), also the smallest range across trials so far. Trials 32 to 46 no longer show any rapid changes in value, with all B_{MPB} results siting above levels seen in nature (Figure 4.30). B_{MPB} continues to have a very strong negative relationship with M_{MPB} (r = -1, p = <.00001).

Figure 4.28. Timeseries plot of biomass values (g C m^{-2}) per time step for trials 32 to 46 for *M. liliana* (a) and MPB (b). Trials are plotted along a colour scale progressing from dark blue to green (MATLAB's 'winter colormap').

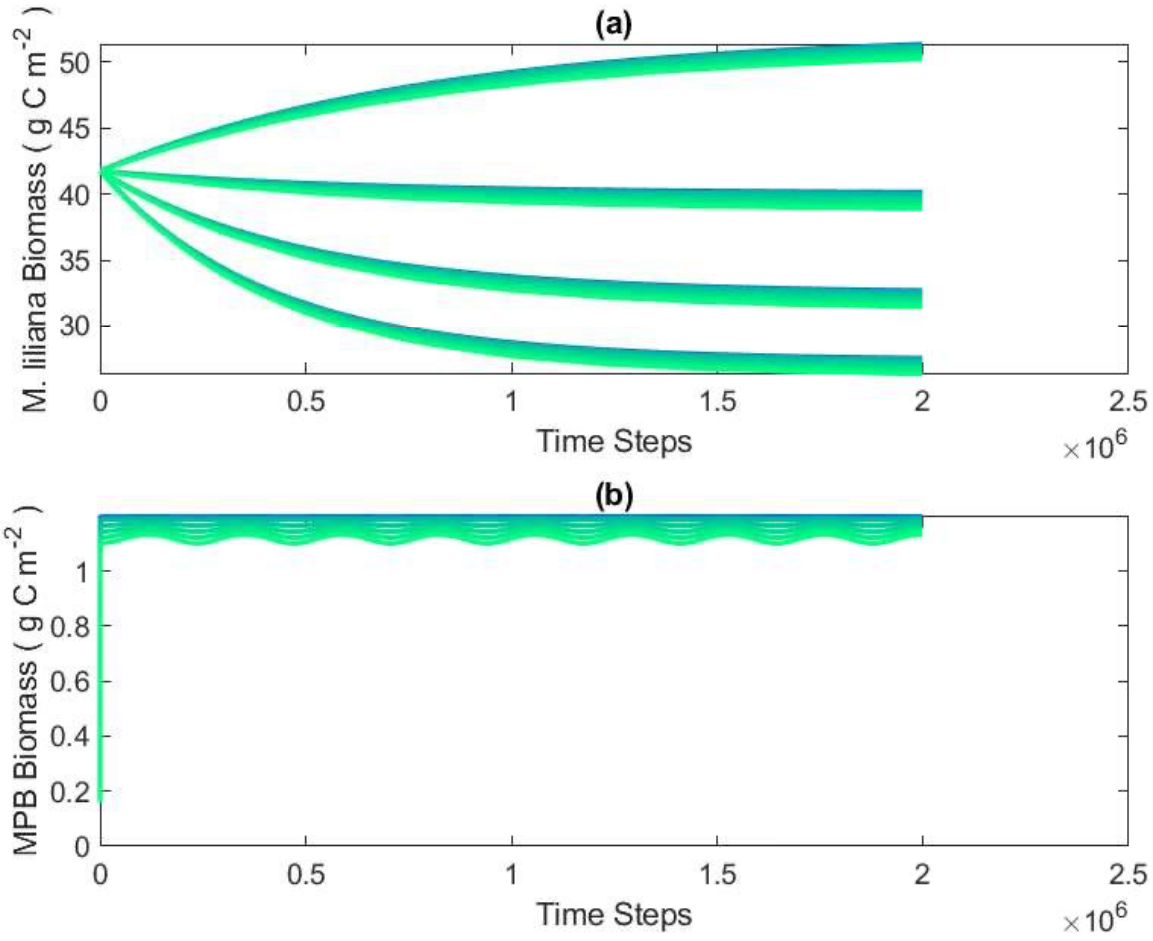

Figure 4.29. Timeseries plot of biomass values (g C m^{-2}) per time step for *M. liliana* (a) and MPB (b). Data was used from trials one to 46, excluding trials 16 & 17 due to errors. Trials are plotted along several colour scales; trials one to ten are plotted in colours progressing from blue to magenta (MATLAB's 'cool colormap'), 11 to 15 are plotted in colours progressing from red to yellow (MATLAB's 'autumn colormap'), 18 to 27 are plotted in colours progressing from dark green to lime (MATLAB's 'summer colormap'), 28 to 31 are plotted in colours progressing from black to copper (MATLAB's 'copper colormap'), and 32 to 46 are plotted in colours progressing from dark blue to green (MATLAB's 'winter colormap').

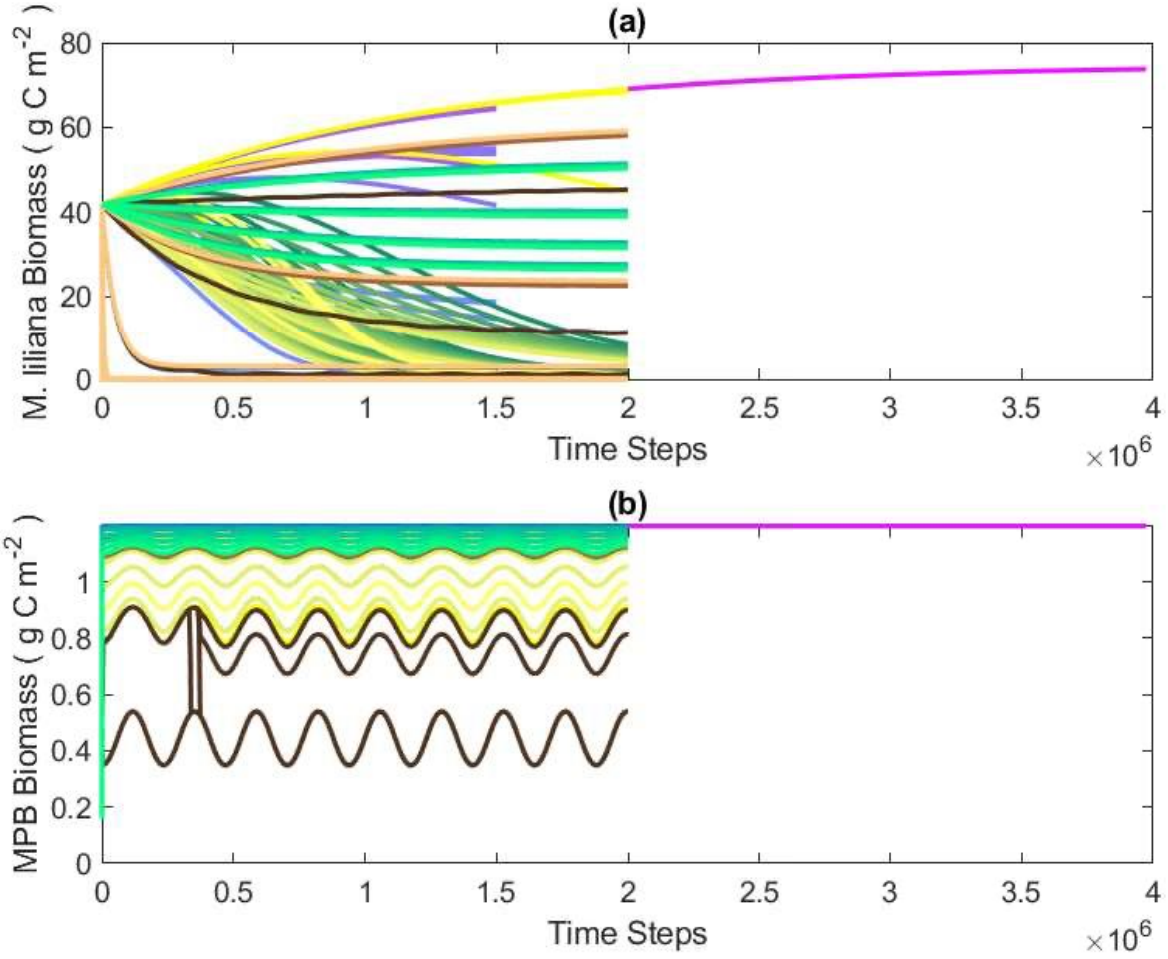

Figure 4.30. Scatter graphs demonstrating the biomass of *M. liliana* and MPB at the conclusion of each trial (excluding trial 16 & 17) from trials one to 46. The vertical red line illustrates an average MPB biomass (1.056 g C m^{-2}) within Tauranga Harbour (Flowers et al., in review) and the horizontal blue line illustrates an average *M. liliana* biomass (41.768 g C m^{-2}) found within Tauranga Harbour (Thrush et al., 2021). The colour scale in (a) denotes the different *M. liliana* mortality rate (per time step) log formed in each trial; the colour scale in (b) denotes the different MPB mortality rates (per time step) log formed in each trial; the colour scale in (c) corresponds to the 'variant' number for MPB mortality across trials (see Table 4.1, 4.2, 4.3, 4.4, 4.5, & 4.6); and the colour scale in (d) refers to the 'trial' number for *M. liliana* mortality rate across trials (see Table 4.1, 4.2, 4.3, 4.4, 4.5, & 4.6).

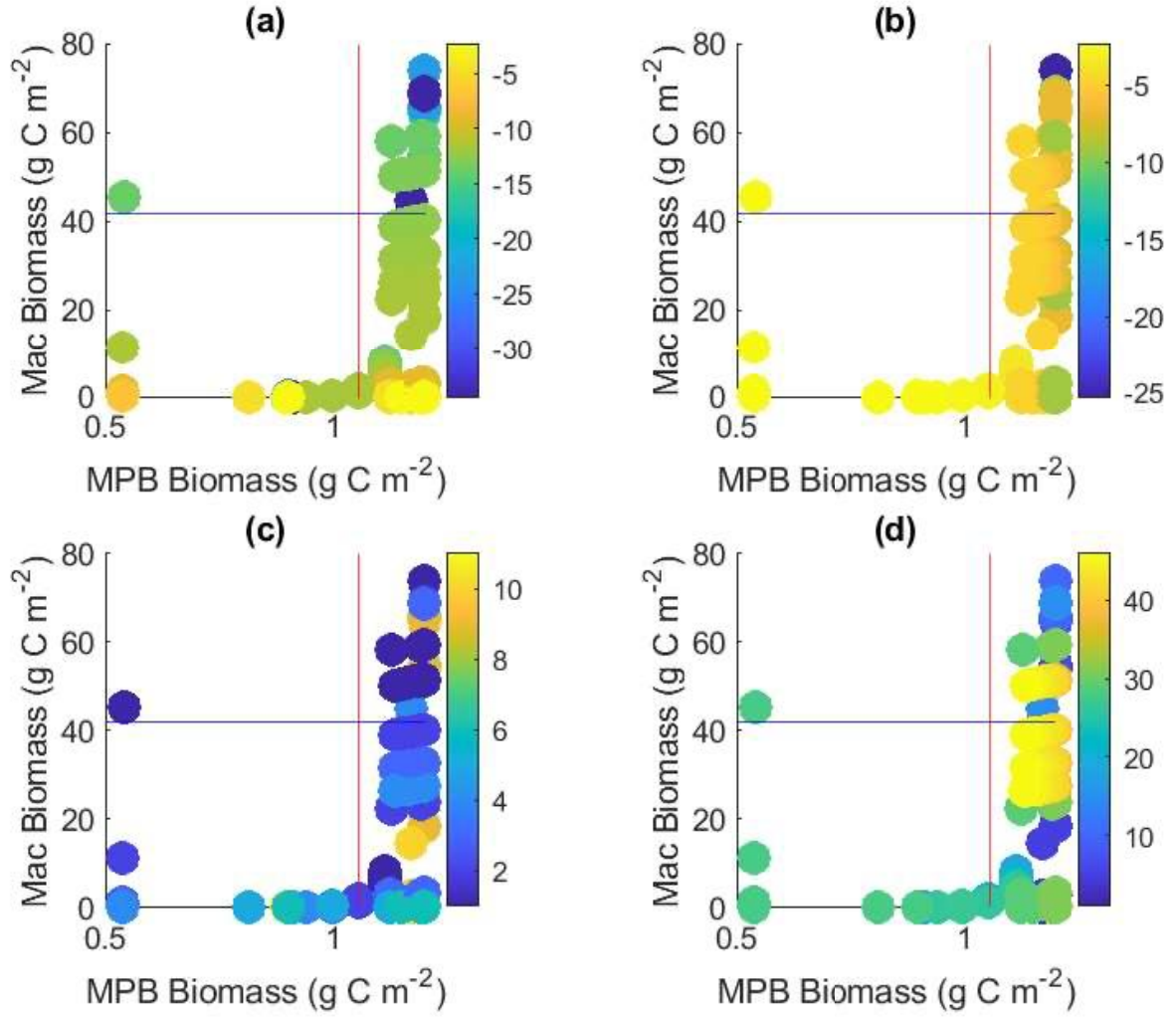

4.7.2 ***Nutrients***

N_{mac} in trials 32 to 46 (Figure 4.31 (a)) vary considerably from trials 28 to 31 (Figure 4.24 (a)). N_{mac} values are highest at their initial value of 49.099 mmol N m^{-2} and immediately reduce to low levels for the remainder of the trial. N_{mac} values range from 0.618 to zero mmol N m^{-2}, with no significant relationship existing with M_{MPB} (r = -.434, p = .106).

N_{MPB} in trials 32 to 46 (Figure 4.31 (b)) show notable change from trials 28 to 31 (Figure 4.24 (b)). Nutrient levels peak at their initial value of 49.04 mmol N m^{-2}, immediately reducing to low levels (opposed to peaking at over 4,000 mmol N m^2 as seen in trial 28).

N_{MPB} values remain above zero across all variants in trials 32 to 46, ranging from 0.849 to 0.00396 mmol N m^{-2}. There is a moderate negative relationship between M_{MPB} and N_{MPB} (r = -.522, p = .0459). Despite this result being significant at the 95% confidence interval, the relationship is not strong enough to conclude that M_{MPB} has an effect on N_{MPB}.

Figure 4.31. Timeseries plot of nutrient values (mmol N m^{-2}) per time step for trials 32 to 46 for *M. liliana* (a) and MPB (b). Trials are plotted along a colour scale progressing from dark blue to green (MATLAB's 'winter colormap').

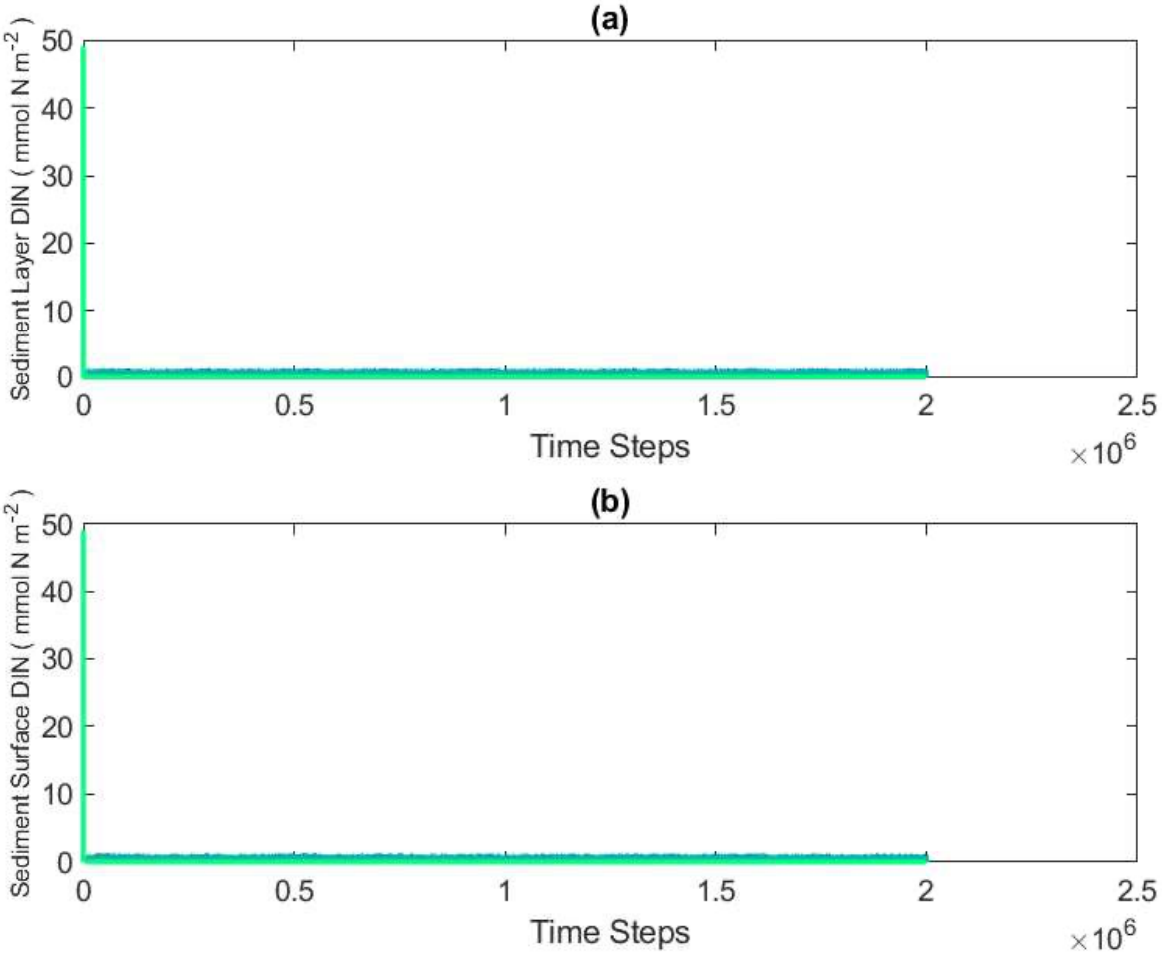

Figure 4.32. Timeseries plot of nutrient values (mmol N m^{-2}) per time step for trials one to 46 for *M. liliana* (a) and MPB (b). Data was used from trials one to 31, excluding trials 16 & 17 due to errors. Trials are plotted along several colour scales; trials one to ten are plotted in colours progressing from blue to magenta (MATLAB's 'cool colormap'), 11 to15 are plotted in colours progressing from red to yellow (MATLAB's 'autumn colormap'), 18 to 27 are plotted in colours progressing from dark green to lime (MATLAB's 'summer colormap'), 28 to 31 are plotted in colours progressing from black to copper (MATLAB's 'copper colormap'), and 32 to 46 are plotted in colours progressing from dark blue to green (MATLAB's 'winter colormap').

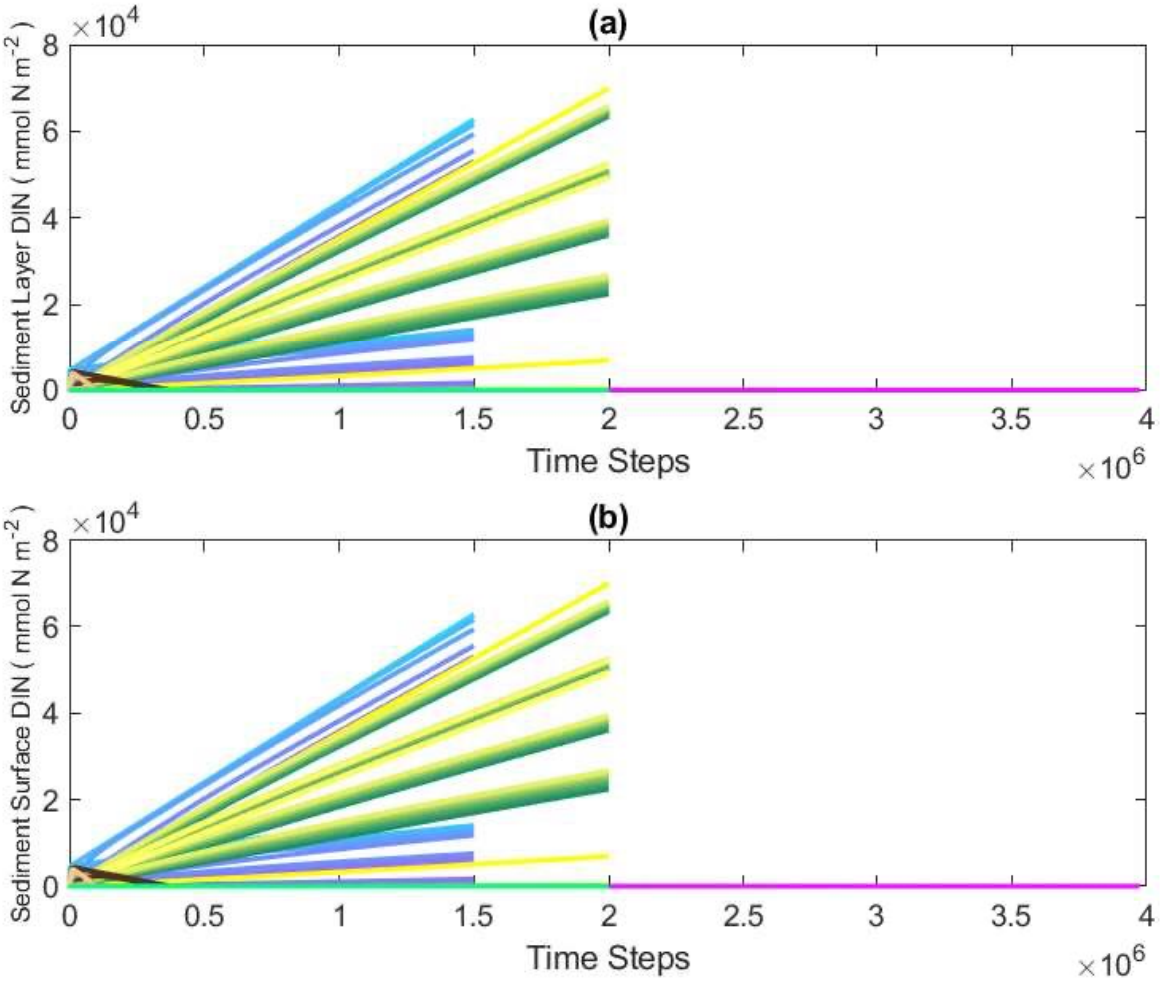

4.7.3 ***Detritus***

Unlike previously seen, D_{mac} do not spike in early the early stages of trials 32 to 46, but sit at low levels throughout the trials' length (Figure 4.33 (a)). D_{mac} values range from 0.154 to 0.0707 g C m^{-2}, and group together based on the M_{mac} value. The same pattern as biomass values in trials 32 to 46 (Figure 4.28) can be seen in Figure 4.33 (a); however, with a much smaller spread. A very strong negative relationship exists between D_{mac} values and M_{MPB} (r = -1, p = <.00001).

D_{MPB} also remain very low throughout trials 32 to 46 (Figure 4.33 (b)), when compared to previous trials. D_{MPB} values range from 0.409 to 0.000481 g C m^{-2}, and rapid

jumps in value are no longer seen. D_{MPB} values increase as the trials progress, showing a very strong positive relationship with M_{MPB} (r = .99, p = <.00001).

Figure 4.33. Timeseries plot of detrital values (g C m^{-2}) per time step for trials 32 to 46 for *M. liliana* (a) and MPB (b). Trials are plotted along a colour scale progressing from dark blue to green (MATLAB's 'winter colormap').

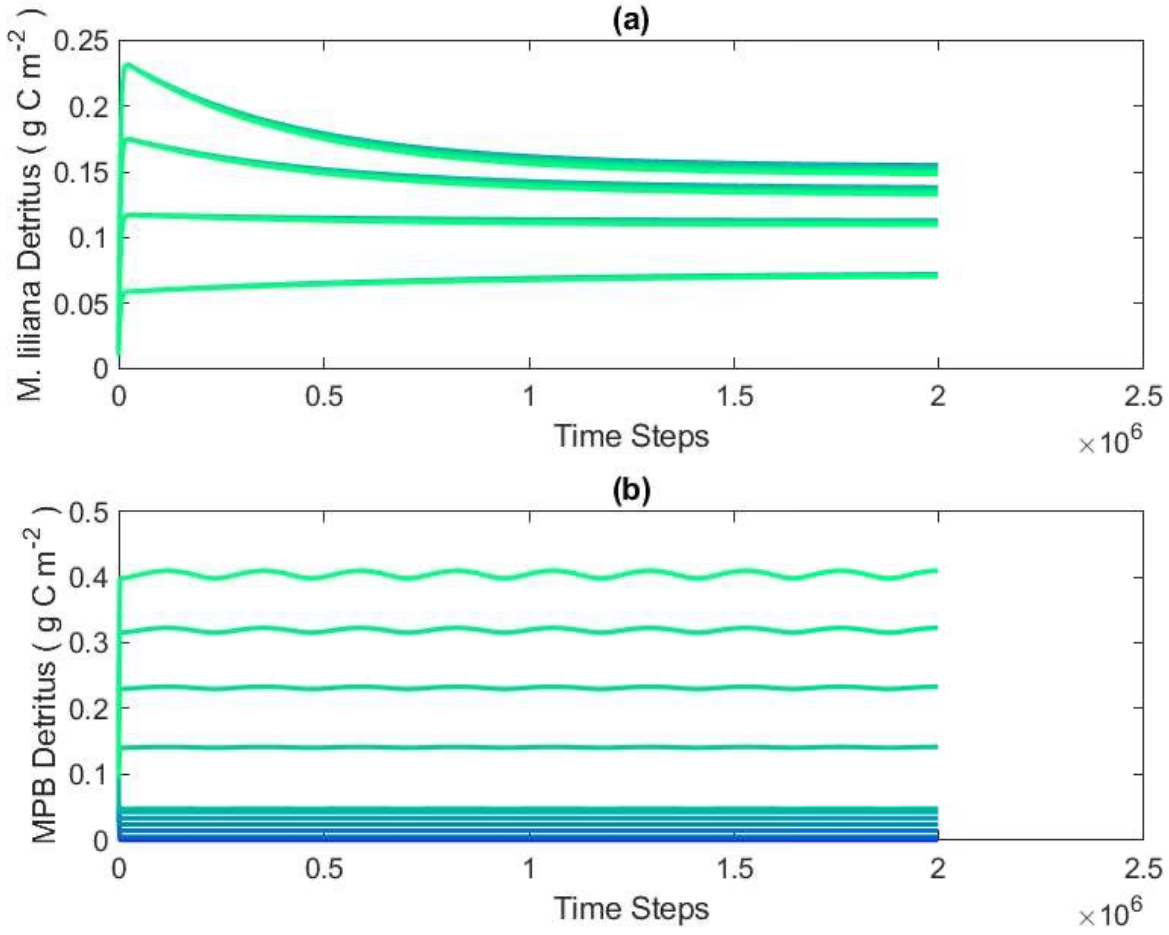

Figure 4.34. Timeseries plot of detrital values (g C m^{-2}) per time step for *M. liliana* (a) and MPB (b). Data was used from trials one to 46, excluding trials 16 & 17 due to errors. Trials are plotted along several colour scales; trials one to ten are plotted in colours progressing from blue to magenta (MATLAB's 'cool colormap'), 11 to 15 are plotted in colours progressing from red to yellow (MATLAB's 'autumn colormap'), 18 to 27 are plotted in colours progressing from dark green to lime (MATLAB's 'summer colormap'), 28 to 31 are plotted in colours progressing from black to copper (MATLAB's 'copper colormap'), and 32 to 46 are plotted in colours progressing from dark blue to green (MATLAB's 'winter colormap').

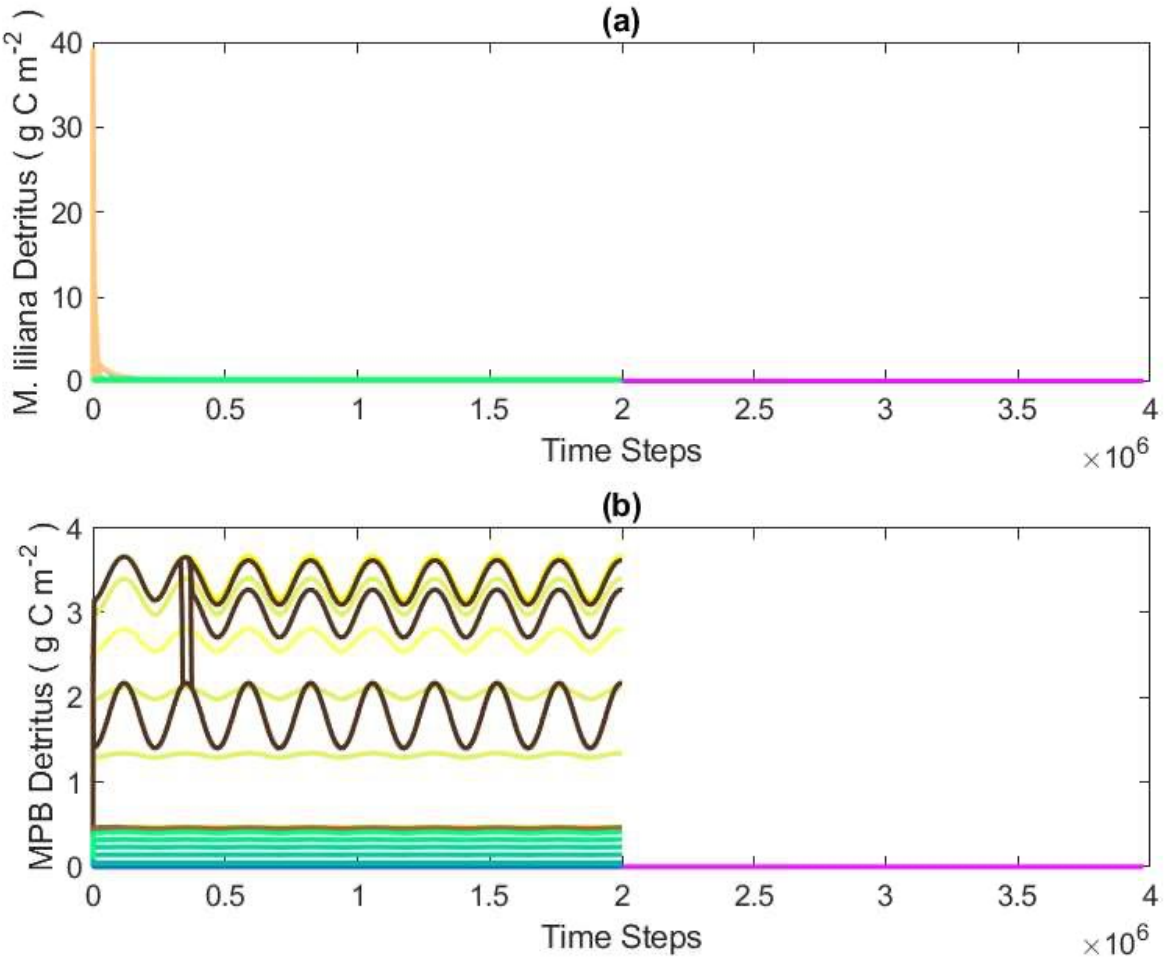

4.7.4 Key findings

- Smallest range of biomass values seen across all trials.
- B_{mac} results across all trials close to that seen in nature.
- Very strong relationships exist between M_{MPB} and B_{MPB}, B_{mac}, D_{mac}, and D_{MPB}.
- M_{MPB} has no significant relationship with N_{mac}, but a moderately negative relationship with N_{MPB}. Can't confirm N_{MPB} impacts water column nutrients.
- D_{MPB} values one order of magnitude smaller in trials 32 to 46, compared to all previous trials.

4.8 Preliminary Results of the Model

We identified B_{mac} and B_{MPB} results from trial 46 variant two (*see Table 4.6 for mortality values*) to be the most reflective of biomass values observed in nature. Values from testing were 38.91 and 1.132 g C m^{-2} for *M. liliana* and MPB respectively, a difference from nature of +2.85 and -0.076 g C m^{-2}. We tested the model's reaction to three external forcing factors that an estuary is likely to encounter: turbidity, sediment mud content, and external nutrient loading. The initial boundary conditions of our three dynamic variables were set to the values produced at the end of trial 46 variant two. Mortality rates were also taken from this trial and variant.

4.9 The Model's Reaction to Changing Turbidity

Turbidity was altered within the model by adjusting light attenuation, or the k_d parameter (Table 4.7) (*see Section 3.4*). The more turbid an environment, the higher the value of k_d, as light cannot penetrate through the sediment particles floating in the water column. The light availability at the bed does vary with water depth variations caused by our long period variations in water depth.

4.9.1 Biomass

There is a wide spread in B_{mac} values (Figure 4.35 (a)), ranging from 38.86 to 12.22 g C m^{-2}. As k_d increases throughout trials, B_{mac} decreases, demonstrating a very strong negative relationship between the two variables (r = -.981, p = <.00001).

The variation of k_d has created the largest oscillations of B_{MPB} we have seen thus far. B_{MPB} values have a range of 0.97 g C m^{-2}, with the largest oscillations in values occurring when k_d is set between 1.4 and 2.4 m (Figure 4.35 (b)). There is a very strong negative relationship between k_d and B_{MPB} (r = -.961, p = <.00001).

Figure 4.35. Timeseries plots of light variation trials one to 19 (excluding trials one, three, five, and seven due to errors). Biomass values (g C m^{-2}) per time step are plotted for *M. liliana* (a) and MPB (b). Results are plotted along a colour scale progressing from blue to magenta (MATLAB's 'cool colormap').

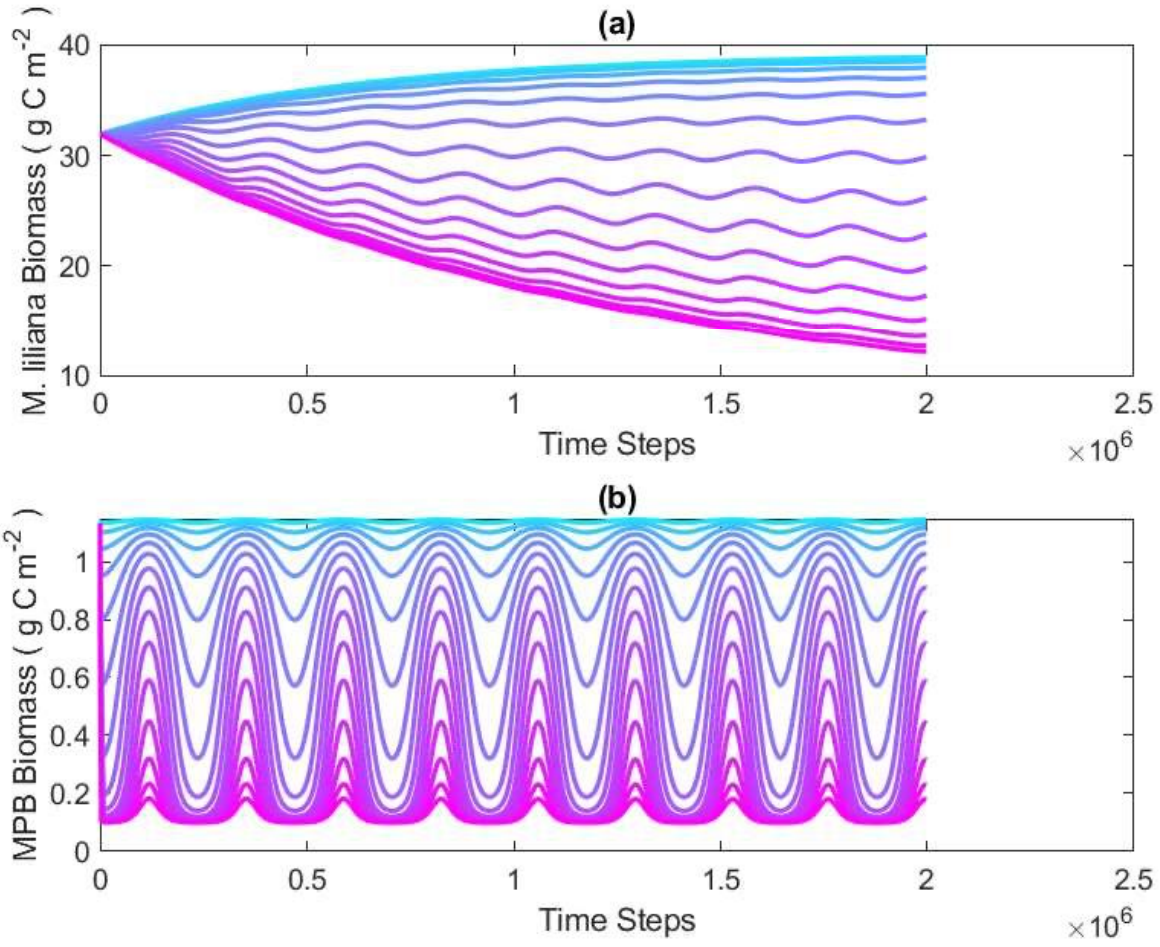

4.9.2 ***Nutrients***

N_{mac} values sit at zero throughout all light variation trials, removed by *M. liliana* pumping behaviour (Figure 4.36 (a)). Therefore, no inference can be made on a relationship between k_d and N_{mac}.

N_{MPB} values immediately drop to low levels, where they remain throughout all turbidity trials, increasing slightly as trials progress (Figure 4.37 (b)). N_{MPB} levels range from 0.00426 to 0.00566 mmol N m^{-2}, showing a strong positive relationship with k_d (r = .773, p = .00073). This makes sense given the negative relationship with B_{MPB} and k_d (*see Section 4.9.1*), as less MPB are available to consume and remove nutrients from the system.

Figure 4.36. Timeseries plot of light variation trials one to 19 (excluding trials one, three, five, and seven due to errors). Nutrient values (mmol N m^{-2}) per time step are plotted for *M. liliana* (a) and MPB (b). Results are plotted along a colour scale progressing from blue to magenta (MATLAB's 'cool colormap').

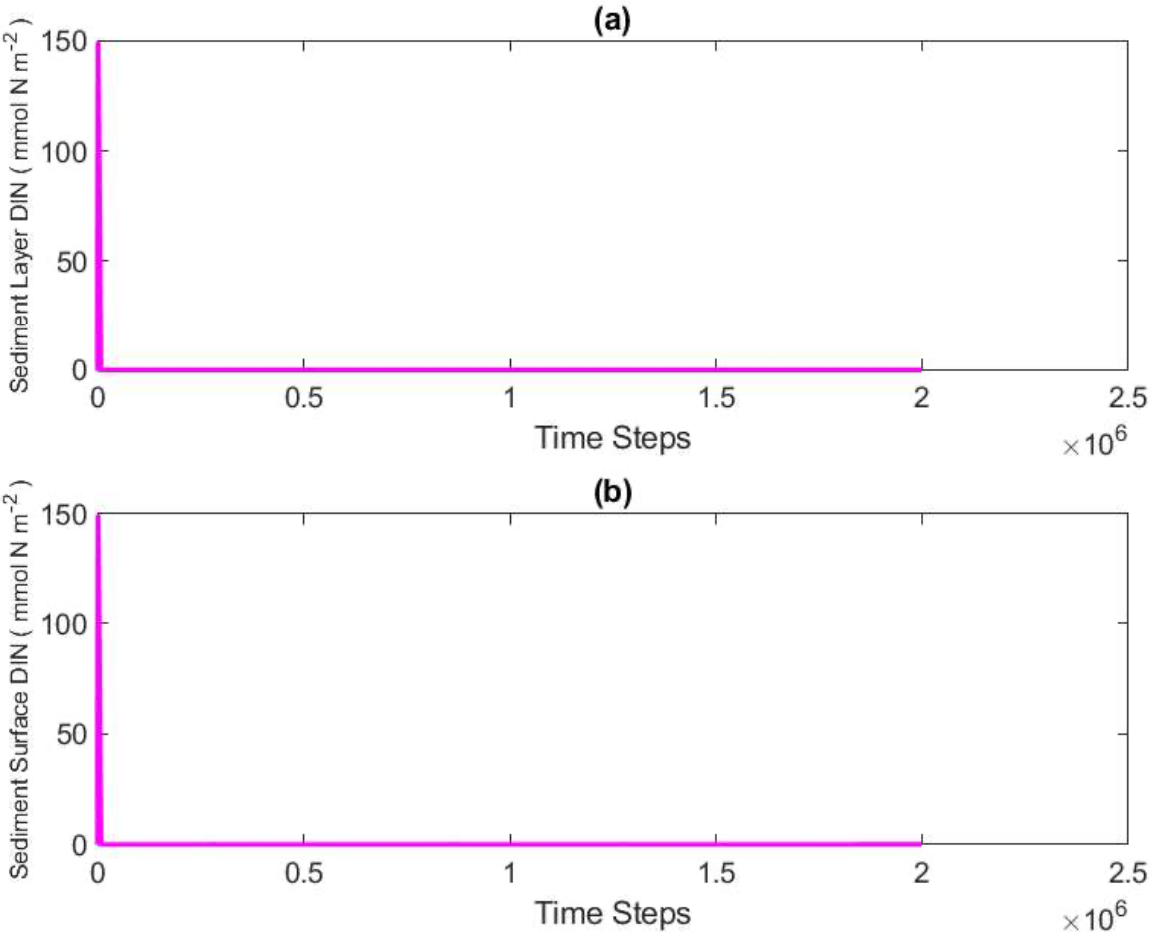

4.9.3 ***Detritus***

D_{mac} (Figure 4.37 (a)) has a similar spread to B_{mac} (Figure 4.35 (a)) in values, although, on a much smaller scale. D_{mac} across all k_d trials quickly drops from its initial value to 0.0924 g C m^{-2} within 7,348 time steps, before it follows the pattern of B_{mac}. D_{mac} has a range of 0.076 g C m^{-2}. There is a very strong negative relationship between D_{mac} and k_d (r = -.984, p = <.00001).

D_{MPB} (Figure 4.37 (b)) also follows the same pattern as B_{MPB} (Figure 4.35 (b)), with large oscillations in value occurring throughout k_d trials. The largest oscillations are seen when k_d has a value between 1.4 and 2.4. D_{MPB} has a range of 0.345 g C m^{-2}, and has a very strong negative relationship with k_d (r = -.962, p = <.00001).

Figure 4.37. Timeseries plots of light variation trials one to 19 (excluding trials one, three, five, and seven due to errors). Detrital values (g C m^{-2}) per time step are plotted for *M. liliana* (a) and MPB (b). Results are plotted along a colour scale progressing from blue to magenta (MATLAB's 'cool colormap').

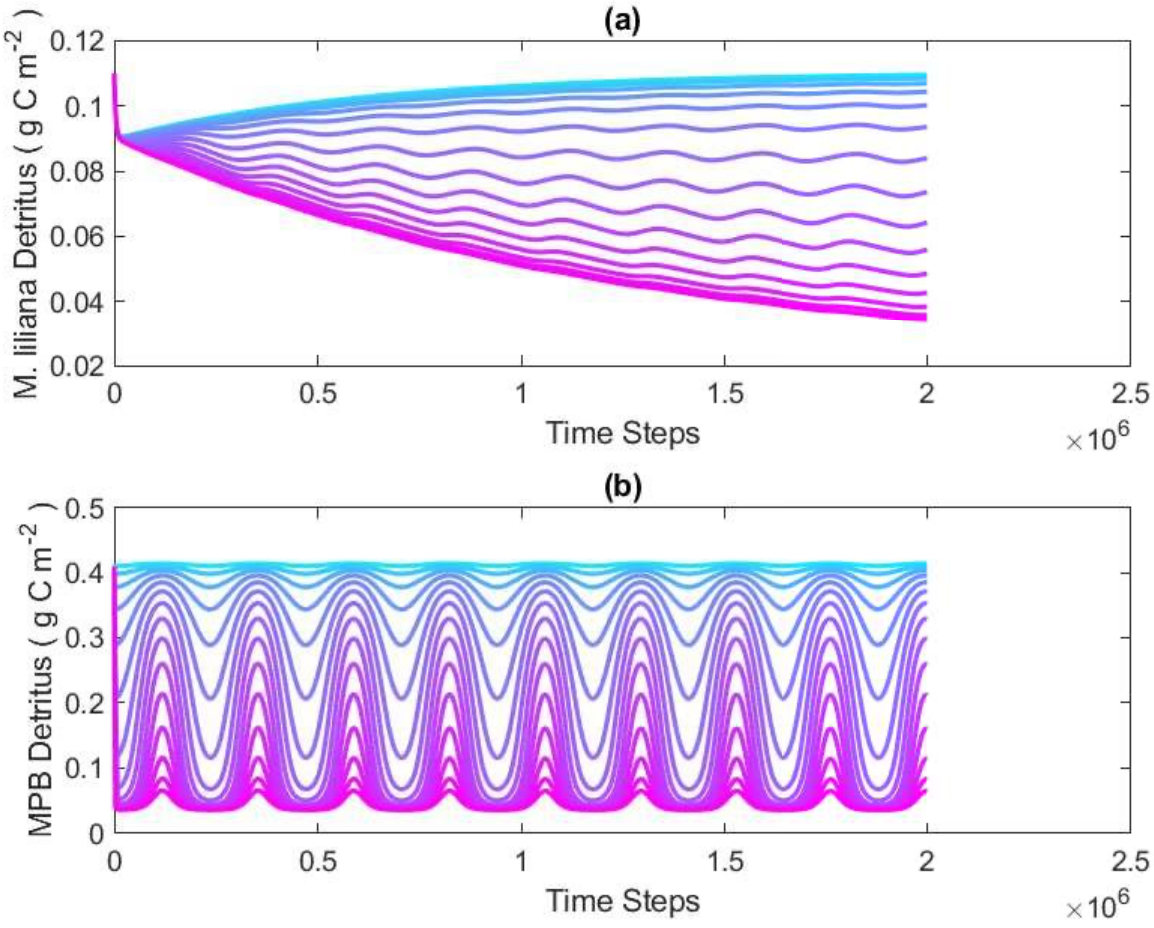

4.9.4 ***Key Findings***

- A very strong negative relationship exists between k_d and B_{mac}, B_{MPB}, D_{mac}, *and* D_{MPB}
- The earlier assumption that the system is light limited, as opposed to nutrient limited, proven by the negative relationship between k_d and B_{MPB}
- Variations of k_d have caused the largest oscillations in B_{MPB} and D_{MPB} (proportionately) throughout all model testing

4.10 The Model's Reaction to Increasing Sediment Mud Content

Sediment mud content (M_c) was increased by 0.1 as trials (Table 4.8). K_{mac} decreases as M_c increases (*see Equation 10*), causing both B_{mac} and D_{mac} values to drop; however, we were unsure how altering this variable would impact our other dynamic variables.

4.10.1 Biomass

B_{mac} has a range of 37.51 g C m^{-2}, showing a clear decrease as M_c increases (Figure 4.38 (a)). The difference in B_{mac} values between trials becomes greater as trials progress from one through seven. The large drop in B_{mac} values in the latter trials is not surprising, but rather demonstrates that the model is behaving appropriately (*see K_{mac} section 3.5*). A very strong negative relationship exists between B_{mac} and M_c throughout trials one through ten (r = -.937, p =.000065). This relationship still exists (r = -.911, p = .00444) when trials eight to ten are removed from statistical analysis, as to the model restricts K_{mac} to 1 g C m^{-2} once M_c reaches 0.8, artificially altering results.

B_{MPB} changes minimally with M_c, increasing by only 0.001 g C m^{-2} from trial one to ten (figure 4.38 (b)) – the smallest range of B_{MPB} across all model testing. However, a very strong positive relationship between these variables exists (r = .924, p = .000133). This relationship also continues to exist following the removal of trials eight to ten from analysis (r = .859, p = .0133). The relationship likely exists due to the reduction in $G_{macgraz}$ caused by increasing M_c values reducing B_{mac}. Trials eight through ten demonstrate a sharp increase in B_{MPB} from boundary conditions to K_{MPB} (within 144 time steps), before B_{MPB} rapidly drops to 1.16 g C m^{-2} (by 40,323 time steps). From here, B_{MPB} begins to stabilise, then rapidly drops again to 1.12 g C m^{-2} by 175,691 timesteps, before the species' biomass resumes its regular oscillation pattern.

Figure 4.38. Timeseries plots of sediment mud content trials one to ten. Biomass values (g C m^{-2}) per time step are plotted for *M. liliana* (a) and MPB (b). Results are plotted along a colour scale progressing from blue to magenta (MATLAB's 'cool colormap').

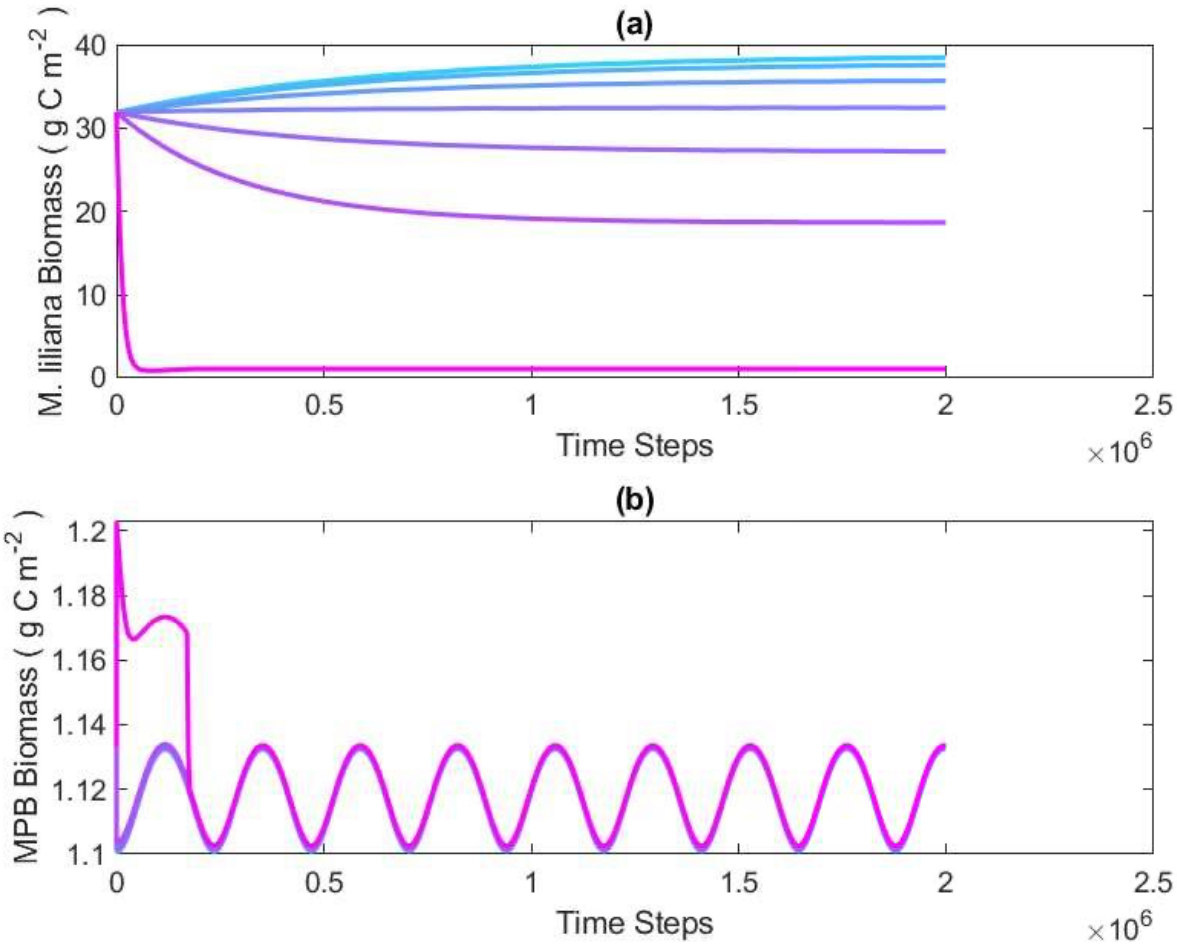

4.10.2 ***Nutrients***

N_{mac} values were zero at the end of all sediment mud content trials, meaning no inference can be made on the relationship between N_{mac} and M_c. For a short period, nutrient values increase 15 fold in trials eight to ten (figure 4.39). This is likely due to a combination of an initial sharp increase in B_{MPB} supplementing the nutrient pool present through decay (*see Equation 18*), the reduced grazing potential of MPB by *M. liliana*, and the mixing coefficient maintaining equilibrium between the nutrient pools. The drop in nutrient values (timestep 34,963) in these latter trials occur almost simultaneously to the first drop in B_{MPB} and D_{MPB} (*see 4.10.1 and 4.10.3*). Nutrients are then removed from the system through *DR*. N_{MPB} values have a range of 0.0665 mmol N m^{-2} and have a very strong positive relationship with M_c (r = .8, p = .00544).

Figure 4.39. Timeseries plots of sediment mud content trials one to ten. Nutrient values (mmol N m^{-2}) per time step are plotted for *M. liliana* (a) and MPB (b). Results are plotted along a colour scale progressing from blue to magenta (MATLAB's 'cool colormap').

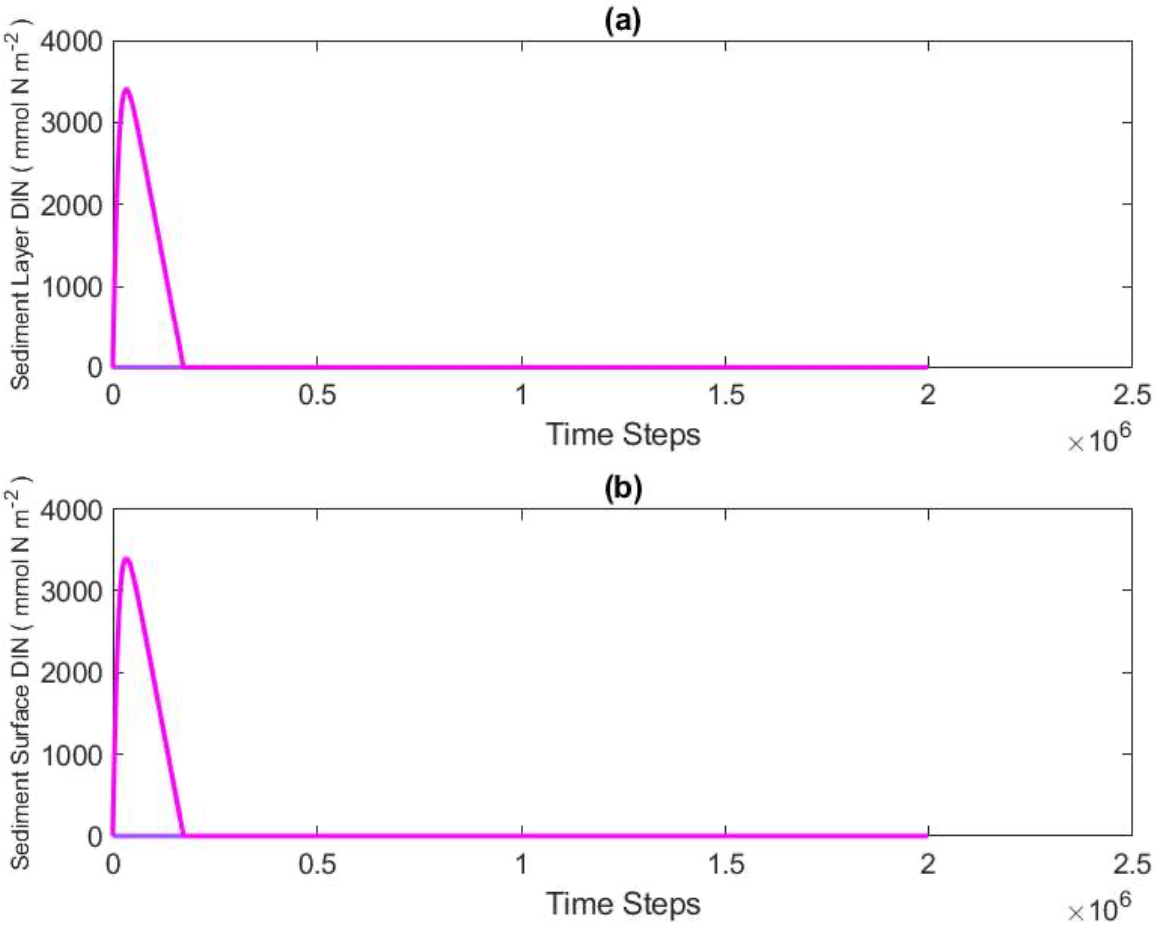

4.10.3 ***Detritus***

D_{mac} (figure 4.40 (a)) follow a similar pattern to B_{mac} (figure 4.38 (a)), only differing in the beginning where D_{mac} rapidly decrease from initial boundary conditions, before stabilising. D_{mac} values in trials one to ten have a range of 0.106 g C m^{-2} and have a very strong negative relationship with M_c (r = -.937, p = .000065). The *r-value* and *p-value* for this relationship is identical to the relationship between B_{mac} and M_c (*see 4.10.*1). Further similarities can be made to B_{mac} results when trials eight to ten are removed from statistical analysis for D_{mac} and M_c (r = -.911, p = .00432).

Alike B_{MPB}, D_{MPB} in trials one to ten have the smallest range throughout all model testing (0.0004 g C m^{-2}). A very strong positive relationship exists between D_{MPB} and M_c (r = .942, p = .000047). The unusual variations in value across trials eight to ten (Figure 4.40 (b)) reflect the species' biomass response (*see 4.10.1*).

Figure 4.40. Timeseries plots of sediment mud content trials one to ten. Detrital values (g C m^{-2}) per time step are plotted for *M. liliana* (a) and MPB (b). Results are plotted along a colour scale progressing from blue to magenta (MATLAB's 'cool colormap').

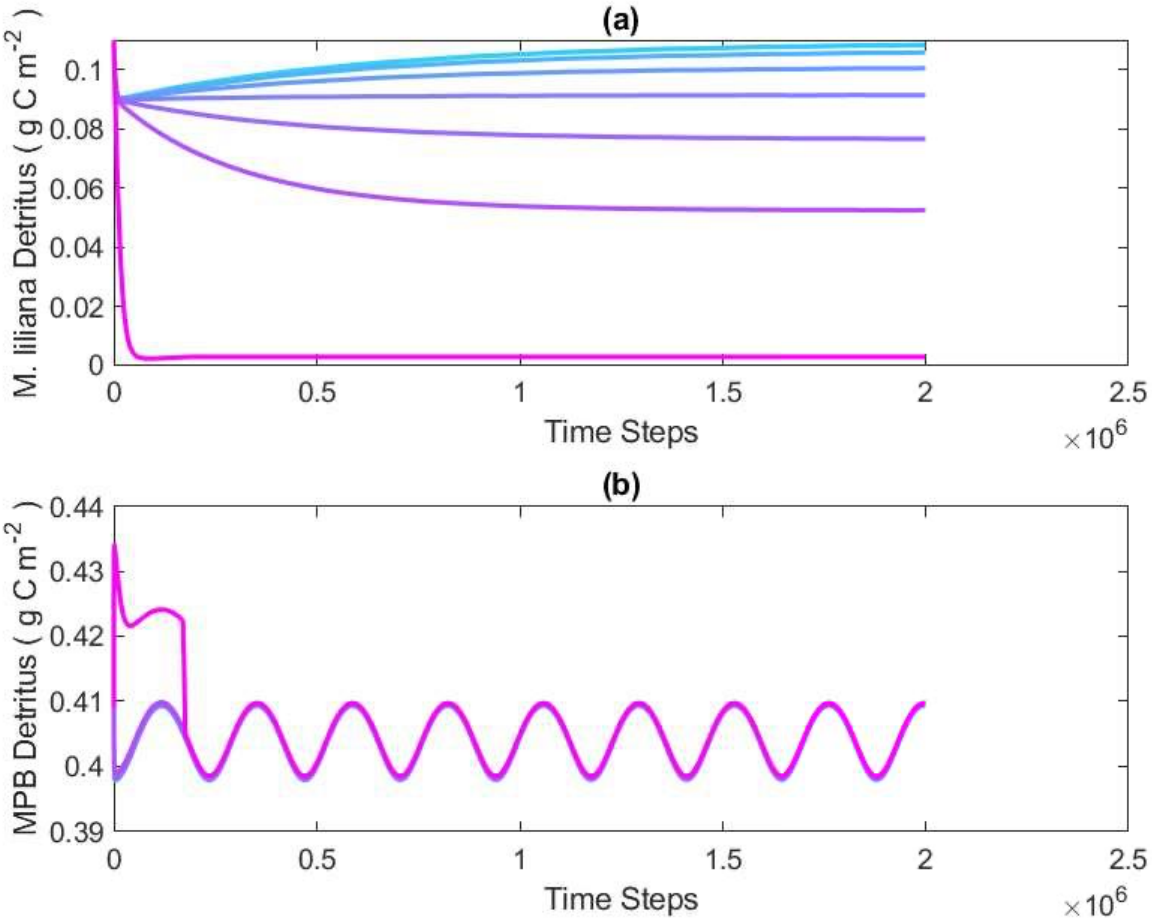

4.10.4 ***Key Findings***

- M_c strongly negatively effects the size of B_{mac} and D_{mac}, while increasing the value of the remaining dynamic variables.
- The sharp decline in nutrient values coincide with rapid shifts in B_{MPB} and $D_{MPB.}$
- Trials eight to ten show the system reacting to a possible regime shift, following the large reduction in B_{mac} due to M_c.

4.11 The Model's Reaction to a Single External Nutrient Loading Event

External nutrient input was altered by increasing the initial external nutrient (*IN*) levels (mmol N m^{-2}) by one order of magnitude per trial (Table 4.9). Six trials were conducted, with the model crashing on a seventh due to the amount of nutrients being too large.

4.11.1 Biomass

B_{mac} values increase from trials one to five, before decreasing by more than 40% from trial five to six (Figure 4.41 (a)). B_{mac} has a range of 15.93 g C m^{-2}. In trial six, B_{mac} responds sharply to external nutrient loading, falling from boundary conditions to 0.281 g C m^{-2}, before the population slowly recovers to 22.52 g C m^{-2} by the end of the trial. These results are promising, as they demonstrate *M. liliana*'s recovery pattern following a significant nutrient loading event. A very strong negative relationship exists between B_{mac} and *IN* (r = -.993, p = .000073).

B_{MPB} follows a similar pattern to B_{mac}. It has a range of 0.0402 g C m^{-2}, going on an upward trend throughout trials until trial six, where it decreases (Figure 4.41 (b)). However, B_{MPB} in trial six remains larger than several earlier trials, only dropping below values seen in trials four and five. B_{MPB} in trial six experiences a sharp increase from initial values to K_{MPB} (within 102 time steps), followed by a steep drop to 1.16 g C m^{-2}. The sharp decline of both B_{mac} and B_{MPB} occur simultaneously, reaching their lowest points between 20,000-25,000 time steps. No significant relationship exists between B_{MPB} and *IN* (r = .251, p = .631).

Figure 4.41. Timeseries plots of external nutrient loading trials one to six. Biomass values (g C m^{-2}) per time step are plotted for M. liliana (a) and MPB (b). Results are plotted along a colour scale progressing from blue to magenta (MATLAB's 'cool colormap').

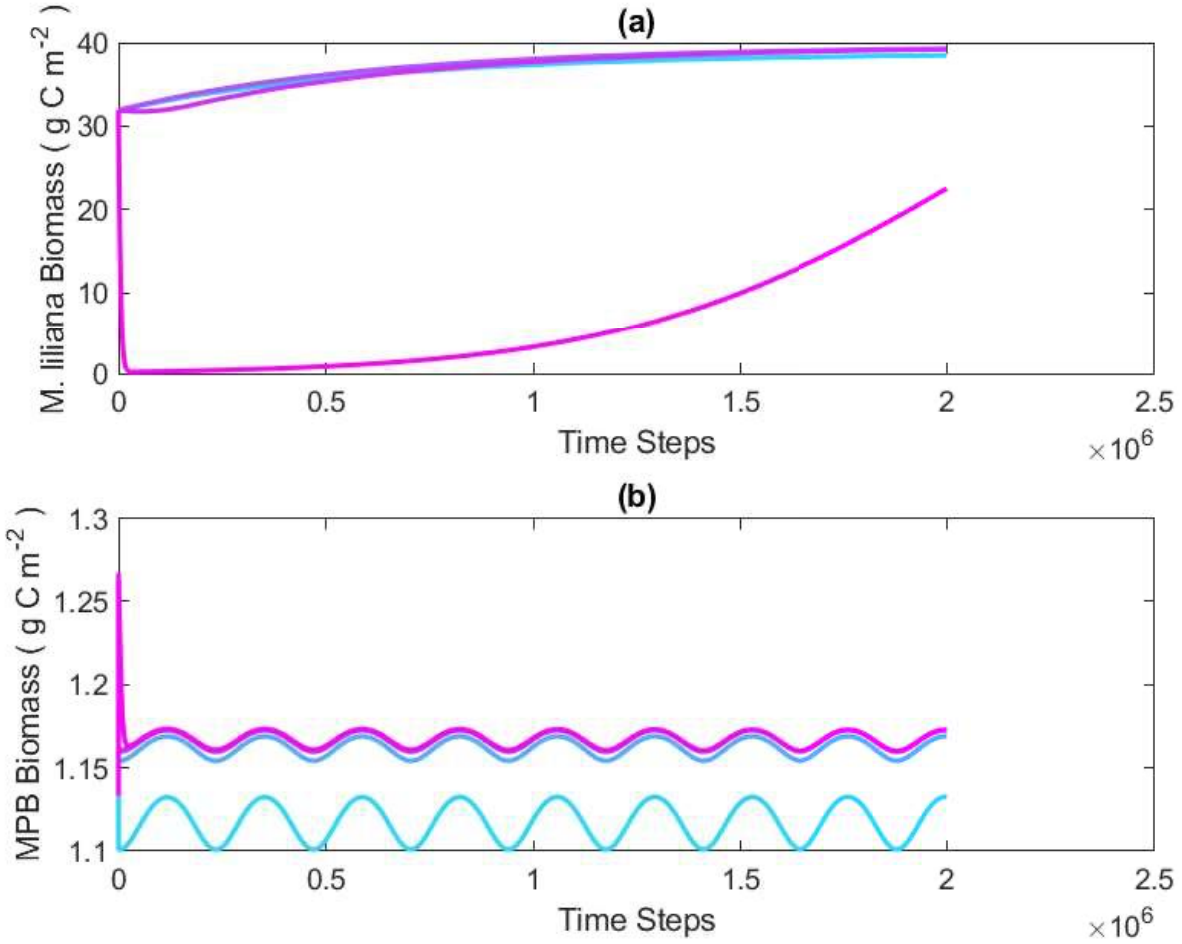

4.11.2 ***Nutrients***

Figure 4.42 was log transformed so that the results from all six trials could be examined. The scale that *IN* increases throughout trials (Table 4.9) produced results too large to fit on a regular timeseries plot..

N_{mac} reduce to zero throughout all six trials (Figure 4.42 (a)), meaning no inference can be made on the relationship with *IN*. However, it is clear that nutrients remain in this layer longer as trials progress, before their removal by the *DR* parameter.

N_{MPB} follow a similar trend to N_{mac}, except levels do not reach zero (Figure 4.42 (b). N_{MPB} has a range of 4.448e^{-4} g C m^{-2}, and surprisingly has a very strong negative relationship with *IN* (r = -.996, p = .000023). This is likely due to the reduced B_{mac} values, as less *M. liliana* are contributing to the pumping of nutrients from within the sediment to the sediment surface. Therefore, nutrients are being sourced from the water column, until *DR* removes the

nutrients from the system following the external loading. As B_{mac} begins to increase, more nutrients will be pumped to the sediment surface to maintain B_{MPB}.

Figure 4.42. Log transformed timeseries plots of external nutrient loading trials one to six. Nutrient values (mmol N m^{-2}) per timestep are plotted for *M. liliana* (a) and MPB (b). Results are plotted along a colour scale progressing from blue to magenta (MATLAB's 'cool colormap').

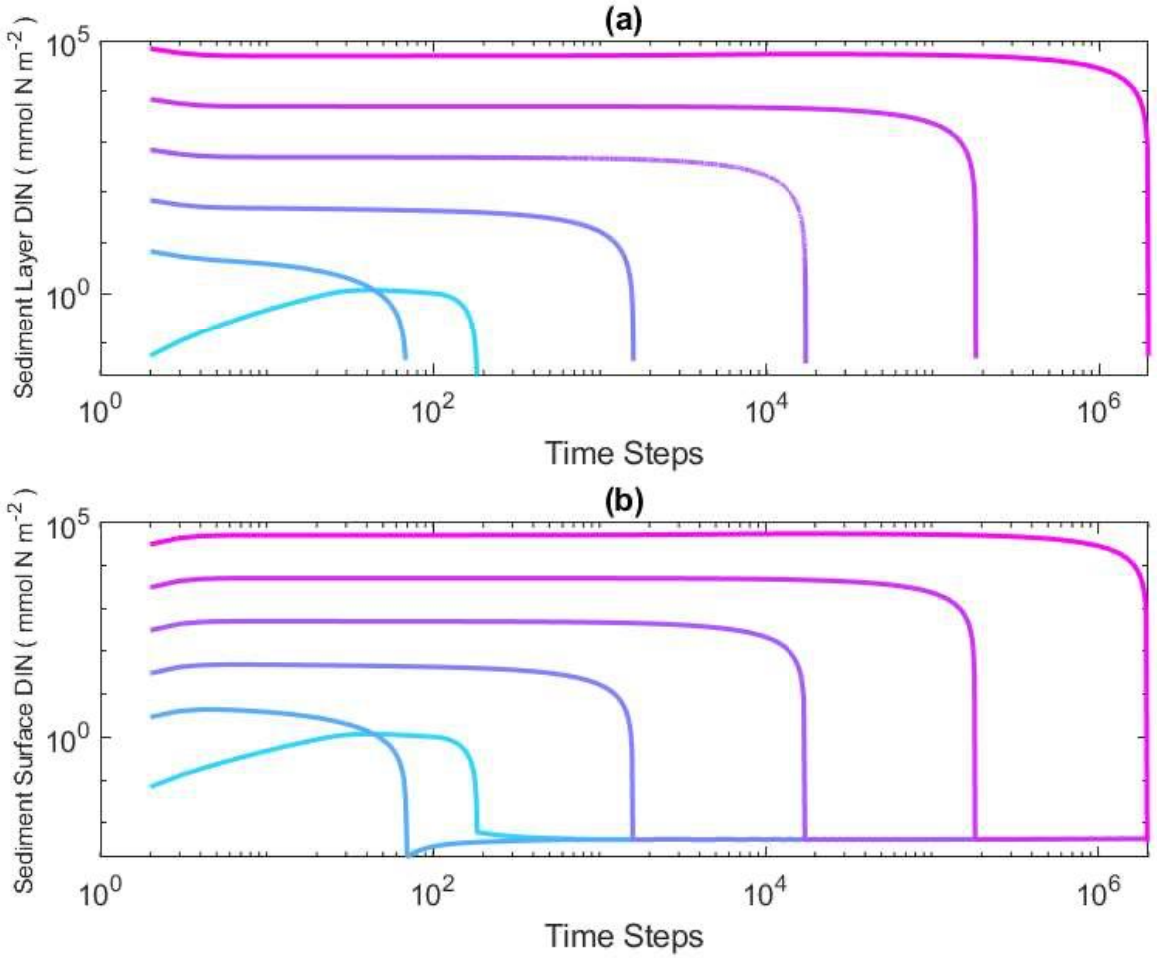

4.11.3 ***Detritus***

Figure 4.43 (a) demonstrates D_{mac} values following a similar pattern to B_{mac} (Figure 4.41 (a)) (*see Section 4.11.1 for analysis*). D_{mac} has a very strong negative relationship with *IN* (r -.994, p = .000069), which is nearly identical to that of B_{mac} and *IN* (*see Section 4.11.1*) D_{mac} has a range of 0.0453 g C m^{-2}.

D_{MPB} (Figure 4.43 (b)) is also very similar to B_{MPB} (*see Section 4.11.1 for analysis*), having no significant relationship with *IN* (r = .251 p = .631). D_{MPB} has a range of 0.0201 g C m^{-2}.

Figure 4.43. Timeseries plots of external nutrient loading trials one to six. Detrital values (g C m^{-2}) per time step are plotted for *M. liliana* (a) and MPB (b). Results are plotted along a colour scale progressing from blue to magenta (MATLAB's 'cool colormap').

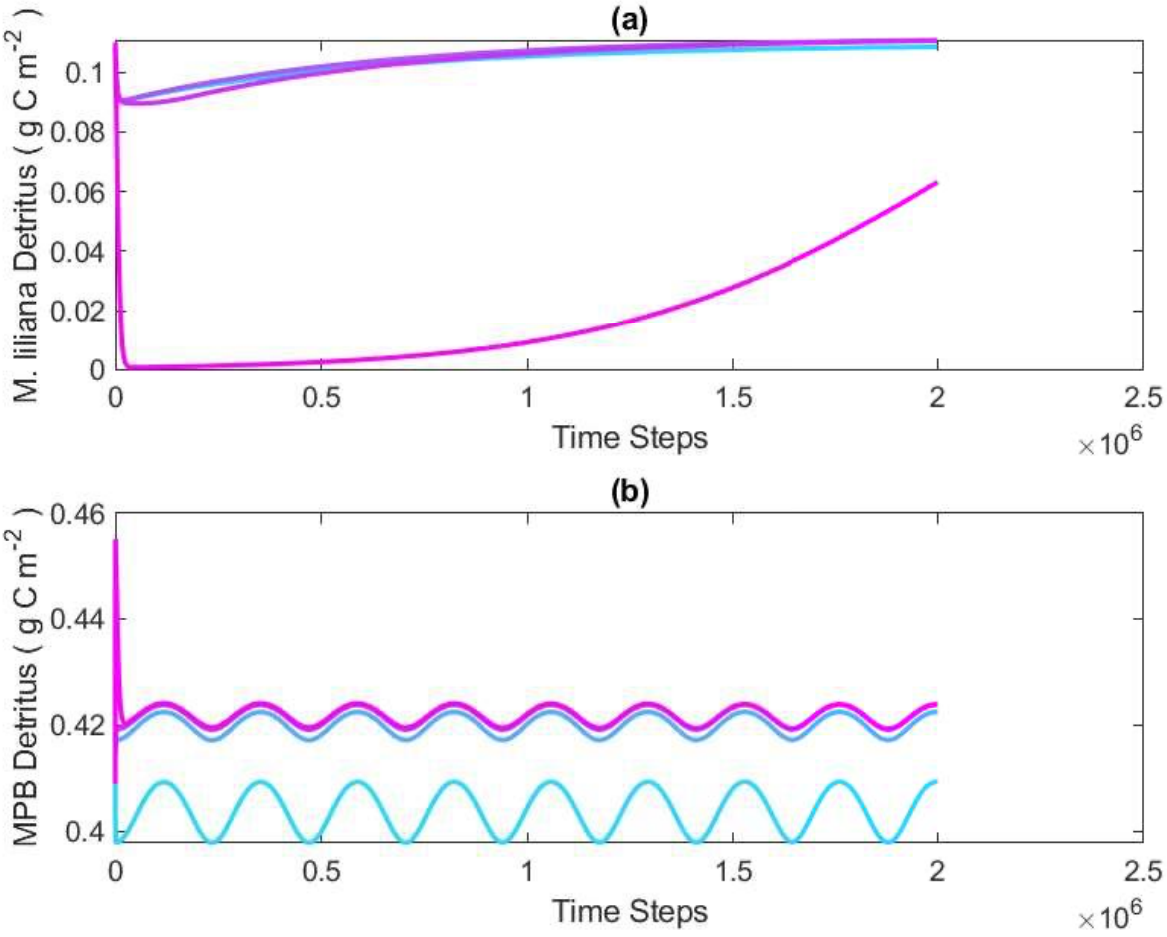

4.11.4 Key Findings

- Very strong negative relationships exist between *IN* and B_{mac}, N_{MPB}, and D_{mac}.
- Increasing *IN* does not result in a MPB bloom until 100,000 mmol N m^{-2} is added to the system. This bloom is not sustained, despite nutrient levels remaining comparatively high throughout the trial.
- No significant relationship exists between *IN* and B_{MPB}, N_{mac}, and D_{MPB}.

Chapter 5

Discussion

5.1 Successful Modelling of Interactions Between Three Dynamic Variables

We were able to successfully create a dynamic model that can accurately synthesise basic ecological relationships within benthic estuarine communities. Following over 260 mortality variation trials, we identified model conditions that produced *M. liliana* and MPB biomasses (B_{mac} and B_{MPB} respectively) that most accurately reflected values seen in nature. Throughout the testing phase, we were able to identify and plot the interactions and relationships between our three dynamic variables, with these interactions becoming more representative of the real world as trials progressed. Our intention for this model was for it to be used within estuarine management, particularly in the scope of tipping points, which we believe our model has identified during testing. We will discuss these occurrences, the observed relationships, and any interesting events within the model below.

5.1.1 Relationships Observed During Model Testing

Throughout our mortality testing, we identified numerous relationships of varying strength between the model's three dynamic variables. In this section, we discuss the evolution of these relationships throughout the mortality testing trials. When reading this section, please consider that the mortality parameter was coded to exclusively update the biomass and detritus of its assigned species. This means we have not manufactured the coupling behaviour identified in our results and can be confident that our model is accurate in its simulation of these behaviours.

According to the literature (*see Sections 2.2 to 2.5*), our finalised model behaved appropriately. Several notable findings were identified throughout the mortality trails: 1) MPB's mortality rate (M_{MPB}) was initially more important than *M. liliana*'s (M_{mac}) for altering conditions within the system; 2) the consumption of MPB by *M. liliana* ($G_{macgraz}$) had less effect than expected on B_{MPB}; and 3) B_{mac} values were much less stable than B_{MPB}.

The first finding was surprising, as we believed that key ecosystem functions performed by *M. liliana* would be more important in determining available nutrients than the

MPB population. For example, we thought that the recycling of nutrients into the water column by *M. liliana* (Ehrenhauss et al., 2004; Volkenborn et al., 2012; Woodin et al., 2012) would be increased as the smaller M_{mac} values allowed for a greater B_{mac}, making M_{mac} an imperative variable regarding nutrient concentrations. However, M_{MPB}'s initial control of the system was so dominant, that throughout trials 11 to 15 the influence of MPB's mortality rate on B_{mac} was stronger than *M. liliana*'s. In line with our initial assumptions, these findings changed as trials progressed, as the relationships M_{mac} shared with other variables became considerably stronger at the 95% confidence interval. We attribute this change to M_{mac} becoming reflective of rates seen in nature and to the addition of the denitrification (*DR*) parameter, both of which enabled the formation of appropriate relationships seen in estuaries.

On the surface, the second finding is consistent with the literature; the positive relationship between B_{MPB} and B_{mac} seen in nature is sustained by *M. liliana*'s pumping behaviour having a greater influence on B_{MPB} than grazing (Thrush et al., 2006). If grazing control over B_{MPB} was more prominent (as we had expected), our results would have shown considerable variations in B_{MPB} coinciding with the amount of *M. liliana* available to graze. The same should be true for B_{MPB} and *M. liliana*'s pumping behaviour; a larger B_{mac} generates more pore-water advection from the sediment to the water column, bringing with it more nutrients to fuel B_{MPB} growth. Figure 4.28 demonstrates a large disparity in B_{mac} values, with very little change in B_{MPB} (*see Section 4.7.1*). Due to the structure of the latter stage of testing, there was insufficient data to test the relationship between M_{mac} and B_{MPB}, which may have clarified this concern. Therefore, can we be sure that our model is demonstrating the relationship seen in Thrush et al. (2006)? It is likely that we created a system that is not nutrient limited and enables B_{MPB} to sustain itself independently from *M. liliana* (due to MPB's ability to source nutrients from the water column), meaning the relationship identified in Thrush et al. (2006) is not imperative for the growth of B_{MPB}. This is consistent with a plethora of studies demonstrating MPB's nutrient uptake from sources outside *M. liliana* (e.g., Sundbäck & Granéli, 1988; Ni Longphuirt et al., 2009; Brito et al., 2010; Brito et al., 2012), and that *M. liliana*'s pumping behaviour and excretion enhance available nutrients for MPB, but are not the only source (Wilcock et al., 1993; Thrush et al., 2006).

Compared to B_{mac}, B_{MPB} was much more stable throughout the mortality trails. Within sets of trials (e.g. trials 1-10, 11-15, etc) B_{MPB} results varied little from each other, while B_{mac} results had a much larger range. B_{MPB} results would oscillate beneath the species' carrying capacity (*K*), a pattern that would continue until the end of trial. Alternatively, B_{mac} values

continued on an upward or downward trend at the end of the trial, until trial 28. From there, B_{mac} began to stabilise and remain relatively constant for the remainder of the trial. Again, we attribute this change to M_{mac} becoming more reflective of natural values and the addition of *DR*. Before the addition of *DR*, nutrients in the system were reaching levels toxic to *M. liliana*, reducing their carrying capacity and lowering their biomass. Once this issue was resolved B_{mac} was able to remain constant, as nutrients were removed from the system before toxic levels could be reached. MPB did not share the same concern, as their growth was only hindered when nutrients became limited within the system, not when in excess.

5.1.2 Possible Tipping Point Events

During mortality rate testing, trials 28 through 31 experienced rapid shifts in B_{MPB} and MPB detrital values (D_{MPB}). Variants of trial 28 experienced the largest shifts (*see Section 4.6.1*). Additionally, during sediment mud content (M_c) testing, trials eight through ten also experienced rapid shifts in B_{MPB} values. In this section, we will discuss our model's ability to identify ecosystem tipping points, with reference to variants of trial 28 from the mortality rate testing and trials eight to ten from M_c testing. Despite the mortality testing trials not experiencing the external forcing that regularly coincides with tipping points (*see Section 2.8*), a change in mortality rates can simulate the response of our chosen species to these forces. Therefore, the response of B_{MPB} within the M_c trials is a more accurate representation of what would be seen in nature. However, we can still look at B_{MPB}'s response in the mortality testing trials to better recognise the model's reaction to a tipping point.

Firstly, we must consider the efficacy of our model in predicting ecosystem tipping points. Recommendations within the literature outline the standards monitoring programmes must meet to accurately predict regime shifts (Hewitt & Thrush, 2019). Judging our model against these guidelines would diminish its efficacy in predicting tipping points, as its design does not align with real world estuarine monitoring programmes with large historic data sets. Our design models future outcomes based upon present day values, rather than using years of repetitive data to track change and make predictive inferences. Therefore, it is more suitable to judge our model's ability based upon the model's design, rather than its applicability to estuarine monitoring programme guidelines.

There are many ways that a model such as ours can become more accurate in predicting tipping points. The literature agrees that creating a multivariate timeseries by monitoring the response of more than one species in the community, adding spatial data, and programming a long-term horizon is imperative for increasing a model's prediction efficiency

(Dakos et al., 2011; Hewitt & Thrush, 2019; Muthukrishnan et al., 2022). Increasing the number of components in the system will improve the model's efficacy in predicting tipping points and allow for insights into the pattern of transition between states (Muthukrishnan et al., 2022). Bestelmeyer et al. (2011) emphasise the importance of environmental context, meaning constructing a model that fits the spatial and biogeochemical context of the chosen location as accurately as possible. Ultimately, a model's capacity to make worthwhile insights into a system's response to drivers is determined by its ability to incorporate broad and rich datasets.

Under the framework of the above guidelines, our model's design is adequate for making predictions of ecosystem tipping points. Although, it may be more appropriate for recognising the signals identifying tipping points, rather than the whole ecosystem response when a system goes through a tipping point. Possible early warning signals may be a change in variance closer to lower frequencies, slower restore rates after disturbance, and larger fluctuations in the dynamics of key ecosystem variables (Carpenter et al., 2007). Our results demonstrate a clear and abrupt change in B_{MPB} in response to variations in mortality rate and M_c, which coincides with two of the three early warning signals outlined above. As the expected dramatic reactions that characterise tipping points are not always correlated to sudden changes in environmental drivers (Hewitt & Thrush, 2019), it is likely that this sudden deviation in biomass is an identifying signal of a tipping point. This finding is further corroborated by what we know of MPB's response to external forcing (*see Sections 2.3, 2.4, & 2.5*). Therefore, we can be confident that this model has achieved our primary objective of this thesis and is appropriate for use in current or future estuarine monitoring programmes. The latter will be particularly true should the recommended additions to the model be implemented in future (*see Section 5.3*).

5.2 Preliminary Results of External Forcing Tests

5.2.1 Turbidity

Our turbidity trials were conducted over a large range of light attenuation (K_d) values, ranging from 0.2 to 3.0m and increasing in 0.2m increments. To maintain simplicity, our model has been designed to operate at a constant light attenuation (K_d) value based on an average reading over 24 hours.

Suspended particles, such as mud or pollutants, are delivered from catchments through freshwater inputs into estuaries, making waters turbid (Cussioli et al., 2019). This

process is especially prominent where soil is exposed and following high rainfall or flood events (Swales et al., 2003; Hancock & Hewitt, 2004). Turbid waters limit light penetration (increase light attenuation) (Dennison, 1987), reducing the photosynthetic potential for, and productivity of, organisms such as MPB. Consequences of decreasing primary production are detrimental to ecosystem health, such as reducing macrofaunal diversity (Morris & Keough, 2003) and intensifying the efflux of dissolved inorganic nitrogen from sediments (Pratt et al., 2014). A positive feedback loop is created, where turbidity and tidal state dictate MPB's ability to consume the increased nutrients from sediment (Meyercordt & Meyer-Reil, 1999; Hillebrand et al., 2000; Stutes et al., 2006), meaning turbid waters can cause nutrient levels within estuaries to remain larger for longer. Furthermore, turbid waters inhibit the biostabilisation of sediments by MPB, facilitating greater turbidity through sediment resuspension (Pivato et al., 2018b). Despite dwelling beneath the sediment surface, suspended sediment can be ingested by *M. liliana*, creating a higher energy demand during feeding, and reducing the energy remaining for reproduction, growth, and maintaining healthy weight (Hancock & Hewitt, 2004).

As K_d was increased in our turbidity trials the system became light limited, reducing MPB's growth rate (G_{MPB}) and biomass. *M. liliana* also decreased in biomass, but this was likely in response to the reduction of their food source, as their growth is not directly dependent on light availability. Our model further imitated an estuary's response to increasing turbidity, as there was a strong positive relationship between nutrients in the water column and the K_d value. This is reflective of the literature (Meyercordt & Meyer-Reil, 1999; Hillebrand et al., 2000; Stutes et al., 2006; Pratt et al., 2014), demonstrating how a reduction in MPB's productivity increases nutrient concentrations. Additionally, our results align with other findings that show how light, rather than nutrient, availability is more important for the productivity of MPB (Mangan et al. 2020) and confirms our assumption that our system is light limited, not nutrient limited. Our results further coincide with a study of a similar nature, where Pivato et al. (2018b) applied a 1-D surface energy balance model to the prior analysis of a shallow tidal flat within the Venice Lagoon (Pivato et al., 2018a). The authors identified that clear water conditions supported the growth of MPB, with light availability at the bottom being the limiting factor for primary productivity. They also found that turbidity and water depth determined the recovery potential following disturbance, as light limitation on bottom sediments prevented sufficient growth rates from occurring. While we did not expose our system to disturbances other than increasing light attenuation in our K_d trials, our results

show that B_{MPB} is does not return to original values following an increase in turbidity. Similarly, to results in Mangan et al. (2020), our results demonstrate that increasing suspended particulate matter in estuaries creates a loss in ecosystem function, reducing its resistance to additional stressors (Gammal et al., 2022). Therefore, our model shows the pattern in which MPB and *M. liliana* populations will respond to fluctuations in turbidity, information that would be useful in future management planning and practice.

5.2.2 *Sediment Mud Content*

Sediment mud content (M_c) was incorporated within the model as a proportion of total sediment composition. *M. liliana's* carrying capacity (K_{mac}) was controlled by the M_c value (*see Equation 10*), meaning B_{mac} (and its coupled variables) were influenced by changing M_c. We tested the system's response to increasing M_c across ten trials, with M_c increasing by 10% in each subsequent trial, and discuss the results below.

M_c increases within estuarine environments through sedimentation, a process occurring due to the tides and surface run off from the catchment (Thrush et al., 2004). Increasing M_c is regularly associated with the modification of benthic community composition, increased nutrient availability, and the reduction of ecosystem functioning (Lovelock et al., 2007; Pratt et al., 2013) (*for an in-depth analysis on sedimentation and the biogeochemical effects of mud within estuaries, please refer to Sections 2.1 & 2.4*). The settlement of MPB, their biomass, and their assemblage diversity is predominantly controlled by tidal exposure and sediment composition (Jesus et al., 2009). Sheltered, muddy environments support a larger biomass than high energy, sandy areas (Cadée & Hegeman, 1977; Tett, 1981; Sundbäck et al., 1991), with MPB facilitating seasonal mud accumulation during their growth (Brückner et al., 2020). However, MPB are likely restricted to where oxygen is still present in the upper millimetres of muddy sediment (Brotas & Serôdio, 1995; Macintyre et al., 1996). Conversely, in high energy, sandy environments MPB penetrate deeper into sediment and are also more diverse in their assemblage (supporting up to three MPB groups, as opposed to only one in muddy substrate) (Fenchel & Straarup, 1971; Fielding et al., 1988; Jesus et al., 2009). These differences are likely in response to the variation in sediment light attenuation, as the photosynthetically active radiation (PAR) light field permeates deeper into sandy sediment (Kühl & Jorgensen, 1994; Jesus et al., 2009). MPB dwelling in sandy sediments also exhibit seasonal fluctuations in taxonomical groups and biomass, indicating that these environments are more stable than their muddy counterparts (Jesus et al., 2009). M_c can have considerable consequences on *M. liliana*

populations also, as the species' biomass has been known to decrease with increasing M_c (Thrush et al., 2003; Anderson, 2008; Pratt et al., 2013).

Unsurprisingly, our results show that as M_c increases, B_{mac} and *M. liliana* detrital values (D_{mac}) decrease. This occurs at a steady rate throughout trials until (as coded) K_{mac} is reduced to 1 g C m^{-2}, demonstrating the negative relationship B_{mac} has with increasing M_c that is seen in the literature. Interestingly, B_{MPB}, MPB detritus (D_{MPB}), and total nutrients within the system (N) increase as M_c increases. As the response of these variables to M_c were not coded into the model, our results highlight the coupled behaviour between our dynamic variables. Most notably, B_{MPB} and N sharply increase in trials eight through ten, coinciding with B_{mac} being below 1 g C m^{-2}. There are several explanations for this effect. Firstly, grazing pressure upon MPB ($G_{macgraz}$) has been considerably reduced when B_{mac} values drop by more than 95% between trial seven and eight, allowing B_{MPB} to increase unregulated. Secondly, nutrients are not being used for *M. liliana* growth (G_{mac}), due to a low K_{mac} value and reduced $G_{macgraz}$. Thirdly, remaining N within the system is mixed between the water column and sediment layer to maintain equilibrium, enabling enlarged N values within both layers. Finally, MPB can access these excess nutrients and maintain their population at their carrying capacity (K) before the denitrification coefficient removes nutrients from the system. When exploring the relationship between B_{MPB} and N across trials eight to ten, we found that B_{MPB} stabilises after its initial sharp decrease from K (1.2 g C m^{-2}) approximately 5,000 timesteps after N begins its decline (Figure 4.38 (b) & Figure 4.39). Moreover, the second sharp decline of B_{MPB} occurs nearly simultaneously (less than 1,000 timesteps apart) with N values bottoming out. Here, it is possible that we are seeing the system return past the threshold of a tipping point, as both N and B_{MPB} return to values seen in 'healthier', low M_c trials. Unfortunately, the simple design of our model that has allowed us to identify this coupling behaviour now becomes a barrier in predicting tipping points. In natural environments, M_c influences many other facets of estuaries, and it is unlikely that B_{MPB} and N would behave exactly in this manor (*see Sections 2.1, 2.4, & 5.2.1*). However, our results are like other studies; documented in Thrush et al. (2005), increasing M_c can exacerbate other stressors within estuaries. This means that the response of one variable can be in direct consequence to increasing M_c or the impacts it has upon other variables. Therefore, to accurately extrapolate upon M_c's effect on benthic communities, it is imperative that models predicting these species-environment interactions include natural history information of the estuary, varying spatial distributions, and test the relationships between variables (Thrush et

al., 2005) – something that we can confidently say our model has achieved. For this reason, the coupling behaviour we have identified within our model is still important information that can be used in the future planning and implementation of management strategies.

5.2.3 External Nutrient Loading Event

Our model was designed to operate through an internal nutrient loading (INL) process, with the full amount of nutrients being present in the system at the beginning of trials. We tested our system's response to six variations of initial external nutrient (*IN*) levels, with the volume of nutrients increasing with each subsequent trial.

INL is the release of nutrients from sediments, either through the rapid process of mineralisation (denitrification) of labile organic material on the sediment surface or a slow, continual release of mineralised material buried at depth (Valdemarsen et al., 2015). ENL is the deposition of nutrients into an estuarine system from sources outside of the water body (*see section 2.1*). External nutrients will increase the total nutrient content of the system, and go on to join the INL cycle once deposited on the seafloor. Nutrients can be released from sediments when they are resuspended by wave and current activity (Niemistö & Lund-Hansen, 2019), which has been shown to as much as double mineralisation rates under the right conditions (Ståhlberg et al., 2006). INL is fundamental in sustaining high biological activity within estuaries (Childers et al., 2006; Murrell et al., 2007), as to some degree, primary production is governed by nutrients sourced from benthic sediment (Cowan and Boynton, 1996; Mortazavi et al., 2012). The sediment-water interface can operate as a nutrient source or sink depending on light availability, which determines the density of denitrification inhibiting sediment microalgae (McGlathery et al., 2001; Sundbäck et al., 2006). Therefore, shallow water estuaries with benthic dominated primary producers may undergo eutrophication following a reduction in submarine light penetration (Kemp et al., 2005). INL is so prevalent within estuaries, that in dry seasons (when less rainfall is depositing nutrients from the catchment) INL can replace water column nutrient pools up to two times faster than ENL (Buzzelli et al., 2013). Consequently, this means the recovery of estuarine systems can be inhibited by the INL process, as nutrients accumulated within the sediment continue to be released following a reduction in ENL (Pitkänen et al., 2001; Carstensen et al., 2006). In enclosed 70L tanks, Valdemarsen et al (2015) discovered that for the first 200 days INL is largely driven by nutrients on the sediment surface, before a reduction in nutrient recycling is seen when nutrients are predominantly sourced from depth. In other words, the extent of organic enrichment in sediment governs denitrification

efficiency (Cook et el., 2004; Hale et al., 2016; Kemp et al., 2005). In natural estuarine systems, the rate of INL is dependent on the filtering capacity, flushing time, and variations in freshwater and external nutrient delivery (Buzzelli et al., 2013).

Our model follows the INL principles outlined above, except for the resuspension of sediment which is not included in the code. Our system deposits nutrients onto the sediment surface through MPB detritus and the pumping behaviour of *M. liliana*, where they are recycled back into sediment through the consumption by MPB. Denitrification also removes nutrients from the sediment layer. We tested six ENL events, simulating a sudden influx of nutrients into an established benthic community. From these tests, we identified both the efficiency of nutrient recycling in a benthic environment and how a large, isolated ENL event impacts B_{MPB} and B_{mac}. Over the course of our trials, excess nutrients were recycled and eventually removed from the system through denitrification, with their removal time dependent on the size of the ENL event. We can only be confident that B_{mac} was significantly affected by the ENL, not B_{MPB}; however, our results are still comparable to the literature (Gladstone-Gallagher et al., 2020; Hope et al., 2020; Thrush et al., 2021). What was interesting to see was how MPB and *M. liliana* responded to *IN* over long periods of time, and how the relationship between the two species changed. Notably, only once *IN* reached 100,000 mmol N m^{-2} did we see a bloom in B_{MPB}. B_{MPB} approached *K* (the carrying capacity), but was not sustained throughout the trial despite nutrients remaining high (Figure 4.41 (b)). MPB's reaction is explainable, as where they source their nutrients from (sediment surface or water column) is dependent on where the highest source of nutrients are. MPB in the model are designed to source their nutrients from *IN* once its volume becomes larger than what is available in the water column. A pronounced reaction from B_{mac} was not seen until nutrient concentrations became relatively high (10,000 mmol N m^{-2}) (Figure 4.41 (a)). When *IN* was set to 100,000 mmol N m^{-2}, both species experienced a sharp drop in biomass simultaneously, reaching their lower limits within 25,000 timesteps. For B_{MPB}, this lower limit was still close to *K*, being maintained by access to sufficient nutrients and light for growth. However, B_{mac} fell well below K_{mac}, and despite continuing on an upward trend throughout the trial it did not fully recover (Figure 4.41). In a study of *A. stutchburyi* (a New Zealand bivalve species that fills a similar ecological niche to *M. liliana*) Tricklebank et al. (2020) found that the species' density within the intertidal flats of Whangateau Harbour had nearly fully recovered in the decade following a mass mortality event (the event caused a decrease from 7.4 to 1.8kg wet weight per m^2). However, the amount of large *A. stutchburyi* (>30mm in length), the most

important size class for completing ecosystem functions, have still not recovered. Similar findings were made following a mass mortality event for bivalves at Monte Hermoso Beach (Argentina) (Fiori & Cazzaniga, 1999). It is evident that disturbance events seriously hinder bivalve populations, due to their slow growth rate or by creating environments that no longer support large individuals. As the mortality events in these studies are unrelated to nutrient enrichment, the results from our study fill a gap in the literature, showing how bivalve populations respond long-term to large scale ENL events. It seems that the recovery of *M. liliana* is more important for regulating B_{MPB} than reducing the concentration of nutrients within the system, an important finding for future management practices within estuaries when considering the focal species and timelines of remediation.

It needs to be noted that the response of the model to this type of testing is not an accurate representation of how an estuary would respond in nature. Due to time restraints, we were unable to alter the code to allow for a continuous external nutrient loading process. Therefore, our tests demonstrate how an estuary would respond to an external nutrient loading (ENL) event if it were also never exposed to external nutrients again.

5.3 Increasing the Model's Efficacy in Predicting Estuarine Tipping Points

Designing a model that remained simple, functioned correctly, and represented an estuarine environment as accurately as possible is a task without end. To gather interesting data in the short timeframe we had, the model design was finalised earlier than we would have hoped. In this section we will discuss future additions that we believe are the most important for increasing the model's efficacy in predicting estuarine tipping points.

5.3.1 Adding Wind, Tidal, and Wave Effects

In its current state, the model is operating as a closed system, with no transport of nutrients, sediments, or both *M. liliana* and MPB. Modelling in this structure only gives us a simple analysis of local impacts, rather than broad scale. There are many ways nutrients and sediments are added to these ecosystems (*see Section 2.1*) – wind effects being one of them. The addition of wind effects would allow for the resuspension of MPB and mud, which has the potential to alter the relationships within the model. The resuspension of MPB would enable the migration and immigration of the species to occur. Most notably this would alter B_{MPB} and other dynamic variables within the model, with constant variables such as $G_{macgraz}$

being impacted also. The resuspension of MPB (from the top 0.5cm of sediment) can be modelled as a linear function of the windspeed averaged over three consecutive highwater periods (effective windspeed) – the same being true for mud (de Jonge & van Beusekom (1995). Within the Ems Estuary (bordering Germany and the Netherlands), de Jonge & van Beusekom (1995) found that up to 25% of benthic diatom's total biomass may be in suspension at any one time. Upon further study within the upper reaches of this estuary, the flux of MPB resuspended from sediment to water column was quantified, being 10×10^3 tonnes annually (de Jonge, 1995). The resuspension of benthic mud can be modelled using effective windspeed, altering the biogeochemical processes within our system by increasing both internal nutrient loading and turbidity values (*see section 5.2.3*). de Jonge (1995) found that even in the sheltered, upper limits of an estuary, the flux of mud from the seafloor to the water column can be as much as 7.5×10^6 tonnes annually. Wind effects are crucial in modelling this process, as a doubling of windspeed from 5 to 10 m s^{-1} can be five times more effective in resuspending mud on intertidal flats than a twofold increase in current velocity from 0.5 to 1.0 m s^{-1} (de Jonge & van Beusekom, 1995). In future iterations of the model, wind effects should be incorporated to include the resuspension and transportation of MPB and mud, coded to coincide with average wind conditions of the modelled estuary. However, while wind is critical in the vertical movement of these variables, tidal currents are the force that govern the horizontal movement of suspended sediment (Green et al., 1997).

Tidal currents are a relatively easy variable to incorporate within the model, as their speed and direction is frequently measured during environmental monitoring by local governing bodies or consistently by ports. Tidal velocities could be modelled as a constant, taken as an average over time, or a dynamic variable changing with ebb/flood tides and the seasons. Incorporating the effects of currents in the model would enable the transport of matter into or outside of the model space. This may include suspended mud and MPB, juvenile *M. liliana* (Cummings et al., 1993), and external nutrients (the latter being sourced from land run-off or coastal upwelling) There is a seaward flux of inorganic nitrogen within the Tauranga Harbour, exporting between 56 and 451 kg N per tidal cycle (Tay et al., 2012) – a process that could be incorporated alongside the denitrification parameter. The transport of mud into the model space would increase M_c and K_d values, having further effects on the model's output (*see Section 3.5 and 2.4 respectfully*). The movement of suspended sediment with tidal currents can be calculated using Equation (7) in Green et al. (1997), which equates the sediment flux as the rate the mean suspended sediment concentration is advected by the

mean current speed. Crucially, Green et al. (1997) notes that sediment settlement times, transporting capacity, and availability are imperative for predicting the transport of total sediment loads. Tuapiro Stream (the stream adjacent to the collection site for much of our model's data) has a sediment yield of 1600t y^{-1}, and a mean suspended sediment concentration of 4.8g m^3 (Surman et al., 1999). Other areas of the Tauranga Harbour have suspended sediment yield of over 37,000t y^{-1} (Surman et al., 1999). Using the sediment load from Tuapiro Stream, alongside Green et al.'s (1997) sediment transport equation, increasing the M_c value could be dynamically modelled. Green et al. (1997) acknowledge that unaided, tidal currents are not able to entrain benthic sediment, expressing that waves on intertidal flats are imperative for this process.

Wave interaction with the seafloor resuspends benthic sediment, creating turbid waters (Green et al., 1997; Green, 2006). Models exist that explain sedimentation patterns across intertidal mudflats (e.g., Malvarez et al., 2001; Green & Coco, 2007), meaning their equations could be incorporated amongst our own wave effects (*see Section 3.10*) to model wave induced sediment movement. For example, the mass of mud resuspended from the seabed by waves can be calculated using an equation by Bailard (1981), which equates the sediment density, transport efficiency, and settling speed against a time interval. Further consideration would need to be taken regarding the burial of MPB, which can occur following strong physical disturbance and vertical mixing from wind waves (Valdemarson et al., 2015).

The incorporation of these three variables would increase the model's efficacy in modelling estuarine ecosystems. It would allow for the transport of MPB, *M. liliana*, nutrients, and sediment in and out of the model space, creating a dynamic (and more natural) way of adding/removing mass to/from the currently closed system. Furthermore, these parameters are often readily accessible, meaning should the model be based around an estuary other than Tauranga Harbour its values could be easily altered.

5.3.2 External Nutrient Loading

Nutrients within our model are currently sourced through two methods: 1) nutrients are added to the model upon initialisation; and 2) internal nutrient loading (*see Section 5.3.2*). To make the model more representative of estuarine systems seen in nature, future iterations should include an open system that allows for continuous external nutrient loading. External nutrients entering the system should be based upon local government records of nutrient loading to the area, or in-situ sampling. For example, total nitrogen (TN) within sediments at

Tuapiro Point (Tauranga Harbour) sit within 200-500 mg kg, with the predicted nutrient load from the Tuapiro Stream being somewhere between 0.5-0.75 parts per billion (ppb) (Ellis et al., 2013). Initial nutrient conditions within sediment can start at a value such as above, with nutrients being added to the system based upon the nearest river's daily input. Nutrients can further be transported to and from the system based upon wind, tidal, and wave effects (*see Section 5.3.1*).

5.3.3 Turbidity

To maintain the simplicity of our model, an average K_d value of 0.4m (from a range of 0.16-0.98m) was used (*see Section 3.4*). A constant value is not reflective of the variable environmental conditions an intertidal flat would be exposed to, as climate conditions and anthropogenic influences vary light exposure constantly. Suspended particle concentrations naturally vary across a wide range in estuaries, controlled by climate oscillations (e.g., La Niña), seasonal variations in rainfall, adjoining land use, and tide and wave-generated currents (Green et al., 1997; Green, 2006; Cussioli et al., 2019). In future iterations of the model, K_d should be set as a range (such as that identified by Cussioli et al. (2019)) that varies upon pre-designated conditions (e.g., average rainfall, sunlight hours, estuarine sedimentation rates). K_d should be linked to additional natural processes, by incorporating it within the sediment resuspension and transportation processes discussed in Section 5.3.1. To increase the accuracy of the model further, sediment stabilisation by MPB should be incorporated, to allow for the modelling of feedback loops associated with MPB, K_d, and benthic sediment resuspension (*see Section 5.2.1*).

5.3.4 Sediment Mud Content

Currently, the model is set to remain at a constant M_c *(mud content)* throughout each trial. While M_c can take some time to increase within benthic environments, it is important that M_c becomes a dynamic variable to increase the efficacy of this model in predicting ecosystem tipping points M_c's variation within the model should be based upon the sediment transport methods outlined in Section 5.3.1, and artificially increased to represent expected M_c increases from external sources with time (*see Section 2.1*). M_c should also be integrated into the functionality of other variables, such as the detrital breakdown coefficients and the denitrification rate. Compared to sandy tidal flats, muddy sediments can increase remineralisation rates tenfold (Nowicki & Nixon, 1985). At its present stage, our denitrification rate (*DR*) is set to a constant rate, and in future iterations should be set to

increase alongside M_c. To maintain simplicity, *DR* could double with each 10% increase in M_c, reaching its maximum ten-fold increase by 100% M_c. This feature should also be incorporated into the biomass decay rates of MPB (C_{MPB}) and *M. liliana* (C_{mac}), as these rates will also increase with M_c. However, what must be considered is that remineralisation rates are highly dependent on local biotic and abiotic factors, and it is difficult to set a universal rate that fits to changing M_c (O'Meara et al., 2020). Therefore, when using this model in future, we recommend using in-situ sampling to identify the M_c and *DR* across an estuary and calculating the range of *DR* based on the coupled *DR*-M_c results. Then, the range of *DR* can be matched proportionately to C_{MPB} and C_{mac}.

Chapter 6

Conclusions and Future Recommendations

6.1 Conclusions

This research successfully created a dynamic model that accurately synthesised basic ecological reactions within an estuarine benthic community. Our design is set apart from the literature due to its unique ability to model pore-water advection currents caused by *M. liliana* pumping behaviour (a behaviour critical for the transportation and regulation of nutrients within New Zealand estuaries). We decided to maintain simplicity in our model for several reasons. The first being the rationalisation given in Fulton et al. (2004); general prediction and learning can be achieved through simpler designs. Physiological details are not always necessary, and their absence reduces costs in development and administration. Another argument in favour of simplicity is 'Occam's razor', a principle that expresses warning in unnecessarily multiplying entities to achieve what can be done with less. Finally, simplicity is beneficial, as minor changes in one parameter in dynamic models may significantly affect another due to the nonlinear nature of their equations (Cale et al., 1983).

Over the course of our study, extensive model testing showed that MPB populations exert a greater influence on the system than *M. liliana*, and that *M. liliana* populations are slow in their recovery following disturbance. Denitrification was found to be an imperative process within estuaries to enable *M. liliana* to maintain a stable population. Importantly, we identified very strong coupling behaviour between our dynamic variables during external forcing testing. Our most notable findings include:1) the growth of MPB populations being more susceptible to light limitation over nutrient limitation, with turbidity variations causing the largest disparity between MPB biomass results across all trials; 2) MPB populations are not diminished by a reduction in *M. liliana* pumping behaviour caused by increasing sediment mud content; and 3) while increasing external nutrient loading was found to decrease *M. liliana* biomass, there was no significant relationship between this process and MPB biomass. Furthermore, external nutrient loading did not cause an MPB bloom until nutrient levels became considerably large (100,000 mmol N m^{-2}). Our results were validated by existing model simulations and field data within the literature. Moreover, our model exceeds guidelines and suggestions within the literature for accurately predicting ecosystem

tipping points, strengthening our confidence that our research successfully identified early warning signals for estuarine tipping points.

6.2 Recommendations for Future Research

Recommendations for increasing the model's efficacy in predicting tipping points have been made in Section 5.3, but caution should be taken in ensuring new parameters are as accurate as possible. With or without these adaptations, the model is well suited for use in future estuarine management strategies; however, not in the context we initially hypothesised. While we are confident in our model's ability, recent research has shown that dynamical models may be better used as a tool for highlighting potential issues in estuaries, rather than predictive instruments in management (Bryan et al., 2022). Where a dynamical model is favoured in its ability to simulate coupling behaviour between variables, this is also its downfall, as small changes in one parameter can markedly change another. In context, a slight mistake in a model parameter can cause major inaccuracies in its outcomes. Therefore, it is recommended that our model be used as an educational tool for estuarine managers to explain outcomes to stakeholders and the public or used to highlight issues within areas of estuaries with little data available. An example of this may be the model's use in gathering explorative information surrounding discharge zones in estuaries without historic data (Bryan et al., 2022).

Our research has successfully created a platform that allows researchers, policy makers, and environmental managers to consider biogeochemical processes previously unavailable in the literature. The inclusion of pore-water advection currents caused by the pumping behaviour of *M. liliana* adds an additional layer of accuracy in our model's prediction capability. Currently in New Zealand, the policies surrounding the management of the coastal marine area (The New Zealand Costal Policy Statement 2010) and freshwater bodies (The National Policy Statement for Freshwater Management 2020) are used in collaboration for deciding estuarine management outcomes. These policy statements are administered by separate governing bodies, with the Department of Conservation overseeing the costal statement and the Ministry for the Environment managing the freshwater. Despite the freshwater policy outlining that management approaches must consider receiving environments, estuaries are not mentioned amongst the guidelines of safe water quality limits. Although some guidance regarding safeguarding estuaries exists (MfE, 2021) and steps are being taken to incorporate estuarine features into policy (Cornelissen et al., 2017), further steps need to be taken. Here, we believe our model can fill this gap, by becoming a tool used

in policy creation and implementation, particularly following the addition of our advised parameters to its design.

References

Adams, J., Taljaard, S., Niekerk, L. V., & Lemley, D. (2020). Nutrient enrichment as a threat to the ecological resilience and health of South African microtidal estuaries. *African Journal of Aquatic Science, 45*(1-2), 23-40. https://doi.org/10.2989/16085914.2019.1677212

Alves de Almeida, E., Celso Dias Bainy, A., Paula de Melo Loureiro, A., Regina Martinez, G., Miyamoto, S., Onuki, J., Fujita Barbosa, L., Carrião Machado Garcia, C., Manso Prado, F., Eliza Ronsein, G., Alexandre Sigolo, C., Barbosa Brochini, C., Maria Gracioso Martins, A., Helena Gennari de Medeiros, M., & Di Mascio, P. (2007). Oxidative stress in Perna Perna and other bivalves as indicators of environmental stress in the Brazilian marine environment: Antioxidants, lipid peroxidation and DNA damage. *Comparative Biochemistry and Physiology Part A: Molecular & Integrative Physiology*, *146*(4), 588–600. https://doi.org/10.1016/j.cbpa.2006.02.040

Anderson, D. M., Burkholder, J. M., Cochlan, W. P., Glibert, P. M., Gobler, C. J., Heil, C. A., Kudela, R. M., Parsons, M. L., Rensel, J. E., Townsend, D. W., Trainer, V. L., & Vargo, G. A. (2008). Harmful algal blooms and eutrophication: Examining linkages from selected coastal regions of the United States. *Harmful Algae*, *8*(1), 39–53. https://doi.org/10.1016/j.hal.2008.08.017

Anderson, M. J. (2008). Animal-sediment relationships re-visited: Characterising species' distributions along an environmental gradient using canonical analysis and quantile regression splines. *Journal of Experimental Marine Biology and Ecology*, *366*(1-2), 16–27. https://doi.org/10.1016/j.jembe.2008.07.006

Anderson, M. J., & Thompson, A. A. (2004). Multivariate Control Charts for ecological and environmental monitoring. *Ecological Applications, 14*(6), 1921–1935. https://doi.org/10.1890/03-5379

Attrill, M. J., & Thomes, R. (1995). Heavy metal concentrations in sediment from the Thames Estuary, UK. *Marine Pollution Bulletin, 30*(11), 742-744. https://doi.org/10.1016/0025-326x(95)98339-x

Auckland Regional Council (2008). *Effects of Suspended Sediment Levels on Suspension-Feeding Shellfish in the Whitford Embayment. Auckland, New Zealand.* NIWA

Bailard, J. A. (1981). An energetics total load sediment transport model for a plane sloping beach. *Journal of Geophysical Research*, *86*(C11), 10938. https://doi.org/10.1029/jc086ic11p10938

Banse, K. (1982). Mass-scaled rates of respiration and intrinsic growth in very small invertebrates. *Marine Ecology Progress Series,9*, 281-297. https://doi.org/10.3354/meps009281

Barbier, E. B. (2017). Marine ecosystem services. *Current Biology*, *27*(11), 507–510. https://doi.org/10.1016/j.cub.2017.03.020

Berberan-Santos, M. N. (1990). Beer's law revisited. *Journal of Chemical Education, 67*(9), 757. https://doi.org/10.1021/ed067p757

Bestelmeyer, B. T., Ellison, A. M., Fraser, W. R., Gorman, K. B., Holbrook, S. J., Laney, C. M., Ohman, M. D., Peters, D. P., Pillsbury, F. C., Rassweiler, A., Schmitt, R. J., & Sharma, S. (2011). Analysis of abrupt transitions in Ecological Systems. *Ecosphere*, *2*(12). https://doi.org/10.1890/es11-00216.1

Biot, M. A. (1941). General theory Of Three-Dimensional Consolidation. *Journal of Applied Physics, 12*(2), 155-164. https://doi.org/10.1063/1.1712886

Birch, G. (2000). Marine pollution in Australia, with special emphasis on central New South Wales estuaries and adjacent continental margin. *International Journal of Environment and Pollution, 13*(1/2/3/4/5/6), 573. https://doi.org/10.1504/ijep.2000.002334

Borja, A., Franco, J., & Pérez, V. (2000). A Marine Biotic index to establish the ecological quality of soft-bottom benthos within European estuarine and Coastal Environments. *Marine Pollution Bulletin*, *40*(12), 1100–1114. https://doi.org/10.1016/s0025-326x(00)00061-8

Borum, J., & Sand-Jensen, K. (1996). Is Total Primary Production in Shallow Coastal Marine Waters Stimulated by Nitrogen Loading? *Oikos*, *76*(2), 406. https://doi.org/10.2307/3546213

Boudouresque, C. F., Bernard, G., Pergent, G., Shili, A., & Verlaque, M. (2009). Regression of Mediterranean seagrasses caused by natural processes and anthropogenic disturbances and stress: A critical review. *Botanica Marina*, *52*(5). https://doi.org/10.1515/bot.2009.057

Boudreau, B. P., & Jørgensen, B. B. (2001). *The benthic boundary layer: Transport processes and biogeochemistry*. Oxford: Oxford University Press.

Bourdeau, P., & Barth, H. (1986). Estuarine, Coastal and Ocean Pollution: EEC Policy and Research. *Water Science and Technology*, *18*(4-5), 1-14. https://doi.org/10.2166/wst.1986.0175

Bradbury, R. H., & Seymour, R. M. (2009). Coral reef science and the NEW COMMONS. *Coral Reefs*, *28*(4), 831–837. https://doi.org/10.1007/s00338-009-0540-6

Bricker, S. B., Longstaff, B., Dennison, W., Jones, A., Boicourt, K., Wicks, C., & Woerner, J. (2008). Effects of nutrient enrichment in the nation's estuaries: A decade of change. *Harmful Algae*, *8*(1), 21–32. https://doi.org/10.1016/j.hal.2008.08.028

Brito, A. C., Newton, A., Fernandes, T. F., & Tett, P. (2010). The role of microphytobenthos on shallow coastal lagoons: A modelling approach. *Biogeochemistry*, *106*(2), 207–228. https://doi.org/10.1007/s10533-010-9539-x

Brito, A. C., Newton, A., Tett, P., & Fernandes, T. F. (2012). Changes in the yield of microphytobenthic chlorophyll from nutrients: Considering denitrification. *Ecological Indicators*, *19*, 226–230. https://doi.org/10.1016/j.ecolind.2011.07.026

Brotas, V., & Serôdio, J. (1995). A mathematical model for the vertical distribution of chlorophyll-a in estuarine intertidal sediments. *Netherlands Journal of Aquatic Ecology*, *29*(3-4), 315–321. https://doi.org/10.1007/bf02084230

Brückner, M. Z., Braat, L., Schwarz, C., & Kleinhans, M. G. (2020). What came first, mud or biostabilizers? Elucidating interacting effects in a coupled model of mud, Saltmarsh, Microphytobenthos, and estuarine morphology. *Water Resources Research*, *56*(9). https://doi.org/10.1029/2019wr026945

Bryan, K. R., Stewart, B. T., Port, A. M., Jones, H. F., & Pilditch, C. A. (2022). The advantages and limitations of biophysical modelling as a tool for informing limit setting in New Zealand's barrier-enclosed estuaries. *New Zealand Journal of Marine and Freshwater Research*, 1–22. https://doi.org/10.1080/00288330.2022.2102045

Buzzelli, C., Chen, Z., Coley, T., Doering, P., Samimy, R., Schlezinger, D., & Howes, B. (2013). Dry Season Sediment-Water Exchanges of Nutrients and Oxygen in Two Florida Estuaries: Patterns, Comparisons, and Internal Loading. *Florida Scientist*, *76*(1), 54–79.

Cadée, G. C., & Hegeman, J. (1977). Distribution of primary production of the benthic microflora and accumulation of organic matter on a tidal flat area, Balgzand, Dutch wadden sea. *Netherlands Journal of Sea Research*, *11*(1), 24–41. https://doi.org/10.1016/0077-7579(77)90019-9

Cahoon, L. B., & Safi, K. A. (2002). Distribution and biomass of benthic microalgae in Manukau Harbour, New Zealand. *New Zealand Journal of Marine and Freshwater Research*, *36*(2), 257–266. https://doi.org/10.1080/00288330.2002.9517084

Cahoon, L. B., Nearhoof, J. E., & Tilton, C. L. (1999). Sediment grain size effect on benthic microalgal biomass in shallow aquatic ecosystems. *Estuaries*, *22*(3), 735. https://doi.org/10.2307/1353106

Cale, W. G., O'Neill, R. V., & Gardner, R. H. (1983). Aggregation error in nonlinear ecological models. *Journal of Theoretical Biology*, *100*(3), 539–550. https://doi.org/10.1016/0022-5193(83)90446-0

Camargo, J. A., & Alonso, Á. (2006). Ecological and toxicological effects of inorganic nitrogen pollution in Aquatic Ecosystems: A global assessment. *Environment International*, *32*(6), 831–849. https://doi.org/10.1016/j.envint.2006.05.002

Cardinale, B. J., Duffy, J. E., Gonzalez, A., Hooper, D. U., Perrings, C., Venail, P., Narwani, A., Mace, G. M., Tilman, D., Wardle, D. A., Kinzig, A. P., Daily, G. C., Loreau, M., Grace, J. B., Larigauderie, A., Srivastava, D. S., & Naeem, S. (2012). Biodiversity Loss and its impact on humanity. *Nature*, *486*(7401), 59–67. https://doi.org/10.1038/nature11148

Carpenter, S. R., Brock, W. A., Cole, J. J., Kitchell, J. F., & Pace, M. L. (2007). Leading indicators of trophic cascades. *Ecology Letters*. https://doi.org/10.1111/j.1461-0248.2007.01131.x

Carstensen, J., Conley, D. J., Andersen, J. H., & Ærtebjerg, G. (2006). Coastal eutrophication and trend reversal: A Danish case study. *Limnology and Oceanography*, *51*(1part2), 398–408. https://doi.org/10.4319/lo.2006.51.1_part_2.0398

Cartaxana, P., Ribeiro, L., Goessling, J. W. L., Cruz, S., & Kühl, M. (2016). Light and O_2 microenvironments in two contrasting diatom-dominated coastal sediments. *Marine Ecology Progress Series*, *545*, 35–47. https://doi.org/10.3354/meps11630

Childers, D. L., Boyer, J. N., Davis, S. E., Madden, C. J., Rudnick, D. T., & Sklar, F. H. (2006). Relating precipitation and water management to nutrient concentrations in the oligotrophic "upside-down" estuaries of the Florida Everglades. *Limnology and Oceanography*, *51*(1part2), 602–616. https://doi.org/10.4319/lo.2006.51.1_part_2.0602

Clark, D. E., Stephenson, F., Hewitt, J. E., Ellis, J. I., Zaiko, A., Berthelsen, A., Bulmer, R. H., & Pilditch, C. A. (2021). Influence of land-derived stressors and environmental variability on compositional turnover and diversity of estuarine benthic communities. *Marine Ecology Progress Series*, *666*, 1–18. https://doi.org/10.3354/meps13714

Cloern, J. (1982). Does the Benthos Control Phytoplankton Biomass in South San Francisco Bay? *Marine Ecology Progress Series, 9*, 191-202. https://doi.org/10.3354/meps009191

Cnudde, C., Moens, T., Werbrouck, E., Lepoint, G., Van Gansbeke, D., & De Troch, M. (2015). Trophodynamics of estuarine intertidal harpacticoid copepods based on stable isotope composition and Fatty Acid Profiles. *Marine Ecology Progress Series*, *524*, 225–239. https://doi.org/10.3354/meps11161

Commito, J. A., Thrush, S. F., Pridmore, R. D., Hewitt, J. E., & Cummings, V. J. (1995). Dispersal Dynamics in a wind-driven benthic system. *Limnology and Oceanography*, *40*(8), 1513–1518. https://doi.org/10.4319/lo.1995.40.8.1513

Consalvey, M., Jesus, B., Perkins, R. G., Brotas, V., Underwood, G. J. C., & Paterson, D. M. (2004). Monitoring migration and measuring biomass in benthic biofilms: The effects of dark/far-red adaptation and vertical migration on fluorescence measurements. *Photosynthesis Research*, *81*(1), 91–101. https://doi.org/10.1023/b:pres.0000028397.86495.b5

Cook, P. L. M., Eyre, B. D., Leeming, R., & Butler, E. C. V. (2004). Benthic fluxes of nitrogen in the tidal reaches of a turbid, high-nitrate sub-tropical river. *Estuarine, Coastal and Shelf Science*, *59*(4), 675–685. https://doi.org/10.1016/j.ecss.2003.11.011

Cornelisen, C., Zaiko, A., Hewitt, J., Berthelsen, A., McBride, G., Awatere, S., Sinner, J., Banks, J., Hudson, N., Bartley, A., & Roper, D. (2017). *Managing upstream: estuaries state and values (Stage 1A report).* Prepared by NIWA for the Ministry for the Environment.

Costanza, R., Kemp, M., & Boynton, W. (1995). Scale and biodiversity in coastal and estuarine ecosystems. *Biodiversity Loss*, 84-126. https://doi.org/10.1017/cbo9781139174329.006

Costanza, R., D'Arge, R., De Groot, R., Farber, S., Grasso, M., Hannon, B., Limburg, K., Naeem, S., O'Niell, R. V., Paruelo, J., Raskin, R. G., Sutton, P., & Van Den Belt, M. (1997). The value of the world's ecosystem services and natural capital. *Nature, 387*(6630), 253-260. https://doi.org/10.1038/387253a0

Costanza, R. (2020). Valuing natural capital and ecosystem services toward the goals of efficiency, fairness, and sustainability. *Ecosystem Services*, *43*, 101096. https://doi.org/10.1016/j.ecoser.2020.101096

Coutteau, P., Castell, J. D., Ackman, R. G., & Sorgeloos, P. (1996). The use of lipid emulsions as carriers for essential fatty acids in bivalves: a test case with juvenile *Placopecten magellanicus*. *J. Shellf. Res.* 15, 259–264.

Cowan, J. L., & Boynton, W. R. (1996). Sediment-water oxygen and nutrient exchanges along the longitudinal axis of Chesapeake Bay: Seasonal patterns, controlling factors and ecological significance. *Estuaries*, *19*(3), 562. https://doi.org/10.2307/1352518

Cummings, V. J., Pridmore, R. D., Thrush, S. F., & Hewitt, J. E. (1993). Emergence and floating behaviours of post-settlement juveniles of *Macomona liliana* (bivalvia: Tellinacea). *Marine Behaviour and Physiology*, *24*(1), 25–32. https://doi.org/10.1080/10236249309378875

Cussioli, M. C., Bryan, K. R., Pilditch, C. A., de Lange, W. P., & Bischof, K. (2019). Light penetration in a temperate meso-tidal lagoon: Implications for seagrass growth and dredging in Tauranga Harbour, New Zealand. *Ocean & Coastal Management*, *174*, 25–37. https://doi.org/10.1016/j.ocecoaman.2019.01.014

Dahlgren, S., & Kautsky, L. (2004). Can different vegetative states in shallow coastal bays of the Baltic Sea be linked to internal nutrient levels and external nutrient load? *Biology of the Baltic Sea,* 249-258. https://doi.org/10.1007/978-94-017-0920-0_23.

Dakos, V., Kéfi, S., Rietkerk, M., van Nes, E. H., & Scheffer, M. (2011). Slowing down in spatially patterned ecosystems at the brink of collapse. *The American Naturalist*, *177*(6). https://doi.org/10.1086/659945

Dauer, D. M. (1993). Biological criteria, environmental health and estuarine macrobenthic community structure. *Marine Pollution Bulletin, 26*(5), 249–257. https://doi.org/10.1016/0025-326x(93)90063-p

Davies-Colley, R. J., & Healy, T. R. (1978). Sediment and hydrodynamics of the Tauranga entrance to Tauranga harbour. *New Zealand Journal of Marine and Freshwater Research, 12*(3), 225-236. https://doi.org/10.1080/00288330.1978.9515747

de Jonge, V. N. (1995). *Wind driven tidal and annual gross transports of mud and microphytobenthos in the Ems estuary, and its importance for the ecosystem.* In: Dyer KR, D'Elia CF (eds.) *Changes in fluxes in estuaries.* (pp. 29−40). Fredensborg, Olsen & Olsen.

de Jonge, V. N., & van Beusekom, J. E. (1995). Wind and tide-induced resuspension of sediment and microphytobenthos from Tidal Flats in the Ems Estuary. Limnology and Oceanography, 40(4), 776–778. https://doi.org/10.4319/lo.1995.40.4.0776

Denis-Roy, L., Ling, S. D., Fraser, K. M., & Edgar, G. J. (2020). Relationships between invertebrate benthos, environmental drivers and pollutants at a subcontinental scale. *Marine Pollution Bulletin*, *157*, 111316. https://doi.org/10.1016/j.marpolbul.2020.111316

Dennison, W. C. (1987). Effects of light on seagrass photosynthesis, growth and depth distribution. *Aquatic Botany*, *27*(1), 15–26. https://doi.org/10.1016/0304-3770(87)90083-0

Douglas, E. J., Lohrer, A. M., & Pilditch, C. A. (2019). Biodiversity breakpoints along stress gradients in estuaries and associated shifts in ecosystem interactions. *Scientific Reports*, *9*(1). https://doi.org/10.1038/s41598-019-54192-0

Douglas, E. J., Pilditch, C. A., Kraan, C., Schipper, L. A., Lohrer, A. M., & Thrush, S. F. (2017). Macrofaunal functional diversity provides resilience to nutrient enrichment in coastal sediments. *Ecosystems*, *20*(7), 1324–1336. https://doi.org/10.1007/s10021-017-0113-4

Douglas, E. J., Pilditch, C. A., Lohrer, A. M., Savage, C., Schipper, L. A., & Thrush, S. F. (2018). Sedimentary Environment Influences Ecosystem Response to Nutrient Enrichment. *Estuaries and Coasts*, *41*(7), 1994-2008. https://doi.org/10.1007/s12237-018-0416-5

Drylie, T. P., Lohrer, A. M., Needham, H. R., Bulmer, R. H., & Pilditch, C. A. (2018). Benthic primary production in emerged intertidal habitats provides resilience to high water column turbidity. *Journal of Sea Research*, *142*, 101–112. https://doi.org/10.1016/j.seares.2018.09.015

Du, G. Y., Son, M., An, S., & Chung, I. K. (2010). Temporal variation in the vertical distribution of microphytobenthos in intertidal flats of the Nakdong River estuary, Korea. *Estuarine, Coastal and Shelf Science, 86*(1), 62-70. https://doi.org/10.1016/j.ecss.2009.10.008

Du, G., Yan, H., Liu, C., & Mao, Y. (2017). Behavioral and physiological photoresponses to light intensity by intertidal microphytobenthos. *Journal of Oceanology and Limnology*, *36*(2), 293–304. https://doi.org/10.1007/s00343-017-6099-0

Ehrenhauss, S., Witte, U., Janssen, F., & Huettel, M. (2004). Decomposition of diatoms and nutrient dynamics in permeable North Sea sediments. *Continental Shelf Research, 24*(6), 721-737. https://doi.org/10.1016/j.csr.2004.01.002

Ellis, J., Clark, D., Hewitt, J., Taiapa, C., Sinner, J., Patterson, M., Hardy, D., Park, S., Gardner, B., Morrison, A., Culliford, D., Battershill, C., Hancock, N., Hale, L., Asher, R., Gower, F., Brown, E., McCallion, A. (2013). *Ecological Survey of Tauranga Harbour. Prepared for Manaaki Taha Moana, Manaaki Taha Moana* (Research Report No. 13. Cawthron Report No. 2321).

Ellis, J. I., Clark, D., Atalah, J., Jiang, W., Taiapa, C., Patterson, M., Sinner, J., & Hewitt, J. (2017). Multiple stressor effects on marine infauna: Responses of estuarine taxa and functional traits to sedimentation, nutrient and metal loading. *Scientific Reports*, *7*(1). https://doi.org/10.1038/s41598-017-12323-5

Eppley, R. W. (1972). Temperature and phytoplankton growth in the sea. *Fish. bull*, *70*(4), 1063-1085.

NIWA. (2014). *Estuary types*. Retrieved January 21, 2022, from https://niwa.co.nz/coasts-and-oceans/nz-coast/learn-about-coastal-environments/estuary-types

Fearman, J. A., Bolch, C. J., & Moltschaniwskyj, N. A. (2009). Energy storage and reproduction in mussels *Mytilus galloprovincialis*: The influence of Diet Quality. *Journal of Shellfish Research*, *28*(2), 305–312. https://doi.org/10.2983/035.028.0212

Fenchel, T., & Straarup, B. J. (1971). Vertical distribution of photosynthetic pigments and the penetration of light in marine sediments. *Oikos*, *22*(2), 172. https://doi.org/10.2307/3543723

Fielding, P. J., Damstra, K. S. J., & Branch, G. M. (1988). Benthic diatom biomass, production and sediment chlorophyll in Langebaan Lagoon, South Africa. *Estuarine,*

Coastal and Shelf Science, *27*(4), 413–426. https://doi.org/10.1016/0272-7714(88)90097-2

Fiori, S. M., & Cazzaniga, N. J. (1999). Mass mortality of the yellow clam, *Mesodesma mactroides* (Bivalvia: Mactracea) in Monte Hermoso Beach, Argentina. *Biological Conservation*, *89*(3), 305–309. https://doi.org/10.1016/s0006-3207(98)00151-7

Fleeger, J. W., Carman, K. R., & Nisbet, R. M. (2003). Indirect effects of contaminants in aquatic ecosystems. *Science of The Total Environment, 317*(1-3), 207-233. https://doi.org/10.1016/s0048-9697(03)00141-4

Flowers, G. J. L., Needham, H. R., Bulmer, R. H., Lohrer, A. M., & Pilditch, C. A. (in review). Going under: the implications of sea-level rise and reduced light availability on intertidal primary production.

Flynn, K. F., Chapra, S. C., & Suplee, M. W. (2013). Modeling the lateral variation of bottom-attached algae in rivers. *Ecological Modelling, 267*, 11-25. https://doi.org/10.1016/j.ecolmodel.2013.07.011

Fransz, H., & Verhagen, J. (1985). Modelling research on the production cycle of phytoplankton in the SOUTHERN Bight of the North Sea in relation to riverborne nutrient loads. *Netherlands Journal of Sea Research, 19*(3-4), 241-250. https://doi.org/10.1016/0077-7579(85)90029-8

Fréchette, M., & Bourget, E. (1985). Energy flow between the pelagic and benthic zones: Factors controlling particulate organic matter available to an intertidal mussel bed. *Canadian Journal of Fisheries and Aquatic Sciences*, *42*(6), 1158–1165. https://doi.org/10.1139/f85-143

Fulton, E. A., Parslow, J. S., Smith, A. D. M., & Johnson, C. R. (2004). Biogeochemical Marine Ecosystem models II: The effect of physiological detail on model performance. *Ecological Modelling*, *173*(4), 371–406. https://doi.org/10.1016/j.ecolmodel.2003.09.024

Galloway, J. N., Townsend, A. R., Erisman, J. W., Bekunda, M., Cai, Z., Freney, J. R., Martinelli, L. A., Seitzinger, S. P., & Sutton, M. A. (2008). Transformation of the

nitrogen cycle: Recent trends, questions, and potential solutions. *Science*, *320*(5878), 889–892. https://doi.org/10.1126/science.1136674

Gammal, J., Hewitt, J., Gladstone-Gallagher, R., Thrush, S., Douglas, E., Lohrer, A., & Pilditch, C. (2022). Stressors increase the impacts of coastal macrofauna biodiversity loss on ecosystem multifunctionality. *Ecosystems*. https://doi.org/10.1007/s10021-022-00775-4

GESAMP (1990). *The state of the marine environment.* Report No.39, GESAMP, IMP, London, UK

Gils, J. A., Ouboter, M. R., & Rooij, N. M. (1993). Modelling of water and sediment quality in the Scheldt estuary. *Netherlands Journal of Aquatic Ecology, 27*(2-4), 257-265. https://doi.org/10.1007/bf02334789

Gladstone-Gallagher, R. V., Mangan, S., Thrush, S. F., & Pilditch, C. A. (2020). Porewater nutrient enrichment alters benthic-pelagic coupling on intertidal sandflats. *Journal of Sea Research*, *159*, 101876. https://doi.org/10.1016/j.seares.2020.101876

Gray, J. S., & Christie, H. (1983). Predicting long-term changes in marine benthic communities. *Marine Ecology Progress Series*, *13*, 87–94. https://doi.org/10.3354/meps013087

Green, M. O., Black, K. P., & Amos, C. L. (1997). Control of estuarine sediment dynamics by interactions between currents and waves at several scales. *Marine Geology*, *144*(1-3), 97–116. https://doi.org/10.1016/s0025-3227(97)00065-0

Green, M. O. (2006). New Zealand's estuaries: how they work and the issue that affect them. *NIWA Information Series, 59,*19. (abbrev version) ISSN 1174-264X.

Green, M. O., & Coco, G. (2007). Sediment transport on an estuarine intertidal flat: Measurements and conceptual model of waves, rainfall and exchanges with a Tidal Creek. *Estuarine, Coastal and Shelf Science*, *72*(4), 553–569. https://doi.org/10.1016/j.ecss.2006.11.006

Green, M. (2013). *Tauranga Harbour sediments in 2051*. NIWA.

Ha, N.-T., Manley-Harris, M., Pham, T.-D., & Hawes, I. (2021). Detecting Multi-decadal Changes in Seagrass Cover in Tauranga Harbour, New Zealand, Using Landsat Imagery and Boosting Ensemble Classification Techniques. *ISPRS International Journal of Geo-Information*, *10*(6), 371. https://doi.org/10.3390/ijgi10060371

Hale, S. S., Cicchetti, G., & Deacutis, C. F. (2016). Eutrophication and hypoxia diminish ecosystem functions of benthic communities in a New England Estuary. *Frontiers in Marine Science*, *3*. https://doi.org/10.3389/fmars.2016.00249

Hall, C. A., Stanford, J. A., & Hauer, F. R. (1992). The Distribution and Abundance of Organisms as a Consequence of Energy Balances along Multiple Environmental Gradients. *Oikos*, *65*(3), 377. https://doi.org/10.2307/3545553

Hancock, N., & Hewitt, J. (2004). Modelling the effects of muddy waters on shellfish. *Water and Atmosphere*, *12*(2), 16–17.

Hancock, N., Hume, T., & Swales, A. (2009). *Tauranga Harbour Sediment Study: Harbour Bed Sediments* (New Zealand, NIWA). Hamilton: NIWA.

Hare, S. R., & Mantua, N. J. (2000). Empirical evidence for North Pacific regime shifts in 1977 and 1989. *Progress in Oceanography*, *47*(2-4), 103-145. https://doi.org/10.1016/s0079-6611(00)00033-1

Henriksen, K., Rasmussen, M. B., Jensen, A. (1983). Effect of bioturbation on microbial nitrogen transformations in the sediment and fluxes of ammonium and nitrate to the overlaying water. *Ecol Bull*, *35*:193–205.

Herring, S. C., Hoerling, M. P., Kossin, J. P., Peterson, T. C., & Stott, P. A. (2015). Explaining Extreme Events of 2014 from a Climate Perspective. *Bulletin of the American Meteorological Society*, *96*(12). https://doi.org/10.1175/bams-explainingextremeevents2014.1

Hewitt, J. E., & Thrush, S. F. (2019). Monitoring for tipping points in the Marine Environment. *Journal of Environmental Management*, *234*, 131–137. https://doi.org/10.1016/j.jenvman.2018.12.092

Hewitt, J. E., Anderson, M. J., Hickey, C. W., Kelly, S., & Thrush, S. F. (2009). Enhancing the Ecological Significance of Sediment Contamination Guidelines through Integration with Community Analysis. *Environmental Science & Technology, 43*(6), 2118-2123. https://doi.org/10.1021/es802175k

Hill, W. R., Rinchard, J., & Czesny, S. (2011). Light, nutrients and the fatty acid composition of stream periphyton. *Freshw. Biol*, *56*, 1825–1836. https://doi.org/10.1111/j.1365-2427.2011.02622.x

Hillebrand, H., Worm, B., & Lotze, H. K. (2000). Marine microbenthic community structure regulated by nitrogen loading and grazing pressure. *Marine Ecology Progress Series*, *204*, 27–38. https://doi.org/10.3354/meps204027

Hope, J. A., Hewitt, J., Pilditch, C. A., Savage, C., & Thrush, S. F. (2020). Effect of nutrient enrichment and turbidity on interactions between Microphytobenthos and a key bivalve: Implications for higher trophic levels. *Frontiers in Marine Science, 7*. https://doi.org/10.3389/fmars.2020.00695

Hope, J. A., Paterson, D. M., & Thrush, S. F. (2019). The role of microphytobenthos in soft-sediment ecological networks and their contribution to the delivery of multiple ecosystem services. *Journal of Ecology, 108*(3), 815-830. https://doi.org/10.1111/1365-2745.13322

Howarth, R. W., & Marino, R. (2006). Nitrogen as the limiting nutrient for eutrophication in coastal marine ecosystems: Evolving views over three decades. *Limnology and Oceanography*, *51*(1part2), 364–376. https://doi.org/10.4319/lo.2006.51.1_part_2.0364

Hsu, J. R., & Jeng, D. S. (1994). Wave-induced soil response in an unsaturated anisotropic seabed of finite thickness. *International Journal for Numerical and Analytical Methods in Geomechanics*, *18*(11), 785–807. https://doi.org/10.1002/nag.1610181104

Huettel, M., Berg, P., & Kostka, J. E. (2014). Benthic Exchange and Biogeochemical Cycling in Permeable Sediments. *Annual Review of Marine Science*, *6*(1), 23-51. https://doi.org/10.1146/annurev-marine-051413-012706

Human, L., Snow, G., & Adams, J. (2016). Responses in a temporarily open/closed estuary to natural and artificial mouth breaching. *South African Journal of Botany*, *107*, 39-48. https://doi.org/10.1016/j.sajb.2015.12.002

Human, L. R. D., Magoro, M. L., Dalu, T., Perissinotto, R., Whitfield, A. K., Adams, J. B., Deyzel, S. H. P., & Rishworth, G. M. (2018). Natural nutrient enrichment and algal responses in near pristine micro-estuaries and micro-outlets. *Science of The Total Environment*, *624*, 945–954. https://doi.org/10.1016/j.scitotenv.2017.12.184

Jäger, C. G., & Diehl, S. (2014). Resource competition across habitat boundaries: Asymmetric interactions between benthic and pelagic producers. *Ecological Monographs*, *84*(2), 287-302. https://doi.org/10.1890/13-0613.1

Jesus, B., Brotas, V., Ribeiro, L., Mendes, C. R., Cartaxana, P., & Paterson, D. M. (2009). Adaptations of microphytobenthos assemblages to sediment type and tidal position. *Continental Shelf Research*, *29*(13), 1624–1634. https://doi.org/10.1016/j.csr.2009.05.006

Joensuu, M., Pilditch, C. A., Harris, R., Hietanen, S., Pettersson, H., & Norkko, A. (2017). Sediment properties, biota, and local habitat structure explain variation in the erodibility of coastal sediments. *Limnology and Oceanography*, *63*(1), 173-186. https://doi.org/10.1002/lno.10622

Johnson, C. R., Banks, S. C., Barrett, N. S., Cazassus, F., Dunstan, P. K., Edgar, G. J., Frusher, S. D., Gardner, C., Haddon, M., Helidoniotis, F., Hill, K. L., Holbrook, N. J., Hosie, G. W., Last, P. R., Ling, S. D., Melbourne-Thomas, J., Miller, K., Pecl, G. T., Richardson, A. J., … Taw, N. (2011). Climate change cascades: Shifts in oceanography, species' ranges and subtidal Marine Community Dynamics in Eastern Tasmania. *Journal of Experimental Marine Biology and Ecology*, *400*(1-2), 17–32. https://doi.org/10.1016/j.jembe.2011.02.032

Jones, H. F., Pilditch, C. A., Hamilton, D. P., & Bryan, K. R. (2016). Impacts of a bivalve mass mortality event on an estuarine food web and bivalve grazing pressure. *New Zealand Journal of Marine and Freshwater Research*, *51*(3), 370–392. https://doi.org/10.1080/00288330.2016.1245200

Kéfi, S., Holmgren, M., & Scheffer, M. (2016). When can positive interactions cause alternative stable states in ecosystems? *Functional Ecology*, *30*(1), 88-97. https://doi.org/10.1111/1365-2435.12601

Kemp, W. M., Boynton, W. R., Adolf, J. E., Boesch, D. F., Boicourt, W. C., Brush, G., Cornwell, J. C., Fisher, T. R., Glibert, P. M., Hagy, J. D., Harding, L. W., Houde, E. D., Kimmel, D. G., Miller, W. D., Newell, R. I. E., Roman, M. R., Smith, E. M., & Stevenson, J. C. (2005). Eutrophication of Chesapeake Bay: Historical Trends and Ecological Interactions. *Marine Ecology Progress Series*, *303*, 1–29. https://doi.org/10.3354/meps303001

Kennish, M. J. (2002). Environmental threats and environmental future of estuaries. *Environmental Conservation*, *29*(1), 78-107. https://doi.org/10.1017/s0376892902000061

Kennish, M. J. (2019). *Ecology of estuaries anthropogenic effects*. CRC press.

Kirk, J. (1977). Attenuation of light in natural waters. *Marine and Freshwater Research*, *28*(4), 497. https://doi.org/10.1071/mf9770497

Kremer, J. N., & Nixon, S. W. (1978). *A coastal marine ecosystem*. Springer.

Kristensen, E., Delefosse, M., Quintana, C. O., Flindt, M. R., & Valdemarsen, T. (2014). Influence of benthic macrofauna community shifts on ecosystem functioning in shallow estuaries. *Frontiers in Marine Science, 1*. https://doi.org/10.3389/fmars.2014.00041

Kromkamp, J., Peene, J., van Rijswijk, P., Sandee, A., & Goosen, N. (1995). Nutrients, light and primary production by phytoplankton and microphytobenthos in the eutrophic, Turbid Westerschelde estuary (The Netherlands). *Hydrobiologia*, *311*(1-3), 9–19. https://doi.org/10.1007/bf00008567

Kühl, M., & Jorgensen, B. B. (1994). The Light Field of microbenthic communities: Radiance Distribution and microscale optics of Sandy coastal sediments. *Limnology and Oceanography*, *39*(6), 1368–1398. https://doi.org/10.4319/lo.1994.39.6.1368

Larson, F., & Sundbäck, K. (2012). Recovery of microphytobenthos and benthic functions after sediment deposition. *Marine Ecology Progress Series,446*, 31-44. https://doi.org/10.3354/meps09488

Lee, R. W., & Rast, W., (1997). *Light Attenuation in a Shallow, Turbid Reservoir. Water-Resources Investigations, Lake Houston, Texas.* Report 97−4064. https://doi.org/10.3133/wri974064.

Lelieveld, S. D., Pilditch, C. A., & Green, M. O. (2004). Effects of deposit-feeding bivalve (*Macomona liliana*) density on intertidal sediment stability. *New Zealand Journal of Marine and Freshwater Research, 38*(1), 115-128. https://doi.org/10.1080/00288330.2004.9517223

Lemley, D. A., Adams, J. B., Bornman, T. G., Campbell, E. E., & Deyzel, S. H. (2019). Land-derived inorganic nutrient loading to coastal waters and potential implications for nearshore plankton dynamics. *Continental Shelf Research, 174*, 1-11. https://doi.org/10.1016/j.csr.2019.01.003

Li, H., Yuan, L., Zhang, L. Q., Li, W., Li, S. H., & Zhao, Z. Y. (2017). Alternative stable states in coastal intertidal wetland ecosystems of Yangtze estuary, China. *The Journal of Applied Ecology, 28*(1), 327-336. https://doi.org/10.13287/j.1001-9332.201701.021

Lingeman-Kosmerchock, M. (1978). *Phytoplankton cells, their nutrient contents, mineralisation and sinking rates*. Delft Hydraulics Laboratory report R1310. Delft

Lohrer, A. M., Thrush, S. F., & Gibbs, M. M. (2004). Bioturbators enhance ecosystem function through complex biogeochemical interactions. *Nature, 431*(7012), 1092-1095. https://doi.org/10.1038/nature03042

Los, F. J. (1982). Mathematical simulation of algae blooms by the model BLOOM II: report on investigations. *r1310*.

Lovelock, C. E., Feller, I. C., Ellis, J., Schwarz, A. M., Hancock, N., Nichols, P., & Sorrell, B. (2007). Mangrove growth in New Zealand estuaries: The role of nutrient enrichment at sites with contrasting rates of sedimentation. *Oecologia, 153*(3), 633–641. https://doi.org/10.1007/s00442-007-0750-y

MacIntyre, H. L., Geider, R. J., & Miller, D. C. (1996). Microphytobenthos: The Ecological Role of the "secret garden" of unvegetated, shallow-water marine habitats. I. Distribution, abundance and primary production. *Estuaries*, *19*(2), 186. https://doi.org/10.2307/1352224

Maes, J., Stevens, M., & Ollevier, F. (2005). The composition and community structure of the Ichthyofauna of the upper Scheldt estuary: Synthesis of a 10-YEAR data collection (1991-2001). *Journal of Applied Ichthyology*,*21*(2), 86-93. https://doi.org/10.1111/j.1439-0426.2004.00628.x

Magni, P., Montani, S., Takada, C., & Tsutsumi, H. (2000). Temporal scaling and relevance of bivalve nutrient excretion on a tidal flat of the Seto Inland Sea, Japan. *Marine Ecology Progress Series, 198,* 139-155. https://doi.org/10.3354/meps198139

Malvarez, G. C., Cooper, J. A. G, Jackson, D. W. T, & Navas, F. (2001). The Role of Wave Action on Sedimentation of Tidal Flats: Application of High Spatial Resolution Numerical Modelling in Strangford Lough, Northern Ireland. *Journal of Coastal Research*, Special Issue (34), 172–182.

Mangan, S., Bryan, K. R., Thrush, S. F., Gladstone-Gallagher, R. V., Lohrer, A. M., & Pilditch, C. A. (2020). Shady business: The darkening of estuaries constrains benthic ecosystem function. *Marine Ecology Progress Series*, *647*, 33–48. https://doi.org/10.3354/meps13410

Marani, M., D'alpaos, A., Lanzoni, S., Carniello, L., & Rinaldo, A. (2010). The importance of being coupled: Stable states and catastrophic shifts in tidal biomorphodynamics. *Journal of Geophysical Research, 115*(F4). https://doi.org/10.1029/2009jf001600

Marinelli, R. L., & Williams, T. J. (2003). Evidence for density-dependent effects of infauna on sediment biogeochemistry and benthic–pelagic coupling in nearshore systems. *Estuarine, Coastal and Shelf Science, 57*(1-2), 179-192. https://doi.org/10.1016/s0272-7714(02)00342-6

Mariotti, G., & Fagherazzi, S. (2012). Modeling the effect of tides and waves on benthic biofilms. *Journal of Geophysical Research: Biogeosciences, 117*(G4). https://doi.org/10.1029/2012jg002064

Matthaei, C. D., Weller, F., Kelly, D. W., & Townsend, C. R. (2006). Impacts of fine sediment addition to tussock, pasture, dairy and deer farming streams in New Zealand. *Freshwater Biology, 51*(11), 2154-2172. https://doi.org/10.1111/j.1365-2427.2006.01643.x

May, R. M. (1977). Thresholds and breakpoints in ecosystems with a multiplicity of stable states. *Nature, 269*(5628), 471-477. https://doi.org/10.1038/269471a0

Mcdowall, R. (1976). The Role of Estuaries in the Life Cycles of Fishes in New Zealand. Proceedings *New Zealand Ecological Society, 23*, 27-32.

McGlathery, K. J., Anderson, I. C., & Tyler, A. C. (2001). Magnitude and variability of benthic and pelagic metabolism in a temperate coastal lagoon. *Marine Ecology Progress Series, 216*, 1–15. https://doi.org/10.3354/meps216001

McGreer, E. R. (1983). Growth and reproduction of *Macoma balthica* (L.) on a mud flat in the Fraser river estuary, British Columbia. *Canadian Journal of Zoology,61*(4), 887-894. https://doi.org/10.1139/z83-116

Mei, C. C., & Foda, M. A. (1981). Wave-induced responses in a fluid-filled poro-elastic solid with a free surface – a boundary layer theory. *Geophysical Journal International, 66*(3), 597-631. https://doi.org/10.1111/j.1365-246x.1981.tb04892.x

Méléder, V., Barillé, L., Rincé, Y., Morançais, M., Rosa, P., & Gaudin, P. (2005). Spatio-temporal changes in microphytobenthos structure analysed by pigment composition in a macrotidal flat (Bourgneuf Bay, France). *Marine Ecology Progress Series*, *297*, 83–99. https://doi.org/10.3354/meps297083

Mermillod-Blondin, F., & Rosenberg, R. (2006). Ecosystem Engineering: The impact of bioturbation on biogeochemical processes in marine and freshwater benthic habitats. *Aquatic Sciences*, *68*(4), 434–442. https://doi.org/10.1007/s00027-006-0858-x

Meyercordt, J., & Meyer-Reil, L. A. (1999). Primary production of benthic microalgae in two shallow coastal lagoons of different trophic status in the southern Baltic Sea. *Marine Ecology Progress Series*, *178*, 179–191. https://doi.org/10.3354/meps178179

MfE (Ministry for the Environment). (2021). *A guide to setting instream nutrient concentrations under clause 3.13 of the National Policy Statement for Freshwater Management 2020.* Wellington: Ministry for the Environment.

Migné, A., Gévaert, F., Créach, A., Spilmont, N., Chevalier, E., & Davoult, D. (2007). Photosynthetic activity of intertidal microphytobenthic communities during emersion: In situ measurements of chlorophyll fluorescence (pam) and CO_2 flux (IRGA) 1. *Journal of Phycology*, *43*(5), 864–873. https://doi.org/10.1111/j.1529-8817.2007.00379.x

Mitbavkar, S., & Anil, A. (2004). Vertical migratory rhythms of benthic diatoms in a tropical intertidal sand flat: Influence of irradiance and tides. *Marine Biology*, *145*(1). https://doi.org/10.1007/s00227-004-1300-3

Montefalcone, M., Parravicini, V., & Bianchi, C. N. (2011). Quantification of coastal ecosystem resilience. *Treatise on Estuarine and Coastal Science*, 49–70. https://doi.org/10.1016/b978-0-12-374711-2.01003-2

Moore, J. C., Berlow, E. L., Coleman, D. C., Ruiter, P. C., Dong, Q., Hastings, A., Johnson, N. C., McCann, K. S., Melville, K., Morin, P. J., Nadelhoffer, K., Rosemond, A. D., Post, D. M., Sabo, J. L., Scow, K. M., Vanni, M. J., & Wall, D. H. (2004). Detritus, trophic dynamics and biodiversity. *Ecology Letters*, *7*(7), 584–600. https://doi.org/10.1111/j.1461-0248.2004.00606.x

Morris, L., & Keough, M. J. (2003). Variation in the response of intertidal infaunal invertebrates to nutrient additions: Field manipulations at two sites within Port Phillip Bay, Australia. *Marine Ecology Progress Series*, *250*, 35–49. https://doi.org/10.3354/meps250035

Morris, E. P. (2005). *Quantifying primary production of microphytobenthos: Application of optical methods* (thesis). s.n., S.l.

Mortazavi, B., Riggs, A. A., Caffrey, J. M., Genet, H., & Phipps, S. W. (2012). The contribution of benthic nutrient regeneration to primary production in a shallow eutrophic estuary, Weeks Bay, Alabama. *Estuaries and Coasts*, *35*(3), 862–877. https://doi.org/10.1007/s12237-012-9478-y

Murrell, M. C., Hagy, J. D., Lores, E. M., & Greene, R. M. (2007). Phytoplankton production and nutrient distributions in a subtropical estuary: Importance of freshwater flow. *Estuaries and Coasts*, *30*(3), 390–402. https://doi.org/10.1007/bf02819386

Muthukrishnan, R., Hayes, K., Bartowitz, K., Cattau, M. E., Harvey, B. J., Lin, Y., & Lunch, C. (2022). Harnessing NEON to evaluate ecological tipping points: Opportunities, challenges, and approaches. *Ecosphere*, *13*(3). https://doi.org/10.1002/ecs2.3989

Naithani, J., Brye, B. D., Buyze, E., Vyverman, W., Legat, V., & Deleersnijder, E. (2016). An ecological model for the Scheldt estuary and tidal rivers ecosystem: Spatial and temporal variability of plankton. *Hydrobiologia*, *775*(1), 51-67. https://doi.org/10.1007/s10750-016-2710-1

New Zealand Ministry for Culture and Heritage Te Manatu Taonga. (2006). *New Zealand's Exclusive Economic Zone*. Te Ara Encyclopedia of New Zealand – Te Ara Encyclopedia of New Zealand. Retrieved March 2, 2022, from https://teara.govt.nz/en/zoomify/6967/new-zealands-exclusive-economic-zone

Newell, R. I. E. (2004). Ecosystem influences of natural and cultivated populations of suspension-feeding bivalve molluscs: A review. *J Shellfish Res*, *23*, 51–61.

Ni Longphuirt, S., Lim, J. H., Leynaert, A., Claquin, P., Choy, E. J., Kang, C. K., & An, S. (2009). Dissolved inorganic nitrogen uptake by intertidal microphytobenthos: Nutrient concentrations, light availability and migration. *Marine Ecology Progress Series*, *379*, 33–44. https://doi.org/10.3354/meps07852

Niemistö, J., & Lund-Hansen, L. C. (2019). Instantaneous effects of sediment resuspension on inorganic and organic benthic nutrient fluxes at a shallow water coastal site in the Gulf of Finland, Baltic Sea. *Estuaries and Coasts*, *42*(8), 2054–2071. https://doi.org/10.1007/s12237-019-00648-5

Nixon, S. W. (1995). Coastal marine eutrophication: A definition, social causes, and future concerns. *Ophelia*, *41*(1), 199-219. https://doi.org/10.1080/00785236.1995.10422044

Nordlund, L. M., Koch, E. W., Barbier, E. B., & Creed, J. C. (2017). Correction: Seagrass ecosystem services and their variability across genera and geographical regions. *PLOS ONE*, *12*(1). https://doi.org/10.1371/journal.pone.0169942

Nowicki, B. L., & Nixon, S. W. (1985). Benthic nutrient remineralization in a Coastal lagoon ecosystem. *Estuaries*, *8*(2), 182. https://doi.org/10.2307/1352199

O'Meara, T. A., Hewitt, J. E., Thrush, S. F., Douglas, E. J., & Lohrer, A. M. (2020). Denitrification and the role of macrofauna across estuarine gradients in nutrient and sediment loading. *Estuaries and Coasts*, *43*(6), 1394–1405. https://doi.org/10.1007/s12237-020-00728-x

Oh, Y., Hamm, S., Chung, S. Y., & Lee, B. D. (2013). Characterizing hydraulic properties by grain-size analysis of fluvial deposits depending on stream path in Korea. *Environmental Engineering Research,18*(3), 129-137. https://doi.org/10.4491/eer.2013.18.3.129

Olds, A. D., Pitt, K. A., Maxwell, P. S., & Connolly, R. M. (2012). Synergistic effects of reserves and connectivity on ecological resilience. *Journal of Applied Ecology*, *49*(6), 1195–1203. https://doi.org/10.1111/jpe.12002

Orvain, F., Galois, R., Barnard, C., Sylvestre, A., Blanchard, G., & Sauriau, P.-G. (2003). Carbohydrate production in relation to Microphytobenthic biofilm development: An integrated approach in a tidal mesocosm. *Microbial Ecology*, *45*(3), 237–251. https://doi.org/10.1007/s00248-002-2027-7

Parsons, T. R., Takahashi, M., & Hargrave, B. (1984). *Biological Oceanographic Processes*. Pergamon Press.

Patil, A. (2011). Protein changes in different tissues of freshwater bivalve *Parreysia cylindrical* after exposure to indoxacarb. *Recent Res. Sci. Technol.* 3, 140–142.

Perretti, C. T., & Munch, S. B. (2012). Regime shift indicators fail under noise levels commonly observed in ecological systems. *Ecological Applications*, *22*(6), 1772–1779. https://doi.org/10.1890/11-0161.1

Peters, R. H. (1991). *A critique for ecology*. Cambridge University Press.

Petuha, E. T., Lundquist, C. J., & Pilditch, C. A. (2006). Estimating spatial scale of post-settlement Transport potential of *Macomona liliana* on an intertidal sandflat. *New Zealand Journal of Marine and Freshwater Research,40*(3), 487-502. https://doi.org/10.1080/00288330.2006.9517438

Pitkänen, H., Lehtoranta, J., & Räike, A. (2001). Internal nutrient fluxes counteract decreases in external load: The case of the Estuarial Eastern Gulf of Finland, Baltic Sea. *AMBIO: A Journal of the Human Environment*, *30*(4), 195–201. https://doi.org/10.1579/0044-7447-30.4.195

Pivato, M., Carniello, L., Gardner, J., Silvestri, S., & Marani, M. (2018a). Water and sediment temperature dynamics in shallow tidal environments: The role of the heat flux at the sediment-water interface. *Advances in Water Resources*, *113*, 126–140. https://doi.org/10.1016/j.advwatres.2018.01.009

Pivato, M., Carniello, L., Moro, I., & D'Odorico, P. (2018b). On the feedback between water turbidity and microphytobenthos growth in shallow tidal environments. *Earth Surface Processes and Landforms*, *44*(5), 1192–1206. https://doi.org/10.1002/esp.4567

Pratt, D. R., Lohrer, A. M., Pilditch, C. A., & Thrush, S. F. (2013). Changes in Ecosystem Function Across Sedimentary Gradients in Estuaries. *Ecosystems, 17*(1), 182-194. https://doi.org/10.1007/s10021-013-9716-6

Pratt, D. R., Pilditch, C. A., Lohrer, A. M., & Thrush, S. F. (2014). The effects of short-term increases in turbidity on sandflat microphytobenthic productivity and nutrient fluxes. *Journal of Sea Research*, *92*, 170–177. https://doi.org/10.1016/j.seares.2013.07.009

Pratt, D. R., Pilditch, C. A., Lohrer, A. M., Thrush, S. F., & Kraan, C. (2015). Spatial distributions of grazing activity and microphytobenthos reveal scale-dependent relationships across a sedimentary gradient. *Estuaries and Coasts*, *38*(3), 722-734. https://doi.org/10.1007/s12237-014-9857-7

Pridmore, R. D., Thrush, S. F., Hewitt, J. E., & Roper, D. S. (1990). Macrobenthic community composition of six intertidal sandflats in Manukau Harbour, New

Zealand. *New Zealand Journal of Marine and Freshwater Research, 24*(1), 81-96. https://doi.org/10.1080/00288330.1990.9516404

Pritchard, D.W. (1967). What is an estuary: physical standpoint. In: *Estuaries*, ed. G.H. Lauff, pp. 3–5. Washington, DC, USA: *American Association for the Advancement of Science, 83*.

Ricciardi, A., & Bourget, E. (1998). Weight-to-weight conversion factors for marine benthic macroinvertebrates. *Marine Ecology Progress Series, 171*, 245-251. https://doi.org/10.3354/meps171245

Robertson, B. P., Gardner, J. P. A., & Savage, C. (2015). Macrobenthic–mud relations strengthen the foundation for Benthic Index Development: A case study from shallow, temperate New Zealand estuaries. *Ecological Indicators, 58*, 161–174. https://doi.org/10.1016/j.ecolind.2015.05.039

Rodil, I. F., Lohrer, A. M., Hewitt, J. E., Townsend, M., Thrush, S. F., & Carbines, M. (2013). Tracking environmental stress gradients using three biotic integrity indices: Advantages of a locally-developed traits-based approach. *Ecological Indicators, 34*, 560–570. https://doi.org/10.1016/j.ecolind.2013.06.023

Roper, D. S., Pridmore, R. D., & Thrush, S. F. (1992). Recruitment to the macrobenthos of *Macomona liliana* (bivalvia: Tellinidae) in Manukau Harbour, New Zealand. *New Zealand Journal of Marine and Freshwater Research, 26*(3-4), 385–392. https://doi.org/10.1080/00288330.1992.9516532

Scheffer, M., Carpenter, S., Foley, J. A., Folke, C., & Walker, B. (2001). Catastrophic shifts in ecosystems. *Nature, 413*(6856), 591-596. https://doi.org/10.1038/35098000

SEDAC. (2011). *Environmental Sustainability Indicators and Trends.* http://sedac.ciesin.columbia.edu/es/csdcoastal.html

Selkoe, K. A., Blenckner, T., Caldwell, M. R., Crowder, L. B., Erickson, A. L., Essington, T. E., Estes, J. A., Fujita, R. M., Halpern, B. S., Hunsicker, M. E., Kappel, C. V., Kelly, R. P., Kittinger, J. N., Levin, P. S., Lynham, J. M., Mach, M. E., Martone, R. G., Mease, L. A., Salomon, A. K., … Zedler, J. (2015). Principles for managing marine

ecosystems prone to tipping points. *Ecosystem Health and Sustainability*, *1*(5), 1–18. https://doi.org/10.1890/ehs14-0024.1

Serôdio, J., Ezequiel, J., Barnett, A., Mouget, J. L., Méléder, V., Laviale, M., & Lavaud, J. (2012). Efficiency of photoprotection in microphytobenthos: Role of vertical migration and the xanthophyll cycle against photoinhibition. *Aquatic Microbial Ecology*, *67*(2), 161–175. https://doi.org/10.3354/ame01591

Simpson, S. L., Batley, G. E., & Chariton, A. A. (2013). Revision of the ANZECC/ARMCANZ sediment quality guidelines. *CSIRO Land Water Rep.* 08/07; CSIRO: Canberra, Australia; 128.

Sinha, S. (2017). Transient evolution of suspended and benthic algae in a riverine ecosystem: A numerical study. *Ecological Modelling, 348,* 78-92. https://doi.org/10.1016/j.ecolmodel.2017.01.008

Skilleter, G. A., & Peterson, C. H. (1994). Control of foraging behavior of individuals within an ecosystem context: The clam *Macoma balthica* and interactions between competition and siphon cropping. *Oecologia, 100*(3), 268-278. https://doi.org/10.1007/bf00316954

Smolders, R., Bervoets, L., De Coen, W., & Blust, R. (2004). Cellular energy allocation in zebra mussels exposed along a pollution gradient: Linking cellular effects to higher levels of biological organization. *Environmental Pollution*, *129*(1), 99–112. https://doi.org/10.1016/j.envpol.2003.09.027

Spanbauer, T. L., Allen, C. R., Angeler, D. G., Eason, T., Fritz, S. C., Garmestani, A. S., Nash, K. L., & Stone, J. R. (2014). Prolonged instability prior to a regime shift. *PLoS ONE*, *9*(10). https://doi.org/10.1371/journal.pone.0108936

Ståhlberg, C., Bastviken, D., Svensson, B. H., & Rahm, L. (2006). Mineralisation of organic matter in coastal sediments at different frequency and duration of resuspension. *Estuarine, Coastal and Shelf Science*, *70*(1-2), 317–325. https://doi.org/10.1016/j.ecss.2006.06.022

Sterner, R. W., Elser, J. J., Fee, E. J., Guildford, S. J., & Chrzanowski, T. H. (1997). The light: Nutrient ratio in lakes: The balance of energy and materials affects ecosystem structure and process. *The American Naturalist*, *150*(6), 663–684. https://doi.org/10.1086/286088

Stutes, A. L., Cebrian, J., & Corcoran, A. A. (2006). Effects of nutrient enrichment and shading on sediment primary production and metabolism in eutrophic estuaries. *Marine Ecology Progress Series*, *312*, 29–43. https://doi.org/10.3354/meps312029

Suding, K. N., & Hobbs, R. J. (2009). Threshold models in restoration and conservation: A developing framework. *Trends in Ecology & Evolution*, *24*(5), 271–279. https://doi.org/10.1016/j.tree.2008.11.012

Sundbäck, K., & Granéli, W. (1988). Influence of microphytobenthos on the nutrient flux between sediment and water- a laboratory study. *Marine Ecology Progress Series*, *43*, 63–69. https://doi.org/10.3354/meps043063

Sundbäck, K., Enoksson, V., Granéli, W., & Pettersson, K. (1991). Influence of sublittoral microphytobenthos on the oxygen and nutrient flux between sediment and water. A laboratory continuous-flow study. *Marine Ecology Progress Series*, *75*, 263–279. https://doi.org/10.3354/meps075263

Sundbäck, K., Miles, A., & Linares, F. (2006). Nitrogen dynamics in nontidal littoral sediments: Role of microphytobenthos and denitrification. *Estuaries and Coasts*, *29*(6), 1196-1211. https://doi.org/10.1007/bf02781820

Surman, M., Clarke, R., & Carter, M. (1999). *Tauranga Harbour Sediment Source Survey* (Operations Report 98/13). Environment B.O.P.

Sutula, M., Green, L., Cicchetti, G., Detenbeck, N., & Fong, P. (2014). Thresholds of adverse effects of macroalgal abundance and sediment organic matter on benthic habitat quality in estuarine intertidal flats. *Estuaries and Coasts*, *37*(6), 1532–1548. https://doi.org/10.1007/s12237-014-9796-3

Suyadi, Gao, J., Lundquist, C. J., & Schwendenmann, L. (2019). Land-based and climatic stressors of mangrove cover change in the Auckland Region, New Zealand. *Aquatic*

Conservation: Marine and Freshwater Ecosystems, 29(9), 1466-1483. https://doi.org/10.1002/aqc.3146

Swales, A., Gibbs, M., Olsen, G., & Ovenden, R. (2015). *Historical changes in sources of catchment sediment accumulating in Whangarei Harbour.* Prepared for by NIWA for Northland Regional Council.

Swales, A., Oldman, J., Radford, J., & MacDonald, I. (2003). What happens in estuaries during floods? *Water & Atmosphere*, *11*(1), 11–13.

Tay, H. W., Bryan, K. R., Pilditch, C. A., Park, S., & Hamilton, D. P. (2012). Variations in nutrient concentrations at different time scales in two shallow tidally dominated estuaries. *Marine and Freshwater Research, 63*(2), 95. https://doi.org/10.1071/mf11102

Tay, H., Bryan, K., Lange, W. D., & Pilditch, C. (2013). The hydrodynamics of the southern basin of Tauranga Harbour. *New Zealand Journal of Marine and Freshwater Research, 47*(2), 249-274. https://doi.org/10.1080/00288330.2013.778300

Tett, P. (1981). The Loch Eil Project: Planktonic pigments in sediments from Loch Eil and the Firth of Lorne. *Journal of Experimental Marine Biology and Ecology*, *56*(1), 101–114. https://doi.org/10.1016/0022-0981(81)90010-1

Thrush, S., Pridmore, R., Hewitt, J., & Cummings, V. (1994). The importance of predators on a sandflat: Interplay between seasonal changes in prey densities and predator effects. *Marine Ecology Progress Series, 107*, 211-222. https://doi.org/10.3354/meps107211

Thrush, S. F., Cummings, V. J., Dayton, P. K., Ford, R., Grant, J., Hewitt, J. E., Hines, A. H., Lawrie, S. M., Pridmore, R. D., Legendre, P., McArdle, B. H., Schneider, D. C., Turner, S. J., Whitlatch, R. B., & Wilkinson, M. R. (1997). Matching the outcome of small-scale density manipulation experiments with larger scale patterns. *Journal of Experimental Marine Biology and Ecology*, *216*(1-2), 153–169. https://doi.org/10.1016/s0022-0981(97)00094-4

Thrush, S. F., & Dayton, P. K. (2002). Disturbance to marine benthic habitats by trawling and dredging: Implications for marine biodiversity. *Annual Review of Ecology and*

Systematics, *33*(1), 449–473. https://doi.org/10.1146/annurev.ecolsys.33.010802.150515

Thrush, S. F., Hewitt, J. E., Norkko, A., Nicholls, P. E., Funnell, G. A., & Ellis, J. I. (2003). Habitat change in estuaries: Predicting broad-scale responses of intertidal macrofauna to sediment mud content. *Marine Ecology Progress Series*, *263*, 101–112. https://doi.org/10.3354/meps263101

Thrush, S. F., Hewitt, J. E., Cummings, V. J., Ellis, J. I., Hatton, C., Lohrer, A., & Norkko, A. (2004). Muddy Waters: Elevating sediment input to coastal and estuarine habitats. *Frontiers in Ecology and the Environment*, *2*(6), 299–306. https://doi.org/10.1890/1540-9295(2004)002[0299:mwesit]2.0.co;2

Thrush, S. F., Hewitt, J. E., Herman, P. M. J., & Ysebaert, T. (2005). Multi-scale analysis of species-environment relationships. *Marine Ecology Progress Series*, *302*, 13–26. https://doi.org/10.3354/meps302013

Thrush, S. F., Hewitt, J. E., Gibbs, M., Lundquist, C., & Norkko, A. (2006). Functional Role of Large Organisms in Intertidal Communities: Community Effects and Ecosystem Function. *Ecosystems*, *9*(6), 1029-1040. https://doi.org/10.1007/s10021-005-0068-8

Thrush, S. F. (2014). *The Life and Time of Macomona liliana, From Humble Bivalve to Fuel for Intercontinental Flights and Provider of Ecosystem Services* [Powerpoint Slides]. MARI450: Marine Science. https://www.otago.ac.nz/marinescience/MARI450BIOL427MARINE701/20140521Thrush/Simon%20Thrush%20seminar%2021-05-2014.pdf

Thrush, S. F., Hewitt, J. E., Parkes, S., Lohrer, A. M., Pilditch, C., Woodin, S. A., Wethey, D. S., Chiantore, M., Asnaghi, V., De Juan, S., Kraan, C., Rodil, I., Savage, C., & Van Colen, C. (2014). Experimenting with ecosystem interaction networks in search of threshold potentials in real-world marine ecosystems. *Ecology*, *95*(6), 1451–1457. https://doi.org/10.1890/13-1879.1

Thrush, S. F., Hewitt, J. E., Kraan, C., Lohrer, A. M., Pilditch, C. A., & Douglas, E. (2017). Changes in the location of biodiversity–ecosystem function hot spots across the seafloor landscape with increasing sediment nutrient loading. *Proceedings of the*

Royal Society B: Biological Sciences, *284*(1852), 20162861. https://doi.org/10.1098/rspb.2016.2861

Thrush, S. F., Hewitt, J. E., Gladstone-Gallagher, R. V., Savage, C., Lundquist, C., O'Meara, T., Vieillard, A., Hillman, J. R., Mangan, S., Douglas, E. J., Clark, D. E., Lohrer, A. M., & Pilditch, C. (2021). Cumulative stressors reduce the self-regulating capacity of coastal ecosystems. *Ecological Applications*, *31*(1). https://doi.org/10.1002/eap.2223

Tobias, C., Giblin, A., McClelland, J., Tucker, J., & Peterson, B. (2003). Sediment din fluxes and preferential recycling of benthic microalgal nitrogen in a shallow macrotidal estuary. *Marine Ecology Progress Series*, *257*, 25–36. https://doi.org/10.3354/meps257025

Tricklebank, K. A., Grace, R. V., & Pilditch, C. A. (2020). Decadal population dynamics of an intertidal bivalve (*Austrovenus stutchburyi*) bed: Pre- and post- a mass mortality event. *New Zealand Journal of Marine and Freshwater Research*, 1–23. https://doi.org/10.1080/00288330.2020.1772323

Turner, D. F., Pelletier, G. J., & Kasper, B. (2009). Dissolved oxygen and pH modeling of a periphyton dominated, nutrient enriched river. *Journal of Environmental Engineering*, *135*(8), 645-652. https://doi.org/10.1061/(asce)0733-9372(2009)135:8(645)

Turner, J., Bindschadler, R. A., Convey, P., Prisco, G. D., Fahrbach, E., Gutt, J., Hodgson, D., Mayewski, P., & Summerhayes, C. P. (2009). *Antarctic climate change and the environment: A contribution to the International Polar Year 2007-2008*. SCAR.

Urlich, S. C., & Handley, S. J. (2020). From 'clean and green' to 'brown and down': A synthesis of historical changes to biodiversity and marine ecosystems in the Marlborough Sounds, New Zealand. *Ocean & Coastal Management*, *198*, 105349. https://doi.org/10.1016/j.ocecoaman.2020.105349

Valdemarsen, T., Quintana, C. O., Flindt, M. R., & Kristensen, E. (2015). Organic N and P in eutrophic fjord sediments – rates of mineralization and consequences for internal nutrient loading. *Biogeosciences*, *12*(6), 1765–1779. https://doi.org/10.5194/bg-12-1765-2015

van Nes, E. H., Amaro, T., Scheffer, M., & Duineveld, G. C. A. (2007). Possible mechanisms for a marine benthic regime shift in the North Sea. *Marine Ecology Progress Series*, *330*, 39–47. https://doi.org/10.3354/meps330039

van Oevelen, D., Soetaert, K., Middelburg, J. J., Herman, P. M., Moodley, L., Hamels, I., Moens, T., & Heip, C. H. (2006). Carbon flows through a benthic food web: Integrating biomass, isotope and Tracer Data. *Journal of Marine Research*, *64*(3), 453–482. https://doi.org/10.1357/002224006778189581

Vitousek, P. M. (1994). Beyond Global Warming: Ecology and Global Change. *Ecology*, *75*(7), 1861-1876. https://doi.org/10.2307/1941591

Volkenborn, N., Meile, C., Polerecky, L., Pilditch, C. A., Norkko, A., Norkko, J., Hewitt, J. E., Thrush, S. F., Wethey, D. S., & Woodin, S. A. (2012). Intermittent bioirrigation and oxygen dynamics in permeable sediments: An experimental and modeling study of three tellinid bivalves. *Journal of Marine Research*, *70*(6), 794–823. https://doi.org/10.1357/002224012806770955

Waikato Regional Council. (n.d.). *Ecosystem Services in Estuaries.* https://www.waikatoregion.govt.nz/assets/PageFiles/41458-coastal-fact-sheets/5263-Estuaries-Facsheet-Ecosystem-Services-WR.PDF

Walker, B., & Meyers, J. A. (2004). Thresholds in Ecological and Social–Ecological Systems: A Developing Database. *Ecology and Society*, *9*(2). https://doi.org/10.5751/es-00664-090203

Walker, B., Holling, C. S., Carpenter, S. R., & Kinzig, A. P. (2004). Resilience, adaptability and transformability in social-ecological systems. *Ecology and Society*, *9*(2). https://doi.org/10.5751/es-00650-090205

Wang, C., & Temmerman, S. (2013). Does biogeomorphic feedback lead to abrupt shifts between alternative landscape states?: An empirical study on intertidal flats and marshes. *Journal of Geophysical Research: Earth Surface*, *118*(1), 229-240. https://doi.org/10.1029/2012jf002474

Warwick, R. M., Ashman, C. M., Brown, A. R., Clarke, K. R., Dowell, B., Hart, B., Lewis Re Shillabeer, N., Somerfield, P. J., & Tapp, J. F. (2002). Inter-annual changes in the biodiversity and community structure of the macrobenthos in Tees Bay and the Tees Estuary, UK, associated with local and regional environmental events. *Marine Ecology Progress Series*, *234*, 1–13. https://doi.org/10.3354/meps234001

Weijerman, M., Lindeboom, H., & Zuur, A. F. (2005). Regime shifts in marine ecosystems of the North Sea and Wadden Sea. *Marine Ecology Progress Series*, *298*, 21–39. https://doi.org/10.3354/meps298021

Wells, S. R., Wing, L. C., Smith, A. M., & Smith, I. W. G. (2019). Historical changes in bivalve growth rates indicate ecological consequences of human occupation in estuaries. *Aquatic Conservation: Marine and Freshwater Ecosystems*, *29*(9), 1452–1465. https://doi.org/10.1002/aqc.3039

Wilcock, R. J., Pridmore, R. D., Thrush, S. F., Cummings, V. J., Hewitt, J. E., & Smith, T. J. (1993). Bioaccumulation and elimination of chlordane by selected intertidal benthic fauna. *Environmental Toxicology and Chemistry*, *12*(4), 733–742. https://doi.org/10.1002/etc.5620120415

Williams, H. F. (2012). Magnitude of Hurricane Ike storm surge sedimentation: Implications for coastal marsh aggradation. *Earth Surface Processes and Landforms*, *37*(8), 901-906. https://doi.org/10.1002/esp.3252

Wilson, J. B., & Agnew, A. D. (1992). Positive-feedback Switches in Plant Communities. *Advances in Ecological Research Advances in Ecological Research Volume 23*, 263-336. https://doi.org/10.1016/s0065-2504(08)60149-x

Woodin, S. A., Marinelli, R. L., & Lindsay, S. M. (1998). Process-specific cues for recruitment in sedimentary environments: Geochemical signals? *Journal of Marine Research, 56*(2), 535-558. https://doi.org/10.1357/002224098321822410

Woodin, S. A., Volkenborn, N., Pilditch, C. A., Lohrer, A. M., Wethey, D. S., Hewitt, J. E., & Thrush, S. F. (2016). Same pattern, different mechanism: Locking onto the role of key species in seafloor ecosystem process. *Scientific Reports, 6*(1). https://doi.org/10.1038/srep26678

Woodin, S. A., Wethey, D. S., & Volkenborn, N. (2010). Infaunal Hydraulic Ecosystem Engineers: Cast of Characters and Impacts. *Integrative and Comparative Biology*, *50*(2), 176-187. https://doi.org/10.1093/icb/icq031

Woodin, S. A., Wethey, D. S., Hewitt, J. E., & Thrush, S. F. (2012). Small scale terrestrial clay deposits on intertidal sandflats: Behavioral changes and productivity reduction. *Journal of Experimental Marine Biology and Ecology, 413*, 184-191. https://doi.org/10.1016/j.jembe.2011.12.010

Yamamoto, T. (1997). Wave induced instability in seabeds. *Proc. Coastal Sediments, 77*, 898-913.